# The control of polymer structure and reactivity using high intensity ultrasound

West, Peter J.

*Award date:*
1993

*Awarding institution:*
University of Bath

# The Control of Polymer Structure

# and Reactivity Using High Intensity Ultrasound

Submitted by PETER J. WEST

for the degree of Ph.D.

at the University of Bath

1993



P.J.West





ProQuest LLC
789 East Eisenhower Parkway
P.O. Box 1346
Ann Arbor, MI 48106-1346

## Acknowledgements

I would like to thank my supervisor Dr. G. J. Price for his encouragement, guidance and friendship throughout my Ph.D., many thanks Gareth.

Special thanks to a great friend Dr. Paul Smith whose enthusiasm added to my interest in the subject, many thanks for the advice and humour over the last few years.

I would also like to thank a large number of friends for making my years in Bath memorable and enjoyable. I would like to thank Joe, our technician, for his help and acknowledge other members of the research group, especially Andy Clifton.

I am grateful to Dr. Steve Holding of RAPRA Technology Ltd. for the assistance with the GPC-viscometry and to Dr. John Maher (University of Bristol) for his training and expert guidance with the ESR spectrometer.

The financial support of the Science and Engineering Research Council and BP Research, Sunbury-on-Thames, is gratefully acknowledged.

Finally to my parents and brother who have given me more support and love during my time at university than I could ever repay - ***thank you***.

## Contents

## Summary

The work described in this thesis concentrates on the application of high intensity ultrasound to the control of polymer structure and reactivity.

Solutions of polyisobutylene were degraded ultrasonically under a range of physical and ultrasonic reaction conditions. The effects of polymer solution concentration and the temperature were investigated, a number of different solvents were employed and a wide range of gases used in order to correlate the results with the properties of the gas. Conclusions were drawn as to the effects of altering the reaction parameters in terms of the process of ultrasonic cavitation. The conformation adopted in solution by the polymer chains will change with the choice of solvent and this factor was correlated with the degradation results by viscometrically determining the Flory-Huggins polymer-solvent interaction parameter.

High temperature degradations involving polyethylene and polypropylene were carried out and the extent of chain branching in the polyethylene system was examined employing the technique of GPC-viscometry. The results concluded that degrees of chain branching were introduced during the sonication process.

Polymer degradation rate models were applied to all of the results showing the presence of an apparent negative Arrhenius activation energy for the degradation and many similarities with the predicted shear degradation mechanism.

The production of macroradicals by homolytic cleavage of the polymer chains was confirmed by electron spin resonance spectroscopy providing the opportunity for their characterisation. The macroradicals were used to synthesise functionalised polyisobutylene chains. The size of the polyisobutylene macroradical could be controlled, predicted and optimised leading to telechelic materials.

Ultrasonic treatment of a mixture of immiscible polymers was found to produce copolymer linkages or miscible, more compatible blends which were studied using conventional scanning electron microscopy.

# CHAPTER ONE

# INTRODUCTION

## 1.1 Polymers, Their Significance and Applications.

By definition, a polymer is a long, chain-like structure characterised by the multiple repetition of one or more species of atoms or groups of atoms linked chemically by covalent bonds in amounts sufficient to provide a set of properties that do not vary markedly with the addition or removal of one of these constitutional units. These repeating segments are termed monomer units.

Polymers have always existed in our natural environment. Biological polymers help dictate many of the important roles played in plant and animal life. The growth of interest and research into synthetic polymers over the past few decades has produced an enormous variety of applications the responsibility for which lying in their vast diversity of properties. Applications vary from materials for aircraft windows to contact lenses and from lightweight, bio-degradable packaging to new breeds of super-lubricants.

Polymers comprising one type of monomer unit only are known as homopolymers, those comprising two or more different types are termed copolymers. Copolymerisation is the most general and powerful method of effecting systematic changes in polymer properties and is widely used in the production of commercial polymers. Copolymerisation modifies the symmetry of the polymer chain and modulates both intramolecular and intermolecular forces, so that properties such as melting point, glass transition temperature, crystallinity, solubility, elasticity, permeability and chemical reactivity may be varied within a wide limit, depending on the monomers.

## 1.2 Polymer Architecture.

A typical sample of commercial polyethylene may contain 50000 atoms and be 25000Å in length. There can be considerable variation in the architecture of the individual molecules in different polymer samples. Polymers will readily adopt a linear, branched or even three-dimensional network as shown in figure 1.1,

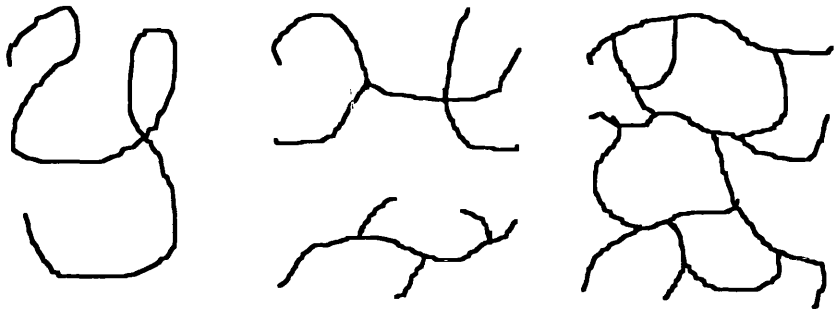


**FIGURE 1.1.** Schematic of Polymer Types.

The structure of the polymer will control the properties of the material both in the solid state and in solution. When a polymeric material is cooled from the liquid or rubber state, it becomes much stiffer as a result of one of two possible events: crystallisation or glass transition. For crystallisation to occur, the polymer molecules must be sufficiently regular along their length to allow the formation of crystalline lattices and the cooling rate must be slow enough to allow the crystallisation process to occur before the molecular motions become too slow. When the polymer fails to crystallise the amorphous, liquid-like structure of the polymer is retained, but the molecular motion becomes frozen and the polymer turns rubbery and as the temperature is reduced further it becomes a relatively hard and elastic polymer *glass*. The temperature at which the polymer undergoes the transformation from a rubber to a glass is known as the *glass transition temperature*, $T_g$. This ability to form a glass is not confined to non-crystallisable polymers. Any material which can be cooled sufficiently below its melting point without crystallising will undergo a glass transition.

Polymers fall broadly into three categories; thermoplastics, rubbers and thermosets.

A thermoplastic polymer can be linear or branched, is capable of being repeatedly softened by heating and hardened by cooling through a characteristic

temperature range and upon the application of heat, whilst in its softened state, the polymer can be shaped by moulding or extrusion. Thermoplastics can be sub-divided into those which crystallise on cooling and those which do not and are normally used as polymer glasses. The ability of the polymers to crystallise depends upon many factors such as the degree of chain branching and regularity of the molecules. The most important types of thermoplastic polymers include polyethylene, polyvinyl chloride, polypropylene and polystyrene.

Rubbers exist in lightly cross-linked macromolecular networks displaying elastomeric properties, molecules slide past each other on deformation but the cross-links prevent permanent flow and the molecules return to their original positions following the removal of the stress. Rubbers exhibit a high degree of chain flexibility and low glass transition temperatures. Vulcanisation of rubber introduces a high degree of cross-linking making melting impossible. Natural rubber is *cis*-polyisoprene, synthetic rubbers include isoprene and isobutylene polymers, styrene-butadiene copolymers and ethylene-propylene copolymers.

A thermoset polymer is heavily cross-linked, rigid and intractable. It adopts a three-dimensional network and, like rubbers, degrades rather than melts on heating. Examples include polyesters and epoxide resins.

### 1.2.1 Copolymer Structure.

Two or more distinct monomer units can be polymerised and incorporated into the same polymer chain. A description of copolymer structure requires the specification of composition, i.e., the relative amounts of comonomers of A and B, sequence distribution, i.e., the order of incorporation of A and B into the chain, and linearity. Copolymers are most often classified according to the latter two characteristics; thus the major classes of copolymers are:

(i) **Statistical (random) Copolymers,** in which comonomers appear in irregular, unspecified sequences long the chain.

~ABBABAAABABBBBA~

(ii) **Alternating Copolymers,** in which the comonomers occur in alternation.

~ABABABABABABABA~

(iii) **Block Copolymers,** in which long linear sequences of comonomer A are joined to long linear sequences of comonomer B.

~AAAAABBBBBAAAAA~

(iv) **Graft Copolymers,** in which chains of one comonomer are pendant from the backbone of the other.

```
~AAAAAAAAAAAAAAA~
   B           B
   B           B
   B           B
```

1.2.2 Configurational Isomerism in Polymers.

Polymer synthesis can produce different stereochemical arrangements along the polymer backbone. The types of configurational isomerism are termed *tacticities*. For the general vinyl monomer $CH_2$=CHR there are two distinct forms. In one type, all of the carbon atoms containing the R substituents have the same configuration, this is said to be an *isotactic* polymer. In the other type, alternate carbon atoms containing the R substituent have the same configuration, this is called a *syndiotactic* polymer. Polymers in which the R substituents are randomly placed are termed *atactic* polymers. These stereochemistries are shown diagrammatically in figure 1.2. The local environments of the protons differ sufficiently between the isomers for them to be determined by $^1$H-nmr spectroscopy.

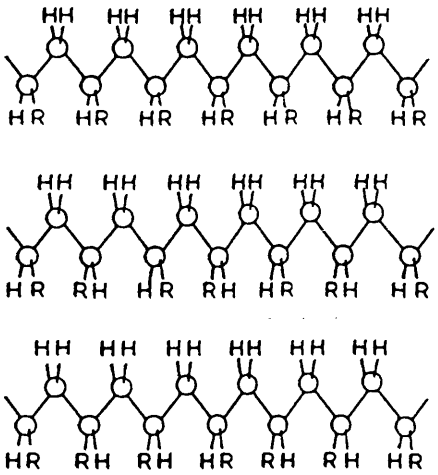


**FIGURE 1.2.** Polymer Stereochemistries.

## 1.3 Molecular Weight Averages of Polymers.

The statistical nature of laboratory and commercial polymer synthesis invariably leads to materials containing a mixture of molecular sizes, hence a distribution of degrees of polymerisation is obtained. The degree of polymerisation, X, is simply defined as the average number of base units per molecule if the molecules are composed of regularly repeating units, or the average number of monomeric units per molecule. These definitions are not necessarily equivalent, except in the case of polymers that are homogeneous with respect to molecular weight. Hence the type of averaging must be specified as explained in the following paragraphs.

A complete description of the molecular weight distribution of a polymer is necessary to understand its physical, rheological and mechanical properties. Molecular weight averages of polymers can be quoted and defined in a variety of ways. It is assumed that the distribution of molar mass can be divided into discrete fractions of molar mass $M_i$, comprising molecules which contain a discrete number of i repeat units, hence $n_i$ is the number of molecules of length i and $W_i$ is the weight of each of the component molecules.

(i) Number-Average Molecular Weight, $M_n$.

This is defined as the sum of the products of the molar mass of each fraction multiplied by its mole fraction, $x_i$.

$$M_n = \sum x_i M_i \qquad 1.1$$

The mole fraction is the ratio of $n_i$ to the total number of molecules, n. It follows therefore that:

$$M_n = \frac{\sum n_i M_i}{\sum n_i} = \frac{\sum W_i}{\sum W_i / M_i} \qquad 1.2$$

It is possible to define a number average degree of polymerisation $X_n$, such that:

$$X_n = \frac{M_n}{M_o} \qquad 1.3$$

where $M_o$ is the molecular weight of the monomer. $M_n$ determines bulk properties of the polymer such as brittleness and tensile strength.

(ii) Weight-Average Molecular Weight, $M_w$.

This is defined as the sum of the products of the molar mass of each fraction multiplied by its weight fraction, $w_i$.

$$M_w = \sum w_i M_i \qquad 1.4$$

The weight fraction $w_i$ is defined as the ratio of the mass of molecules of length i, to the total mass of all molecules such that:

$$w_i = \frac{n_i M_i}{\sum n_i M_i} \qquad 1.5$$

Combining equations 1.4 and 1.5 gives the more familiar expression for $M_w$ in terms of the number of molecules and in terms of the weight of its components, $W_i$.

$$M_w = \frac{\sum n_i M_i^2}{\sum n_i M_i} = \frac{\sum W_i M_i}{\sum W_i} \qquad 1.6$$

As in the case of $M_n$, a weight average degree of polymerisation $X_w$, can be defined,

$$X_w = \frac{M_w}{M_o} \qquad 1.7$$

$M_w$ is greatly influenced by high molecular weight species as each molecule contributes in proportion to the square of its mass. Hence, with the exception of monodisperse polymer systems, $M_w$ is always greater than $M_n$. $M_w$ determines properties such as hardness of the solid polymer.

(iii) Higher Molecular Weight Averages, $M_Z$ and $M_{Z+1}$.

Not finding common usage, these values are determined mathematically by back-calculating averages from the distribution and applied to correlate sedimentation and diffusion properties.

$$M_z = \frac{\sum n_i M_i^3}{\sum n_i M_i^2} = \frac{\sum W_i M_i^2}{\sum W_i M_i} \qquad 1.8$$

$$M_{z+1} = \frac{\sum n_i M_i^4}{\sum n_i M_i^3} = \frac{\sum W_i M_i^3}{\sum W_i M_i^2} \qquad 1.9$$

(iv) Viscosity-Average Molecular Weight, $M_V$.

The intrinsic viscosity $[\eta]$, described later, can be related to the molar mass of a monodisperse polymer M, through a semi-empirical equation of the form:

$$[\eta] = KM^{\alpha} \qquad 1.10$$

where K and $\alpha$ are the Mark-Houwink parameters and M is the viscosity-average molecular weight, $M_V$. This value is an average one when measuring a polydisperse sample hence:

$$M_v = \left[ \frac{\sum n_i M_i^{1+\alpha}}{\sum n_i M_i} \right]^{\frac{1}{\alpha}} \qquad 1.11$$

The value $\alpha$ lies between 0.5 and 1 therefore it follows that the value $M_V$ falls between $M_W$ and $M_n$.

Quoting one molecular weight average does not adequately characterise a polymer. Two polymer samples possessing identical values for one molecular weight average may have a vastly different distribution of chain lengths. The breadth of this distribution is described in terms of a heterogeneity index or *polydispersity*, $\gamma$, such that:

$$\gamma = \frac{M_w}{M_n} \qquad 1.12$$

For a monodisperse polymer $\gamma$=1 whereas for wider distributions, or *polydisperse* systems, values exceed unity. Common polymerisation techniques produce materials around $\gamma$=2 but $\gamma$ values in excess of 10 are known. Anionic polymerisation procedures produce the lowest values of 1.02 - 1.05. Only natural polymers, or biological polymers, like DNA, possess true monodisperse properties.

### 1.4 Molecular Weight Determination of Polymers.

Most polymeric materials are composed of mixtures of molecules of various sizes caused by the statistical nature of the polymerisation process.

Various methods exist, both chemical and physical, to determine the molecular weight. Most techniques are only capable of yielding one of the molecular weight averages of the distribution. End-group analysis and measurement of colligative properties by osmometry, ebulliometry and cryoscopy determine $M_n$, light-scattering determines $M_w$, solution viscometry determines $M_v$ and higher molecular weight averages such as $M_z$ can be determined by ultracentrifugation. All of which are absolute techniques in that they require no reference to a calibration, with the exception of viscometry. The majority of analytical techniques require the solubility of the polymer, many involve the extrapolation to infinite dilution or operation in a theta solvent in which ideal-solution behaviour is attained.

Gel permeation chromatography, GPC, was the main technique employed in the work documented in this thesis and has the advantage of yielding more than one molecular weight average. Solution viscometry and combined GPC-viscometry were also used to determine other polymer properties such as chain conformation in solution and the degree of chain branching, the theory of these will be discussed in sections 1.5 and 1.11.

### 1.4.1 Gel Permeation Chromatography.

#### a.) Underlying Principle.

Essentially GPC is a process for the separation of macromolecules according to their size. Its general application to synthetic polymer chemistry in the 1970's onwards has revolutionised the procedure for polymer characterisation and molecular weight determination and has now become a widely accepted method[1,2] of analysis.

Dilute polymer solutions, perhaps containing a broad molecular weight distribution of polymer chains, are allowed to flow through a column, or series of columns, packed with finely divided solid particles, each particle being permeated by pores or tunnels with a diameter of typically a few microns. As the dissolved solute passes each particle the small molecules, with dimensions less than the pore-size, will enter the pores and be *delayed* in their elution through the column. On the other hand, the larger polymer molecules (those with a random coil radius greater than the pore-size) will be unable to penetrate the pores and will be swept along with the solvent front and eluted ahead of the smaller molecules.

In practice, if the substrate particles have only one uniform pore-size the process can separate molecules that form part of a continuous molecular weight distribution. In principle, this single pore-size column would be expected to *separate* high molecular weight molecules from the rest and *fractionate* the smaller molecules according to their size. Therefore those molecules possessing a coil diameter close to that of the pore diameter will be fractionated the most effectively.

The effectiveness of the fractionation process for a complete molecular weight distribution can be improved by the use of several different columns in series, each of which containing particles with different pore-sizes. Alternatively, mixed-bed columns are employed which contain a range of pore-sizes in the same column. Figure 1.3 shows a typical column and its packing.

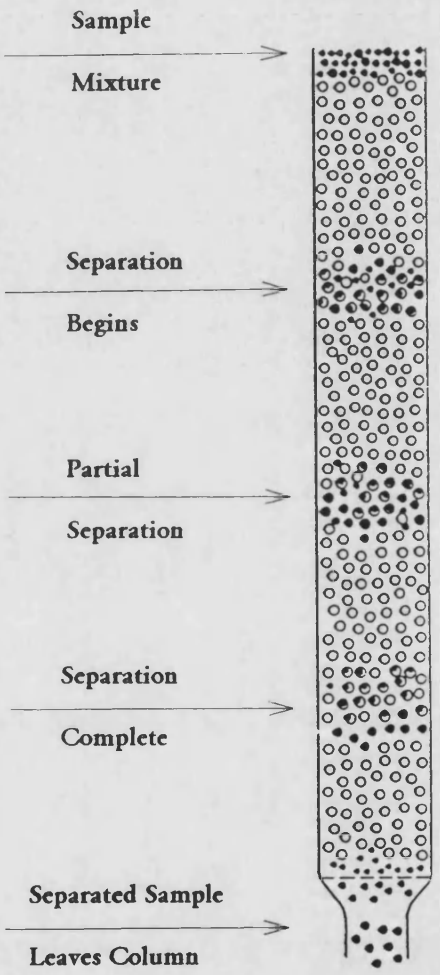


**FIGURE 1.3.** Diagram of a GPC Column.

Thus GPC fractionates polymers according to their size and therefore according to their molecular weight. Molecular weights cannot be determined directly but only after calibration in terms of the elution time or volume of solution eluted.

b.) Experimental Equipment.

The apparatus for GPC or size-exclusion chromatography, SEC, is shown schematically in figure 1.4.

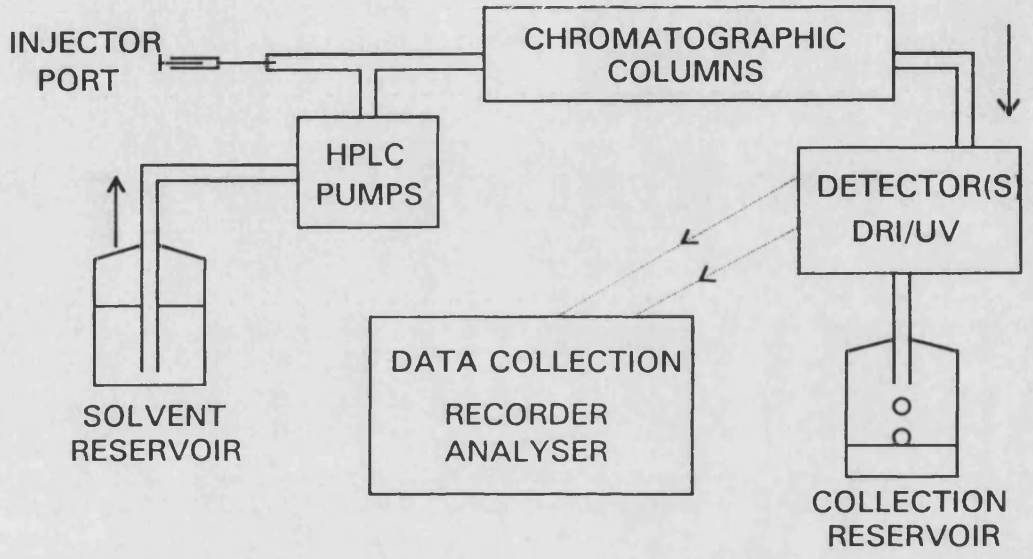


**FIGURE 1.4.** Schematic of a Gel Permeation Chromatograph.

The accuracy and reproducibility of the system relies on the pump being able to deliver a pulse-free, accurately known flow-rate of eluent into which the dilute polymer sample is injected. The flow-rate and column pore-sizes must remain constant throughout the analysis, both of these factors may change if the column temperature varies or the solvent composition changes. The equipment is designed to avoid such problems.

Typically the elution solvent is forced through the columns at a constant flow-rate of 1.0 $cm^3$ $min^{-1}$ at pressures approaching 100 bar. Commonly used packings for organic mobile phases include styrene-divinyl benzene copolymers and Sephadex for aqueous systems. There are a wide range of solvents and solvent mixtures used in GPC.

Following fractionation, the concentration of all eluted species is determined by either a differential refractometer, DRI, which compares the refractive indices of the column effluent containing the fractionated polymer and the reference of pure solvent, or an ultraviolet spectrophotometer which is employed for polymers with UV chromophores e.g. the spectrometer is set to a single wavelength corresponding to the aromatic absorbance region for a polymer containing phenyl rings. Detectors are usually non-destructive, this is particularly useful if the samples are valuable or preparative work is required. An example of a typical chromatogram obtained in this work using a DRI detector is shown in figure 1.5.

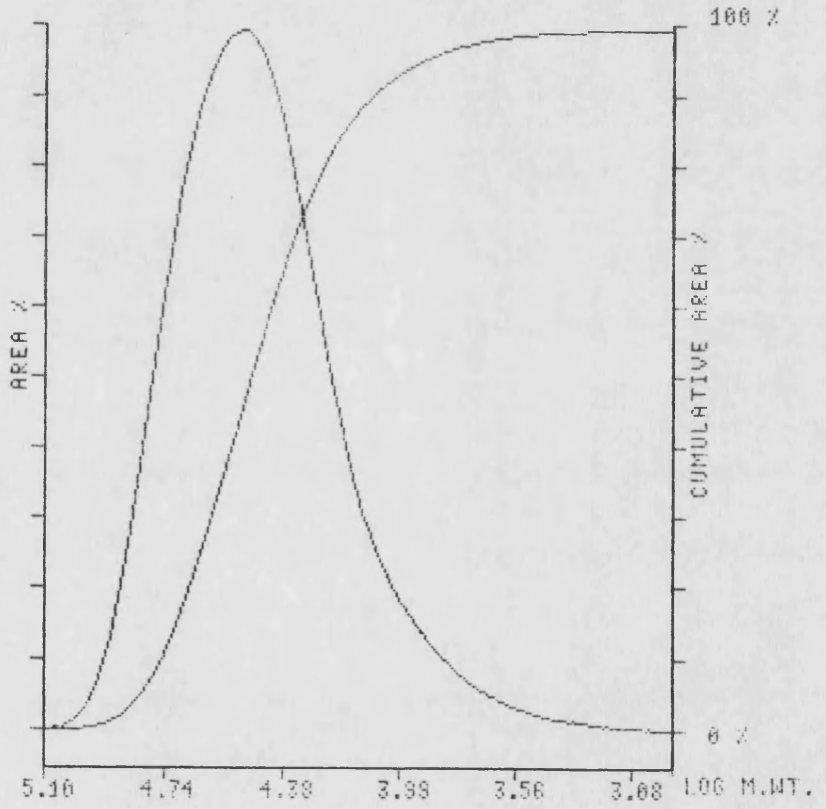


**FIGURE 1.5.** GPC chromatogram obtained with DRI detector.

c.) Theory of GPC.

GPC is a secondary method of polymer analysis in that it requires calibration. Such a calibration establishes a relationship, for a given polymer-solvent system,

between the volume of solution eluted (or equivalently, the elution time for a given flow-rate) and the molecular weight of monodisperse fractions of polymer. Samples are available for a few specific polymers possessing near monodisperse properties. A notable example is polystyrene for which samples having a molecular weight range of $10^3$ to $10^6$ and $\gamma$ values of less than 1.10 can be obtained commercially.

Calibration can be achieved in a variety of ways[3], the simplest being calibration with narrow distribution standards of the same polymer which is to be analysed. A calibration curve is then plotted of logM against $V_R$, the elution volume. The elution volume is proportional to the logarithm of molecular weight.

$$V_R = f \log M \qquad 1.13$$

This is shown in figure 1.6 for a series of polystyrene standards taken from a universal calibration carried out during the analysis of polyisobutylene samples in the work described in chapter 3 of this thesis.

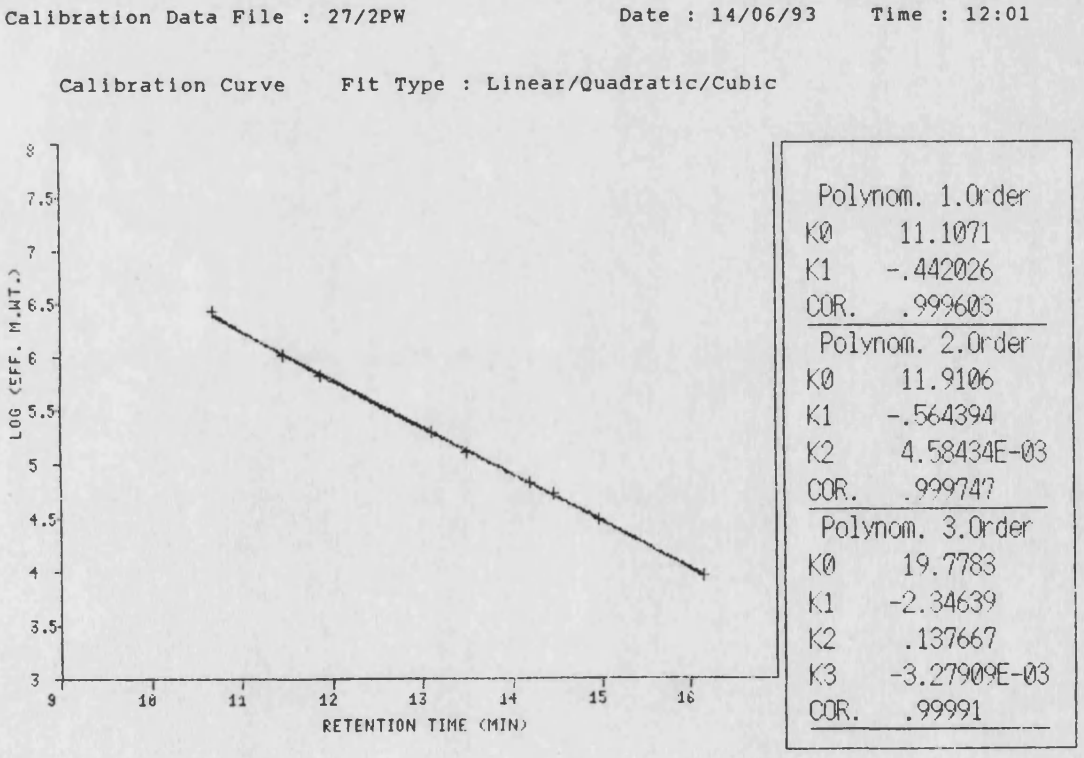


**FIGURE 1.6.** A Typical GPC Calibration Curve for Polystyrene.

Calibration with a set of monodisperse samples of a single polymer leaves the problem of establishing the relationship between the elution volume and the molecular weight of a chemically different polymer. To do this, Benoit[4] devised a *universal calibration* technique. This suggests that a plot of log[η]M against $V_R$ is identical for all polymers, where [η] is the intrinsic viscosity. The product of [η]M is the *universal calibration parameter*, often termed the hydrodynamic volume, HV.

$$HV = [\eta]M \tag{1.14}$$

log[η]M is assumed to be a constant for all polymers in a given solvent, at a given temperature, at the same elution volume. Hence it is possible to write,

$$\log[\eta]_x M_x = \log[\eta]_s M_s \tag{1.15}$$

where subscripts x and s relate to the unknown polymer under examination and the standard polymer respectively. If each intrinsic viscosity term in equation 1.15 is replaced by its Mark-Houwink expression from equation 1.10 it follows that,

$$\log M_x - \log M_s = \log \frac{[\eta]_s}{[\eta]_x} \tag{1.16}$$

then it can be solved for the elution calibration curve for $M_x$,

$$\log M_x = \left(\frac{1}{1+\alpha_x}\right)\log\frac{K_s}{K_x} + \left(\frac{1+\alpha_s}{1+\alpha_x}\right)\log M_s \tag{1.17}$$

Providing Mark-Houwink parameters $K_s$, $K_x$, $\alpha_s$ and $\alpha_x$ are known in the particular solvent then the method will be satisfactory.

In this study, for example, the Mark-Houwink parameters for the standard polymer, polystyrene, and the unknown polymer, polyisobutylene, were known in THF so it was possible to utilise the calibration curve constructed for polystyrene and relate it to injections of polyisobutylene of unknown molecular weight.

## 1.5 The Behaviour of Polymers in Solution.

In solution, polymers can adopt a large number of possible conformations which will govern their behaviour in solution. The major influence on the conformation is the degree of interaction between the polymer and the solvent. In a thermodynamically 'good' solvent, contacts between polymer segments and solvent molecules are energetically favourable so that the coil expands to maximise these interactions. Conversely, if the contacts are unfavourable, the polymer chain will minimise the interactions by adopting a tightly coiled conformation in a thermodynamically 'poor' solvent. The intermediate stage where the polymer adopts an undisturbed conformation is termed a *theta* solvent.

The conformation in solution may be quantified in a number of ways. They include the root mean square end-to-end distance, R, or more commonly the radius of gyration, š, which is the root mean square distance of the polymer segments from the centre of gravity[5], C.

Figure 1.7 shows the parameters often used to describe a polymer chain in solution.

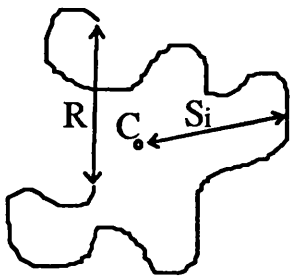


**FIGURE 1.7.** Representation of a Polymer Chain in Solution.

$S_i$ is the distance of a segment i from the centre of gravity, C. The radius of gyration, š, is the root mean square of all such distances and is most commonly measured by light scattering techniques.

Alternatively, thermodynamic qualities such as the Flory-Huggins interaction parameter, $\chi$, may be quoted. Derived by Flory[6,7] and Huggins[8,9] independently, the theory is based on a statistical mechanical treatment of a lattice model of polymer solutions. The free energy of mixing of a polymer solution, $\Delta G_m$, is predicted from equation 1.18,

$$\Delta G_m = RT(n_1 \ln \phi_1 + n_2 \ln \phi_2 + \chi n_1 \phi_2) \qquad 1.18$$

where R is the molar gas constant, T is the absolute temperature, $n_1$ and $n_2$ are the number of moles of solvent and polymer respectively, $\phi_1$and $\phi_2$ are the volume fractions of solvent and polymer respectively and $\chi$ is the Flory-Huggins interaction parameter.

A polymer in a theta solvent will have a $\chi$ value equal to 0.5, polymers in 'good' solvents will have lower interaction parameters and those in 'poor' solvents will have higher values. This is shown in figure 1.8.

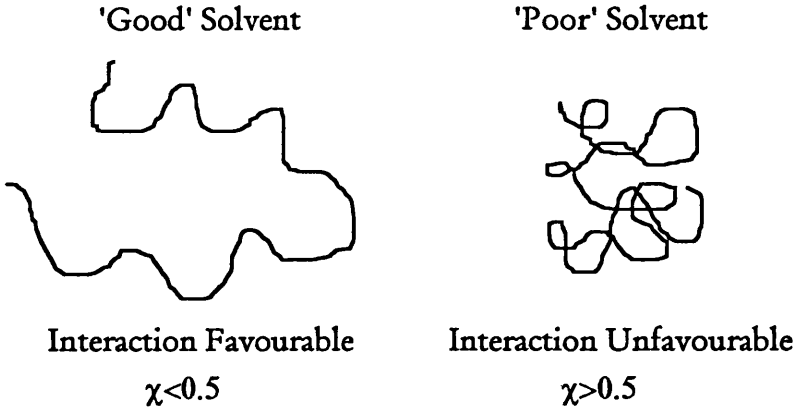


**FIGURE 1.8.** Polymer Conformations in Solution.

Commonly used techniques for the measurement of the Flory-Huggins interaction parameter include gas-liquid chromatography[10,11], light-scattering[12,13] and solution viscometry[14-16]. Viscometry was employed in this study in order to evaluate $\chi$ parameters owing to its availability and ease of use, its theory is discussed in the following section.

### 1.5.1 Solution Viscometry and the Determination of the Flory-Huggins Interaction Parameter.

Polymer molecular weights have been determined by solution viscometry since the 1930s[17] yielding a viscosity average value $M_v$, which falls between $M_w$ and $M_n$. No indication of the breadth of the distribution of molecular weights is obtained using this technique.

Solution viscometry was used in the study documented in this thesis in order to determine intrinsic viscosities, $[\eta]$, which were then employed in the calculation leading to the Flory-Huggins interaction parameter, $\chi$.

Determination of $[\eta]$ by solution viscometry is a time consuming process. This was alleviated by the use of a dilution viscometer and two 'single-point' methods to calculate $[\eta]$ were compared with the results from the normal extrapolation procedure. These values of $[\eta]$ were then used to determine $\chi$ in order to examine whether single-point viscometry could be a viable technique for the fast determination of $\chi$ without introducing large errors.

#### a.) Theory of Solution Viscometry.

Long chain polymers dissolved in solvents markedly increase the solution viscosity even at low concentrations. This is calculated by measuring the flow times of the polymer solution and pure solvent through a capillary tube. The two main types of viscometers are the Ostwald viscometer and the modified Ubbelohde or suspended-level viscometer. The Ubbelohde viscometer has the

advantage that its pressure head depends only upon the volume of liquid in an above the capillary and is independent of the total volume of liquid in the viscometer by having a third arm open to the atmosphere and it is possible to dilute the solution undergoing measurement *in situ.*

A *relative viscosity*, $\eta_r$, is defined such that,

$$\eta_r = \frac{t_s \rho_s}{t_o \rho_o} \qquad 1.19$$

where $t_s$ and $t_o$ are the flow times of the polymer solution and solvent respectively and $\rho_s$ and $\rho_o$ are their corresponding densities. Very dilute solutions are used and it is often assumed that $\rho_s \approx \rho_o$. Since $\eta_r$ becomes unity for an infinitely dilute solution the *specific viscosity*, $\eta_{sp}$, is defined such that $\eta_{sp} = \eta_r - 1$. The change in viscosity is concentration dependent and can be expressed using the equations,

$$[\eta] = \frac{\eta_{sp}}{c} - K_H[\eta]^2 c \qquad 1.20$$

$$[\eta] = \ln\frac{\eta_r}{c} + K_H[\eta]^2 c \qquad 1.21$$

equation 1.20 is the Huggins equation[18] where $K_H$ is the Huggins constant related to the size and shape of polymer molecules in solution[19,20] and equation 1.21 is the Kraemer equation[21]. Both equations are found to hold well at low concentrations and graphical extrapolation produces similar values of $[\eta]$, the *intrinsic viscosity*, for a particular solvent. Extrapolation to infinite dilution yields a value for $[\eta]$, the simple relationship in equation 1.22 can be used.

$$[\eta] = \lim_{c \to 0} \left( \frac{\eta_r - 1}{c} \right) \qquad 1.22$$

The intrinsic viscosity is related to the viscosity average molecular weight of the polymer via the Mark-Houwink equation[22] (equation 1.10). The Mark-Houwink constants, K and $\alpha$ are determined experimentally by measuring $[\eta]$ as a function of molecular weight for a series of monodisperse polymer standards and plotting log $[\eta]$ versus log M which yields a straight line graph of gradient $\alpha$ and intercept log K. The value of $\alpha$ varies between 0.5 and 1.0 depending on the geometry of the polymer in solution. Solution viscosity is affected less by low molecular weight polymers and a single-pair of Mark-Houwink constants is only valid over a narrow molecular weight distribution making this an unsuitable technique for following the ultrasonic degradation of polymers over a wide range of molecular weights.

b.) 'Single-Point' Determination of Intrinsic Viscosity.

The conventional graphical extrapolation of experimental results requires measurements of $\eta_r$ at a number of concentrations, this involves repetition of runs, greater volumes of solvent and is therefore a time consuming procedure. A number of workers[23-31] have proposed methods for the estimation of $[\eta]$ from the determination of relative viscosity at a single concentration. In this study, two single-point estimations were used and their applicability was tested by comparing the values of $[\eta]$ found with those obtained by the usual method of graphical extrapolation from a series of concentrations. Solomon and Ciuta[24], by combining the Huggins[18] and Kraemer[21] equations (equations 1.20 and 1.21) suggested that $[\eta]$ could be found from a single measurement of $\eta_r$ using the equation overleaf.

$$[\eta] = \frac{\sqrt{2}}{c}\sqrt{\eta_{sp} - \ln\eta_r} \qquad 1.23$$

This equation is valid for a wide range of polymer-solvent systems where an operating concentration of about 0.2% w/v is used.

Rudin and co-workers[23,31,32] proposed a mathematical treatment relating $\eta_r$ to $[\eta]$ with a wider applicability that would be of use in predicting values in more concentrated solutions. Their model assumes the existence of non-interpenetrating solvated spherical polymer entities. From consideration of Newtonian flow of large spheres in a solution, a relationship was derived between the relative viscosity and the volume fraction of solvated polymer molecules.

The volume fraction, $\phi$, of swollen polymer molecules in solution at a concentration, c (g $cm^{-3}$) is given by,

$$\phi = \frac{0.524c\varepsilon_o}{0.524\rho + c(\varepsilon_o - 1)} \qquad 1.24$$

where $\rho$ is the density (g $cm^{-3}$) of the polymer at the solution temperature and $\varepsilon_o$ is the infinite dilution swelling factor, given by,

$$\varepsilon_o = \frac{\rho[\eta]}{2.5} \qquad 1.25$$

Use of equation 1.24 is confined to concentrations such that $0 \leq c \leq 0.524\rho$, due to the model's assumption of a high concentration boundary condition corresponding to cubic packing of uniform spheres.

With $\phi$ from equation 1.24 it was shown[33] that Newtonian flow of suspensions of rigid spheres at low and moderate concentrations can be described by an empirical equation, a version of which provides agreement with results for polymer solutions,

$$\frac{\eta_o}{\eta} = \eta_r^{-1} = 1 - 2.5\phi + 11\phi^5 - 11.5\phi^7 \qquad 1.26$$

where $\eta_o$ and $\eta$ are the solvent and solution viscosities respectively.

The value of $\phi$ can be calculated from equation 1.26 using a Newton-Raphson iterative procedure where only one of the seven roots is real, positive and in the range $0 \leq \phi \leq 0.524$ as required by the model.

Thus from a single measurement of $\eta_r$, $\phi$ can be calculated and by combining equations 1.24 and 1.25 $[\eta]$ can be determined,

$$[\eta] = \frac{\phi(1.31\rho - 2.5c)}{c\rho(0.524 - \phi)} \qquad 1.27$$

c.) Calculation of the Interaction Parameter.

The thermodynamic quality of solvent is often described using the interaction parameter, $\chi$, it describes the conformation adopted by polymer chains in solution and hence influences the viscosity.

Kok and Rudin[14-16] developed a model showing that the second virial coefficient, $A_2$, could be calculated from,

$$A_2 = \frac{16\pi N_o[\eta]}{M(9.3x10^{24} + 4\pi N_o c([\eta] - [\eta]_\theta))}\left\{1 - \frac{[\eta]_\theta}{[\eta]}\right\} \qquad 1.28$$

where [η] is the intrinsic viscosity ($cm^3g^{-1}$) of the polymer in the given solvent, $[\eta]_\theta$ is the intrinsic viscosity under theta conditions, c is the concentration ($gcm^{-3}$), $N_0$ is Avogadro's constant and M is the average polymer molecular weight.

The value of $[\eta]_\theta$ can be calculated according to,

$$[\eta]_\theta = K_\theta M^{0.5} \qquad 1.29$$

The value of $K_\theta$, the unperturbed viscosity coefficient, for polyisobutylene[34] is $1.02 \times 10^{-1}$ $cm^3g^{-1}$, the value of $\chi$ can then be calculated from,

$$\chi = 0.5 - A_2\rho^2 V_1 \qquad 1.30$$

where $V_1$ is the molar volume of the solvent ($cm^3mol^{-1}$) and ρ is the density of the polymer ($gcm^{-3}$), for polyisobutylene[35] this is taken as 0.917 $gcm^{-3}$.

Values of $\chi$ can be obtained up to a concentration of $0.5c_x$, where,

$$c_x = \frac{9.3 \times 10^{24}}{4\pi N_0 [\eta]_\theta} \qquad 1.31$$

This model did not account for the variation of $\chi$ with solution concentration, it did however account for dependence on molecular weight.

Tseng and Lloyd[36] employed an alternative approach in calculating $\chi$ from [η]. By combining the Flory-Huggins lattice model of polymer solutions with the Flory-Fox treatment of solution viscosity[37,38], the interaction parameter was given by,

$$\chi = \frac{1}{2} - \frac{V_1}{2C'_m kM}\left\{\frac{[\eta]^{5/3}}{[\eta]_\theta^{2/3}} - [\eta]\right\} \qquad 1.32$$

where $V_1$ is the molar volume of the solvent and $C'_m k$ is a constant dependent only on the specific volume of the polymer at a given temperature and is equal to $3.53 \times 10^{-3}$ for polyisobutylene[39].

A similar equation was also derived by applying the modified Fox-Flory viscosity treatment proposed by Kurata *et al*[40] designed to take into account the non-Gaussian character of polymer chains in solution,

$$\chi = \frac{1}{2} - \frac{V_1}{2C'_m kM}\left\{\left(\frac{[\eta]^5}{[\eta]_\theta^{2.57}}\right)^{1/2.43} - \left(\frac{[\eta]^3}{[\eta]_\theta^{0.57}}\right)^{1/2.43}\right\} \qquad 1.33$$

Chee[41] has developed an extrapolation method for estimating the unperturbed parameter, $K_\theta$, and the second virial coefficient by correlation with the Mark-Houwink constants, this technique requires prior knowledge of the Mark-Houwink constants for the polymer in each of the solvents used or prediction of these parameters by further mathematical approaches.

## 1.6 General Principles of Ultrasound.

By definition, ultrasound is defined as sound waves possessing frequencies higher than the upper limit of human hearing, usually taken as 16 kHz. In gases the upper limit of ultrasonic frequency is taken as 5 MHz, in liquids it is 500 MHz.

1.6.1 Applications of Ultrasound.

Sonochemistry[42] is a term appearing with increasing regularity in the chemical literature in the context of its use to improve reaction rates and/or product yields. It is however not a new term but has received a resurgence of interest over the last decade.

Ultrasound is best known for its use in medicine for foetal imaging, in underwater range finding (SONAR) used to locate sunken ships or shoals of fish, in non-destructive testing of metals for flaws or in animal communication and bat navigation. However, ultrasound can be a form of energy for the excitation or promotion of a chemical reaction.

Due to its wide range of frequencies, shown in figure 1.9, ultrasound can be broadly divided into two regions.

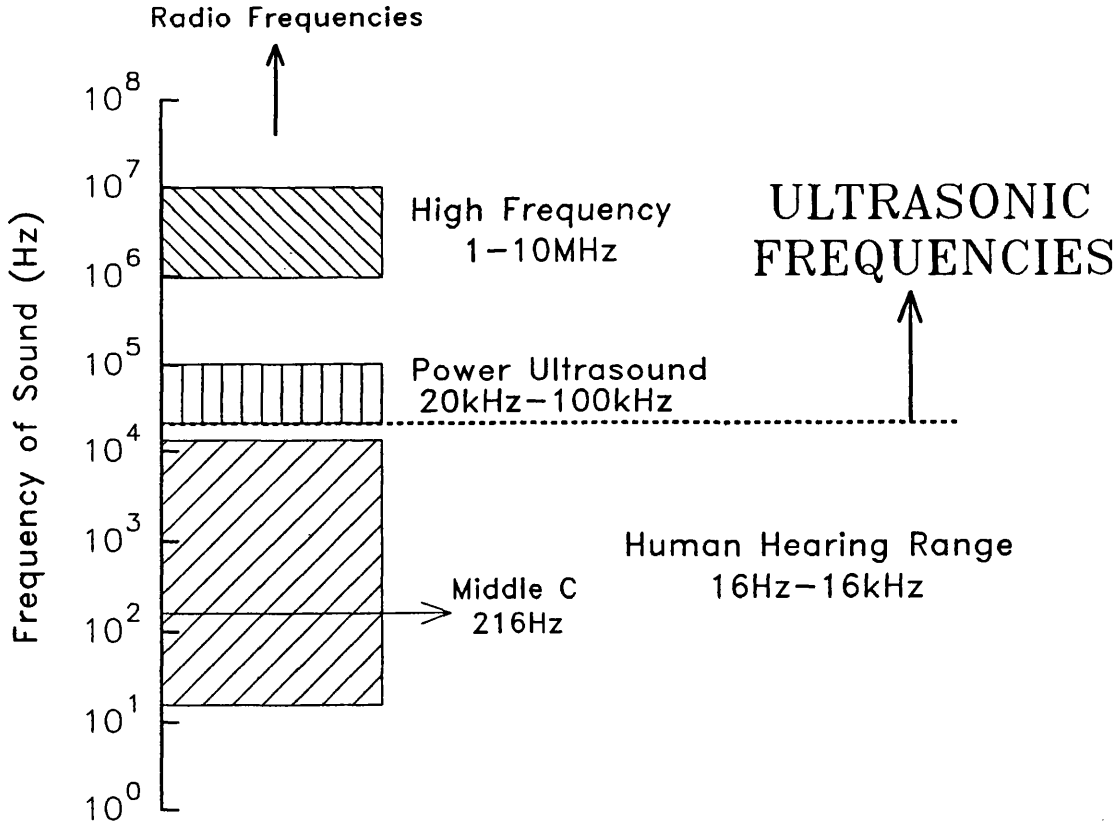


**FIGURE 1.9.** The Frequencies of Sound.

(i) High frequency, low power ultrasound - concerned with the effect of the medium on the wave. This is used in medical scanning (obstetrics) for observing the foetus, guiding subcutaneous surgical instruments, the non-destructive testing of various materials and in chemical analysis in the 1-10 MHz range.

(ii) High power, lower frequency ultrasound - often termed power ultrasound operating in the range 20-100 kHz. This is used for ultrasonic cleaning, plastic welding, emulsification and effecting chemical reactivity. The work documented in this thesis concentrates on power ultrasound at 23 kHz.

Power ultrasound offers many advantages when applied to chemical reactions:

a.) the reaction may be accelerated or less forcing conditions employed,

b.) induction periods are often significantly reduced along with possible reductions in the exotherms normally associated with such reactions,

c.) reactions are often promoted without additives like radical initiators,

d.) the number of steps in a synthetic route may be reduced,

e.) alternative pathways may be followed.

1.6.2 Propagation of Ultrasound in Liquids.

Sound waves can be transmitted through any substance, solid, liquid or gas which possesses elastic properties. Ultrasound is concerned with sinusoidal motion and in the case of liquids, with longitudinal waves only. At these frequencies, transverse waves are propagated in liquids but as their attenuation with distance is very high, they need not be considered. Longitudinal waves are those in which the vibration or displacement of the particle occurs in the direction of propagation of the wave. Thus the passage of sound through a liquid can be regarded as an alternating series of compressions and rarefactions of the medium. This is depicted in figure 1.10.

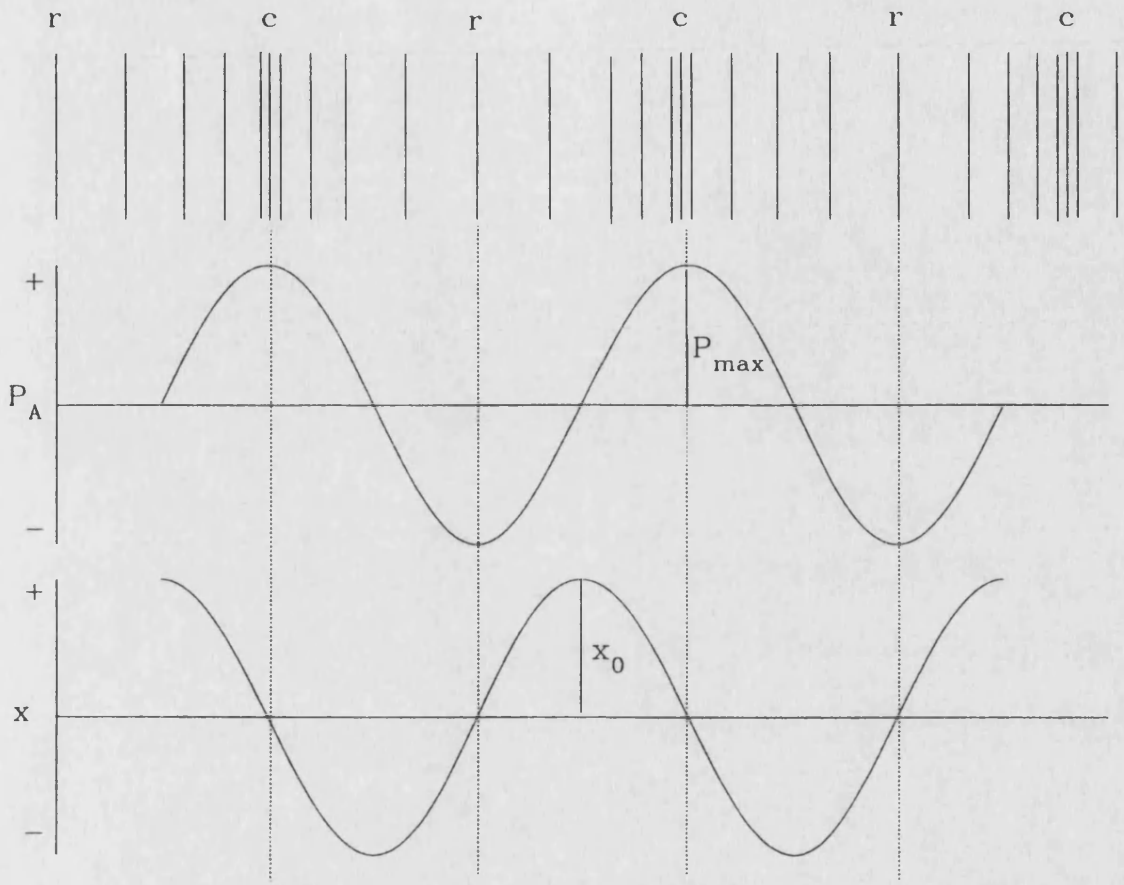


**FIGURE 1.10.** The Passage of Sound Through a Liquid.

At any time t, the displacement x of an individual molecule from its mean position is given by,

$$x = x_o \sin 2\pi ft$$

where $x_o$ is the maximum displacement of the molecule and f, the frequency of the sound. An expression for the particle velocity, V, is obtained by differentiation of equation 1.34,

$$\frac{dx}{dt} = V = V_o \cos 2\pi ft$$

where $V_o$ is the maximum particle velocity, $2\pi f x_o$.

The succession may also be expressed as an acoustic pressure, $P_A$, which varies with time, t.

$$P_A = P_{max} \sin 2\pi ft \qquad 1.36$$

where $P_{max}$ is the maximum acoustic pressure generated.

The intensity, I, of the wave is defined as the energy transmitted through unit area of liquid in unit time and is given by,

$$I = \frac{P_{max}^{\ 2}}{2\rho c} \qquad 1.37$$

where c is the velocity of sound in the medium of density $\rho$.

The sound intensity is attenuated during propagation due to energy transfer to the medium, usually manifested as a slight increase in temperature arising from vibrational interactions. Attenuation can be expressed as,

$$I_d = I_o \exp(-2\alpha d) \qquad 1.38$$

where $I_d$ is the intensity of the sound at a distance d from a source radiating with an intensity of $I_o$. The $\alpha$ term is the coefficient of absorption and is dependent on the viscosity, thermal conductivity, specific heat capacity of the liquid, the density and velocity of sound in that medium[43].

In particular, $\alpha$ is proportional to the square of the sound frequency so that higher intensities are required to produce equivalent effects at the same distance when using higher frequency ultrasound. The value $\alpha/f^2$ is a constant at a given temperature in one medium.

As for any sound wave, the wavelength, $\lambda$, of ultrasound at a particular frequency, f, is given by $c=\lambda f$, where c is the velocity of sound in the medium. Hence for a typical sonochemical reaction (20-50 kHz) the wavelengths produced, assuming the velocity of sound in a liquid to be 1500 $ms^{-1}$, are in the range of 7.5-3.0 cm. Obviously these wavelengths are not comparable to bond lengths hence it can be stated that sonochemical effects are not a result of direct interactions between reagent and wave as is the case in photochemistry. Hence the phenomenon of ultrasonic cavitation should be introduced.

## 1.7 The Phenomenon of Ultrasonic Cavitation.

The progression of a sound wave through a medium causes the molecules to oscillate about their mean position. During the compression cycle of the wave, the average distance between adjacent molecules decreases whilst this distance increases during the rarefaction cycle. If a sufficiently large negative pressure is applied to the liquid during the rarefaction period, such that the average distance between adjacent molecules exceeds the critical molecular distance necessary to hold the liquid intact, the liquid structure will break down forming voids or cavitation bubbles[44].

Cavitation has at least three distinct stages shown in figure 1.11.

a.) nucleation

b.) bubble growth

c.) implosive collapse.

Estimates for the pressures required to overcome the tensile strength in liquids exceed 100 bar, however in practice cavitation occurs at much lower acoustic pressures, this is undoubtedly attributed to flaws in the liquid structure or so-called *weak-spots*. Sources of weak-spots include the presence of dissolved gas molecules in the liquid and the presence of particulate matter. In rigorously degassed[45,46] systems and those which have undergone ultrafiltration[47] the cavitational threshold (the value

of applied acoustic pressure necessary before cavitation occurs) is increased dramatically.

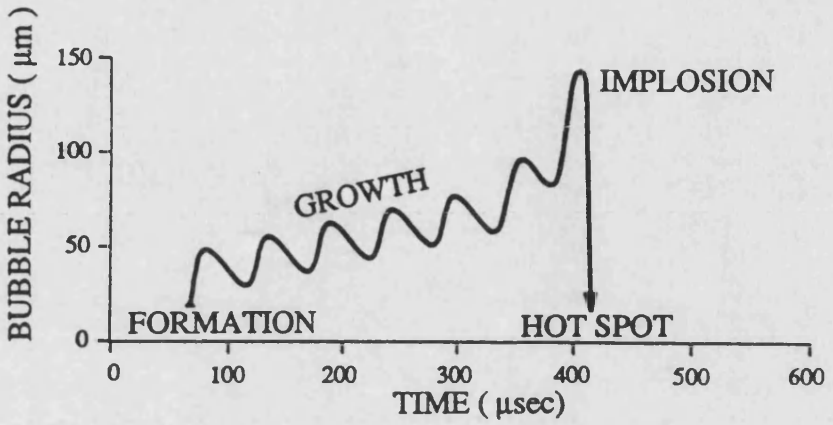


**FIGURE 1.11.** Cavitation Bubble Formation.

Trapped gas nuclei in the crevices of particulate matter can act as nucleation sites, as shown in figure 1.12.

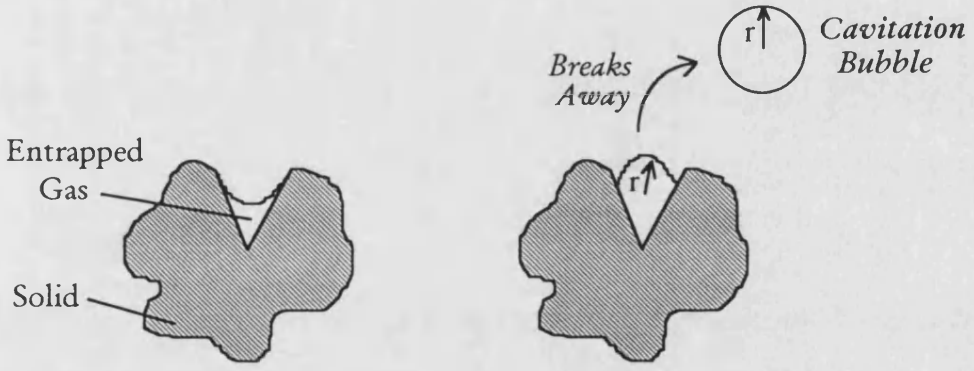


(i) Positive external pressure

(ii) Negative external pressure (Rarefaction)

**FIGURE 1.12.** Particulate Matter Acting as Nucleation Sites.

During rarefaction, as the pressure decreases, the liquid-gas interface becomes more convex until at sufficiently low pressure, the gas breaks away to produce a bubble of radius r.

Cavitation bubbles can exist as empty, vapour, or gas-filled cavities and these are believed to be responsible for the observed sonochemical effects.

Cavities, or microbubbles, formed in one rarefaction cycle will not necessarily collapse in the immediately succeeding compression cycle. The lifetime of the cavity will depend on factors including whether there has been sufficient time during rarefaction to allow the influx of solvent vapour or gas into the bubble. Depending on their size, some cavities will have a lifetime of a few acoustic cycles giving rise to *transient* cavitation but others will oscillate in the acoustic field for much longer and give rise to *stable* cavitation. Hence cavitation can be classified into its two main types[44,48].

**(i) Transient Cavitation** - these cavities exist for one, or at most two, acoustic cycles and involve the exponential rise of the bubble radius to at least twice its original size followed by a violent collapse on compression. On collapse, they can fragment into smaller bubbles which may act as nuclei for further cavitation events. The short lifetime of these cavities gives little opportunity for the diffusion of gas into the bubbles although solvent evaporation can occur. Hence, transient cavities are either voids or vapour-filled cavities.

Estimations based on theoretical considerations by Noltingk and Neppiras[49,50] and Flynn[51] indicate that during the adiabatic collapse of a cavitation bubble, very high localised temperatures (~4000K) and pressures (~1000 bar) occur. It is these conditions which form the basis of the explanation of chemical reactivity in particular radical production by bond cleavage due to power ultrasound. This is discussed in more detail in section 1.9. The rapid compression of gas and vapour during cavitational collapse leads to nearly

adiabatic heating of the contents of the bubble, simply because thermal transport is slower than the collapse itself. Thus a short-lived, localised hot-spot is formed. Homogeneous sonochemistry and sonoluminescence arise from hot molecules and radicals formed in the cavitational hot spot by bond cleavage or rearrangement. The thermal theory of sonochemistry and sonoluminescence proposes that the high temperatures found in the cavitation event are responsible for the observed effects and the experimental evidence of Suslick[52] predicts the effective localised temperatures to be in excess of 5000 K.

**(ii) Stable Cavitation** - these exist for many acoustic cycles oscillating about an equilibrium size. Stable cavities contain gas and vapour and as they grow there is a possibility that they will transform into transient cavities and collapse. The intensity of the disruptions[53,54] to liquid molecules caused locally by the resonating bubbles is undoubtedly responsible for many of the mechanical effects of ultrasound. The nature of the collapse will be strongly dependent on the contents of the bubbles prior to implosion. It is therefore important to examine how various experimental and irradiation conditions affect the cavitation.

1.7.1 Factors Affecting Ultrasonic Cavitation.

Considerable experimental evidence[55-58] suggests that cavitation plays an important role in both the polymerisation and degradation of polymers as well as many other chemical processes.

a.) Ultrasonic Frequency.

There is a minimum sound frequency required in order to produce ultrasonic cavitation and an optimum value where maximum effects are observed. An increase in the ultrasonic frequency above the optimum value results in a decrease in the amount of cavitation[59]. This is explained[60] by the fact that at high frequency, when the time between successive compression and rarefaction

cycles is very short, there is insufficient time to permit bubble growth to a size sufficient to cause any effect.

b.) Solvent.

Cavitation requires that the negative pressure during the rarefaction cycle of the wave must overcome the cohesive forces in the liquid. Hence high viscosity solutions, or those with a high surface tension, have the highest cavitational thresholds. However, the vapour pressure of the solvent is far more important[61] than the effects arising from surface tension[62] and viscosity[63]. In a volatile solvent, more vapour will enter the cavitation bubble thus shortening its lifetime, cushioning its collapse[51] and ultimately reducing the extent or rate of reaction.

c.) Temperature.

Raising the temperature increases the vapour pressure of the liquid and lowers the surface tension and therefore the cavitation bubbles formed will contain more vapour. Hence collapse of the bubble will be cushioned.

d.) Ultrasonic Intensity.

Generally an increase in the intensity of the ultrasound will give rise to enhanced sonochemical effects, this is due to the production of more bubbles, or cavitation events[64]. The intensity of the bubble collapse is independent of this factor.

From equation 1.37 it can be seen that the intensity I is proportional to $P_{max}^2$. The temperatures and pressures produced on collapse will increase with intensity, as can be seen from equations 1.39 and 1.40.

$$T_{max} = T_o\left[\frac{P_{max}(\gamma - 1)}{P}\right] \qquad 1.39$$

$$P_{max} = P\left[\frac{P_m(\gamma-1)}{P}\right]^{\frac{\gamma}{(\gamma-1)}} \qquad 1.40$$

where $T_{max}$ and $P_{max}$ are the temperatures and pressures generated within the bubble at the moment of collapse, $T_o$ is the ambient temperature, P is the pressure in the bubble at its maximum size, $P_m$ is the pressure in the liquid at the moment of collapse and $\gamma$ is the polytropic index, or the ratio of the specific heats of the gas or vapour. It should be appreciated that intensity cannot be increased indefinitely[49,50] as the bubble may grow so large on rarefaction that the time remaining for collapse may prove insufficient.

e.) Applied External Pressure.

An increase in the externally applied pressure increases both the cavitational threshold and the intensity of bubble collapse. Under pressure, the bubbles produced will be smaller and those below a certain critical size will be unable to grow[49] due to surface tension forces, hence the number of cavitation events will decrease unless a sufficiently large increase in intensity is made.

f.) Effect of Dissolved Gases.

Equations 1.39 and 1.40 for the temperature and pressure within the bubble prior to collapse, show that by employing gases with large $\gamma$ values, the polytropic ratio, will lead to enhanced sonochemical effects from gas-filled bubbles. Monatomic gases like helium have higher $\gamma$ values than diatomics such as nitrogen for example. Gases with a high solubility will reduce both the cavitational threshold, as a consequence of an increased number of gas nuclei (or weak-spots) to act as nucleation sites, and the intensity of the bubble collapse, as a result of the cushioning effect in the microbubble. The latter is shown by replacing P by $(P_v + P_g)$ where $P_g$ is the vapour pressure inside the bubble. Increasing gas content increases the value of $P_g$ resulting in a lowering of both $T_{max}$ and $P_{max}$ explaining the reduced sonochemical effects. Another

factor is that the more soluble the gas, the more likely it is to re-dissolve in the medium during the compression cycle.

## 1.8 Generation of Ultrasound.

The piezoelectric effect was discovered in 1880 by the Curies[65,66] and it is this which forms the basis for the present day generation of ultrasound. The earliest ultrasound transducer was a whistle developed by Galton[67] in 1883 who was interested in measuring the threshold of hearing for both animals and humans. In 1917, Langevin's echo-sounding technique for the estimation of depths of water was the first commercial application of ultrasound, this lead to the development of SONAR.

The cavitation phenomenon was first reported in 1895 by naval investigators[68] following the discovery that the rapid motion of a ship's propeller produced cavitation thus damaging it. Further understanding of cavitation together with advances in transducer design and technology led to increased availability of ultrasonic equipment after 1945.

### 1.8.1 The Piezoelectric Effect.

The piezoelectric effect is the most commonly employed method for the generation of ultrasound using such crystals as quartz[69] and more recently ceramics like barium titanate ($BaTiO_3$), lead metaniobate ($PbNb_2O_6$) and the mixed crystal of lead zirconate titanate[70].

Piezoelectricity is the electric charge developed in anisotropic crystals when subjected to stress, e.g. the application of pressure across the crystal faces results in the generation of charge on each face equal in size but of opposite sign. The inverse of this effect is used in the generation of ultrasound when equal, but opposite, charges are applied to the faces of the crystal then the whole crystal will either expand or contract. In the case of ultrasound, an alternating current produces a mechanical vibration.

By varying the type and size of piezoelectric material used, ultrasonic generators of different frequencies can be constructed.

1.8.2 Ultrasonic Apparatus.

Ultrasound can be introduced into a reaction vessel using a variety of techniques, the most common laboratory and industrial-scale equipment is described:

(i) Ultrasonic Cleaning Bath. (Figure 1.13)

This is the most commonly used due to its availability, simplicity and large working volume. It consists of a stainless-steel tank with transducers fixed to its base. The power generated is attenuated by the water in the bath but there are limitations·

a.) The efficiency and overall power generated by the bath are governed by its size and the position of the reaction vessel within it.

b.) Inconsistent results can be obtained due to inevitable heating of the water in the bath unless a thermostat is fitted.

c.) Fully representative, reproducible results are not obtained since not all baths operate at the same frequency or power, hence direct comparisons between different baths cannot easily be made.

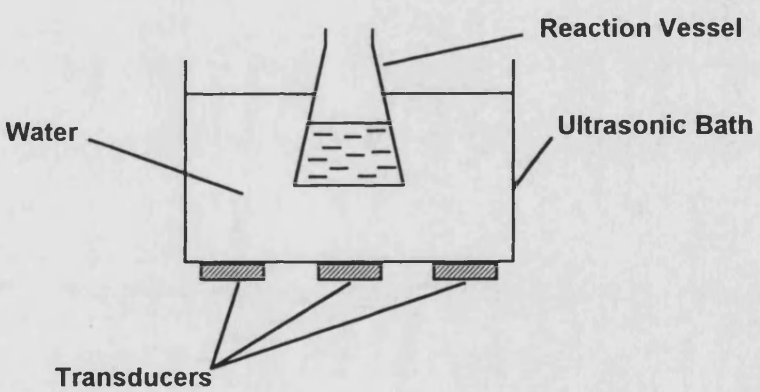


**FIGURE 1.13.** Ultrasonic Cleaning Bath.

(ii) Direct Immersion Sonic Horn. (Figure 1.14)

Ultrasonic energy is transmitted directly into the heart of the reaction therefore making it capable of producing higher powers and being a far more efficient

technique than the bath. Its main advantage being that it can be tuned to deliver optimum cavitation. However, during prolonged use, erosion of the probe tip can cause contamination of the reaction with metallic particles making it necessary to monitor and maintain its condition. The piezoelectric crystal is coupled to a titanium alloy horn, the length of which should be an exact number of half wavelengths producing an anti-node at the probe tip which is responsible for producing the mechanical vibration. This type of ultrasonic apparatus was used throughout the experiments described in this thesis and temperature rises were overcome by incorporation of an outer jacket into the reactor design through which thermostatted liquid was circulated. This design is discussed in section 2.2.1.

Other apparatus for small-scale reactions include the cup horn and the whistle reactor but more interest is being focused on the possibilities of *scale-up* of reactions involving ultrasound.

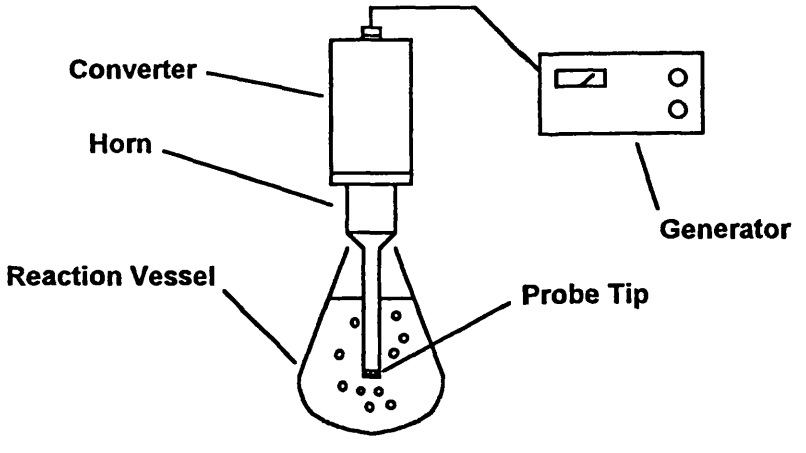


**FIGURE 1.14.** Direct Immersion Horn System.

(iii) Scale-Up Equipment.

The possible application of ultrasound to industrial processes relies on the availability of suitable equipment. Cost effectiveness, safety and overall efficiency are factors which must be considered before multi-litre scale ultrasonic reactions become common-place.

Batch reactors offer one possibility, the simplest of which being a larger version of the laboratory cleaning bath. Taking into account the number of transducers required to be fitted to the outside of the reactor and the high running costs this is an expensive option. An alternative is a sonochemical reactor incorporating immersible transducers. This would enable far higher ultrasonic intensities to be generated within the reactor and could be a simple adaptation to an existing chemical reactor. Problems associated with the immersible transducers include non-uniformity of the ultrasonic field generated (the addition of mechanical stirrers may prove difficult) and a difficulty in sealing the transducers to prevent problems arising from the corrosive nature of many of the chemicals employed.

Continuous reactors offer an alternative with many inherent advantages. One such system involves the incorporation of wall-mounted transducers to a pipeline. This provides the opportunity to ultrasonically irradiate reagents as they flow through the 'sonicating section' which can be easily fitted to existing pipelines. Figure 1.15 shows wall-mounted transducers on a pipe.

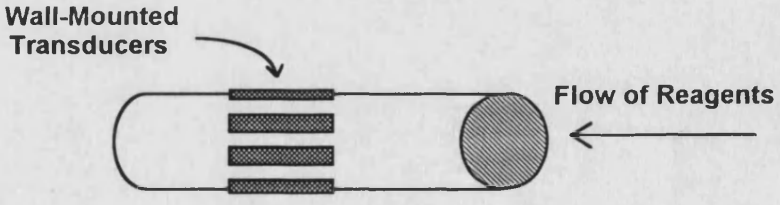


**FIGURE 1.15.** Ultrasonic Treatment of Reagents in a Pipeline.

A single ultrasonic probe or an array of probes can be fitted into a continuous flow situation. Ultrasound can be applied to a process by incorporating an 'insonation chamber' which can enable pre-treatment of reagents prior to the main process or as an integral part of the reaction loop. Figure 1.16 shows the inclusion of two probes into a flow situation.

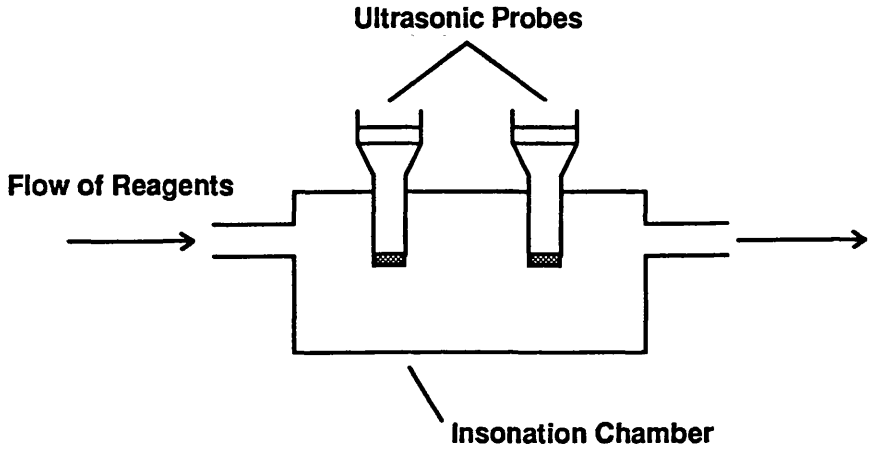


**FIGURE 1.16.** Insonation Chamber Incorporated into a Continuous Reactor.

Improved control over the ultrasonic conditions is achieved industrially using small volumes of reactants, typically 1 - 5 litres, making the inclusion of an insonation chamber or flow-reactor preferable rather than a batch reactor which typically operates on volumes in excess of 100 litres.

## 1.9 Degradation of Polymers under Ultrasonic Irradiation.

Most macromolecular compounds undergo significant modification when exposed to high intensity ultrasound, polymers are no exception. The earliest work dates from the 1930s following studies on several natural polymers. Flosdorf and Chambers[71] found that ultrasound caused the instant coagulation of egg albumen, the reduction of agar and starch and promoted the rapid hydrolysis of sucrose to glucose. Similar effects were noted by Szalay[72] on gelatin and Gyorgyi[73] on starch, gum arabic

and gelatin. The latter attributed the effects to the possible breakdown of the polymer structure.

Freundlich[74-76] however noted a non-permanent reduction in viscosity for solutions of gelatin and methyl cellulose in water and rubber in benzene. It was concluded that the reduction was a thixotropic effect and not due to molecular degradation and Freundlich attributed the effect to rapid dehydration of the gel with relatively slow rehydration to form the gel. This was compounded by work reported by Heyman[77] who showed that viscosity could be reduced by vigorous shaking.

The evidence for bond breakage was firmly established by Brohult[78] who used an ultracentrifugation technique to study the effect of sonication on haemocyanin and found that the molecule fragmented into monodisperse fragments. Schmid and Rommel[79,80] were the first to observe an irreversible and permanent reduction in the viscosity of solutions of polystyrene, poly(acrylates) and nitrocellulose when exposed to ultrasonic irradiation. They noted that the viscosity decrease was initially quite rapid but slowed with time and reached a limiting value below which no further reduction occurred.

These workers excluded oxidative fission as being responsible for the degradation by working in an atmosphere of nitrogen and obtaining the same rate of breakdown as that found under air. The possibility of cavitation being responsible for the degradation was investigated by sonicating solutions under sufficient pressure so as to prevent cavitation events. They noted that an increase in pressure caused a decreased degradation achieved by increasing the gaseous pressure over the solutions. Effectively this varied two factors simultaneously, the external applied pressure and, due to increased solubility, more gas would be present. As described earlier, the increased pressure would be expected to suppress cavitation whereas the increased gaseous concentration counter-acted this effect by providing more nucleation sites for cavitation

This effect was clarified by Brett and Jellinek[81,82] who performed the degradation of polystyrene in benzene by firstly exerting gaseous pressure and

observing a relatively small decrease in degradation rate to a constant value, and secondly exerting pressure via mercury column observing a rapid decrease in rate to zero. These two effects, the existence of a limiting molecular weight, $M_{lim}$, below which no further degradation occurs and the more rapid degradation at high molecular weights have since been noted by a number of workers and may now be regarded as characteristic of ultrasonic degradation[83] in common with other mechanical processes.

1.9.1 The Products of Polymer Chain Scission.

Cleavage of a covalent bond can occur in two ways[84,85], *homolytically*, resulting in one electron from the bond going to each fragment to produce radical species, or *heterolytically*, with both electrons going to one fragment leading to the formation of an ion pair. Both of these have been observed in polymer degradation.

(i) **Homolytic Cleavage**, two free macroradicals are formed.

$$P_{n+m} \rightarrow P_n^{\cdot} + P_m^{\cdot}$$

For example, in the case of polyisobutylene,

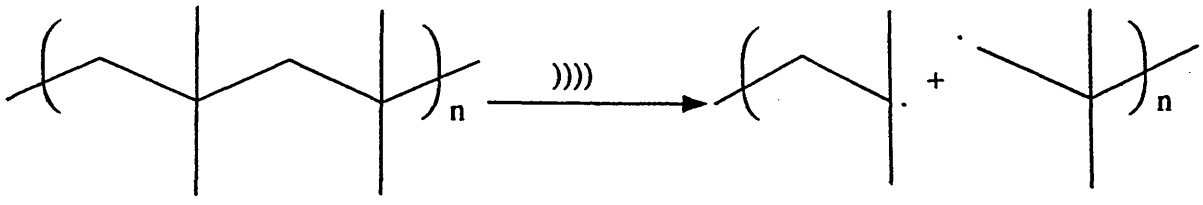


This is the most common chain cleavage observed during ultrasonic degradation the first evidence for which was obtained by Melville and Murray[86] who performed sonications in the presence of unsaturated, polymerisable monomers and by Henglein[85] who used 2,2-diphenyl-1-picrylhydrazyl, DPPH, as a radical scavenger.

More recently, direct evidence of radical production has been confirmed during sonications of polystyrene, poly(methyl methacrylate), polypropylene and poly(vinyl acetate) solutions in benzene with the spin-trap pentamethyl nitrosobenzene by Tabata[87,88] using the very sensitive technique of electron paramagnetic resonance spectroscopy, EPR or ESR, which detects the spin properties of the unpaired radical electron.

Tabata and Sohma[89] showed that by sonicating benzene alone did not produce detectable radicals and compared the results with those obtained using high energy γ-radiation where radicals were produced from both the polymer and the solvent.

ESR has been used in the work described in this thesis to confirm the presence, and attempt the identification, of radicals produced in a variety of systems. The theory is detailed in section 1.11.2.

(ii) **Heterolytic Cleavage**, two macromolecular ions are formed.

$$P_{n+m} \rightarrow P_n^+ + P_m^-$$

The production of ions by heterolytic cleavage under ultrasonic irradiation is illustrated by poly(dimethyl siloxane), PDMS, in the presence of methanol[90]. Methanol, being a strong nucleophile, reacts rapidly with carbonium and siliconium ions thus indicating the heterolytic cleavage of the Si-O bond.

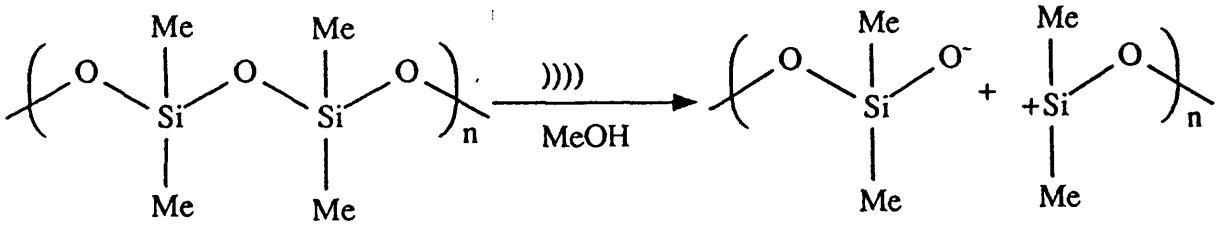

This has been confirmed by ESR results documented in section 3.8.

Alternatively, in the absence of methanol or similar nucleophile, a disproportionation reaction may occur,

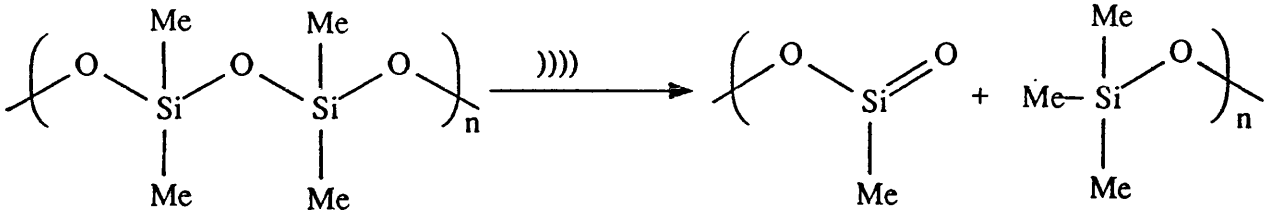

Thomas and DeVries[90], in the sonication of PDMS, detected no radicals using DPPH. When the sonication was carried out in the presence of $^{14}C$ enriched methanol they observed the radioactive label was incorporated into the polymer chain. More importantly, similar experiments with polyisobutylene and polystyrene, both in the presence and absence of DPPH, showed zero incorporation of the radio-labelled molecule, confirming their homolytic cleavage. This was repeated for PDMS which was refluxed in benzene and no radioactivity was incorporated in the recovered polymer.

1.9.2 Effect of Sonication on Molecular Weight Distribution of Polymers.

Prior to the advent of GPC by Moore[91] in 1964, few studies were reported on the effect of sonication on the polydispersity of the polymer[57,92]. This was due to the lack of techniques available for its accurate determination, those employed were tedious fractionation processes. The first study of this type was by Jellinek and White[57] who calculated the distribution of ultrasonically degraded polystyrene by fractional precipitation from methyl ethyl ketone using methanol, determining the molecular weight of each fraction viscometrically.

Similar conclusions were reported in work by Mostafa[93] and Schmid *et al*[94] on a wide distribution polystyrene sample, the latter showing that the polydispersity changed throughout the sonication with initially narrow distribution samples broadening before narrowing as the limiting molecular weight was approached.

Initial work focused on polystyrene degradation and whilst examining its distribution by turbimetric titration, Gooberman and Lamb[95,96] reported secondary peaks at lower molecular weights, suggesting a non-random degradation process.

Once established, GPC was applied to a variety of systems notably poly(isobutylene) degradation studied by Porter and co-workers[97]. Secondary peaks were not observed in these degradations and the polydispersity did not change significantly but was seen to decrease from its initial value of 2.03 at long sonication times.

Shaw and Rodriguez[98] used GPC to study degraded poly(dimethyl siloxanes) with initial molecular weights of 1300000 and 240000 and found that the samples with different initial polydispersities approached the same polydispersity after long sonication times. Similar findings were reported by Malhotra[99] who showed that the polydispersities of a series of poly(alkyl methacrylates) approached a value of 1.5 as the limiting chain length was reached.

Molecular weights and distributions of sonicated poly(methyl methacrylate) solutions in tetrahydrofuran were studied by Wu *et al*[100]. It was found that narrow polydispersity fractions broadened their initial distributions before narrowing at long sonication times. This was in agreement with earlier work by Schmid[94]. Wider distribution samples only narrowed in polydispersity.

Polyisobutylene, PIB, can be considered as one of the simplest polymers studied to date since its structure is that of a branched hydrocarbon chain having one extra substituted carbon atom in its monomeric unit. When comparing the degradation behaviour of this polymer with that of polypropylene, which has a similar structure but which cross-links, the importance of the change from a tri-substituted to a tetra-substituted carbon atom becomes clearly apparent.

Much of the early work involved mechanical degradation of PIB solutions. Porter and Johnson[101] studied PIBs with molecular weights of 40000 to $>10^6$ at several temperatures and concentrations in n-hexadecane reporting permanent viscosity losses due to polymer degradation.

Mechanical degradation of high molecular weight PIB in dilute solution was performed by Yu *et al*[102] and reported that shear degradation is controlled by the shear stress not by the shear rate and is independent, at a given stress, of initial molecular weight and viscosity of the solvent. Molecular weights were determined by GPC and showed that the degradation of broad molecular weight distribution PIB narrowed its distribution mainly through the break down of large molecules.

Fujiwara and Goto[103] studied the mechanics of PIB solution degradation by violent stirring using an homogeniser. The degradation was found to depend on the circumferential velocity of the motor and occurred preferentially in polymers with a high degree of polymerisation. The molecular weight distribution was found to narrow and the number of bonds broken increased with stirring time.

Importantly, Nakano and Minoura[104] studied PIB chain scission in a variety of solvents stirred at 30000 rpm. Lower scission rate constants were observed for the polymer in a solvent where the polymer existed in a relatively more extended form, while the polymer in a solvent where it existed in an entangled form, showed a higher scission rate constant.

Much less attention has been focused on the ultrasonic degradation of PIB in solution.

The phenomenon of chain scission occurring preferentially near the centre of the chain appears to be characteristic of the ultrasonic degradation process and differentiates it from thermal, chemical or photochemical degradation. Computer models by Van der Hoff[105-108] simulating the distributions of degraded polymers found that centre cleavage best fitted their experimental results.

### 1.9.3 Parameters Influencing Ultrasonic Degradation.

The fundamental vibration frequency associated with chemical bonds lies in the range of $10^{12}$-$10^{14}$ Hz[109] which is far in excess of the frequency of the applied ultrasound at ~20 kHz, hence it can be concluded that there is no direct effect of ultrasound on the polymers. However, all of the parameters governing the

phenomenon of ultrasonic cavitation can, along with physical parameters, be associated with those influencing the degradation and will therefore be examined.

The rate of degradation was found to be dependent on the ultrasonic frequency applied by Mostafa[110] in 1958. Mostafa reported an optimum frequency at which cavitation intensity attains a maximum value and at this frequency maximum degradation occurs, this was 1 MHz for polystyrene in benzene. As explained in section 1.6 an increase in frequency requires an increased intensity to obtain equivalent effects and the results may have been due to a decrease in intensity rather than a frequency effect.

Reports in theoretical work[81] showed that the degradation rate should be independent of frequency up to 500 kHz, which was proved experimentally[111] for solutions of poly(methyl methacrylate) in benzene irradiated at 10, 175 and 300 kHz at an intensity of 1 $Wcm^{-2}$.

Frequency effects are probably the least reported in the literature owing to the relative lack of available equipment when compared to intensity effects. The vast majority of commercial, laboratory ultrasound equipment has variable intensity controls.

The first intensity study was reported by Mostafa[112] for polystyrene in benzene. The degradation was clearly faster at higher intensities as predicted. Jellinek[81] showed that the rate constant obtained was a linear function of intensity. More recently, the effect of ultrasonic intensity has been reported for a variety of systems including poly(methyl methacrylate)[113], poly(dimethyl siloxane)[114], hydroxyethyl cellulose and poly(ethylene oxide) in aqueous solutions[115] and poly(acrylamide)[116].

Most workers conclude that the limiting molecular weight, $M_{lim}$, decreases with increasing ultrasound intensity. Okuyama[64] and Thomas and Alexander[117] predicted that $M_{lim}$ should, in fact, be independent of intensity. Schoon and Rieber[118], working with poly(dimethyl siloxane), poly(chloroprene) and natural rubber arrived at similar conclusions. These results compete with the theory which predicts that the severity of bubble collapse is affected directly by the ultrasound intensity.

Degradation is known to proceed faster at higher molecular weights with several workers including Jellinek[81] and Basedow and Ebert[119,120] suggesting that the rate constant varies linearly with molecular weight. Mostafa[121], however, showed that at long sonication times, the limiting molecular weight was independent of the molecular weight of the starting material.

Correlations between the limiting molecular weight and the chemical nature of the polymer have been attempted. Most notably, Schoon and Rieber[118,122] studied the degradation of a variety of polymers including polystyrene, polyisobutylene, styrene-butadiene copolymers, poly(dimethyl siloxane) and natural rubber and found that under the same conditions, similar values of $M_{lim}$ were reached, suggesting that the chemical nature of the polymer was unimportant. Malhotra[99] degraded a series of poly(alkyl methacrylates) with alkyl side chains ranging between methyl and octadecyl. Chain structure and monomer molecular weight were put forward as being the important factors governing the kinetics of the degradation rather than the bulk size of the alkyl substituents. This was supported by Thomas[123] who found that polystyrene, poly(methyl methacrylate) and polybutene degraded at similar rates but that poly(lauryl methacrylate) degraded 3.5 times faster.

Many workers have ascribed the effects observed during the ultrasonic degradation of polymers in solution to mechanochemical processes or shock waves, this will be discussed further in section 1.9.4. In this case, it would be reasonable to expect that the nature of the solvent will play an important role as this will largely govern the size and shape adopted by the polymer chains in solution.

Schmid and Beuttenmuller[124] showed that poorly solvated polymer molecules were difficult to degrade by adding a non-solvent (acetone) to solutions of polystyrene in benzene. They also found that there was no change in molecular weight when a polymer was irradiated with ultrasound as a suspension in a non-solvent.

There is now evidence that the degradation is largely dependent on the nature of the solvent employed. However, a small number of workers have reported rate constants for degradation as being similar for a range of solvents. Nelkenbaum[125],

working with polyisobutylene, reported the same degradation kinetics in solvents including benzene, toluene, chlorobenzene, nitrobenzene and isopropylbenzene. Thomas and Alexander[117] found similar rate constants for the degradation of cellulose nitrate in ethyl acetate (a solvent) mixtures with ethanol (a non-solvent).

The kinetic results documented in this thesis show a dependence on the nature of the solvent and a correlation between the degradation and the thermodynamic 'quality' (in terms of the configuration adopted by the polymer in solution) of the solvent has been attempted. The Flory-Huggins interaction parameter has been employed for this purpose[82,126,127] and its theory has been introduced in section 1.5.

The effects of a number of factors concerning the solvent on the degradation have been studied mainly in an attempt to elucidate evidence concerning the mechanism of ultrasonic depolymerisation. Schmid and Beuttenmuller[128] investigated the effect of bulk reaction temperature on the ultrasonic degradation process for solutions of polystyrene in toluene and nitrocellulose in n-butyl acetate over the range 40-120°C. Their results showed that the process was slower and yielded higher limiting molecular weights at higher reaction temperatures. This important result confirmed that direct thermal effects were not responsible for the depolymerisation since in that case, the opposite results would be expected.

This effect was explained by considering the process of cavitation. At higher temperatures, the solvent will have a higher vapour pressure, more vapour will enter the cavitation bubble so that its collapse will be cushioned, reducing the forces in the liquid and hence the degree of degradation.

Malhotra *et al* also reported increased rates for polystyrene in tetrahydrofuran[129] and for a series of poly(alkyl methacrylates) in toluene and tetrahydrofuran[99] at -20°C.

In addition to the cushioning effect, Malhotra suggested that at lower temperatures, the increase in the viscosity of the solution led to better transference of energy from the transducer to the solution and also reduced the polymer chain mobility leading to increased effects.

The volatility of the solvent will govern the amount of vapour entering the cavitation bubble, hence the lower the enthalpy of vaporisation, $\Delta H_{vap}$, the higher the solvent volatility, the more vapour will enter the bubble thus lowering the rate of degradation.

Basedow and Ebert[119,120] reported a linear relationship between the rate constant of degradation and the heat of vaporisation of the solvent for dextran in a range of solvents.

Apart from solvent vapour, dissolved gases can enter the cavitation bubbles and influence the cushioning effects. A gas with a high solubility in the solvent should lessen the effects of the bubble collapse and so lower the degradation rate. Melville and Murray[86] found that the degradation rates for polystyrene and poly(methyl methacrylate were virtually identical in air and nitrogen saturated solutions in toluene but were reduced slightly in oxygen saturated solutions, an effect that they attributed to the high reactivity of oxygen with radical species.

Relatively few literature reports study the effects of various gaseous atmospheres on the ultrasonic degradation process. In the work documented in this thesis a wide variety of gases were employed and the results are documented subsequently.

The effect of polymer solution concentration on the degradation has been studied by a few workers. Previous work by Schmid and Rommel[130], Thomas and Alexander[131], Gooberman and Lamb[95,96] and Jellinek and White[58] all showed that the degradation rate decreased with increasing concentration. The results of Gooberman and Lamb[95,96] and Jellinek and White[58] studying solutions in benzene, were attributed to a reduction in cavitation efficiency as chains begin to overlap at high concentrations.

Recent work by Smith[127] characterised many of the parameters influencing the ultrasonic solution degradation of polystyrene leading to conclusions regarding the control of the size and reactivity of the macromolecular radicals produced.

1.9.4 Mechanism of Ultrasonic Degradation.

The various mechanisms proposed for the degradation of polymers must be introduced and discussed if the results from the degradation studies to follow are to be fully explained.

The primary requirement of any proposed mechanism is that it must allow for sufficient energy to break the C-C covalent bond of the polymer backbone. This force is[132] approximately $5.64 \times 10^{-9}$ N.

Early mechanisms proposed by Schmid and Rommel[79,80] assumed that the frictional forces arising between solvent molecules and polymer chains were sufficient to rupture C-C bonds. Indeed, calculations found frictional forces exerted by an oscillating solvent on a polymer fixed at one end were of the same order as the force required to break the C-C bond. Schmid also proposed a formula for the case of the chains not being rigidly fixed and this led to a much smaller, insufficient frictional force. To account for this Schmid suggested that in practice the polymer chains were neither rigidly fixed nor freely mobile but were sufficiently entangled so that the frictional forces were increased. This led to the incorrect assumption that degradation would only occur under conditions where the polymer chains were prevented from moving by entanglement.

Jellinek and White[133] suggested that bond breakage occurred as a result of impact forces when solvent molecules collided with the chains. These forces were calculated assuming that the time of impact was so short that the chain appeared rigid and were found to be considerably less than the force required to break the C-C bond.

Evidence now suggests that degradation occurs as a direct result of the cavitation process and subsequent theories about the mechanism of ultrasonic degradation have concentrated on this process. The precise effect caused by cavitation has been, and remains, the subject of considerable discussion. The possibilities addressed include; (i) thermal effects arising from collapsing bubbles[53], (ii) shock waves produced from bubble implosion during transient cavitation[123] and (iii) shear forces arising from pulsating resonant bubbles during stable cavitation[134,135].

Thermal effects have now been discounted as this is known to lead to a random degradation rather than the non-random chain scission observed under ultrasonic irradiation.

a.) Shock-wave Degradation.

The collapse of cavitation bubbles is believed to generate large hydrodynamic pressures and velocity gradients in the surrounding liquid. The bubble collapse produces intense flow fields of solvent molecules carrying some parts of the polymer chain towards the site of the implosion leading to stresses within the molecule capable of cleaving a C-C bond.

Thomas[123] proposed a model whereby the side of the polymer chain nearest the implosion will move faster than the other, setting up stresses along the backbone that first stretch the chain out into a rod-like conformation and then bond cleavage occurs. The model assumed that the polymer resembles a string of spherical beads and that the concentration of polymer in solution was so low that the molecules did not overlap or entangle. The mathematical treatment predicted centre cleavage of the chain and a linear dependence of the degradation rate on the molecular weight.

Okuyama and Hirose[136] extended Thomas' treatment and proposed that stress forces only acted on regions of the chains which would be extended and stretched prior to centre cleavage, this is depicted in figure 1.17.

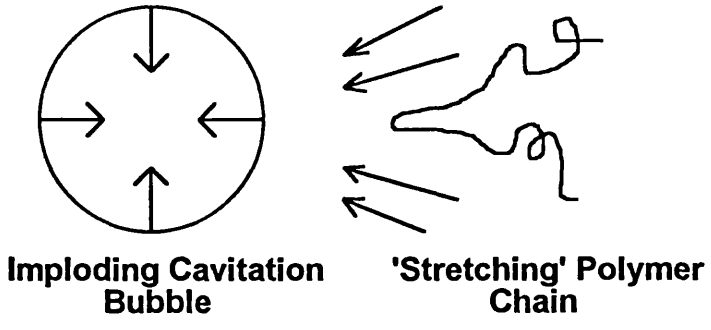


**FIGURE 1.17.** Polymer Molecule being 'Stretched'.

Their model predicted a limiting degree of polymerisation at infinite sonication time and calculations were performed for two types of cavitation bubbles, stable gas-filled cavities and transient cavities. The results showed that the limiting degree of polymerisation for a stable cavity was far in excess of the experimental prediction unlike the results for a transient cavity. It was concluded that ultrasonic degradation of polymers occurred primarily as a results of transient cavity collapse.

Cavitation produces another hydrodynamic effect, first used by Gooberman[137] in the explanation of degradation, the generation of a shock-wave as a result of the collapse of a transient cavity. The stress forces exerted on the polymer chain are due to the shock-wave radiating outwards from the site of an imploded cavity, this wave was described as a rapid pressure rise followed by an exponential pressure drop. During the pressure rise, solvent molecules are compressed and the number of solvent molecules within the volume enclosed by a macromolecule increases. During the subsequent pressure drop, the solvent molecules flow rapidly out of the macromolecule and set up stresses which are of the correct order to cause bond cleavage.

Schoon and Rieber[138] extended the shock-wave mechanism after studying polymer microstructure by electron microscopy. They concluded that the polymer resembled a 'string of pearls' and that the molecular weight of these spherical structures corresponded to the limiting molecular weight following sonication.

b.) Shear Degradation.

Depolymerisation is known to occur[134] in polymer solutions when subjected to hydrodynamic shear such as being forced through a narrow capillary or being rapidly stirred. Non-laminar flow under high shear has proved to be a difficult mechanism to quantify but several treatments have been attempted[139].

Harrington and Zimm[135] showed that the critical stress was different in various solvents reporting ranges of results for thermodynamically 'good' through to 'poor' solvents.

Shear stresses during cavitation are thought to arise from the rapid movement of solvent molecules around pulsating cavitation bubbles. Hughes and Nyborg[140] designed apparatus to simulate resonant bubbles without causing cavitational collapse by employing a needle vibrating at high frequency but with a low power. It was found that shearing effects were produced in the eddy currents around the needle tip. Pritchard *et al*[141,142] used a similar approach studying the effect on calf thymus DNA with a molecular weight of $6.5 \times 10^6$ and significantly, their work showed the characteristic limiting molecular weight and high probability of centre cleavage. Thus it appears that shear stresses can cause degradation of high molecular weight polymers even in the absence of transient cavitation bubble collapse.

Neither mechanism receives unanimous agreement amongst present workers in this field but it is generally accepted that the mechanism of degradation is caused by some combination of the effects discussed.

## 1.10 Homopolymer and Copolymer Synthesis Using Ultrasound.

Ultrasound has been used in the polymerisation of monomers to form homopolymers, in the degradation of a variety of polymers and in combinations of the two to produce copolymers.

### a.) Polymerisation of Monomers to Form Homopolymers.

Ultrasonic polymerisation was first reported in 1951 by Lindstrom and Lamm[143] for acrylonitrile in an aqueous medium under an atmosphere of nitrogen. The hydroxyl radicals from the decomposition of water were thought to be the initiating species. This was confirmed by Berlin[144] during the polymerisation of

polystyrene in the presence of styrene monomer who reported enhanced yields following the addition of small amounts of water.

Ultrasonic polymerisation of pure monomer was thought to be unlikely to occur following the statement in a 1964 review by El'Piner[145] that "polymerisation of monomers in an ultrasonic field does not occur if these monomers are thoroughly dried and do not contain substances in the polymerised state." The initial presence of pre-formed polymer was thought necessary for the production of initiating radicals obtained from their breakdown. However, this was disproved by Kruus[146] in 1983 when initiation of polymerisation in pure styrene monomer by high intensity ultrasound was reported. Since then other systems have been investigated including vinyl acetate and methyl methacrylate[147-150].

Variation of the conditions for sonication of monomers has been shown, in our laboratory, to be able to produce polymers with different tacticities[150]. For example, lowering the reaction temperature favours the production of syndiotactic poly(methyl methacrylate) whereas at higher temperatures, the thermodynamically favoured syndiotactic polymer predominates.

Activation energies have been reported for the bulk polymerisation of methyl methacrylate in the presence of ultrasound[151] and the value obtained, provided that the initiation step is excluded, was very close to that observed for bulk thermal polymerisation. This suggests that the activation energy for initiation of ultrasonic polymerisation is negligible as in photopolymerisation.

b.) Formation of Copolymers.

The primary product of the ultrasonic degradation process is a short-lived macromolecular radical. If this radical is formed in the presence of a polymerisable monomer, and in the absence of all radical traps, then the radical can initiate the polymerisation of the monomer[152] and the formation of block copolymers.

Melville and Murray[86] were the first to use this approach in their attempt to confirm the presence of these macromolecular radicals during ultrasonic degradation.

Copolymers may also be formed during the sonication of a solution comprising a mixture of two homopolymers. Henglein[84,85] produced block copolymers of acrylonitrile and acrylamide in aqueous solution in this manner. The two homopolymers employed must both possess molecular weights above the limiting values expected from their ultrasonic degradation[153] otherwise radicals would not be formed from chain scission.

Much copolymer work has focused on poly(styrene-b-methyl methacrylate) copolymers[154,155]. Malhotra studied systems including polystyrene in the presence of poly(alkyl methacrylates)[156] and he investigated the degradation of various substituted polystyrenes in the presence of flexible chain polymers such as poly(vinyl methyl ketone) or poly(vinyl methyl ether). It was concluded that, in general, sonication of two polymers with relatively 'stiff' inflexible chains in solution led to copolymer production but where flexible chain polymers were used, no copolymerisation was found.

More complex systems have been addressed including poly(acrylonitrile) and poly(ethylene oxide)[157] and poly(acrylamide)[158], the block copolymers of the latter two monomers are difficult to prepare conventionally but were prepared in reasonable yield by the sonochemical technique[146].

In addition to the production of copolymers there is considerable interest in producing miscible polymer blends. Ultrasound has been used in the work documented in this thesis to address this area.

c.) Polymer Blends.

Several reviews of miscible polymer mixtures have been published with listings of up to fifty mixtures exhibiting some degree of miscibility[159-162]. Reviews by Krause[161,162] list both miscible and immiscible blends.

Polymer miscibility is not only regarded as important in the case of simple homopolymer mixtures but also determines the physical nature of block and graft

copolymers, interpenetrating networks and thermosetting networks of polymer mixtures. The term *miscibility* is used to describe single-phase polymer-polymer blends often confused with the term *compatibility* which is used to describe single phase behaviour but also describes good adhesion between constituents, an average of mechanical properties, behaviour of two-phase block and graft copolymers and ease of blending. *Solubility* describes molecular mixing in polymer blends and for single-phase solvent-solvent and polymer-solvent mixtures solubility is the accepted term.

Electron microscopy provides an excellent insight into the degree of mixing, often heterogeneous structures can be observed at high magnification despite macroscopic properties indicating single-phase behaviour. Heterogeneous structures (domains) have been observed in amorphous polymers (atactic polystyrene), thus confusing the interpretation of polymer blend miscibility[163].

In other words, the determining factor is how large is the size of a domain required to be in order to yield macroscopic properties, such as glass transition temperature, distinctly different from other domains of different molecular structures[164,165]?

A truly miscible blend is one possessing a single glass transition temperature, $T_g$. Generally immiscibility will reveal itself as opacity, double glass transition or a combination of properties.

From a thermodynamic point of view, every polymer will exhibit some degree of solubility in every other polymer but the magnitude is, in most cases, exceedingly low. For example, polystyrene and poly(methyl methacrylate) will result in a two-phase mixture regardless of length or intensity of mixing, however, fluxing polystyrene with poly(2,6-dimethyl-1,4-phenylene oxide) results in one stable phase only. Equal amounts of polystyrene and poly(vinyl methyl ether) fluxed at 80°C results in a clear single-phase mixture but when the temperature is raised to 140°C, two phases appear and a return to 80°C restores one phase[166]. The three systems define polymer miscibility. The first represents an immiscible blend, the second a miscible blend and the third illustrates that miscibility and immiscibility can be exhibited by the same

mixture depending on the ambient conditions. The last example shows that the driving forces for the transition from the single-phase (miscible) to the two-phase (immiscible) state are thermodynamic in origin and do not depend on the extent of mixing.

For polymer mixtures, the transition point, often termed a cloud point, is measured using a thin film made from a thoroughly dried mixed blend. The film is illuminated and observed as it is heated at a very low rate such that temperature increases at an infinitesimally slow rate. The temperature is recorded as cloudiness appears and this is repeated for a series of compositions and then a temperature-composition plot is generated, known as a cloud-point curve. Problems identifying the transition arise because it can only be observed after large enough clusters have formed to create sufficient refractive index differences for scattering an observable quantity of light.

Work documented in this thesis concentrates on the effects of ultrasound on polymer mixtures and uses electron microscopy to give indications of blending.

## 1.11 Specialist Characterisation Techniques.

A number of techniques were used to analyse the systems studied in the work documented in this thesis other than those already introduced.

### 1.11.1 The Estimation of the Degree of Chain Branching by GPC-Viscometry.

Long chain branching greatly affects the rheological and mechanical properties of polymers. Viscometry has been recognised as a primary method for determining the degree of long chain branching. A branched polymer will have a lower intrinsic viscosity than a linear polymer with the same retention volume. With the advent of GPC-viscometry, the laborious collection of GPC fractions to measure viscosities off-line has been replaced by a technique which gives the intrinsic viscosity distribution point-by-point across the chromatogram much more quickly.

Branching is normally caused by transfer reactions within polymer molecules. The reactivity of the active centre determines the likelihood for transfer and hence

branching is more common in polymers produced by free radical reactions. Ultrasonic degradation produces radicals on the polymer chain ends due to the homolytic cleavage of a bond along the polymer backbone, it is therefore feasible to examine whether branching is introduced during sonication and whether concentrated solutions produce more branching due to the close proximity of the polymer chains.

A common GPC-viscometry technique utilises the Haney[167] capillary bridge differential viscometer which measures differential pressure on separate capillary flow streams of solvent and solution.

The differential viscometer, DV, in principle, can be connected in three different positions with respect to the concentration detector (typically a differential refractometer, DRI), each of these configurations presents particular problems. If the DV is placed before the DRI the GPC effluent is diluted by a factor of two as it passes through the viscosity detector, if the DV is placed after the DRI it may present a back pressure on the RI cell causing it to break and if the DV and DRI are placed in parallel this requires fine adjustment to ensure the flow resistance of each detector remains equal. The parallel configuration is generally favoured and is shown schematically in figure 1.18.

A theory of chain branching was proposed by Zimm and Stockmayer[168] which led to the relationship,

$$g' = \frac{[\eta]_{br}}{[\eta]_l} \qquad 1.41$$

where g' is an experimentally determined quantity providing information concerning branching in polymers, it is defined as the ratio of intrinsic viscosities of the branched (subscript br) and the linear (subscript l) isomers at the same molecular weight.

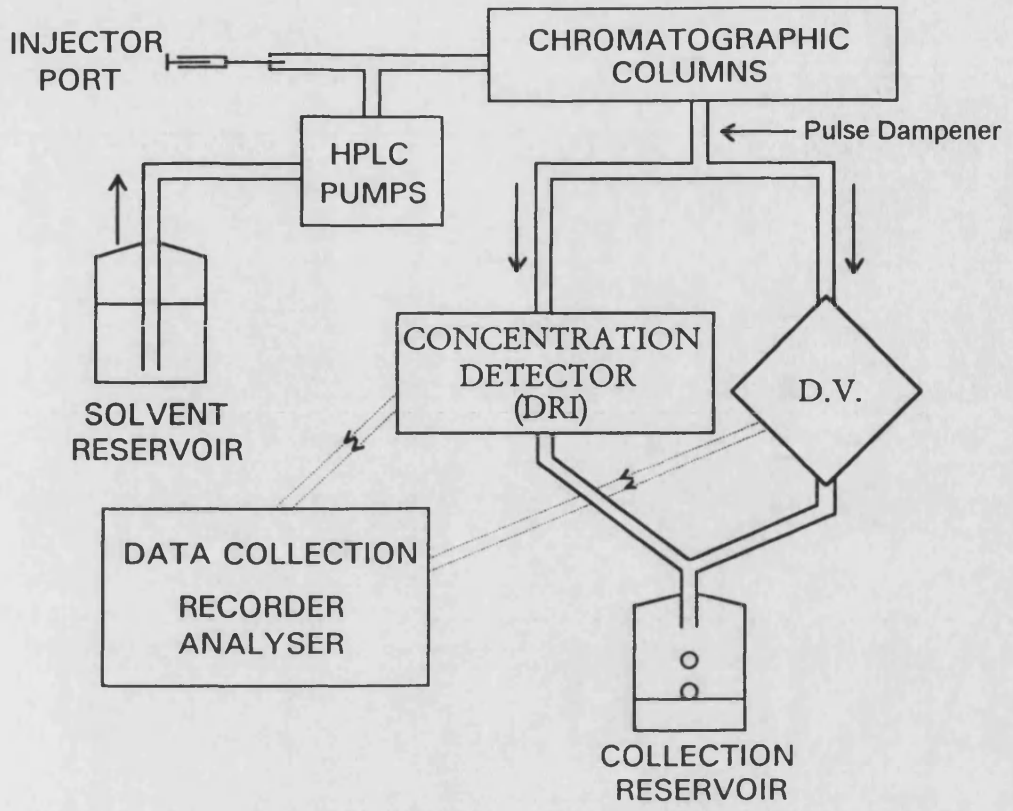


**FIGURE 1.18.** Schematic of GPC-Viscometry Apparatus.

From g', an estimate of $g_o$, the ratio of unperturbed radii of branched and linear isomers is inferred,

$$g_o = \frac{\left\langle r_g^2 \right\rangle_{br}^{1/2}}{\left\langle r_g^2 \right\rangle_{l}^{1/2}} \qquad 1.42$$

where $\langle r_g^2 \rangle_{br}$ and $\langle r_g^2 \rangle_l$ are the radii of gyration of the branched and linear polymers respectively.

Relations between g' and $g_o$ are semi-empirical and approximate[169,170]. It is assumed that g' is independent of solvent conditions and that a theta solvent for a linear

polymer is a theta solvent for its branched analogue. Neither of these assumptions is well founded[169]. In practical applications, exponential relations between g' and $g_o$ of the form,

$$g' = g_o^{\,k} \qquad 1.43$$

have been proposed. A well studied example of a branched polymer is low-density polyethylene, LDPE, for which k = 1.2, k is an arbitrary constant.

The number of branches per macromolecule, n, is calculated through one of the Zimm-Stockmayer[168] relationships such as,

$$g_o = \left[\left(1+\frac{n}{7}\right)^{1/2} + \frac{4n}{9\pi}\right]^{-1/2} \qquad 1.44$$

The branching frequency, λ, the number of branches per molecule, per repeat unit of molecular weight M is given by,

$$\lambda = \frac{Rn}{M} \qquad 1.45$$

where R is the molecular weight of a repeat unit.

A typical procedure for calculating n using a differential viscometer in parallel with a concentration detector would be to first establish a universal calibration then obtain chromatograms of the 'branched' polymers together with the value of $[\eta]_{br}$. $M_{br}$ would be calculated directly from the universal calibration and an estimate of $[\eta]_l$ would be obtained using a suitable Mark-Houwink relationship thus enabling the calculation of g' and hence n. Alternatively if no reliable Mark-Houwink constants are

available, the unknown 'branched' polymer could be compared with a sample of the same polymer known to be linear.

GPC-viscometry has become an accepted method for the determination of chain branching in polymers. This technique has been developed[171-174] and specific applications to branching in polyethylene samples have been reported[175,176]. Recently, light-scattering detectors have been applied to determine branching in polystyrene[177] and polyethylene[178]. The branching study documented in this thesis focuses on the ultrasonic degradation of polyethylene in solution and application of GPC-Viscometry to quantify any change in the degree of branching. It is believed to be the first study of this nature concentrating on polyethylene under ultrasonic irradiation.

### 1.11.2 Electron Spin Resonance Spectroscopy of Polymers.

Electron spin resonance (ESR), also known as electron paramagnetic resonance (EPR), is a form of microwave absorption spectroscopy in which transitions are induced between energy levels arising from the interaction of paramagnetic electrons with an externally applied magnetic field.

The majority of stable molecules have bonds in which electron spins are opposed resulting in no net overall electron spin, no electronic magnetic moment and therefore no interaction between electron spins and an applied magnetic field. However, some molecules contain one or more electrons with unpaired spins hence exhibit electron spin resonance and bulk paramagnetism, examples include $O_2$, NO, $NO_2$ and notably, free radicals. A simplified ESR spectrometer is shown in figure 1.19.

Experimentally, incident radiation is supplied at a fixed frequency from the Klystron and the magnetic field is swept through a range. Energy absorbed by the sample is plotted versus field strength. For sensitivity reasons a small a-c magnetic field is superimposed on the magnetic field sweep and the resulting signal is phase detected. The resultant is a first derivative spectral line whose intensity is a measure of

the number of electrons participating in resonance absorption and whose shape provides information about the local chemical environment of the electrons.

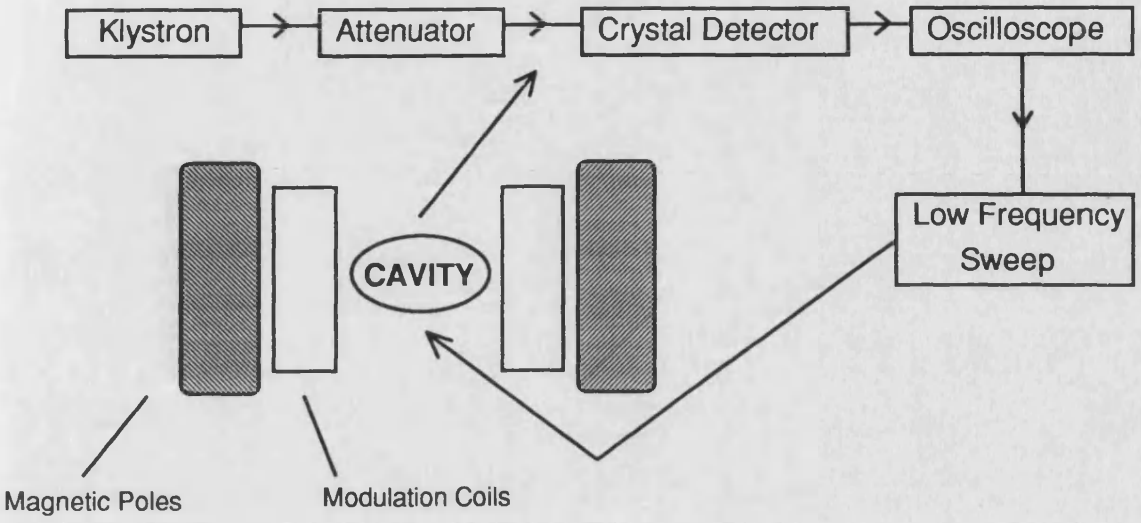


**FIGURE 1.19.** Schematic of an ESR Spectrometer.

Most experimental results based on ESR are used primarily to corroborate reaction mechanisms. The ESR study documented in this thesis attempts to both confirm the presence of a free radical mechanism in the ultrasonic degradation of PIB and identify the nature of this radical. Spin-traps known to react with short-lived radicals were employed and thus gave the opportunity to isolate the radicals as they were formed. ESR was also applied to the ultrasonic polymerisation of methyl methacrylate.

### 1.11.3 Polymer Morphology as Viewed by Scanning Electron Microscopy.

Increased use of electron microscopy applied to polymer research has been the result of widespread acceptance of the techniques and extended property requirements of the materials. It is well known that the structure present in a polymer reflect the process variables and further that they greatly influence the physical and mechanical

properties. Thus, the properties of polymer materials are influenced by their chemical composition, process history and the resulting morphology. Structural observations of the polymers must be correlated with the properties of the material in order to gain a full understanding of the system.

Polymer microscopy is the study of fine structure and morphology. There are many different techniques available, each individual technique having its own unique advantages. Scanning electron microscopy, SEM, has high resolution (10nm), a fairly wide magnification range, incurs little radiation damage on the easily prepared sample and has the ability to study the surface morphology of polymers.

The essential feature of an SEM is that the image is formed point by point by scanning a probe across the specimen. The probe of an SEM is a focused electron beam and a detected signal is displayed as a TV type image. Several texts[179-182] fully describe the technique of SEM and its application to polymer samples has been reviewed by White and Thomas[183].

Other advantages of SEM include higher resolution than in optical microscopy, with a much larger depth of field. The specimen chamber in the SEM is large and samples from several millimetres to several inches in diameter can be accommodated. This makes SEM ideal for studying polymer films cast directly onto a specimen plate. Non-conductive polymers require conductive coatings, sputter-coaters commonly being used[184] for SEM to provide a conductive layer of about 1-100 nm thickness, typically gold, which emits secondary electrons producing SEM images.

Thin films can be cast from solutions of crystalline or non-crystalline polymers where the film thickness is controlled by the solution concentration, for example polyethylene films have been cast from boiling dilute solutions in xylene[185].

Vadimsky[186] described thin film preparation from solution, this involved evaporation of carbon onto freshly cleaved mica or fractured NaCl crystal substrates. The thin polymer film was then cast directly onto the carbon coated substrate, the solvent removed and the film scored and 'raised' from the support by floating it onto a water surface. Alternatively, polymers may be deposited directly onto the substrate

and coated after solvent evaporation. Documented in this thesis, the study includes solvent evaporation in this manner and some samples were heated above the glass transition temperatures of the component polymers to ensure removal of trapped solvent molecules.

Cast films exhibit a range of morphologies due to the effect of solvent and orientation. In the case of block copolymers, the choice of solvent is important to the final structure. In this study the solvent was not varied so that the effect of sonication could be isolated and interpreted.

Polymer-solvent interaction has been studied by electron microscopy by Hsiue and Yang[187] who examined the morphology and properties of α-methylstyrene butadiene diblock copolymer films cast from several solvents. The microstructure was shown to differ for films cast from different solvents, this effect was out of the range of the study documented in this thesis.

# CHAPTER TWO

# EXPERIMENTAL

## 2.1 Materials

The GPC eluent used for the analysis of PIB molecular weights and polydispersities was tetrahydrofuran (Aldrich Ltd., 99+% HPLC grade.) The THF was used as received, inhibited with butylated hydroxytoluene (0.025%.) to avoid peroxide formation and subsequent column damage.

Polyisobutylene was high molecular weight material (approx. MW=1400000) supplied by Janssen Chemicals and the study was performed on a single batch of polymer to avoid variations in starting molecular weight. Degradation studies were performed on polyethylene (BPD 2133) and polypropylene (Amoco Chemical Belgium, M.F.I.=11.0) and were analysed by high temperature GPC using 1,2-dichlorobenzene at RAPRA Technology Ltd.

The solvents used in the degradation studies were all used as received, obtained from Aldrich Ltd. unless otherwise stated. The purity is shown in parentheses: tetrahydrofuran (99+%), toluene (BDH HiPerSolv 99.9%), tetrachloromethane (99%), trichloromethane (99.9%), pentane (99.6%), hexane (99+%), octane (99+%), decane (99+%), dodecane (99%), tetradecane (99%), decahydronaphthalene (decalin, 99% mixture of cis and trans isomers). Other solvents used other than those already specified were reagent grade or better.

Gases employed were supplied by BOC Ltd (unless otherwise stated) and were all used as received, helium, hydrogen, nitrogen (oxygen-free), oxygen, argon, methane, carbon dioxide, ethene (Argo International Ltd.), propane (Argo International Ltd.).

Solution viscometry was performed using the range of n-alkanes listed above, these were all filtered prior to use using 0.2μm 'Nylaflo' membrane filters (Gelman Sciences) to remove microparticles which would inhibit the flow in the viscometer.

Functionalised PIBs were synthesised and analysed using the following (supplied by Aldrich Ltd.), 9-bromoanthracene (96%), 1-amino-4-bromonaphthalene (99%), 1-bromonaphthalene (98%), 9-methylanthracene (98%), 1-methylnaphthalene

(97%), Rose Bengal (94% dye content) and 2,2-diphenyl-1-picrylhydrazyl (98%). The spin traps used in the ESR studies were nitrosobenzene and N-t-butyl-α-phenylnitrone.

Other polymers were used as supplied by Aldrich Ltd. including polystyrene (secondary standard, Mn = 120000), styrene-butadiene copolymer (45% styrene content), poly(methyl phenylsilane), cis-polybutadiene and poly(ethylene oxide).

Polystyrene standards were used to calibrate the GPC, they were supplied by Polymer Laboratories Ltd. and are detailed in section 2.3.1.

## 2.2 Sonication Experiments.

All reactions documented in this thesis were performed using a Lucas Dawe ultrasonic probe system with a Branson Ultrasonics converter. Far more control, variation of reaction conditions and overall effect was produced with a probe system hence this was used in favour of an ultrasonic bath. The probe was inserted directly into the reaction using a cell designed and constructed for this study.

### 2.2.1 Reaction Cell Design.

The shape of the reaction cell used in sonochemistry has been found to greatly affect the extent of reaction[70]. For this study, a specially designed glass cell was employed throughout, its design is shown in figure 2.1.

The reaction cell incorporates a jacket through which water (or a glycol/water mixture) can be circulated to control the bulk reaction temperature to within ± 0.5°C. Temperature control is an important factor in sonochemistry as a significant amount of heat is produced during sonication, this thermostatted jacket also ensured that any kinetic measurements were made at the correct temperature.

The cell has three quick-fit joints which serve as ports for a thermometer, a sampling syringe and gas inlet/outlet needles. The seal around the probe was made by two o-rings inset into the cell neck which ensured that a controlled gaseous atmosphere could be maintained inside the reaction cell.

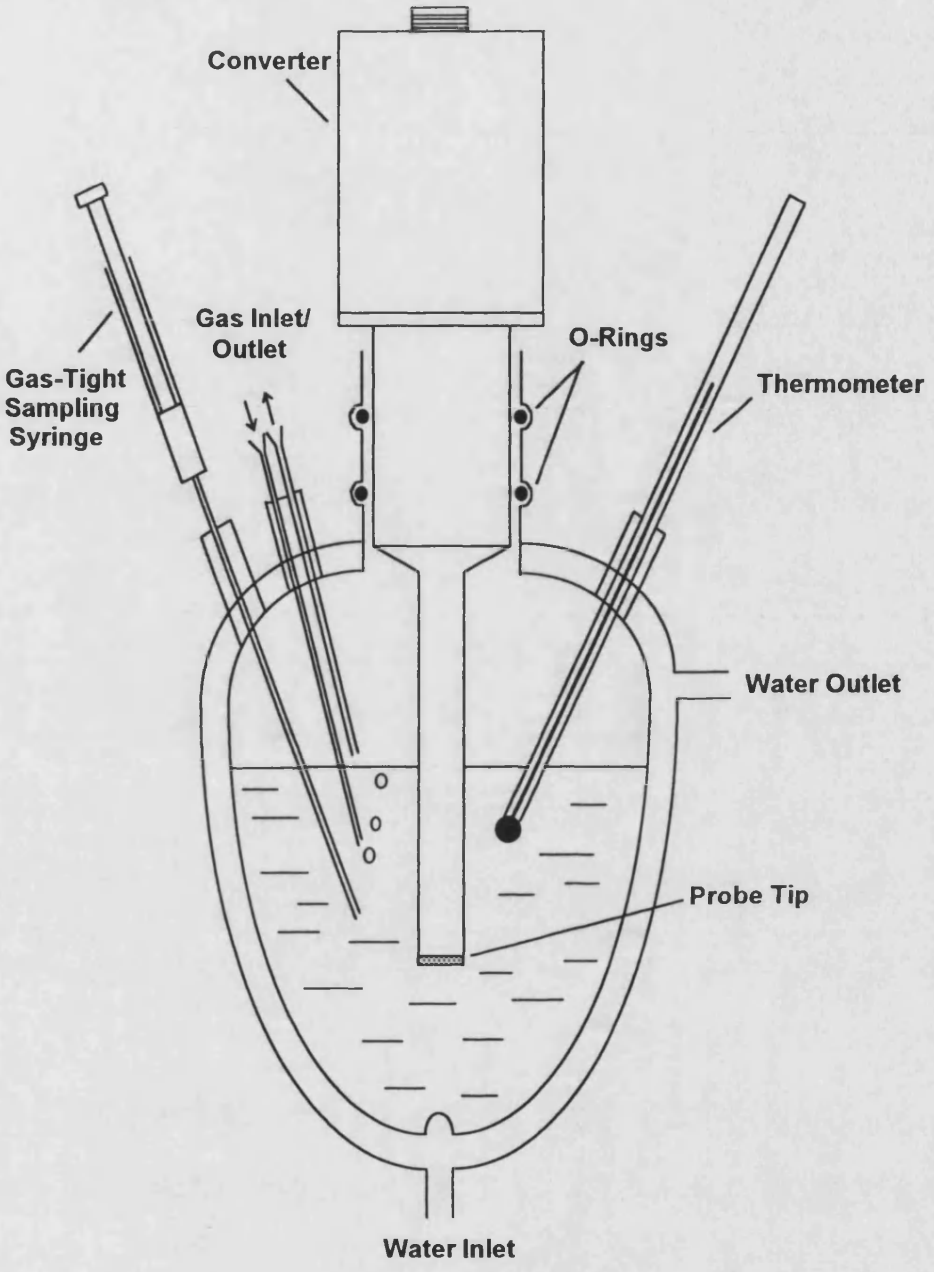


**FIGURE 2.1.** Ultrasonic Reaction Vessel, 100 $cm^3$ Capacity.

The ultrasonic probe was inserted into the reaction cell to a reproducible depth of 3 cm. The internal flask was designed with a modified base directly below the probe tip, this provides efficient mass transfer during the sonication and thus ensured that all reactants were sonicated to the same degree, obviating additional stirring.

2.2.2 Calibration of the Ultrasonic Probe Intensity.

Ultrasonic equipment can be calibrated in a variety of ways so that the operating intensity can be quoted. Nominal output is often quoted by manufacturers but relates to the energy supplied to the transducer(s) and not to the amount of energy being transferred to the reaction medium.

El'tsefon and Berlin[188,189] suggested that the total energy input should be quoted defining a parameter q, such that,

$$q = \frac{Ut}{Vc} \qquad 2.1$$

where U is the intensity, t is the irradiation time, V is the volume of solution and c is the polymer concentration.

In this study all reactions were performed on the same volume, it was therefore decided that a calorimetric treatment would provide reliable measurements. A value was recorded measuring a temperature rise in a volume of distilled water over a set period of time. Other workers may use vessels possessing different total thermal capacities, but this approach should enable comparisons to be drawn between the experiments performed.

Experimentally, the reaction vessel was set up as for a degradation, the jacket of the cell was filled with water (not circulating) and 100 $cm^3$ of distilled water was pipetted into the vessel. An electric heater and a thermocouple probe were inserted so that the temperature rise could be monitored at regular intervals automatically. The voltage, V, and current, I, drawn by the electric heater were noted and a series of readings were recorded once the cell had equilibrated at 20°C. The energy, E, supplied to the heater over a period of time, t, was calculated,

$$E = VIt \qquad 2.2$$

A total heat capacity, C, was calculated from the linear temperature rise over the initial period of time such that,

$$C = \frac{E}{\Delta\theta} \qquad 2.3$$

where $\Delta\theta$ is the rise in temperature over a set time period.

The procedure was repeated substituting the ultrasonic probe for the electric heater, each intensity setting on the ultrasonic generator could then be calibrated. The ultrasonic power, P, was calculated by monitoring the temperature rise, $\Delta\theta$, over a period, t, using C calculated previously,

$$P = \frac{C\Delta\theta}{t} \qquad 2.4$$

The heating curves showing the temperature rise produced from each source are shown in figure 2.2.

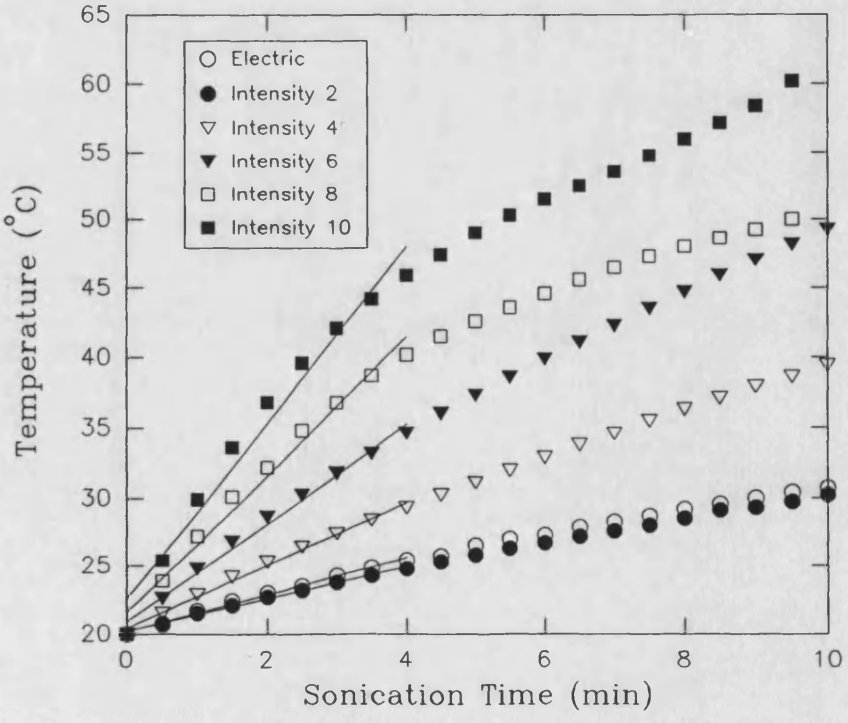


**FIGURE 2.2.** Heating Curves for the Calibration.

Intensity Calibration

a.) Electric Heater, Current, I = 1.11 A, Voltage, V = 15.00 V

| Source | Δθ over 240s |
|---|---|
| Electric Heater | 5.4°C |

E=3996 J, therefore total heat capacity of reaction cell, C=740 $JK^{-1}$.

b.) Lucas Dawe Ultrasonic Probe

| Generator Setting | Δθ over 240s |
|---|---|
| 2 | 4.8°C |
| 4 | 9.3°C |
| 6 | 14.6°C |
| 8 | 20.2°C |
| 10 | 25.9°C |

Hence the power, P, for each setting is calculated and has been converted into ultrasonic intensity (taking into account the area of the probe tip) as shown in Table 2.1 with the estimated errors included.

Many workers use differential calculus taking the initial slope of the heating curves, however for the purposes of correlating the electric heating results with those obtained ultrasonically it was felt sufficient to use a mean temperature rise over a short period of time.

c.) Estimation of Errors in the Intensity Calibration

The main sources of error arise from temperature and time readings, each temperature reading was subject to ± 0.1°C. For the electric heating $\Delta\theta=T_2-T_1$ where $T_2>T_1$,

$$\text{Error in temperature, } \Delta\theta, = \sqrt{\{(0.1)^2+(0.1)^2\}} = \pm 0.14^{o}C$$

Each time reading is subject to an error of ±1sec, hence the error can be estimated.

$$\text{Error in time ,t, } = \sqrt{\{(1)^2+(1)^2\}} = \pm 1.4 \text{ sec}$$

Normal methods of differentiation were applied in order to calculate the errors in electrical energy, E, and ultrasonic power, P. These compounding errors enabled absolute errors for the ultrasonic intensity to be quoted.

The area of the probe tip was measured and found to be 1.202 $cm^2$ so that the intensity of the ultrasound produced could be quoted as shown in Table 2.1.

**TABLE 2.1.** Ultrasonic Intensities Generated by Probe System.

| Generator Setting | Intensity ($Wcm^{-2}$) |
|---|---|
| 2 | 12.3 ± 1.2 |
| 4 | 23.9 ± 2.2 |
| 6 | 37.4 ± 3.4 |
| 8 | 51.8 ± 4.7 |
| 10 | 66.5 ± 6.0 |

A linear calibration plot is shown in figure 2.3 so that intermediate intensities can be selected if required.

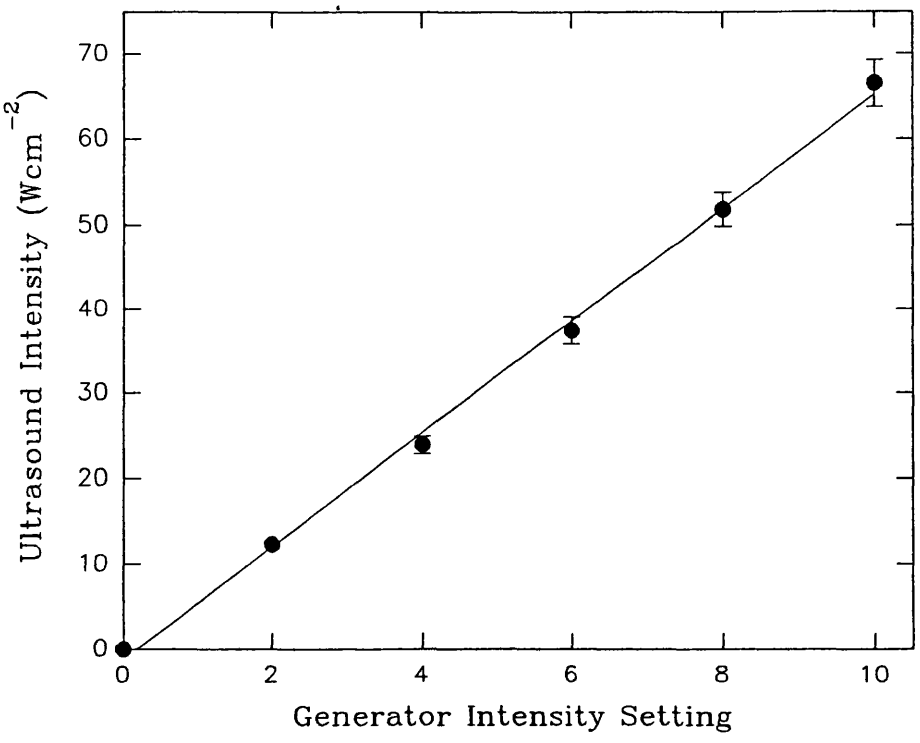


**FIGURE 2.3.** Calibration Plot for Ultrasonic Probe.

Other errors exist such as heat losses to the surroundings and non-efficient heat transfer during the electric heating, these were minimised but are difficult to quantify. Hence approximate values for intensity can be used to make comparisons with other researchers' work.

2.2.3 Ultrasonic Degradation Experiments.

Each reaction in the series of polyisobutylene degradations was performed using an identical procedure. An accurately weighed sample of polymer was dissolved in 100 $cm^3$ of solvent at 25°C. When dissolution was complete the solution was added to the reaction cell set-up as shown in figure 2.1 previously.

A Haake D8 digital heater/circulator was used to control the temperature in the water jacket or, in order to maintain sub-ambient temperatures, a Grant circulating bath was used substituting an ethylene glycol/water mixture as the coolant.

All reactions were carried out under a nitrogen (oxygen-free) atmosphere unless the effect of another gas was being studied. In each case the solution was degassed for 45 minutes by bubbling the gas through the solution. During the sonication the gas flow was maintained over the solution to maintain a slight positive pressure of gas in the reaction cell to prevent air re-entering the system.

At regular intervals, a 0.5 $cm^3$ sample was removed from the cell, for analysis, using a Hamilton gas-tight syringe. The reaction was allowed to proceed for 6 hours in each case.

An identical procedure was carried out for the sonications involving polyethylene and polypropylene except the solvent in this case was decahydronaphthalene, all sonications were performed at 80°C and the reactions were allowed to proceed for 24 hours. The resulting polymers were precipitated into acetone prior to analysis.

2.2.4 Production of Functionalised Polyisobutylene.

Solutions of polyisobutylene (1% w/v) in tetrahydrofuran were sonicated as described in section 2.2.3 in the presence of 0.5% w/v of the following molecules to produce end-capped or telechelic polymers. This amount ensured that the capping molecules were in excess but not likely to affect the degree of degradation by inhibiting the ultrasound.

(i) 9-bromoanthracene

(ii) 1-amino-4-bromonaphthalene

(iii) 1-bromonaphthalene

(iv) Rose Bengal

After 6 hours sonication at 25°C under a nitrogen atmosphere the resulting polymers were precipitated into a ten-fold excess of acetone (a non-solvent for PIB) and rigorously purified by re-dissolving in THF and precipitating into acetone three

times. This would ensure that no unreacted cap remained, this was tested for by repeated UV absorbance readings for the newly 'capped' material remaining constant.

The degree of functionalisation or capping efficiency was measured using a Perkin-Elmer 330 UV/Vis Spectrophotometer. Molecules mimicking the structure of the functionalised polymer chain were used in order to measure the extinction coefficient of the materials synthesised. The absorbance of the 'capped' polymer samples was then measured and a value for the number of caps per chain could be calculated.

The efficiency of capping was further investigated by sonicating polyisobutylene solutions in THF with the addition of an excess of 2,2-diphenyl-1-picrylhydrazyl (DPPH). DPPH is known to be an efficient radical trap as it exists as a stable free radical with the structure,

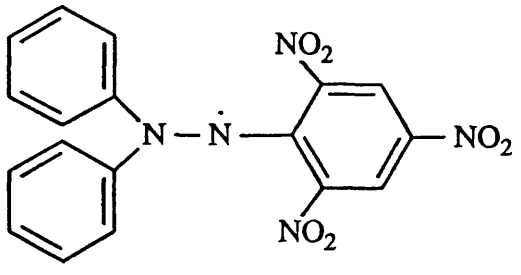


By calculating the number of chain breaks from the degradation of polyisobutylene under identical conditions in the absence of DPPH and by sonicating DPPH in the solvent alone, it was possible to predict the rate of DPPH consumption and hence from the experiment gain a value for the efficiency of the ultrasonic technique for the functionalisation reactions.

2.2.5 Ultrasonic Copolymerisation Reactions.

a.) Copolymerisation Reactions Analysed by $^1$H-NMR.

The degradation of one homopolymer in the presence of a polymerisable monomer or a second homopolymer gives the opportunity to synthesise block copolymers. The systems chosen were as follows (the selective solvents for each

homopolymer being shown in parentheses, each being a non-solvent for the other homopolymer),

(i) PS + *cis*-Polybutadiene/THF (hexane, acetone)

(ii) PIB + PEO/$CHCl_3$ (hexane, water)

(iii) PIB + PMMA/THF (hexane, acetone)

Each homopolymer (1% w/v respectively) mixture was prepared in the co-solvent indicated and sonicated at 25°C, under a nitrogen atmosphere for 6 hours. In addition, *cis*-polybutadiene was dissolved in 100 $cm^3$ of styrene monomer, degassed thoroughly with nitrogen and sonicated under the same conditions.

In each case, the products of the reaction were precipitated into an ice-cold excess volume of methanol (acetone used in (ii)) and dried under vacuum. Selective precipitation was repeatedly preformed on each product to separate the component homopolymer and isolate any resulting copolymer. All products were analysed by NMR in order to estimate the copolymer composition.

b.) Ultrasonic Blending Experiments Analysed by SEM.

Solutions of polymer mixtures (1% w/v) were prepared in toluene and sonicated under a nitrogen atmosphere at 25°C for 6 hours sampling at the beginning, after 1 hour and 6 hours of sonication. The solutions were sonicated as follows,

(i) Polystyrene + styrene-butadiene copolymer (45% styrene content) in the ratio 80:20.

(ii) Polystyrene + cis-polybutadiene in the ratio 80:20.

(iii) Polystyrene + poly(methyl phenylsilane) in the ratio 80:20.

The resulting samples were analysed by conventional scanning electron microscopy as described in section 1.11.3.

## 2.3 Polymer Analysis.

### 2.3.1 Molecular Weight Determination by GPC.

a.) Polyisobutylene Samples.

The analysis of degraded samples of polyisobutylene was carried out using a Bruker LC41 gel permeation chromatograph. The GPC was fitted with a Polymer Laboratories Ltd. PL Gel 5μm mixed pore-size 600mm column and was controlled from an Epson QX16 data station.

All of the samples injected were adjusted to a concentration of 0.5% w/v to avoid any concentration effects and the eluent (THF) was pumped at a constant 1.0 $cm^3\ min^{-1}$. A dual detector system comprising a Knauer ultraviolet spectrometer and a differential refractive index detector was used for the analysis.

A universal calibration technique was necessary owing to the lack of PIB standards to characterise the polymer samples. The GPC was calibrated with a range of polystyrene standards ($\gamma \approx 1.02$) supplied by Polymer Laboratories Ltd. with the following molecular weights, 2650000, 1030000, 675000, 200000 ,127000, 68000, 52000, 30300, 9200. The Mark-Houwink parameters (determined by RAPRA Technology Ltd.) for polyisobutylene and polystyrene in tetrahydrofuran at 25°C were used in the data handling and calibration files of the analysis procedure respectively. The values used were:

| Polymer | logK | α |
|---|---|---|
| Polystyrene | -3.293 | 0.600 |
| Polyisobutylene | -2.849 | 0.541 |

b.) Polyethylene and Polypropylene Samples.

The analysis was performed at RAPRA Technology Ltd. by Dr. Steve Holding. The GPC was set up with a PL Gel mixed gel-B 10μm 300mm column with 1,2-dichlorobenzene as the eluent. The column was maintained at 140°C and the eluting

polymers were detected by an infra-red (3.4 microns) detector. The polymers were prepared as 0.1%w/v solutions and gently boiled in the solvent for 20 minutes. A part of each solution was filtered through a fibre pad at 160°C and re-heated to boiling immediately prior to the chromatography. The system had been calibrated with polystyrene and a universal calibration procedure applied mathematically and the results were expressed as polyethylene (high-density) or polypropylene as appropriate.

2.3.2 Viscometric Determination of Intrinsic Viscosity and the Flory-Huggins Interaction Parameter.

A calibrated Ubbelohde viscometer (Camlab), size 0a, was used to measure the relative viscosities of polyisobutylene solutions in a series of n-alkanes. Flow times of at least 200 seconds were obtained to minimise drainage errors[22].

The Ubbelohde viscometer used incorporated a dilution reservoir to enable additions of pure solvent to be made to change the concentration thus reducing the time taken by cleaning and charging the viscometer.

Before use, the series of n-alkanes was filtered through 0.2μm 'Nylaflo' filters to remove microparticles. A stock solution of polyisobutylene in each n-alkane was prepared with an initial concentration of between 0.1 and 3.0 g $dm^{-3}$ depending on the viscosity of the solvent. The polymer was dissolved at a constant 25°C to ensure an accurate solution concentration in the volumetric flask. All further dilutions were performed with pure, filtered solvent at 25°C inside the viscometer.

The polymer solutions were filtered again directly into the viscometer and allowed to equilibrate to 25°C. The viscometer was suspended vertically with the aid of a plumb-line in a thermostatted water bath at 25 ± 0.1°C controlled by a Haake D8 digital water heater/circulator. Temperature fluctuations were minimised as the viscosities of most solvents vary greatly with temperature[190].

The viscometer was modified to operate with an automatic timer by incorporating a set of LED sensors which switched the timer on/off as the solution passed the two marks successively under gravity. The flow-times were recorded to an

accuracy in excess of ± 0.05 seconds. An average value was calculated over a set of three successive readings that had a flow-time variation of less than 0.2 seconds in each case.

Intrinsic viscosities were calculated by conventional extrapolation techniques and the values of $\eta_r$, the relative viscosity, were used in the single-point determination approximations of intrinsic viscosity (Rudin and Solomon and Ciuta) as explained previously in section 1.5.1.

The Flory-Huggins interaction parameters were calculated from the values of intrinsic viscosity using the methods introduced in section 1.5.1.

2.3.3 Chain Branching by GPC-Viscometry.

The degree of chain branching in sonicated samples of polyethylene was studied by GPC-viscometry at RAPRA Technology Ltd. The samples were analysed similarly to the procedure outlined for high temperature GPC of polyethylene and polypropylene in section 2.3.1 except in this case the solution concentrations were prepared more accurately and the viscosity detector was placed in series between the column and the infra-red concentration detector. During sample preparation, techniques were adopted designed to minimise solvent loss (and hence changes in concentration) and the solutions were not filtered.

The theory relating to the calculation of the degree of chain branching was discussed in section 1.11.1. Two approaches were examined, the degree of chain branching in the sonicated samples was related to the unsonicated material and to parameters inserted into the calibration file of the analysis relating to a known linear sample of polyethylene. Hence the effect of sonication on the introduction of chain branching could be discussed.

2.3.4 Electron Spin Resonance Spectroscopy.

The ESR spectroscopy was performed at the University of Bristol under the guidance of Dr. John Maher. The ESR spectra were obtained with a Bruker ESP-

300E spectrometer operating at ~9.5 GHz using a standard rectangular cavity TE102. The spectrometer was calibrated with respect to a DPPH signal, field measurements were taken from the Bruker ER032M Hall field controller and the frequency was measured via a Hewlett Packard 5350B microwave frequency meter. Samples were measured in 5mm o.d. x 3mm i.d. silica tubes.

Polyisobutylene was sonicated in tetrahydrofuran (at Bristol) in the presence of nitrogen containing radical traps so that any radicals formed could be isolated, their presence confirmed and their identification attempted. This was repeated with polystyrene. Poly(dimethylsiloxane), a polymer thought not to produce radicals[90] under ultrasonic irradiation, was examined to confirm this.

2.3.5 Nuclear Magnetic Resonance Spectroscopy.

All copolymer and homopolymer fractions isolated from the separation procedures performed were analysed by $^1$H-NMR spectroscopy in order to determine their composition. All spectra were recorded on a JEOL GX-270 spectrometer, deuterated chloroform was used as the solvent and TMS as the reference.

2.3.6 Scanning Electron Microscopy.

All of the images were obtained on a JEOL T-330 scanning electron microscope. The morphology of the polymer samples was studied and photographs taken of unreacted and sonicated blends. The systems examined were sonicated as described in section 2.2.5. The theory of SEM was discussed in section 1.11.3. The negatives were developed and the photographs printed in the School of Chemistry.

# CHAPTER THREE

# CONTROLLED ULTRASONIC DEGRADATION OF POLYISOBUTYLENE

## 3.1 Controlled Ultrasonic Degradation of Polyisobutylene.

The primary product of an ultrasonic degradation is a macromolecular radical. In order to use this radical in copolymer synthesis or compatibilising polymer blends, the control of its structure must be addressed.

Experimentally, there are many ultrasonic and physical factors which can be varied. The parameters studied include the intensity of the ultrasound, the bulk solution temperature, the concentration of polymer and its conformation adopted in solution and the effect of dissolved gases.

The properties of the polymer investigated were the variation of molecular weight with time, the rate of degradation and the final, or limiting, molecular weight reached during the process. In subsequent sections the nature of the macroradicals measured by ESR-spectroscopy will be described and the extent of chain branching introduced will be investigated by GPC-viscometry.

Before a rigorous examination of the various factors affecting the degradation, it is necessary to define rate constants and introduce rate models for the degradation processes.

## 3.2 Rate Models for the Ultrasonic Degradation Process.

The kinetics of a degradation process are studied to characterise the reaction in terms of a rate constant, k. The statistical nature of polymer molecular weight distributions introduced in section 1.3 and the physical nature of polymer molecules makes the assignment of a particular rate equation very difficult. Essentially the solution degradation process consists of a series of polymer chains of varying degrees of polymerisation undergoing parallel reactions, this introduces complexity into the kinetic treatment of the results.

Rate equations have been proposed for the degradation of polymers by a number of workers. The following section aims to introduce a small number of these models, chosen from a range of mechanisms applied to various systems, and select the most applicable to the ultrasonic process.

3.2.1 Rate Models.

(i) **Schmid Model**[191]. This was the first attempt to apply a kinetic analysis to a monodisperse polymer sample. The model proposed that the rate of degradation dB/dt (number of chain breaks per unit time) of a molecule with a degree of polymerisation at time t, $P_t$, was proportional to the fraction of a total chain which exceeded the limiting degree of polymerisation, $P_{lim}$, thus,

$$\frac{dB}{dt} = k(P_t - P_{lim}) \qquad 3.1$$

Conversion of the degree of polymerisation to molecular weight and integration of the above equation leads to the Schmid rate equation,

$$\frac{M_{lim}}{M_t} + \ln\left(1 - \frac{M_{lim}}{M_t}\right) = -\frac{k}{c}\left(\frac{M_{lim}}{M_o}\right)^2 t + \frac{M_{lim}}{M_i} + \ln\left(1 - \frac{M_{lim}}{M_i}\right) \qquad 3.2$$

where $M_o$ is the monomer molecular weight, $M_i$ is the initial molecular weight of starting material, $M_t$ is the molecular weight at time t, $M_{lim}$ is the limiting molecular weight and c is the solution concentration in base moles $dm^{-3}$.

A plot of $[(M_{lim}/M_t) + \ln(1-M_{lim}/M_t)]$ against t should yield a straight line with a gradient of $k(M_{lim}/M_o)^2/c$. The model does not consider the variation in molecular weight distribution during the degradation and although the molecular weights were defined as number averages, $M_n$, the values plotted by Schmid were viscosity averages. Schmid obtained straight line plots and it was suggested that this was due to the use of wide distribution polymers whose polydispersity changed with time. This suggests that the model may suit the ultrasonic degradation process and has been found to give good linear fits for a range of systems[191,192].

The Schmid model has been the most extensively used for the calculation of ultrasonic rate constants. With an understanding of cavitation theory, Jellinek and White[57], Mostafa[93] and Simha[193] extended the theory of the model but the improvements were negligible and will not be examined.

(ii) **Ovenall Model.** Henglein[84,85] was the first of many workers to measure the number of bonds broken in the polymer as a function of time. He proposed that breakage of a covalent bond led to two macromolecular radicals which could be monitored by the use of a radical scavenger like 2,2-diphenyl-1-picrylhydrazyl, DPPH. It is assumed that DPPH was a completely efficient scavenger, every radical arising in the system is removed by a DPPH molecule, and that two DPPH molecules are consumed for every polymer bond broken. The rate of bond breakage and ultimately the limiting molecular weight should not be affected by the presence of DPPH.

Using Henglein's results, Ovenall *et al*[192,194] produced a fundamental rate equation for the rate of bond breakage, this is based on the extent of degradation over the first 10 minutes irradiation for a series of poly(methyl methacrylate) fractions using DPPH,

$$\frac{dB}{dt} = k \ln\left(\frac{P_t}{P_{lim}}\right) \qquad 3.3$$

resulting in the following rate equation,

$$\ln\left(\frac{1}{M_{lim}} - \frac{1}{M_t}\right) = \ln\left(\frac{1}{M_{lim}} - \frac{1}{M_o}\right) - k\left(\frac{M_{lim}}{cM_o}\right)t \qquad 3.4$$

A plot of $\ln(1/M_{lim}-1/M_t)$ against time produces a straight line graph with a gradient of $-k/c(M_{lim}/M_o)$.

(iii) **Fujiwara Model.** Fujiwara *et al*[195] derived a rate of mechanical degradation as follows,

$$\frac{1}{(P_t - P_{lim})} = kt + \frac{1}{(P_i - P_{lim})} \qquad 3.5$$

where $P_i$, $P_t$ and $P_{lim}$ are the degrees of polymerisation of the polymer at time t=0, t=t and the limiting degree of polymerisation respectively.

(iv) **Sato and Nalepa Model**[196]. A degradation rate equation was derived by Sato and Nalepa during the ultrasonic degradation of cellulose using a model put forward by Jellinek[197] for a random degradation process, although ultrasonic degradation is known to follow a non-random degradation mechanism. A relationship between the number average degree of polymerisation $P_t$, and the time t, is given by,

$$-\ln\left(1-\frac{1}{P_t}\right) = kt - \ln\left(1-\frac{1}{P_o}\right) \qquad 3.6$$

When the number average degree of polymerisation, $P_n$, is large this can be approximated to,

$$\frac{1}{P_t} = \frac{1}{P_i} + kt \qquad 3.7$$

The number average molecular weight, $M_n$, is given by,

$$M_n = M_o P_n \qquad 3.8$$

where $M_O$ is the monomer molecular weight, hence equation 3.7 can be reduced further to,

$$\frac{1}{M_t} = \frac{1}{M_i} + k't \qquad 3.9$$

where $M_t$ and $M_i$ are the number average molecular weight averages of the polymer at time t=t and t=0 respectively and $k'=k/M_O$.

(v) **Xu Model**[198]. After studying the degradation of polybutadiene a basic first order empirical rate model was suggested,

$$\ln\left(\frac{M_t}{M_i}\right) = -kt \qquad 3.10$$

Xu *et al* reported linear fits for the initial stages of the degradation.

3.2.2 Application of the Rate Models to an Experimental System.

Each of the five rate models outlined were applied to a set of polyisobutylene degradation results in order to determine which models best describe the process of the ultrasonic solution degradation. The results chosen were those of an ultrasonic intensity study. The number average molecular weight values were used in each model and the linear correlation coefficients (for the first 60 minutes) were calculated for the rate models. These values are shown in Table 3.1. This section does not aim to

discuss the nature of the effect as this will be dealt with more comprehensively in a subsequent section, only the applicability of the rate models will be examined.

TABLE 3.1. Linear Correlation Coefficients for the Ultrasonic Degradation of Polyisobutylene at Various Ultrasonic Intensities for Five Proposed Rate Models.

| | LINEAR CORRELATION COEFFICIENTS | | | | |
|---|---|---|---|---|---|
| Intensity ($Wcm^{-2}$) | (i) Schmid | (ii) Ovenall | (iii) Fujiwara | (iv) Sato&Nalepa | (v) Xu |
| 12.3 | 0.9956 | 0.9423 | 0.9723 | 0.9026 | 0.7558 |
| 23.9 | 0.9988 | 0.9677 | 0.9785 | 0.9548 | 0.8023 |
| 37.4 | 0.9995 | 0.9634 | 0.9745 | 0.9503 | 0.7744 |
| 51.8 | 0.9942 | 0.9770 | 0.9853 | 0.9664 | 0.7850 |
| 66.5 | 0.9953 | 0.9753 | 0.9855 | 0.9619 | 0.7727 |
| Average | 0.997 | 0.965 | 0.979 | 0.947 | 0.778 |

3.2.3 Discussion of Rate Models.

(i) **Schmid Model**, gave excellent linear fits for the initial period of the degradation. The model holds well for other degradation studies and deviations from linearity only occur at long sonication times.

(ii) **Ovenall Model**, near-linear correlations are observed for the degradation process for approximately 200 minutes in all of the systems studied.

(iii) **Fujiwara Model**, good linear correlation coefficients are found for the initial period of the degradation, deviations occur at longer sonication times.

(iv) **Sato and Nalepa Model**, poor correlations are observed using the random degradation model proposed as expected when applied to the non-random ultrasonic degradation process.

(v) **Xu Model,** this model does not apply to the system studied.

3.2.4 Choice of Rate Models.

Of the five models examined, three had potential applications for studying rates in the ultrasonic degradation process. It was decided to apply these models to the results. The chosen rate models were those proposed by Schmid, Ovenall and Fujiwara. Plots are shown for all five of the suggested models using the results for the ultrasonic intensity study in figures 3.1 - 3.5. Clear deviations from linearity are observed in the two discarded models. In addition, figures 3.6 - 3.17 show the linear plots obtained for the Schmid, Ovenall and Fujiwara rate models for the remaining four parameters studied. These parameters will be discussed in more depth in the following sections.

### 3.3 Effect of the Ultrasound Intensity on the Degradation.

The probe system was calibrated as described in section 2.2.2, five generator intensity settings were used,

| Generator Setting | Intensity ($Wcm^{-2}$) |
|---|---|
| 2 | $12.3 \pm 0.5$ |
| 4 | $23.9 \pm 1.0$ |
| 6 | $37.4 \pm 1.6$ |
| 8 | $51.8 \pm 2.2$ |
| 10 | $66.5 \pm 2.8$ |

Figure 3.18 shows the variation of the number average molecular weight, $M_n$, with sonication time for the various intensities. The solution under examination was 1% w/v polyisobutylene in tetrahydrofuran sonicated at 25°C under a nitrogen atmosphere. The results indicate that the severity of bubble collapse is independent of

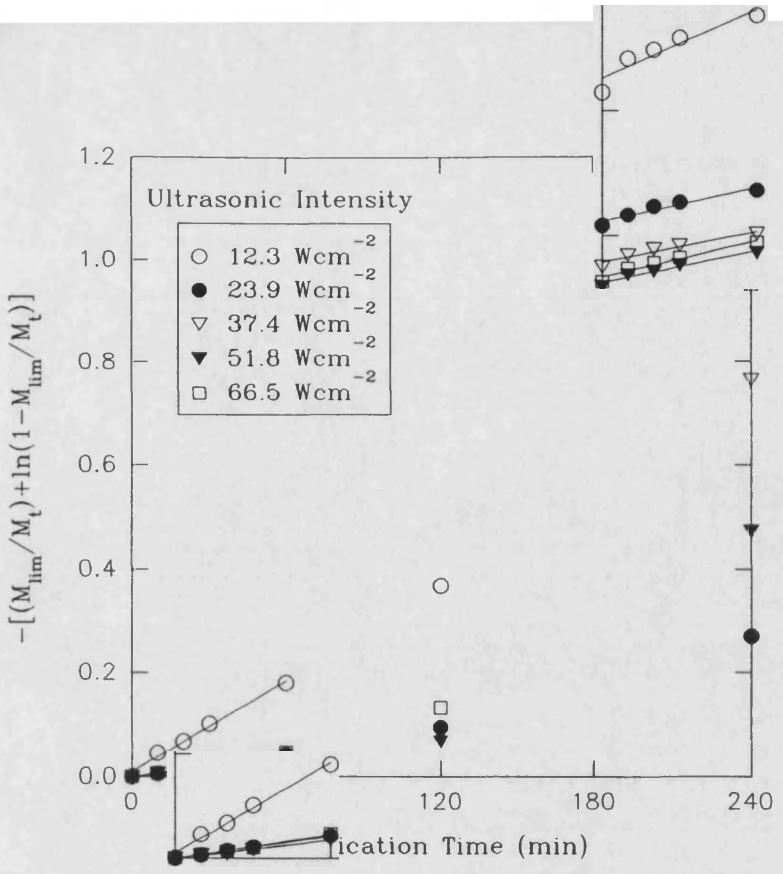


**FIGURE 3.1.** Schmid Rate Model Plot for the Sonication of 1% w/v PIB in THF at Various Ultrasonic Intensities.

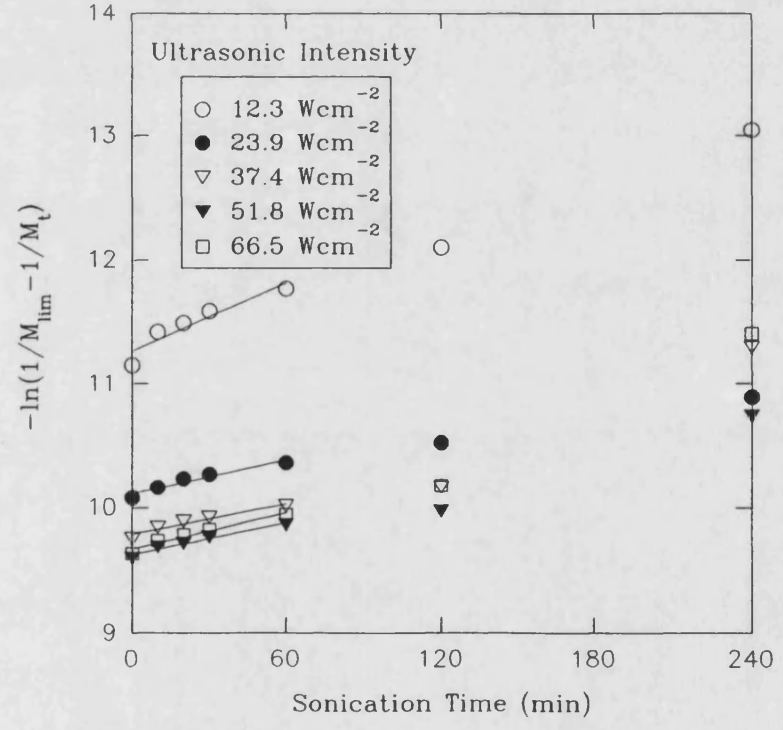


**FIGURE 3.2.** Ovenall Rate Model Plot for the Sonication of 1% w/v PIB in THF at Various Ultrasonic Intensities.

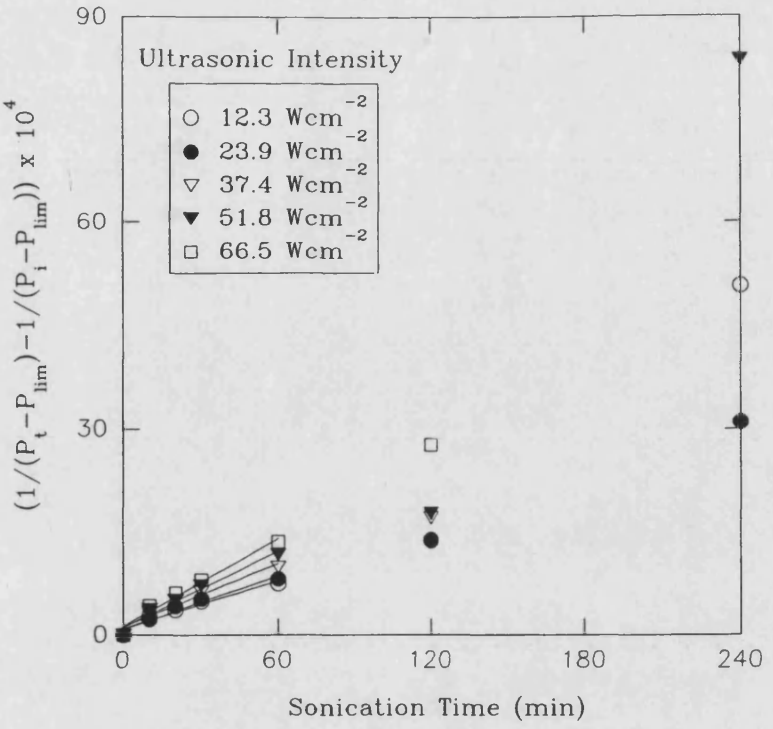


**FIGURE 3.3.** Fujiwara Rate Model Plot for the Sonication of 1% w/v PIB in THF at Various Ultrasonic Intensities.

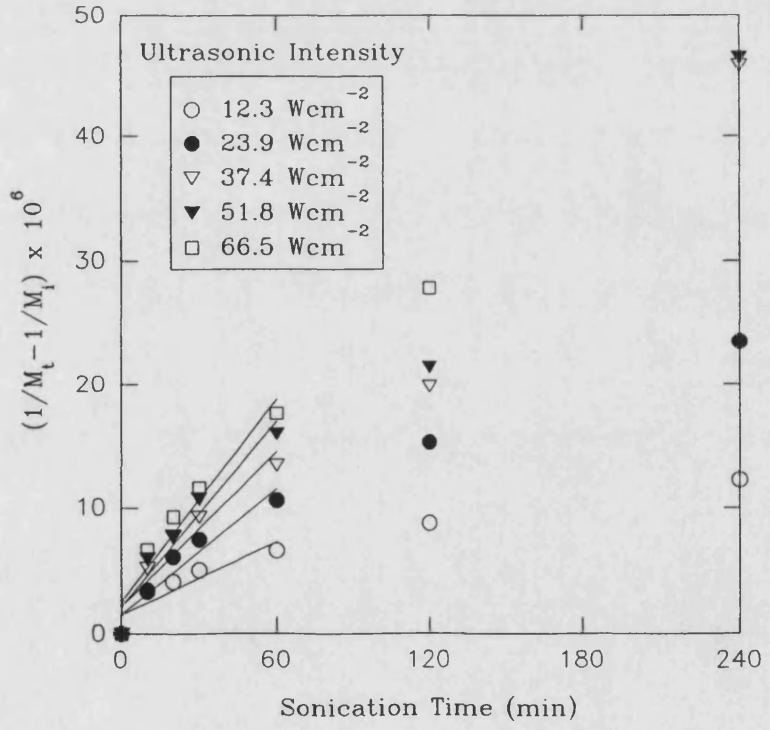


**FIGURE 3.4.** Sato and Nalepa Rate Model Plot for the Sonication of 1% w/v PIB in THF at Various Ultrasonic Intensities.

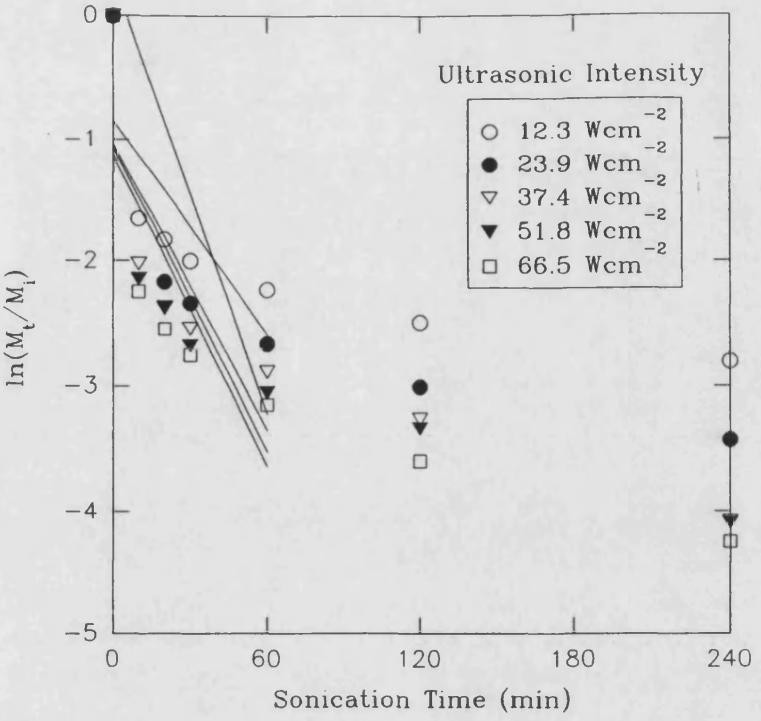


**FIGURE 3.5.** Xu Rate Model Plot for the Sonication of 1% w/v PIB in THF at Various Ultrasonic Intensities.

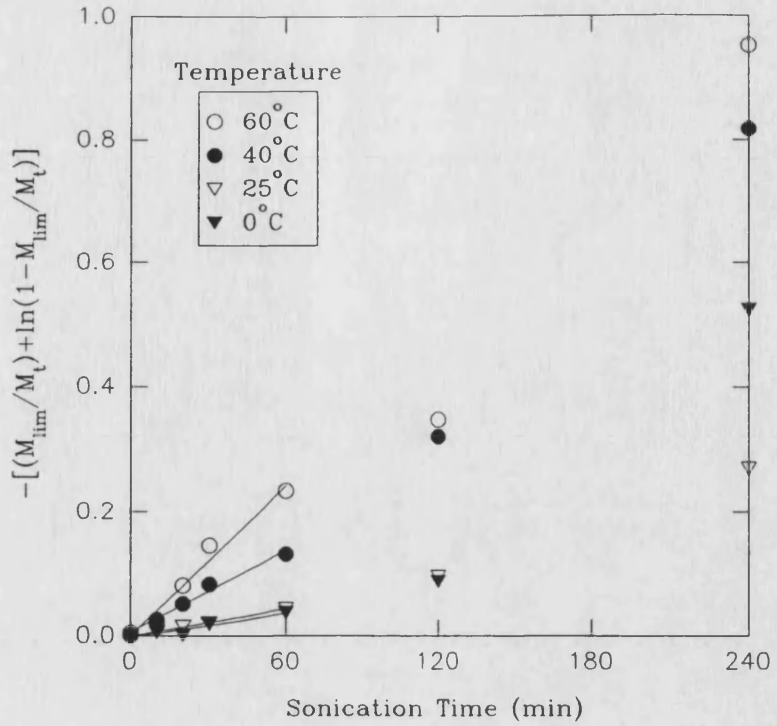


**FIGURE 3.6.** Schmid Rate Model Plot for the Sonication of 1% w/v PIB in THF at Various Temperatures.

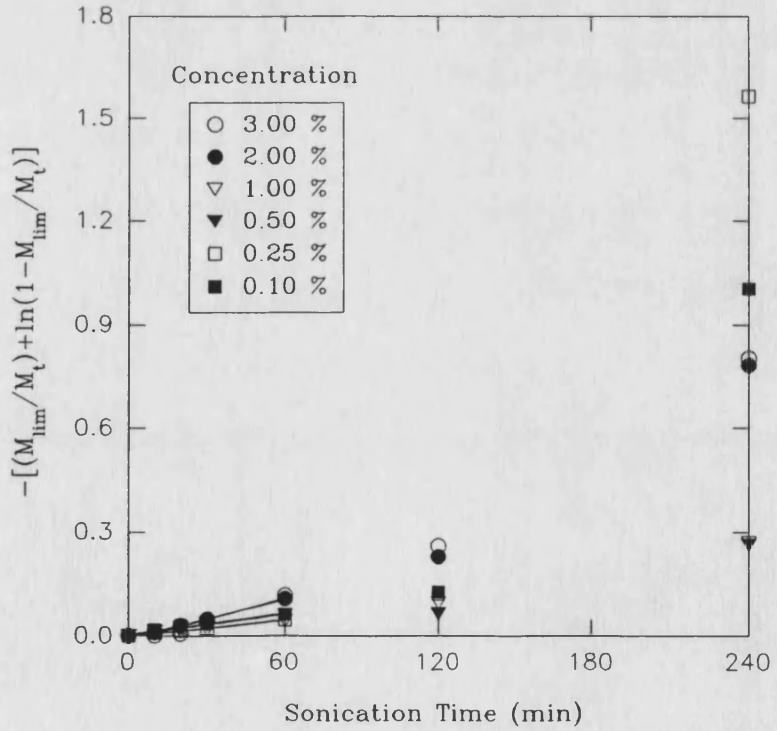


**FIGURE 3.7.** Schmid Rate Model Plot for the Sonication of PIB in THF at Various Concentrations.

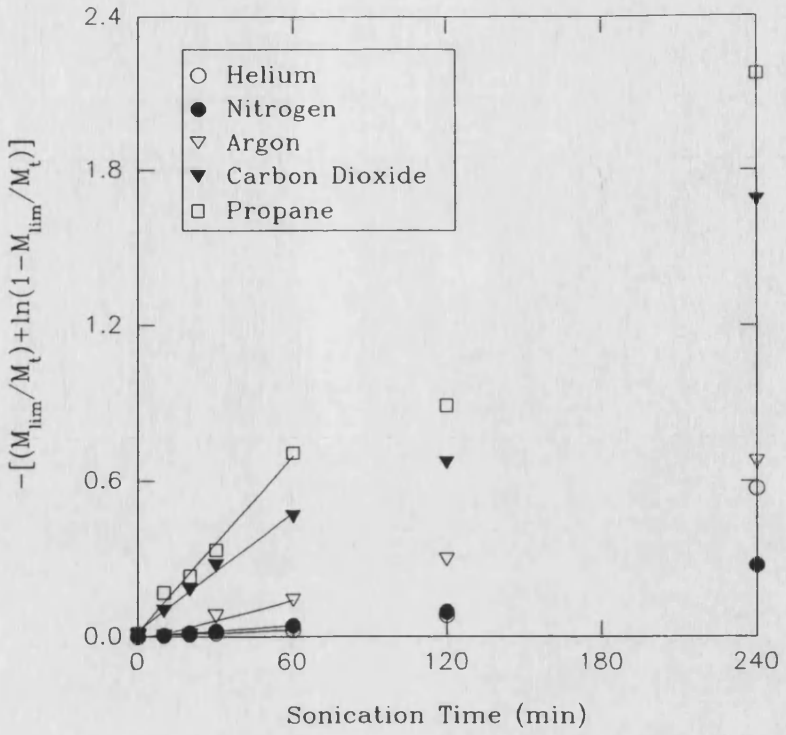


**FIGURE 3.8.** Schmid Rate Model Plot for the Sonication of 1% w/v PIB in THF Under Various Gaseous Atmospheres.

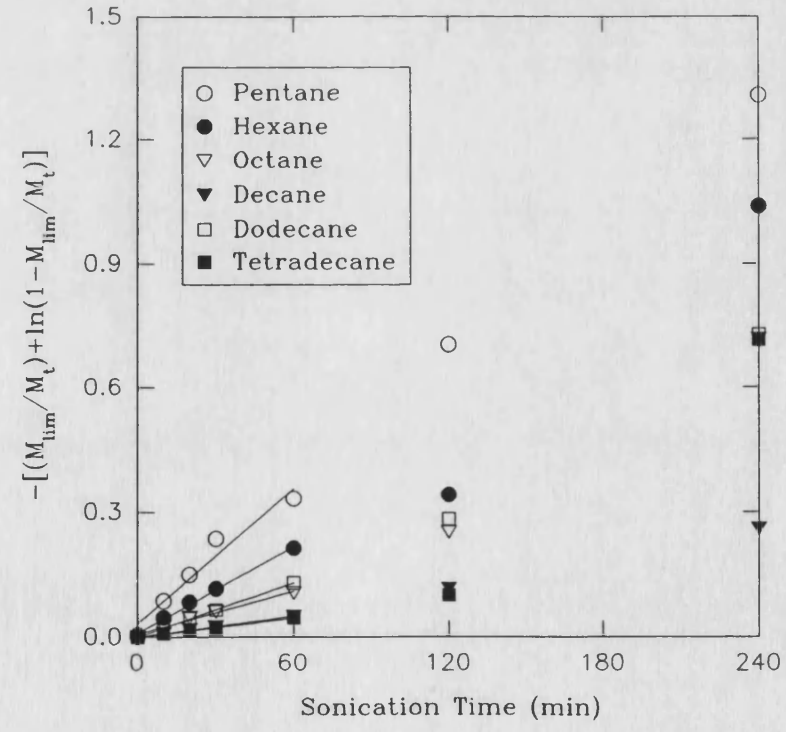


**FIGURE 3.9.** Schmid Rate Model Plot for the Sonication of 1% w/v PIB in Various n-Alkane Solvents.

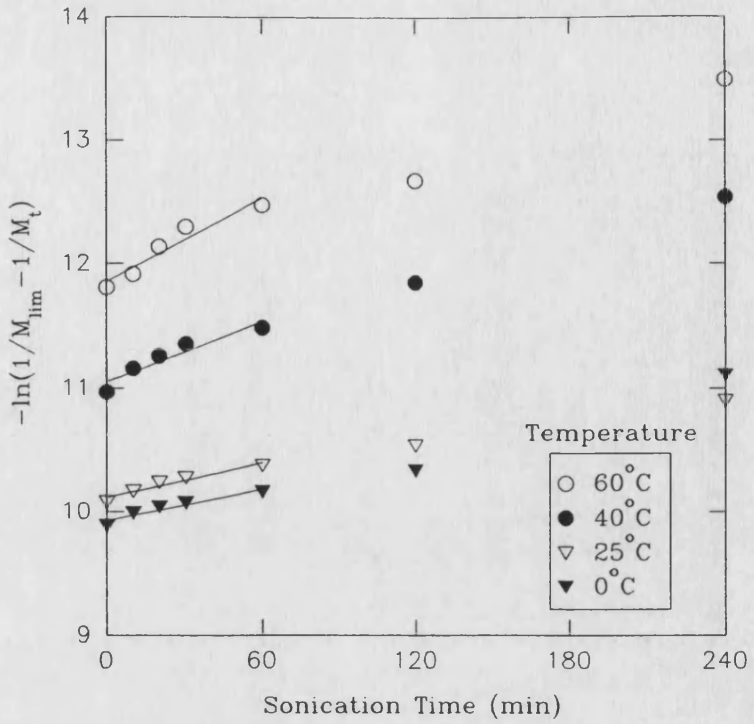


**FIGURE 3.10.** Ovenall Rate Model Plot for the Sonication of 1% w/v PIB in THF at Various Temperatures.

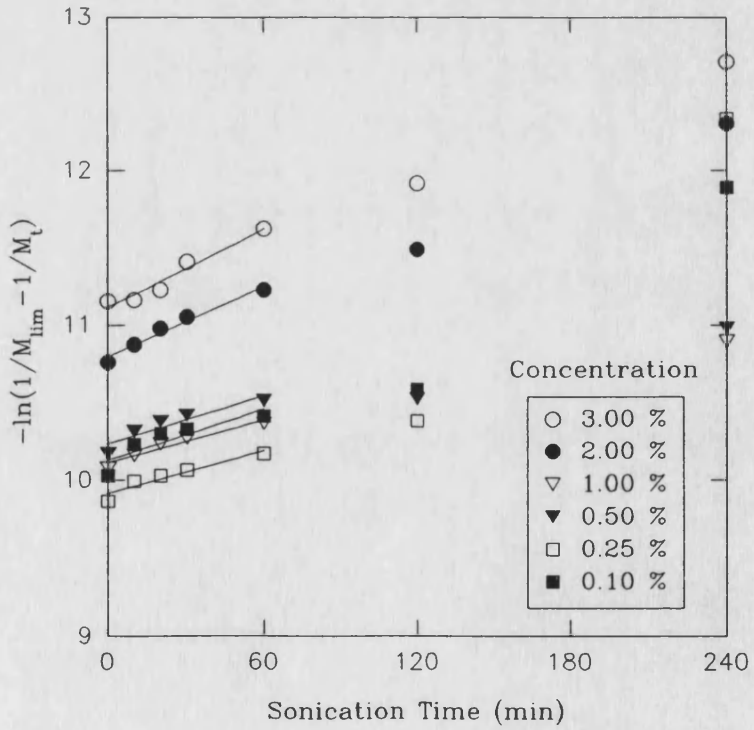


**FIGURE 3.11.** Ovenall Rate Model Plot for the Sonication of PIB in THF at Various Concentrations.

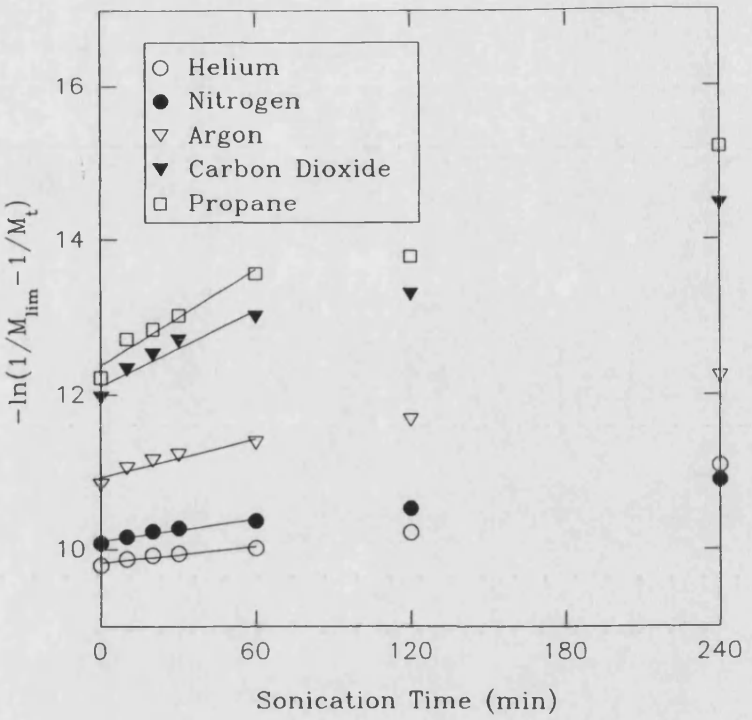


**FIGURE 3.12.** Ovenall Rate Model Plot for the Sonication of 1% w/v PIB in THF Under Various Gaseous Atmospheres.

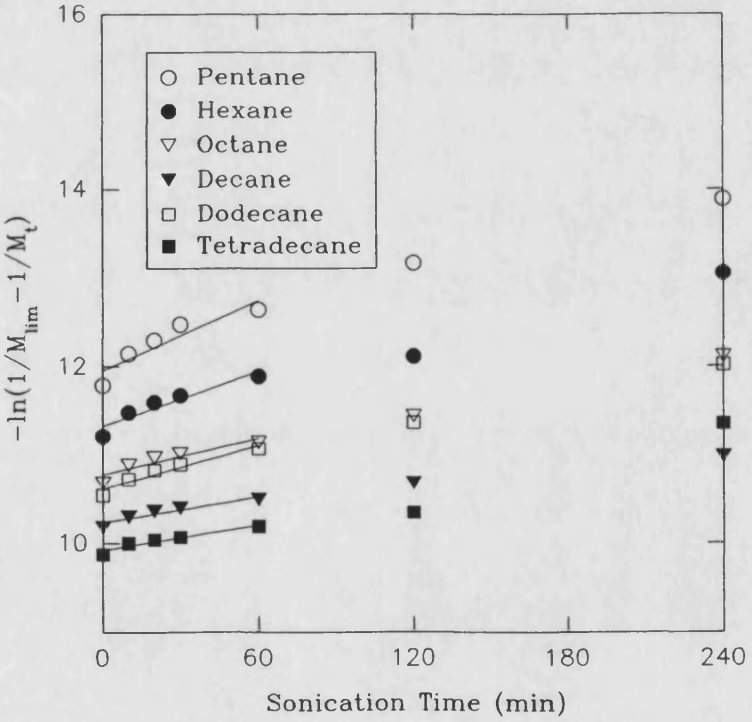


**FIGURE 3.13.** Ovenall Rate Model Plot for the Sonication of 1% w/v PIB in Various n-Alkane Solvents.

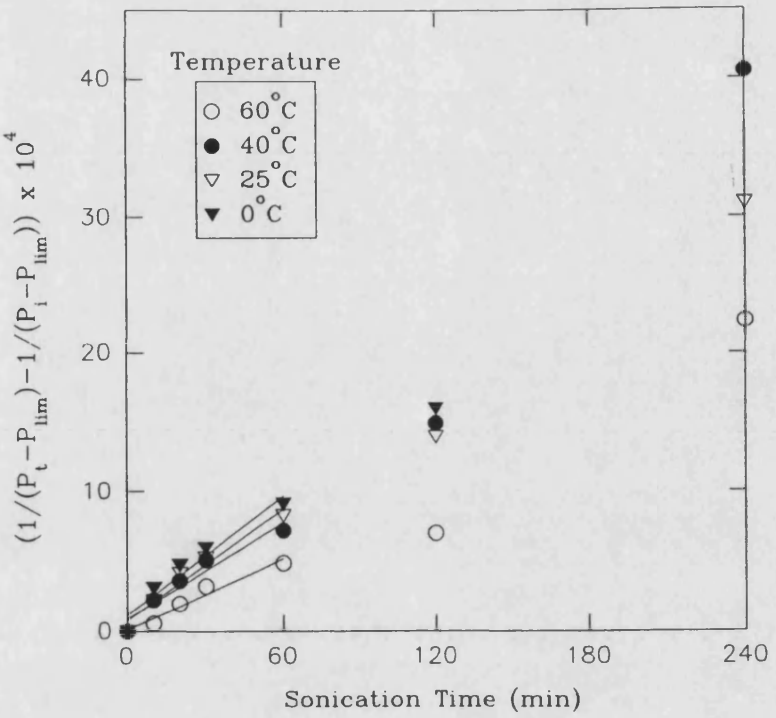


**FIGURE 3.14.** Fujiwara Rate Model Plot for the Sonication of 1% w/v PIB in THF at Various Temperatures.

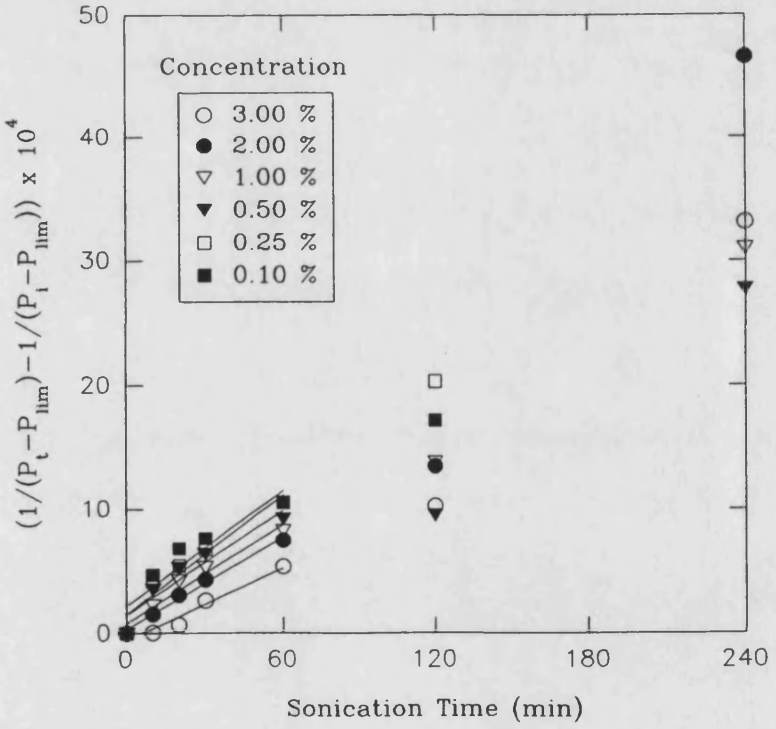


**FIGURE 3.15.** Fujiwara Rate Model Plot for the Sonication of PIB in THF at Various Concentrations.

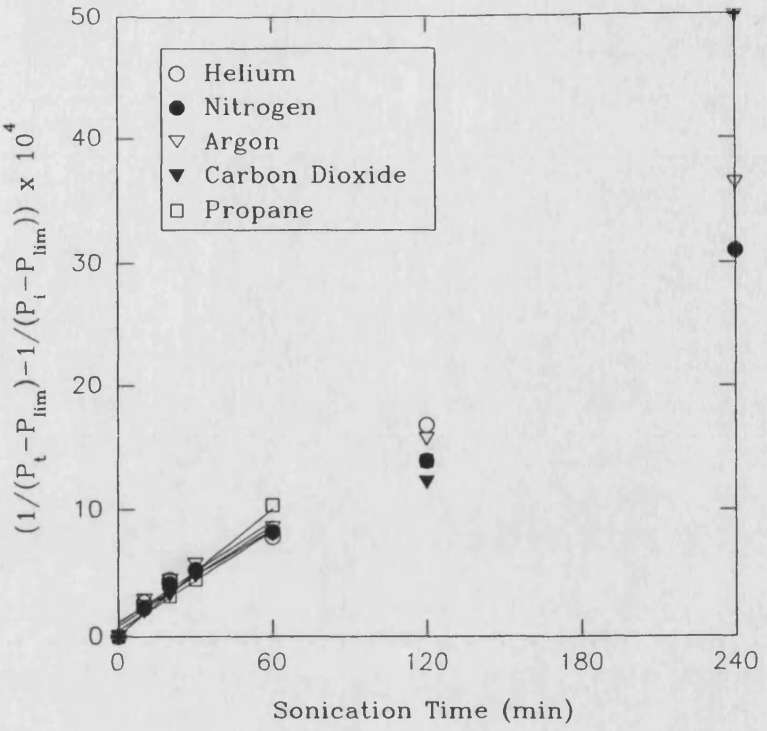


**FIGURE 3.16.** Fujiwara Rate Model Plot for the Sonication of 1% w/v PIB in THF Under Various Gaseous Atmospheres.

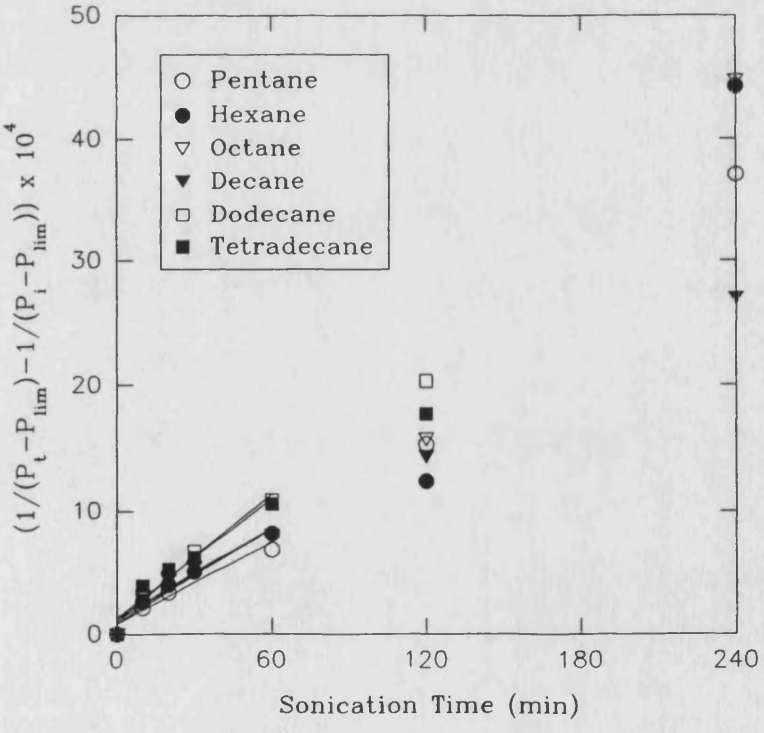


**FIGURE 3.17.** Fujiwara Rate Model Plot for the Sonication of 1% w/v PIB in Various n-Alkane Solvents.

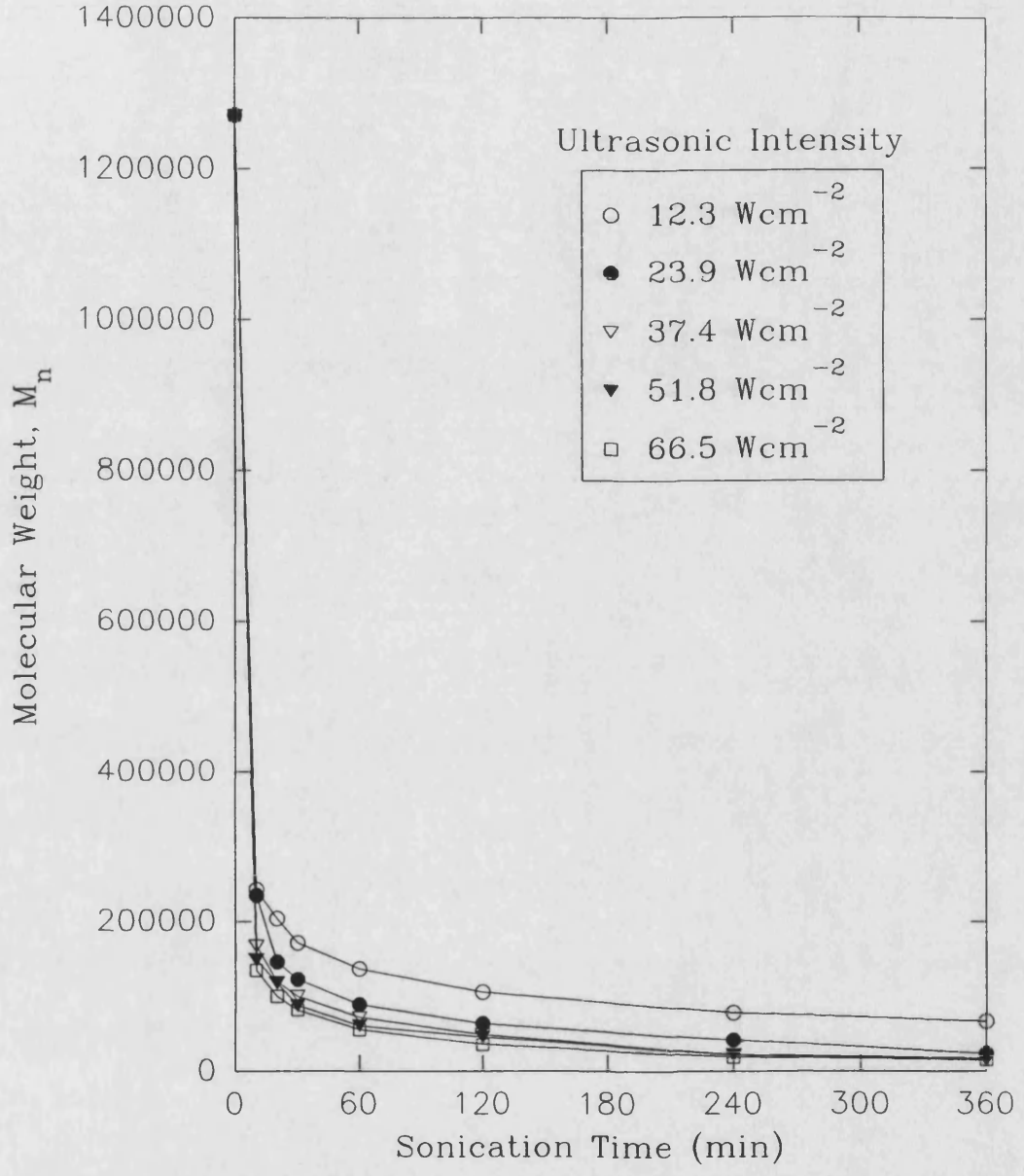


**FIGURE 3.18.** Variation of Number Average Molecular Weight During the Sonication of 1% w/v PIB in THF at Various Ultrasonic Intensities.

the ultrasound intensity as a significant effect is observed at the lowest power studied. At higher ultrasound intensities more cavitation events occur.

As predicted, at higher intensities, the degradation proceeds further and thus the limiting molecular weight reached, $M_{lim}$, decreases with increasing ultrasound intensity. This relationship is shown in figure 3.19. The curve appears to level out at higher intensities suggesting that at a certain intensity little further effect on $M_{lim}$ is observed.

As $M_n$ decreases, a similar effect is observed for $M_w$ resulting in an overall reduction in the molecular weight distribution or polydispersity, $\gamma$.

Figures 3.20 - 3.22 show the effect of intensity on the Schmid, Ovenall and Fujiwara degradation rate constants. The relationships are roughly linear with the linear correlations coefficients being 0.996, 0.985 and 0.997 respectively. A similar effect was observed by Jellinek[81] for the degradation of polystyrene in benzene using a rate model similar to the Schmid model applied here. This has also been observed by other workers including Mostafa[112]. In this study, a wide range of intensities were used, 12 - 67 $Wcm^{-2}$ and the linear relationship appeared to hold over the range. The equipment used would not allow higher intensities to be studied. Other workers[127] in our laboratory have noted a reduction in rate as an apparent intensity maximum is exceeded, above which no further effect is observed.

Figures 3.23 and 3.24 show the effect on the discarded rate models (Sato and Nalepa and Xu). There are deviations from the predicted linear relationship justifying their exclusion from future studies. The errors in all of the rate constants calculated arise mainly from uncertainties in the molecular weight averages determined by GPC estimated at ~5% throughout the range. The direct effect of this error on the absolute value of the rate constant is addressed in a subsequent section.

The linear trend observed would be expected considering the ultrasound theory proposed by Noltingk and Neppiras[50]. They suggested that the maximum radius, $R_m$, of a cavitation bubble reached during its growth is a function of the ultrasound intensity,

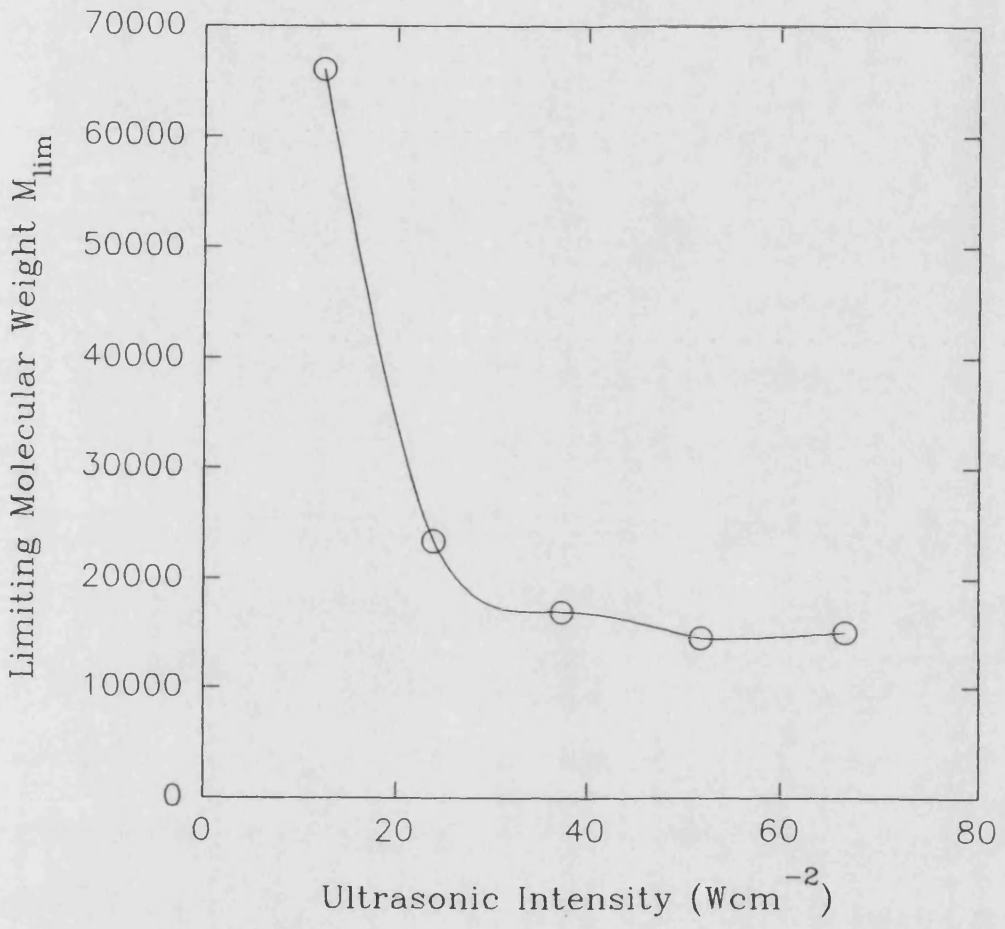


**FIGURE 3.19.** Effect of Ultrasonic Intensity on the Limiting Molecular Weight of PIB for the Sonication of a 1% w/v Solution in THF.

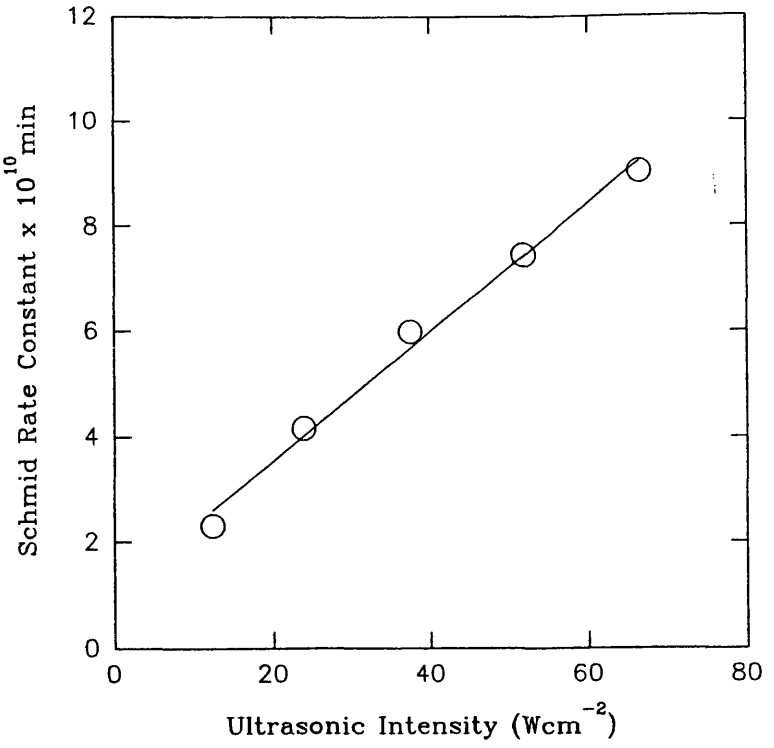


**FIGURE 3.20.** Effect of Ultrasonic Intensity on the Schmid Rate Constant for the Sonication of 1% w/v PIB in THF.

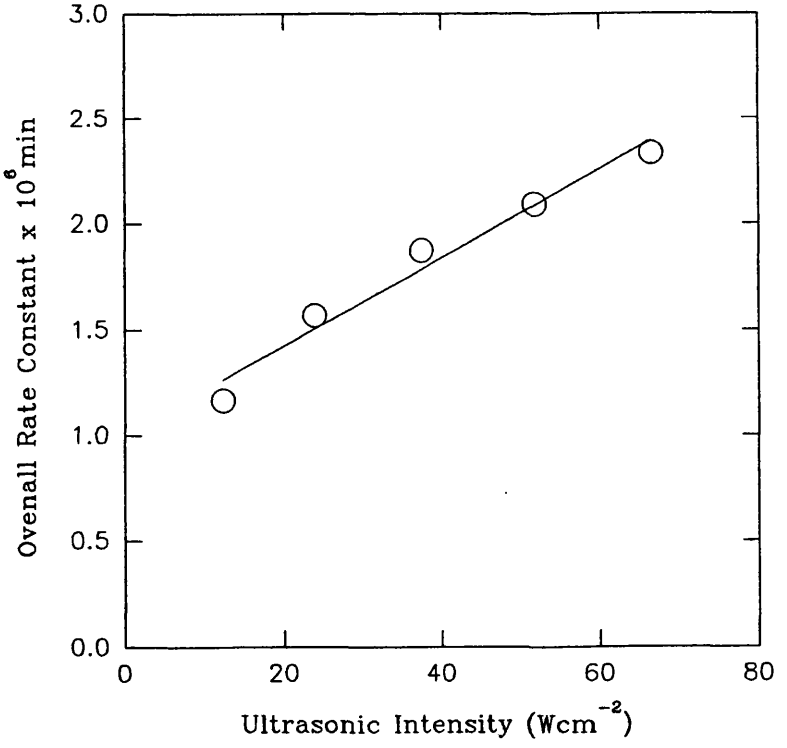


**FIGURE 3.21.** Effect of Ultrasonic Intensity on the Ovenall Rate Constant for the Sonication of 1% w/v PIB in THF.

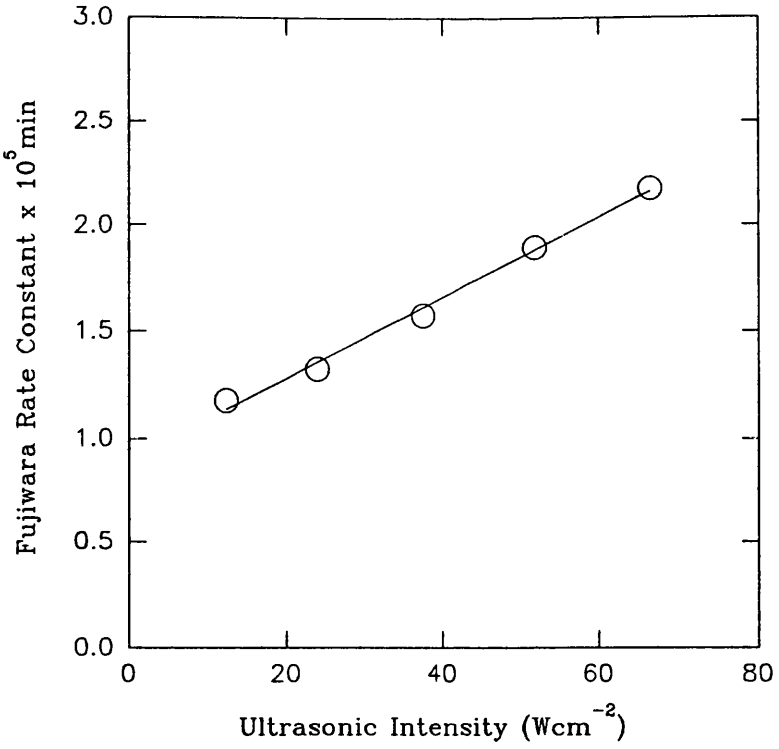


**FIGURE 3.22.** Effect of Ultrasonic Intensity on the Fujiwara Rate Constant for the Sonication of 1% w/v PIB in THF.

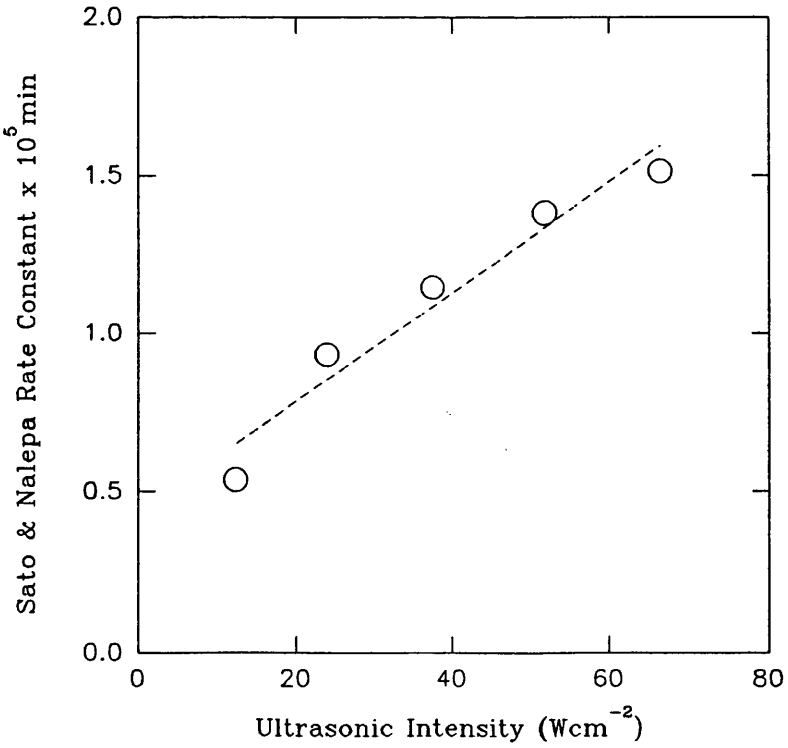


**FIGURE 3.23.** Effect of Ultrasonic Intensity on the Sato and Nalepa Rate Constant for the Sonication of 1% w/v PIB in THF.

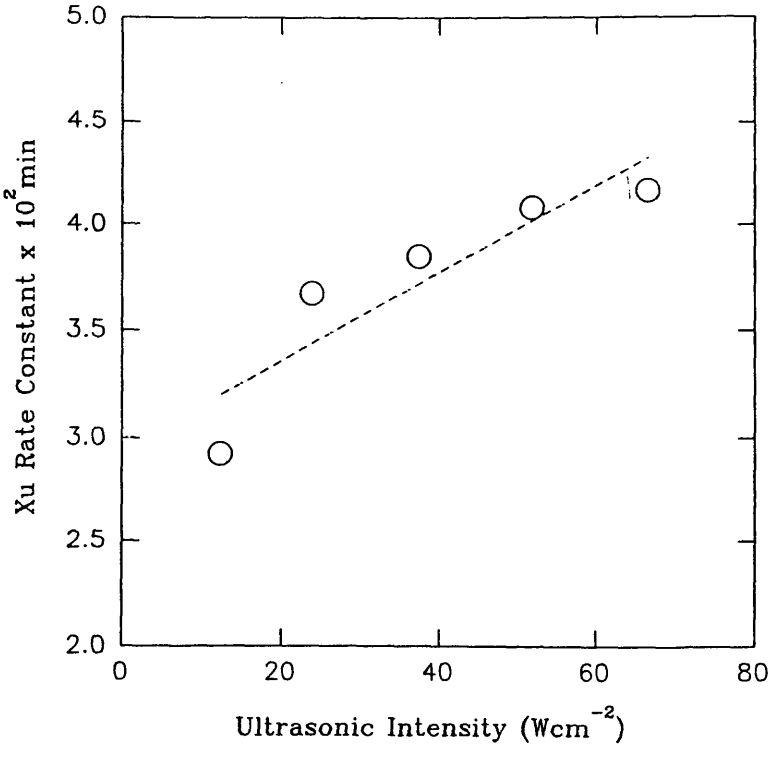


**FIGURE 3.24** Effect of Ultrasonic Intensity on the Xu Rate Constant for the Sonication of 1% w/v PIB in THF.

$$R_m = f(I^{1/2}) \qquad 3.11$$

hence, they predicted that any increase in ultrasound intensity will increase the size of the cavitation bubble produced resulting in greater forces acting following its collapse.

It should be appreciated, however, that intensity cannot be increased indefinitely and if it were increased to such an extent that there would be insufficient time between adjacent acoustic cycles for a transient collapse. This would result in a decrease in rate at very high ultrasound intensities.

### 3.4 Effect of Bulk Reaction Temperature on the Degradation.

The cavitational properties and behaviour of dilute polymer solutions are greatly affected by changes in temperature. Properties such as the saturated vapour pressure of the solution would be expected to influence the collapse of cavitation bubbles and thus affect the degradation of polymers in solution as this governs the gaseous contents of the bubbles immediately prior to collapse.

The effect of bulk reaction temperature on the degradation of 1%w/v polyisobutylene in tetrahydrofuran under a nitrogen atmosphere can be seen in figure 3.25. The graph shows that a faster rate of degradation is exhibited at lower temperatures reaching a lower limiting molecular weight, $M_{lim}$, as depicted in figure 3.26.

The results agree qualitatively with those of Malhotra[99] who reported enhanced degradation at -20°C for a series of poly(alkyl methacrylates) in toluene and tetrahydrofuran and Schmid and Beuttenmuller[128] who reported slower rates of degradation leading to higher limiting molecular weights at elevated temperatures when studying the solution degradation of polystyrene in toluene over the temperature range 40 - 120°C.

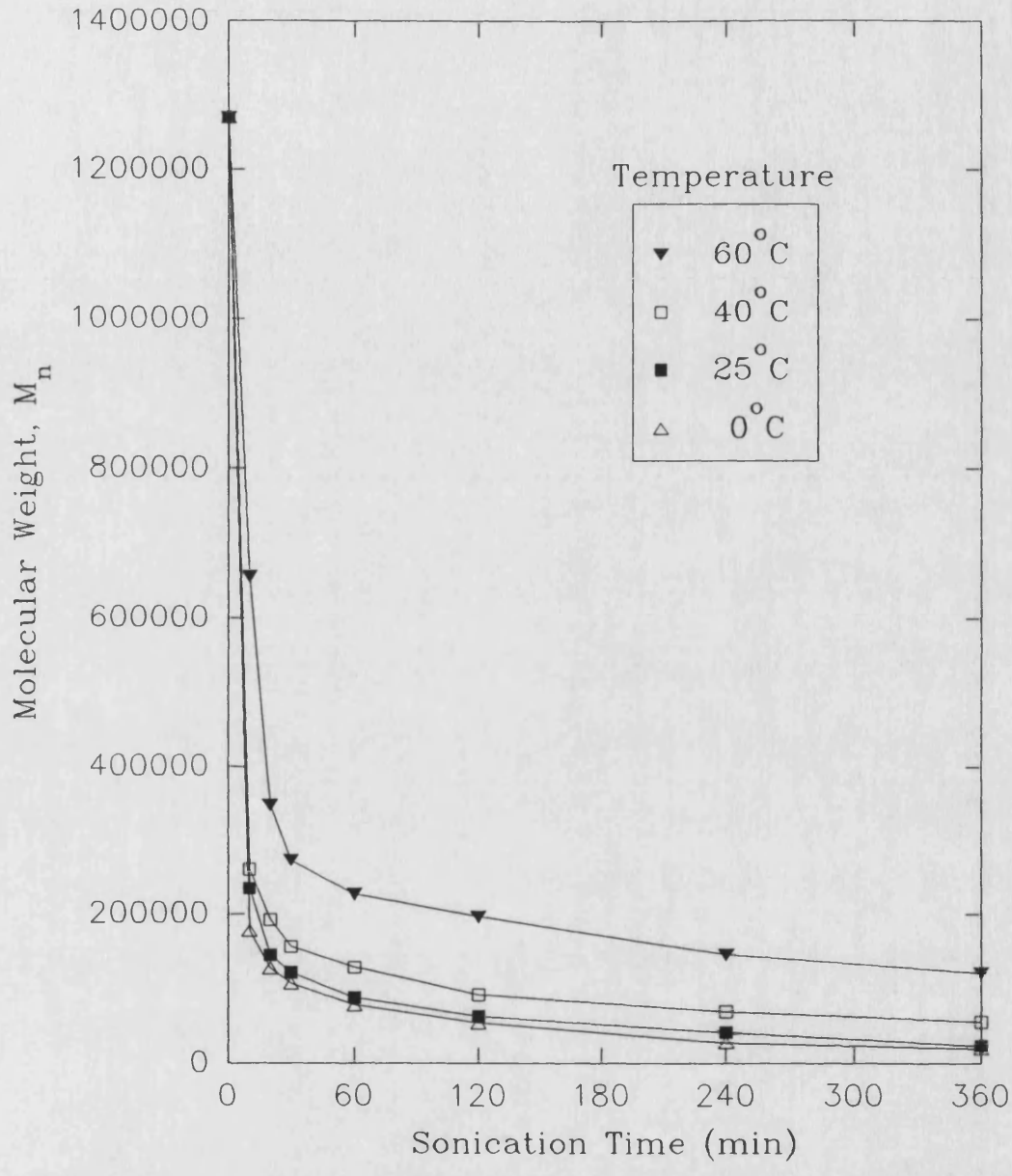


**FIGURE 3.25.** Variation of Number Average Molecular Weight During the Sonication of 1% w/v PIB in THF at Various Temperatures.

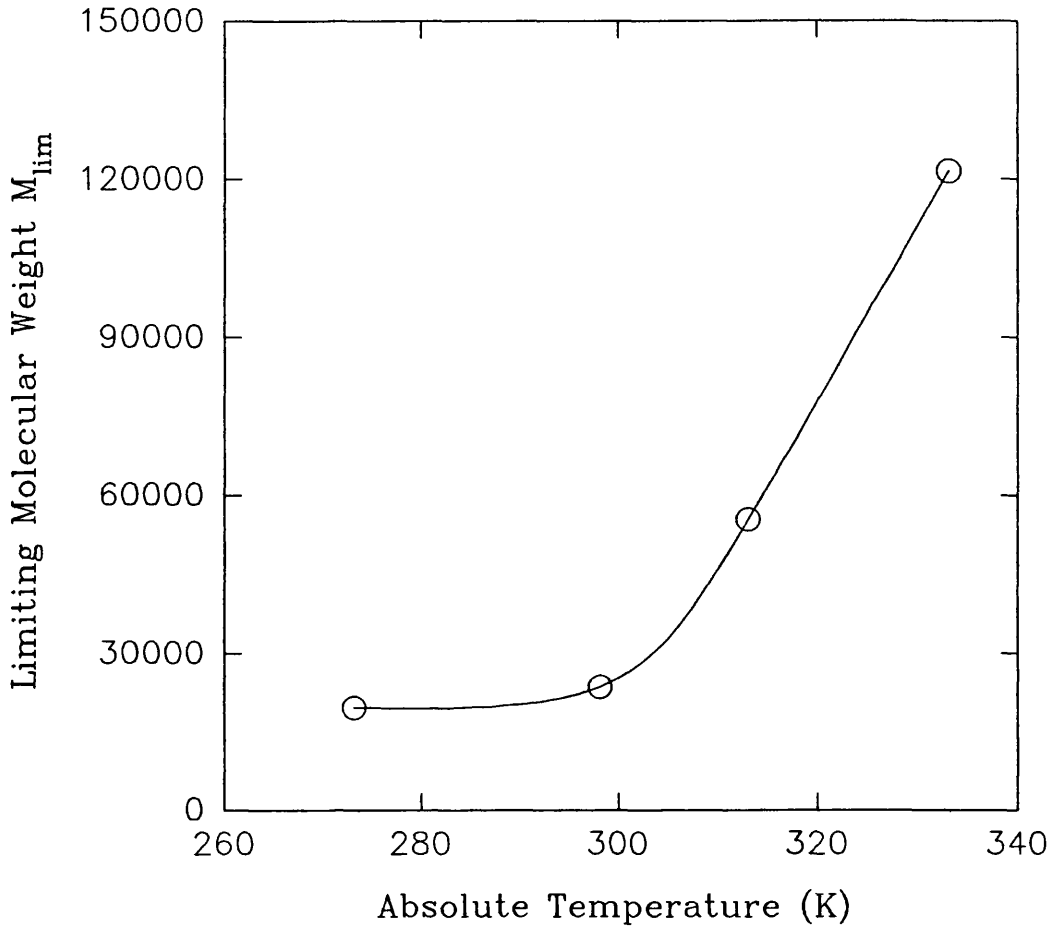


**FIGURE 3.26.** Effect of Absolute Temperature on the Limiting Molecular Weight of PIB for the Sonication of a 1% w/v Solution in THF.

The majority of chemical reactions are promoted by increases in temperature, the opposite effect is a characteristic of sonochemistry. This effect can be explained by considering the cavitation process. More solvent vapour will enter the cavitation bubble at higher temperatures producing a higher saturated vapour pressure and hence the cavitation bubble will be cushioned on collapse and the shock wave produced will be lessened.

This simple relationship can be seen in the Clausius-Clapeyron equation,

$$\ln P = -\frac{\Delta H_{vap}}{RT} + \text{constant} \qquad 3.12$$

where $\Delta H_{vap}$ is the heat of vaporisation of the solvent, R is the molar gas constant, T is the absolute temperature of the solution and P is the saturated vapour pressure.

At lower temperatures less solvent vapour will enter the cavitation bubble and thus the implosive collapse will be less cushioned so that the shock wave produced will be more severe causing more degradation.

Temperature therefore has a pronounced effect on the rate of degradation, Table 3.2 shows the magnitude of the rate constants at various absolute temperatures. The associated absolute error predicted from the errors arising from the determination of molecular weights by GPC is also shown in the table.

**TABLE 3.2.** Degradation Rate Constants for 1% w/v Polyisobutylene in THF at Various Absolute Temperatures.

| | RATE CONSTANT / $min^{-1}$ | | |
|---|---|---|---|
| **Absolute Temperature (K)** | **Schmid x $10^{10}$** | **Ovenall x $10^{6}$** | **Fujiwara x $10^{5}$** |
| 333.15 | 1.02 ± 0.15 | 0.78 ± 0.07 | 1.11 ± 0.16 |
| 313.15 | 2.77 ± 0.38 | 1.29 ± 0.10 | 1.66 ± 0.19 |
| 298.15 | 4.15 ± 0.48 | 1.57 ± 0.10 | 1.77 ± 0.14 |
| 273.15 | 5.18 ± 0.60 | 1.74 ± 0.11 | 1.94 ± 0.15 |

All of the chosen rate models show the highest rate constant at 273.15K (0°C). Figures 3.27 - 3.29 show the relationship between the rate constants and the absolute temperature with the estimated error bars included. It is possible to apply the values to the Arrhenius equation,

$$\ln k = \ln A - \frac{E_A}{RT} \qquad 3.13$$

where k is the rate constant at the absolute temperature, T, $E_A$ is the Arrhenius activation energy, R is the molar gas constant and A is the pre-exponential factor which is independent of temperature. This gives the opportunity to calculate an activation energy for the degradation process. A plot of lnk versus 1/T is shown in figure 3.30, the value of $E_A$ is calculated from the gradient of $-E_A/R$. Error bars are included on the graph allowing an error in $E_A$ to be quoted.

Normally the activation energy yields a positive value as chemical reaction rates usually increase with increasing temperature. In the case of the ultrasonic degradation an effective negative Arrhenius activation energy is found emphasising the fact that

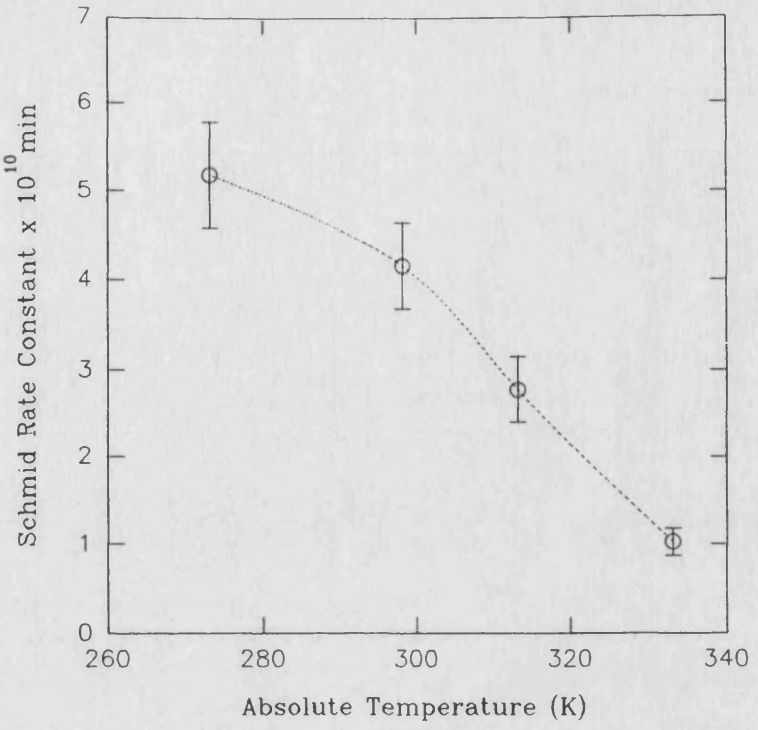


**FIGURE 3.27.** Effect of Absolute Temperature on the Schmid Rate Constant for the Sonication of 1% w/v PIB in THF.

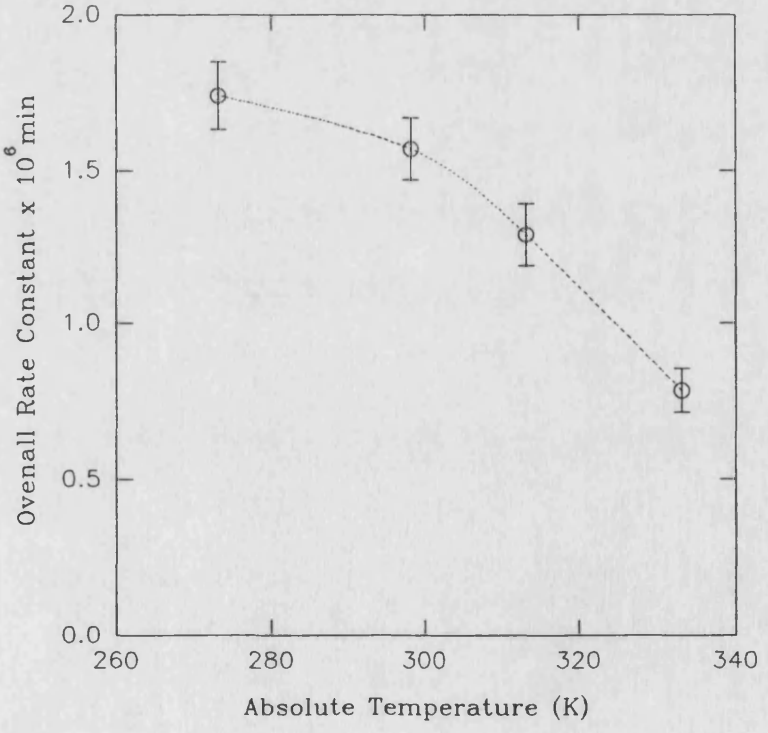


**FIGURE 3.28.** Effect of Absolute Temperature on the Ovenall Rate Constant for the Sonication of 1% w/v PIB in THF.

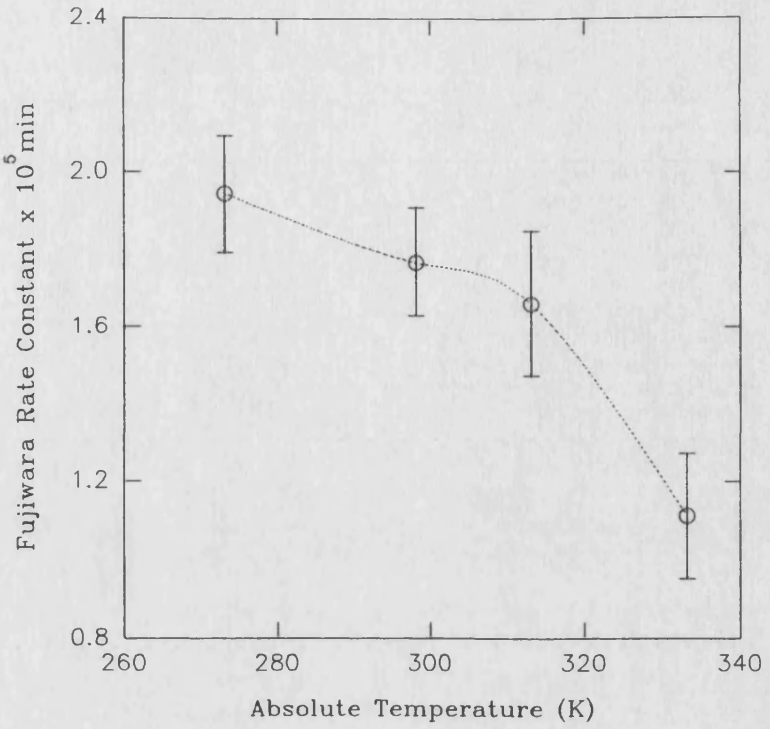


**FIGURE 3.29.** Effect of Absolute Temperature on the Fujiwara Rate Constant for the Sonication of 1% w/v PIB in THF.

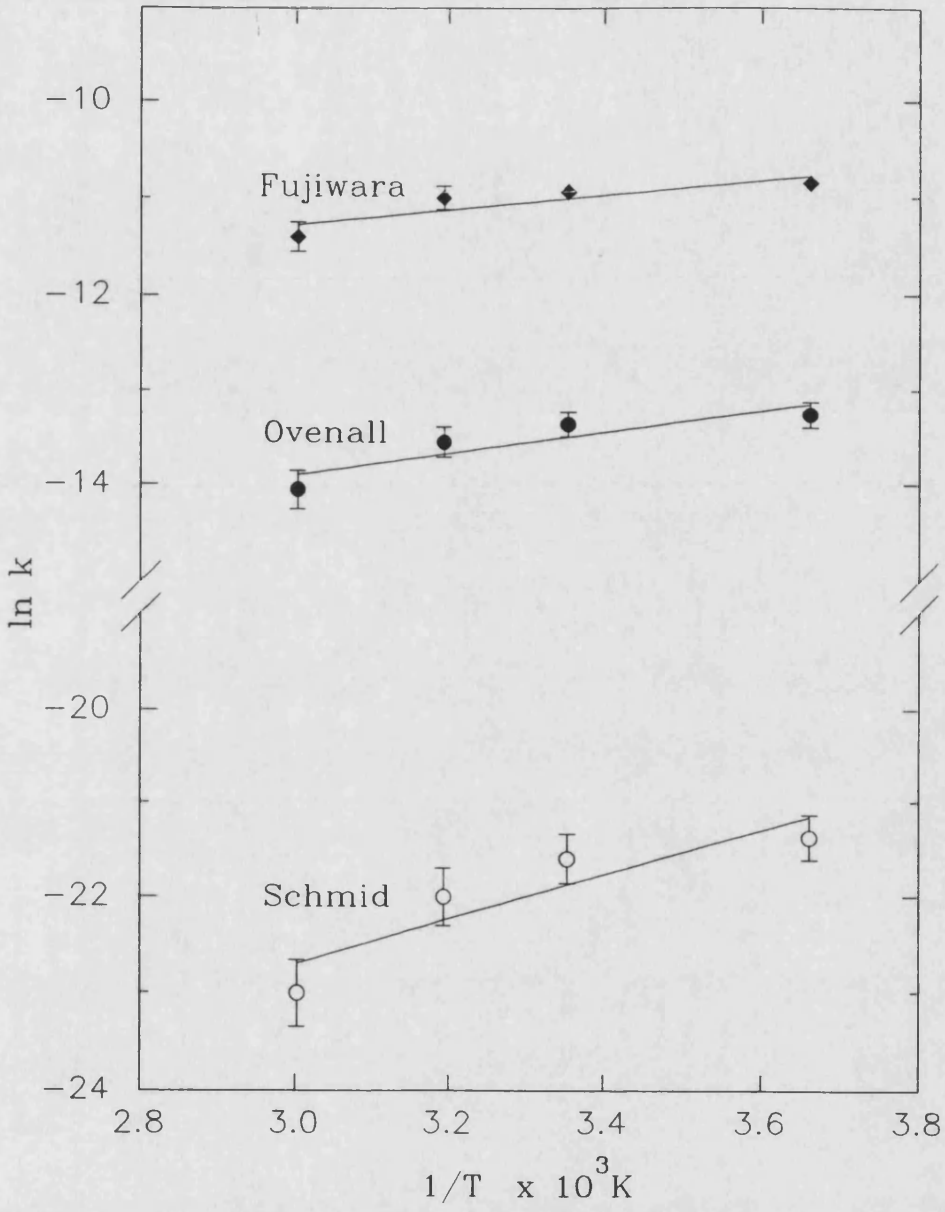


**FIGURE 3.30.** Arrhenius Plot to Calculate the Activation Energy for the Degradation of 1% w/v PIB in THF Using Different Rate Models.

ultrasonic reactions proceed more quickly at reduced temperatures. The results are shown in Table 3.3.

TABLE 3.3. Apparent Arrhenius Activation Energies for Rate Models Employed.

| | APPARENT ARRHENIUS ACTIVATION ENERGY, $E_A$. |
|---|---|
| Schmid Rate Model | $-19 \pm 4$ kJmol$^{-1}$ |
| Ovenall Rate Model | $-10 \pm 2$ kJmol$^{-1}$ |
| Fujiwara Rate Model | $-6 \pm 2$ kJmol$^{-1}$ |

Each rate model predicts a small negative activation energy for the process, with the associated errors this value approximates to -12 kJmol$^{-1}$ for polyisobutylene.

### 3.5 Effect of Polymer Solution Concentration on the Degradation.

The effect of polymer solution concentration was studied in two solvents, tetrahydrofuran and hexane as the proximity of the polymer chains would be expected to affect a mechanical degradation process. In each solvent, concentrations were sonicated ranging from 0.1% w/v up to 3.0% w/v which was found to be the maximum concentration attainable due to the solubility limit of the high molecular weight polymer.

Figures 3.31 and 3.32 show that the degradations are similar in character for both of the solvents studied. The degradations appear much faster in the less concentrated solutions reaching a lower limiting molecular weight. The effect of polymer solution concentration on the value of $M_{lim}$ in both solvents can be seen in figure 3.33.

Other researchers[95,96] have also reported a decrease in degradation at high solution concentrations and this can be explained by considering the motion of polymer

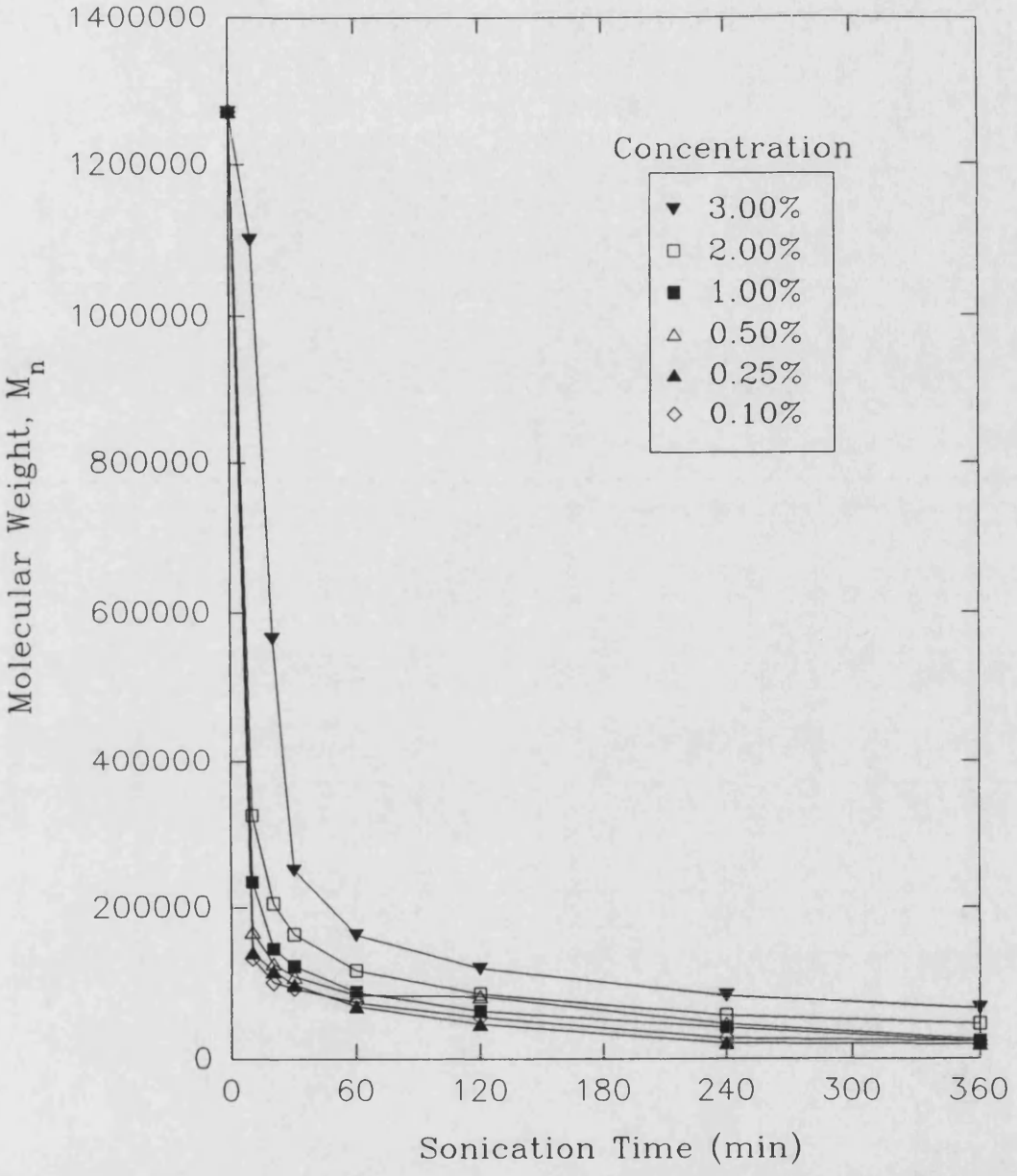


**FIGURE 3.31.** Variation of Number Average Molecular Weight During the Sonication of PIB in THF at Various Concentrations.

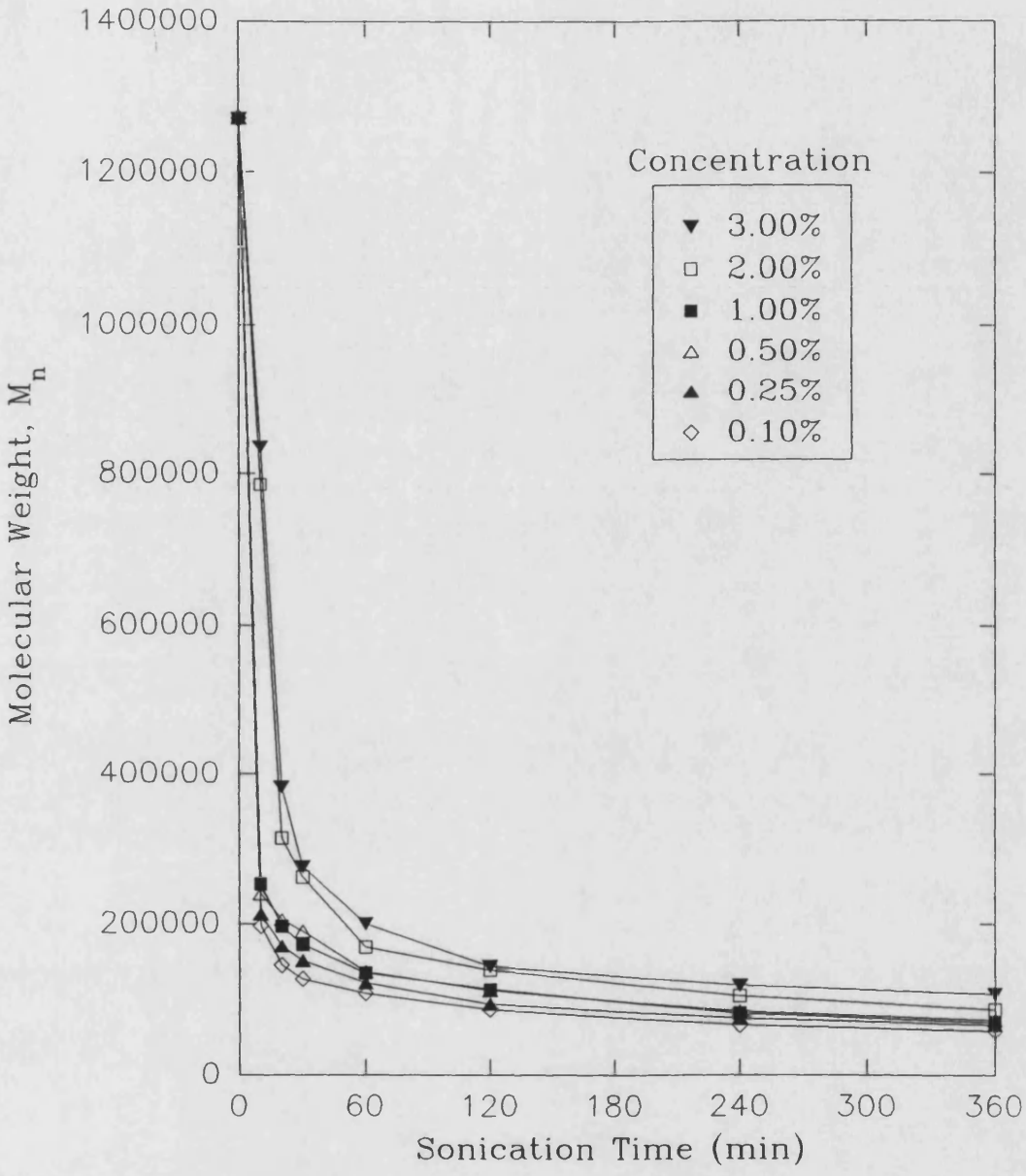


**FIGURE 3.32.** Variation of Number Average Molecular Weight During the Sonication of PIB in Hexane at Various Concentrations.

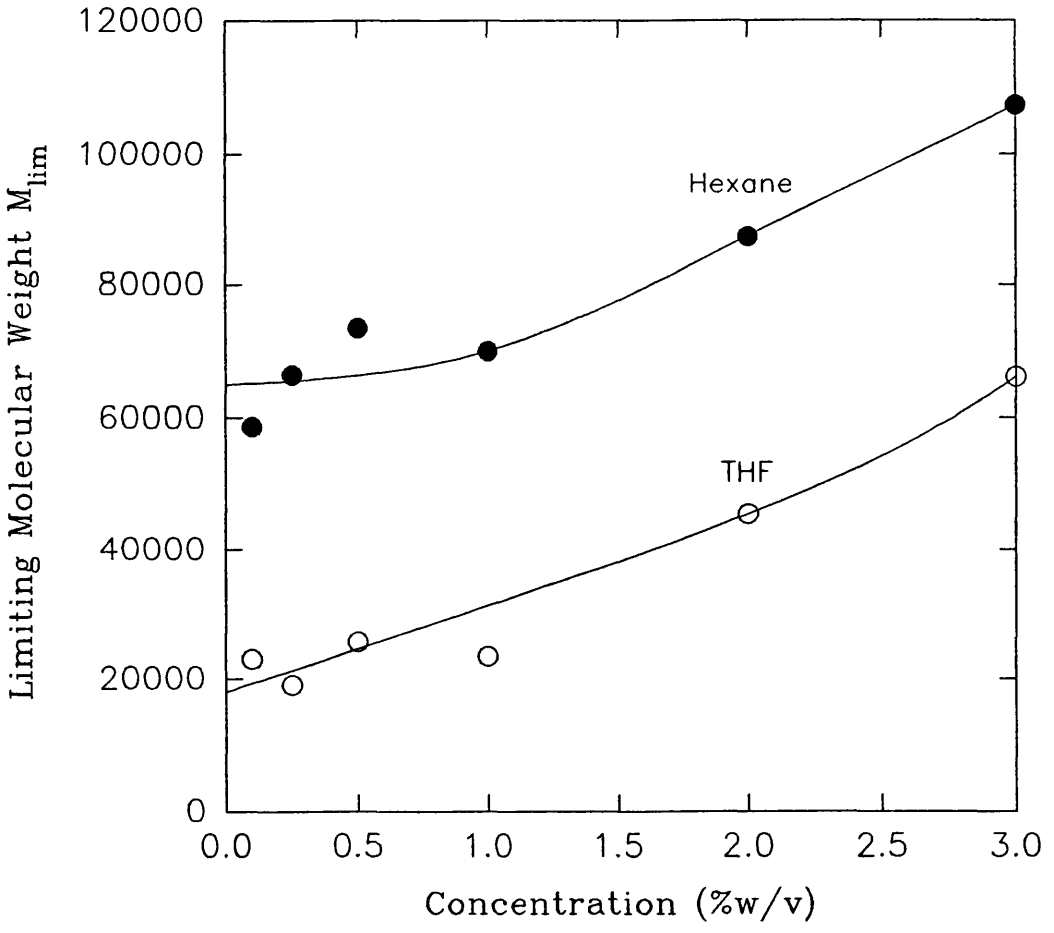


**FIGURE 3.33.** Effect of Concentration on the Limiting Molecular Weight of PIB for the Sonication in THF and Hexane.

chains around imploding cavities[123]. In very dilute polymer solutions it can be assumed that there will be no association between polymer molecules. When the cavitation bubble implodes, very large pressures and velocity gradients are produced in the surrounding liquid. Since the polymer chain occupies a relatively large volume, with sufficiently large velocity gradients, the side of the polymer chain nearest to the side of the collapsing cavity will move at a higher velocity than the side of the chain away from the site. This produces stresses in the polymer chain responsible for bond cleavage, reduction in molecular weight and hence degradation.

As the solution concentration is increased, the effect produced by the flow field of polymer chains in solution will be less important due to the large number of chains hindering the flow and motion of polymer molecules towards the site of the imploding cavities and hence lessening the effect. In this more concentrated solution, the polymer molecules nearest the site of the implosion will still be affected but the range of the shock wave produced will be greatly reduced as a result of the increased viscosity of the solution, hence the overall reduction in the molecular weight will be less.

The effect of concentration on the three degradation rate constants can be seen in figures 3.34 - 3.39. The results in tetrahydrofuran show, for the Schmid and Ovenall rate models, an increase in rate with concentrations up to approximately 2.0% w/v after which higher concentrations result in a decrease in rate. In hexane, the Schmid and Ovenall rate models appear to indicate that the rate constant continues to increase with concentration. This suggests that the polymer adopts a different conformation in hexane. The Fujiwara rate model shows a decrease in rate with increasing concentration as would be expected.

The reduction in rate at high concentrations in THF can be attributed to the point where the polymer chains begin to overlap. This will result in a marked reduction in cavitational efficiency. This critical overlap concentration, C*, at which the chains begin to entangle is shown in figure 3.40.

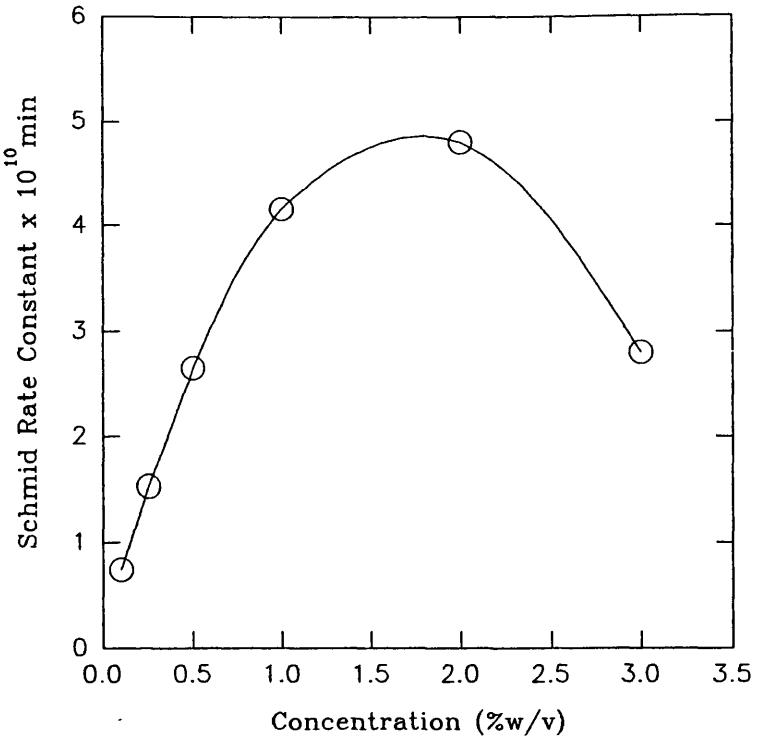


**FIGURE 3.34.** Effect of Concentration on the Schmid Rate Constant for the Sonication of PIB in THF.

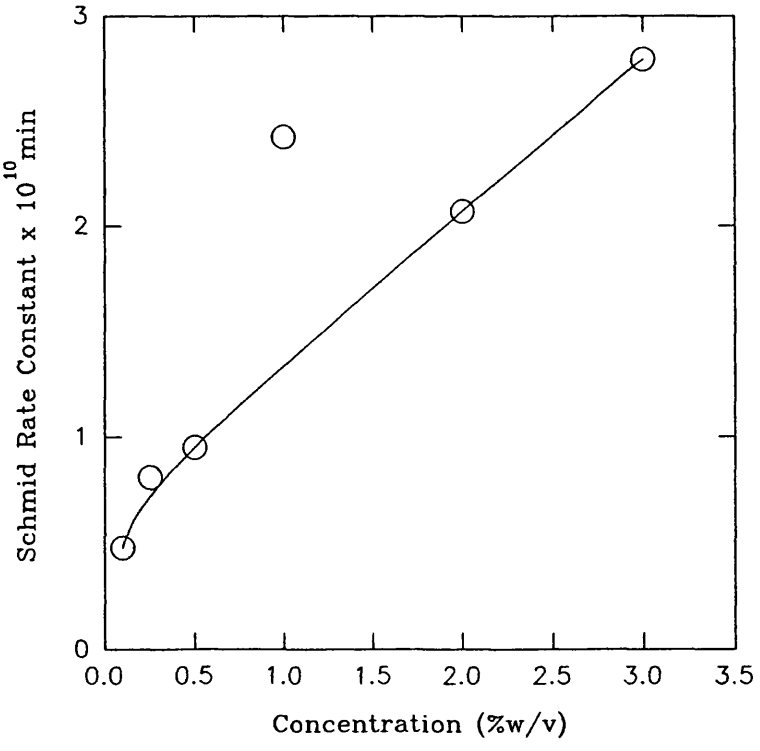


**FIGURE 3.35.** Effect of Concentration on the Schmid Rate Constant for the Sonication of PIB in Hexane.

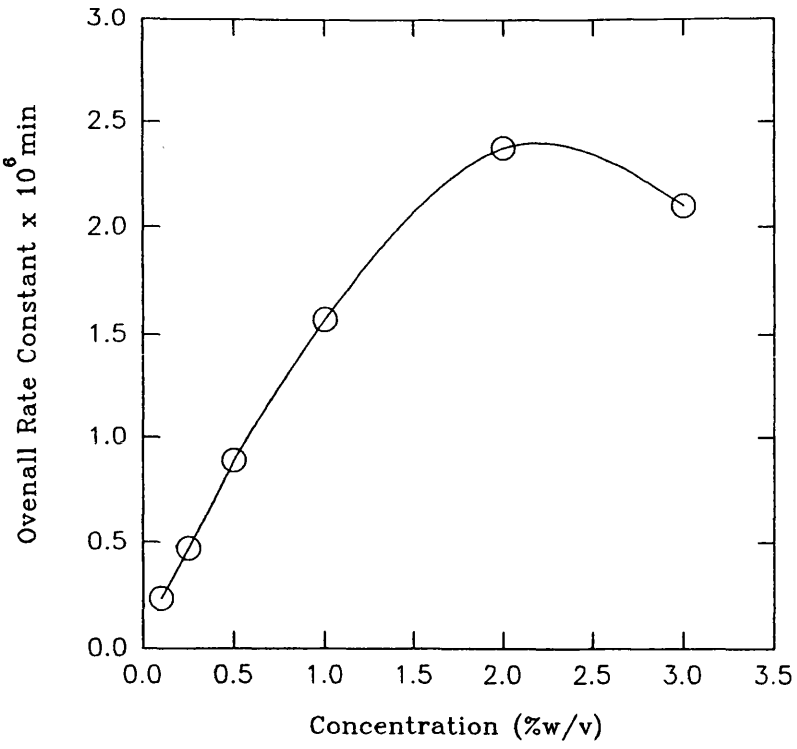


**FIGURE 3.36.** Effect of Concentration on the Ovenall Rate Constant for the Sonication of PIB in THF.

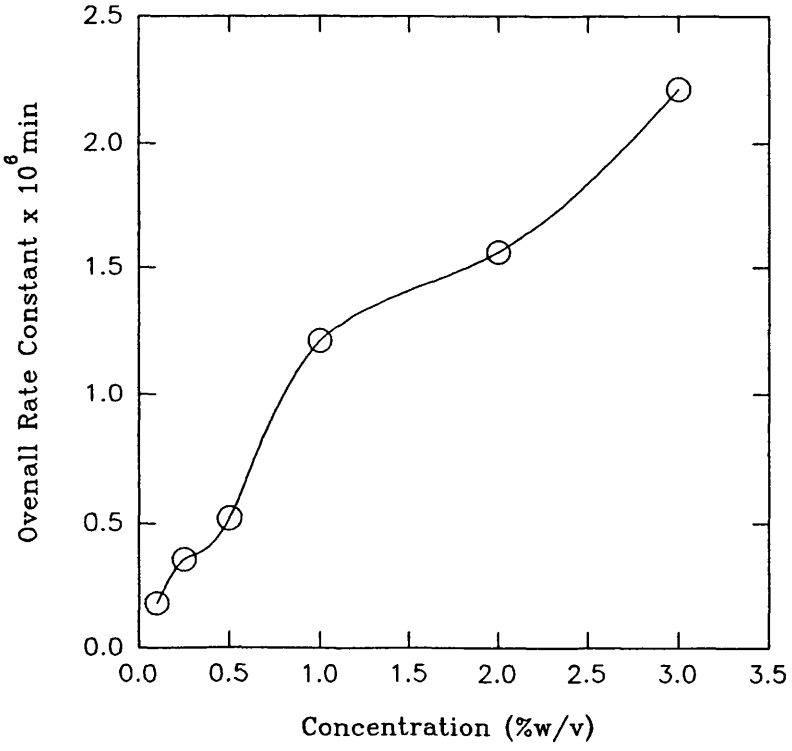


**FIGURE 3.37.** Effect of Concentration on the Ovenall Rate Constant for the Sonication of PIB in Hexane.

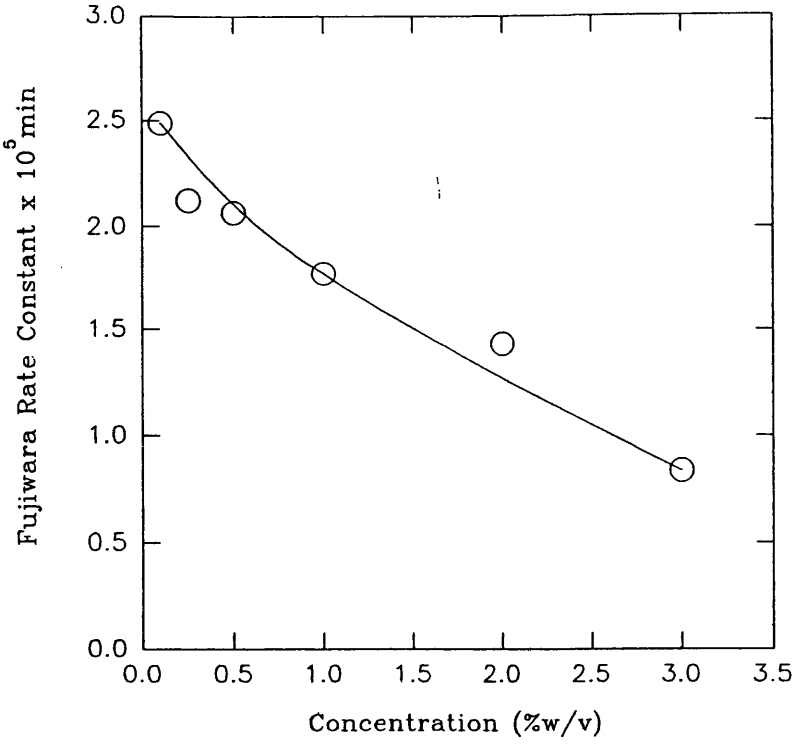


**FIGURE 3.38.** Effect of Concentration on the Fujiwara Rate Constant for the Sonication of PIB in THF.

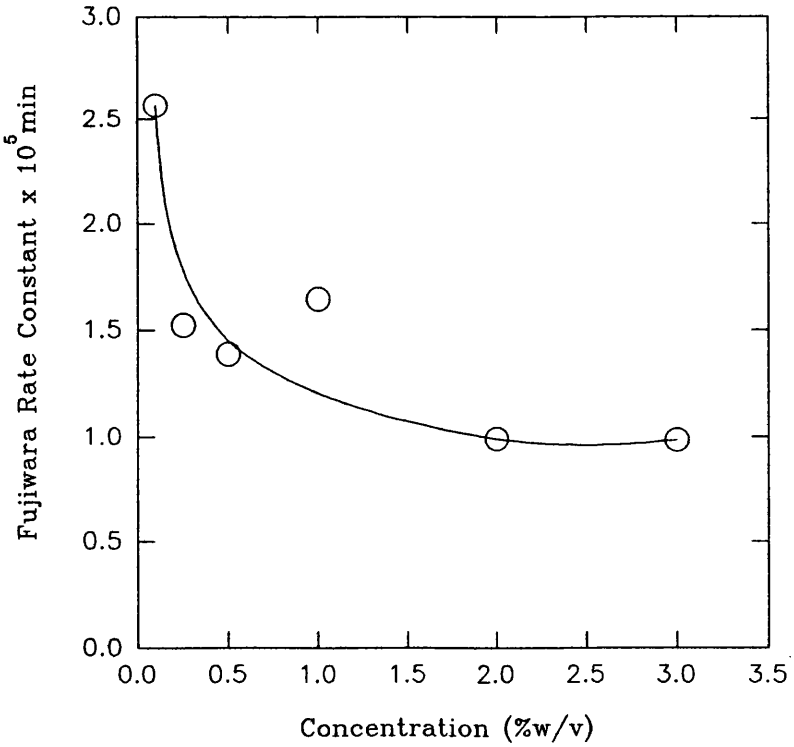


**FIGURE 3.39.** Effect of Concentration on the Fujiwara Rate Constant for the Sonication of PIB in Hexane.

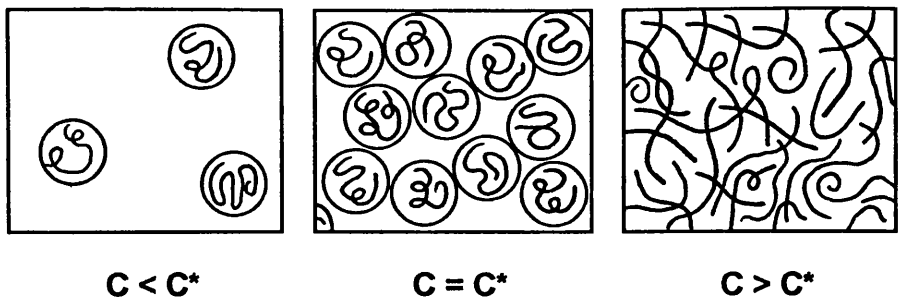


**FIGURE 3.40.** Conformations of Chains in Solution Showing the Critical Overlap Concentration, C*.

As the chains begin to overlap, there is more restriction to movement and on cleavage, a greater probability of chains recombining. Hence the degree of degradation is reduced and the value of $M_{lim}$ increases.

Using the Schmid and Ovenall models, the study appears to have exceeded the critical overlap concentration in THF but this is perhaps not the case in hexane. From the degradation curves 3.31 and 3.32 it is shown that the rate obviously decreases with increasing concentration from 0.1 - 3.0% w/v and neither the Schmid nor the Ovenall rate model agrees with these observed results, this is due to the fact that both rate equations contain a concentration term which is proportional to the rate constant which is found not to be the case in the experimental results. The Fujiwara rate model differs however and follows the predicted trend showing a decreasing rate with an increasing solution concentration.

### 3.6 Effect of Dissolved Gases on the Degradation.

As introduced in section 1.7.1, the gaseous contents of the cavitation bubbles would be expected to greatly affect the nature and severity of their implosive collapse. This study concentrates on polyisobutylene dissolved in three different solvents saturated with one of up to nine gases.

All other factors known to influence the cavitation process were kept constant throughout the study, employing an ultrasonic intensity of 23.9 $Wcm^{-2}$, a reaction

temperature of 25°C and a polymer solution concentration of 1% w/v so that the effect of the gas could be isolated. Prior to sonication, each solution was saturated with the gas under examination and the solution was blanketed with the gas throughout the ultrasonic reaction to prevent air from re-entering the system.

There are many ways to express the solubility of a gas[199] in a liquid[200]. The Ostwald coefficient, L, is defined as,

$$L = \frac{V_2}{V_1} \qquad 3.14$$

where $V_2$ is the volume of gas absorbed by the volume $V_1$ of the solvent. The mole fraction of dissolved gas, $X_A$, can be given by,

$$X_A = \left\{ \left( \frac{RT}{LP_2 V_1^o} \right) + 1 \right\}^{-1} \qquad 3.15$$

where R is the molar gas constant, T is the absolute temperature, $P_2$ is the partial pressure of the gas and $V_1^o$ is the molar volume of the pure solvent, this equation assumes ideal gas behaviour. $X_A$, the mole fraction of dissolved gas is defined as,

$$X_A = \frac{N_A}{1 + N_A} \qquad 3.16$$

where $N_A$ is the number of moles of A absorbed per mole of the solvent at 1 atmosphere pressure and 298 K. A large value of $X_A$ indicates a high solubility[199].

The three solvents used in the study were THF, hexane and toluene. A series of gases were chosen with a wide range of properties. There are many relevant

sources of gas solubility data[201-203] and slight differences in quoted values are not uncommon. In this study each complete series used was taken from the same source to ensure that trends could be studied.

The physical properties of the gases used are documented in Tables 3.4 - 3.6. For THF and toluene, gas solubilities were taken, where available, directly from the literature[204]. For hexane, the Ostwald coefficients measured by Makranczy *et al*[205] were used and had to be converted to gas solubilities as shown.

TABLE 3.4. Tetrahydrofuran.

| Gas | Solubility[204] $X_A \times 10^3$ | $M_{lim}$ | Thermal Conductivity[206] / $mJcm^{-1}K^{-1}s^{-1}$ | Cp/Cv |
|---|---|---|---|---|
| He | 0.18 | 17800 | 1.51 | 1.67 |
| $H_2$ | 0.27 | 27900 | 1.83 | 1.40 |
| $N_2$ | 0.52 | 23400 | 0.26 | 1.40 |
| $O_2$ | 0.82 | 49300 | 0.27 | 1.40 |
| Ar | 1.00 | 48700 | 0.18 | 1.67 |
| $CH_4$ | - | 73700 | 0.34 | - |
| $CO_2$ | 1.94 | 140100 | 0.17 | 1.30 |
| Ethene | - | 146500 | 0.21 | - |
| Propane | - | 175100 | 0.18 | - |

TABLE 3.5. Hexane.

$V_1^o = 131.4 \times 10^{-6}$ $m^3mol^{-1}$, $P_2 = 101325$ Pa ($Nm^{-2}$) at 298 K

| Gas | Ostwald Coeff.[205] L | Solubility $X_A \times 10^3$ | $M_{lim}$ |
|---|---|---|---|
| He | 0.0425 | 0.228 | 41100 |
| $H_2$ | 0.134 | 0.719 | 62800 |
| $N_2$ | 0.255 | 1.368 | 70000 |
| $O_2$ | 0.365 | 1.957 | 82700 |
| Ar | 0.496 | 2.659 | 87200 |
| $CH_4$ | 1.095 | 5.847 | 113000 |
| $CO_2$ | 2.236 | 11.867 | 126900 |

TABLE 3.6. Toluene.

| Gas | Solubility[204] $X_A \times 10^3$ | $M_{lim}$ |
|---|---|---|
| He | 0.10 | 15400 |
| $N_2$ | 0.54 | 20600 |
| Ar | 1.10 | 44500 |
| $CH_4$ | 2.34 | 63400 |
| $CO_2$ | 10.70 | 121600 |

The degradation curves showing the variation of molecular weight with sonication time for 1% w/v polyisobutylene in each of the three solvents under various gaseous atmospheres are figures 3.41 - 3.43. The curves are strongly dependent on

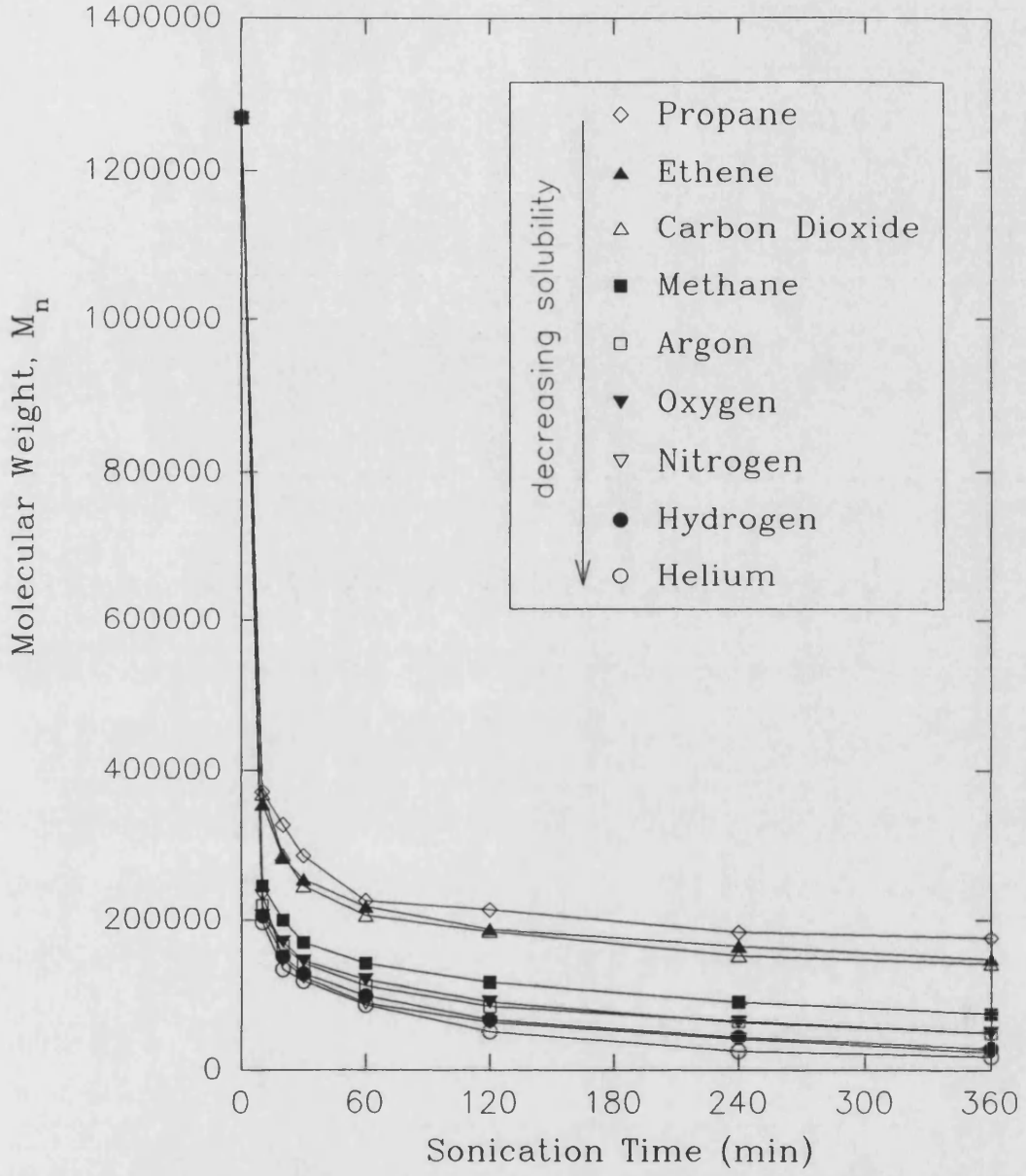


**FIGURE 3.41.** Variation of Number Average Molecular Weight During the Sonication of 1% w/v PIB in THF Under Various Gaseous Atmospheres.

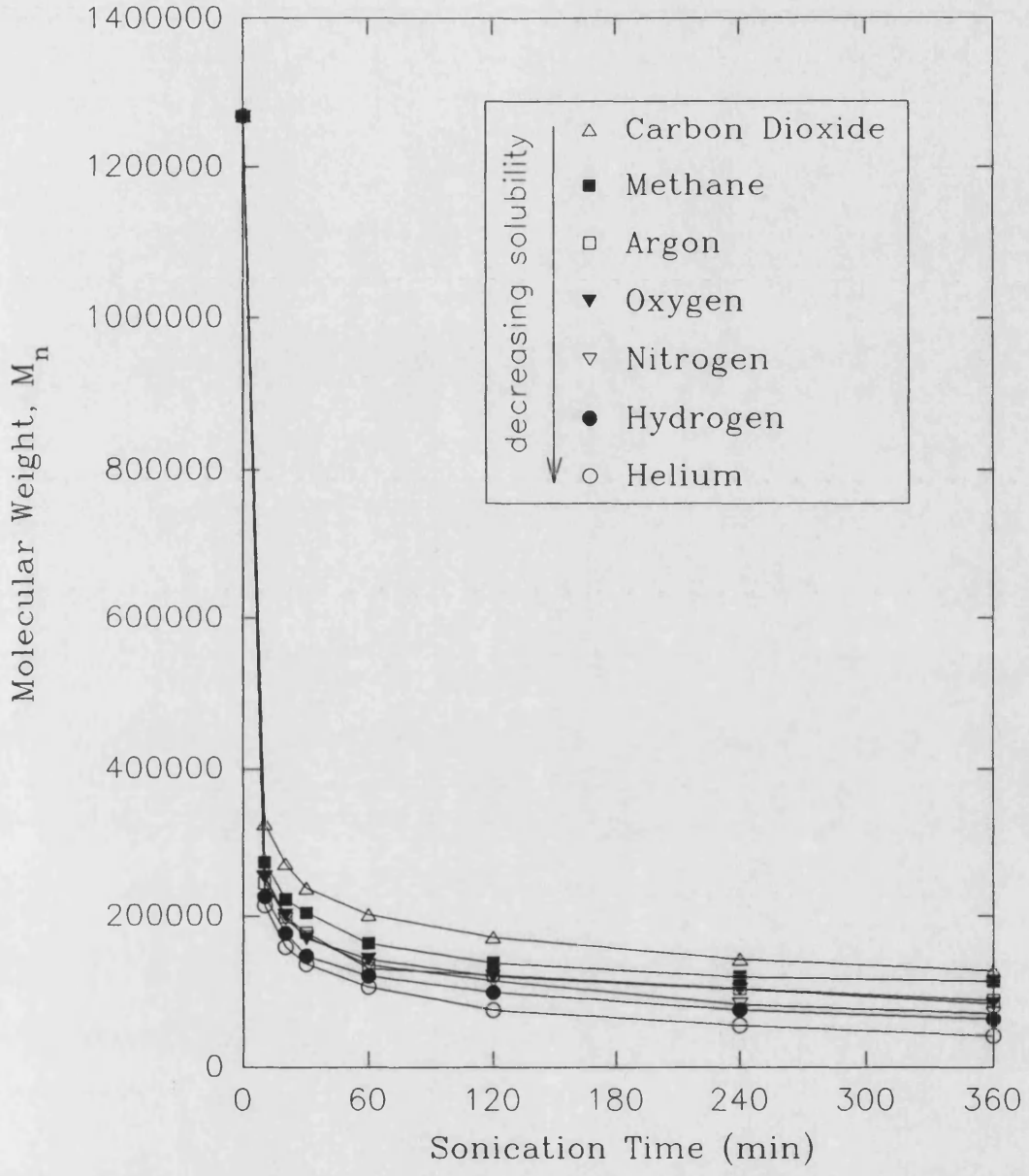


**FIGURE 3.42.** Variation of Number Average Molecular Weight During the Sonication of 1% w/v PIB in Hexane Under Various Gaseous Atmospheres.

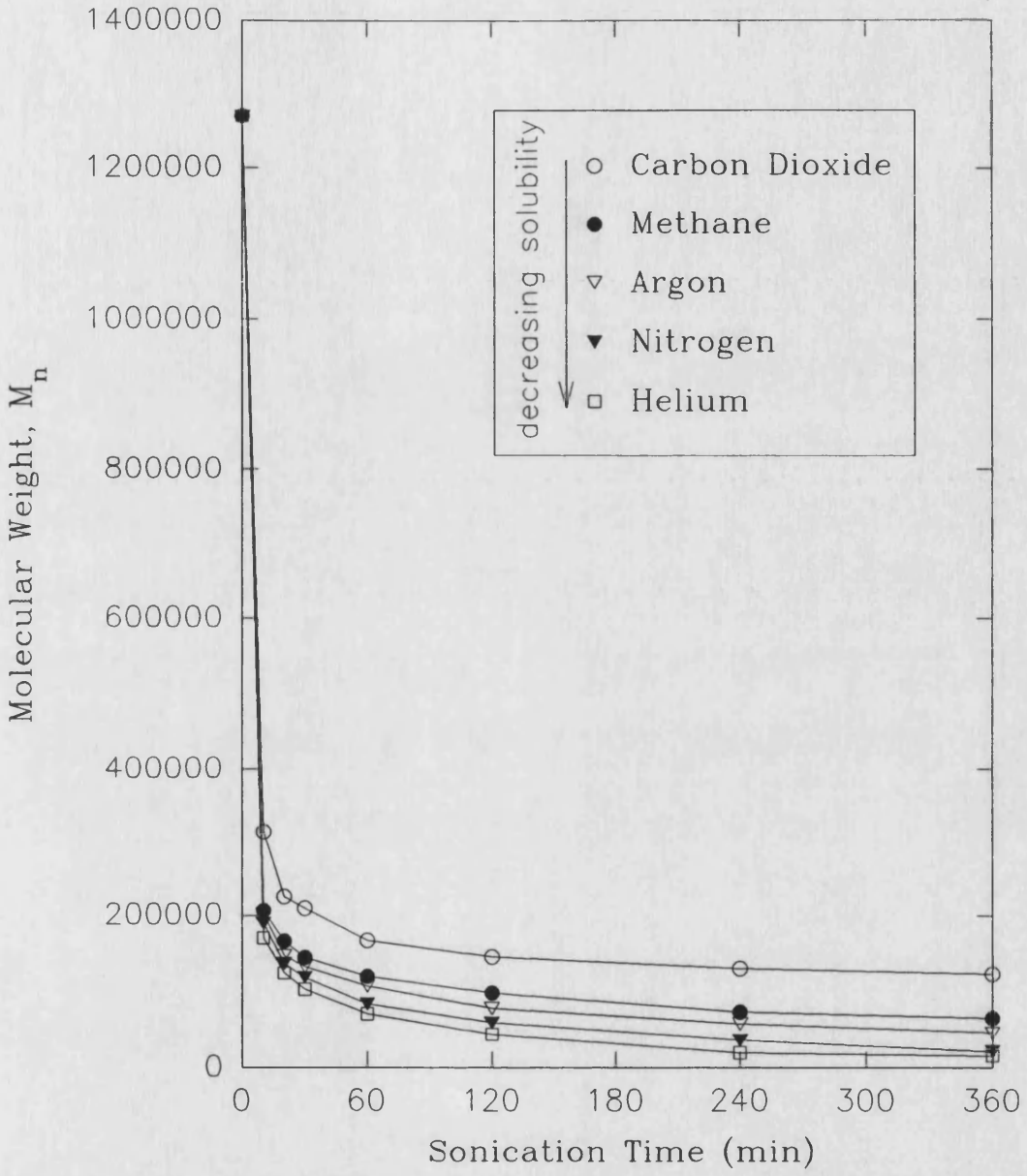


**FIGURE 3.43.** Variation of Number Average Molecular Weight During the Sonication of 1% w/v PIB in Toluene Under Various Gaseous Atmospheres.

the nature of the gas employed and the effect on $M_{lim}$ is shown in Tables 3.4 - 3.6 and graphically in figures 3.44 - 3.46. As the gas solubility increases, the limiting molecular weight increases. The availability of reliable gas solubility data dictated the nature of the gases employed throughout this study.

A gas with a high solubility in the solvent will be expected to diffuse more readily into the cavitation bubble thus cushioning its implosion, as explained earlier in section 1.7.1, increasing the gas content of the solvent reduces the pressure, $P_{max}$, produced on bubble collapse. This would affect the shock wave mechanism. The cushioning effect will reduce the severity of the shock wave produced resulting in less force acting on the polymer chains. The speed of bubble collapse would be slower owing to the increased gas content of the bubble. Oppositely, gases with relatively low solubilities like helium would be less likely to diffuse into the cavities and thus produce more violent implosions leading to lower limiting molecular weights.

Dissolved gases have an effect on the degradation rate constant as shown in Table 3.7 for each system studied.

As expected, gases with a high solubility in the solvent dictate slow degradation rates. All data is shown graphically for the Schmid (figures 3.47 - 3.49), Ovenall (figures 3.50 - 3.52) and Fujiwara (figures 3.53 - 3.55) rate models. The gases employed follow this predicted trend with few deviations, however, the Fujiwara rate model does not exhibit the trends shown by the other two models.

There is no correlation between the extent degradation of polyisobutylene with the thermal conductivity or polytropic ratio of the gas. This proves that the effects observed are not due directly to the hot-spot theory and cannot be explained in terms of thermal contributions from the cavitation nuclei; the major effect, as predicted, remains a mechanochemical one.

Finally in this study of the effects of dissolved gases a series of n-alkanes was chosen and solutions of polyisobutylene in each alkane were sonicated under a nitrogen atmosphere. The solubility of nitrogen varies across the series of alkanes, the values of solubility were calculated from Ostwald coefficients[205], values are shown in Table 3.8.

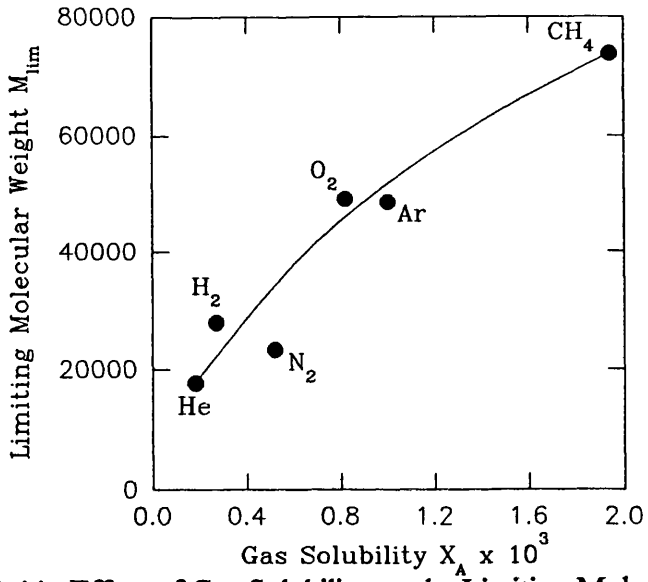


**FIGURE 3.44.** Effect of Gas Solubility on the Limiting Molecular Weight of PIB for the Sonication of a 1% w/v Solution in THF.

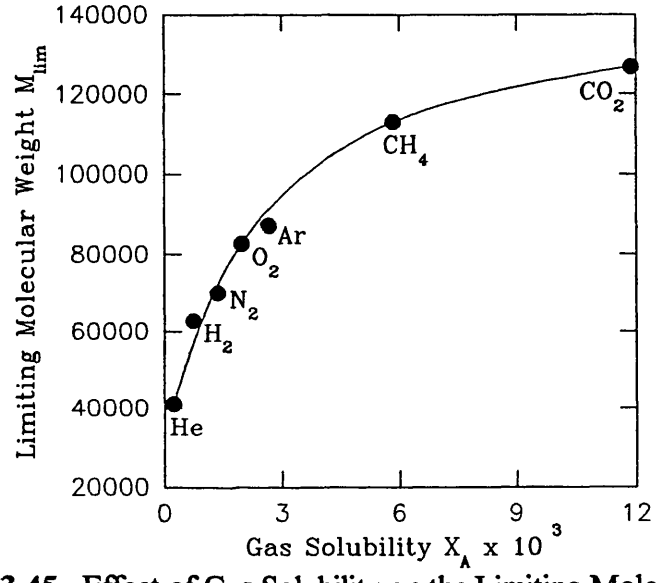


**FIGURE 3.45.** Effect of Gas Solubility on the Limiting Molecular Weight of PIB for the Sonication of a 1% w/v Solution in Hexane.

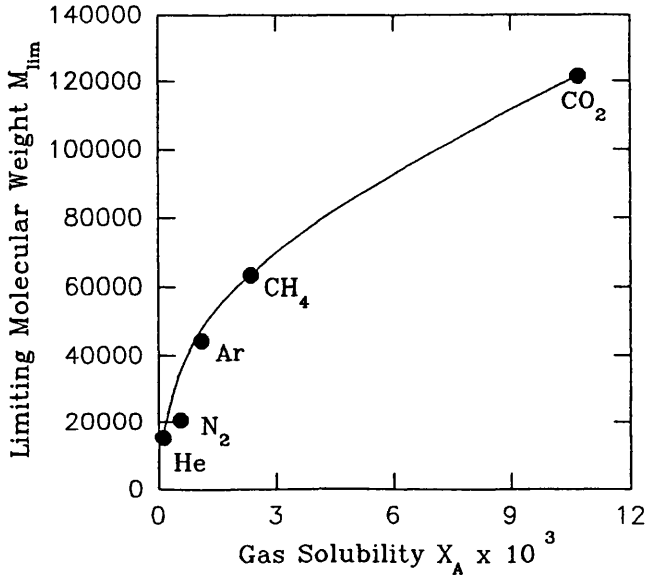


**FIGURE 3.46.** Effect of Gas Solubility on the Limiting Molecular Weight of PIB for the Sonication of a 1% w/v Solution in Toluene.

TABLE 3.7. Effect of Dissolved Gases on the Rate Constant for the Degradation.

| | RATE CONSTANTS / $min^{-1}$ | | | | | | | | |
|---|---|---|---|---|---|---|---|---|---|
| | THF | | | Hexane | | | Toluene | | |
| Gas | Schmid x $10^{10}$ | Ovenall x $10^{6}$ | Fujiwara x $10^{5}$ | Schmid x $10^{10}$ | Ovenall x $10^{6}$ | Fujiwara x $10^{5}$ | Schmid x $10^{10}$ | Ovenall x $10^{6}$ | Fujiwara x $10^{5}$ |
| He | 4.342 | 1.578 | 1.732 | 3.558 | 1.458 | 1.792 | 5.628 | 1.806 | 1.978 |
| $H_2$ | 3.815 | 1.486 | 1.711 | 3.387 | 1.464 | 2.018 | - | - | - |
| $N_2$ | 4.154 | 1.569 | 1.769 | 2.425 | 1.211 | 1.643 | 4.323 | 1.575 | 1.756 |
| $O_2$ | 3.184 | 1.374 | 1.746 | 2.689 | 1.313 | 1.937 | - | - | - |
| Ar | 3.460 | 1.453 | 1.854 | 2.481 | 1.254 | 1.867 | 3.996 | 1.568 | 1.990 |
| $CH_4$ | 2.558 | 1.255 | 1.752 | 2.032 | 1.148 | 1.861 | 3.587 | 1.511 | 2.114 |
| $CO_2$ | 1.399 | 0.971 | 1.561 | 1.426 | 0.933 | 1.477 | 2.090 | 1.194 | 2.018 |
| Ethene | 1.317 | 0.908 | 1.526 | - | - | - | - | - | - |
| Propane | 1.047 | 0.799 | 1.424 | - | - | - | - | - | - |

TABLE 3.8. Solubility of Nitrogen in n-Alkane Solvents.

| n-Alkane | Ostwald Coeff.[205], L | Molar Volume $V_1^o$ / x $10^6$ $m^3mol^{-1}$ | Solubility $N_A$ x $10^3$ | $M_{lim}$ |
|---|---|---|---|---|
| Pentane | 0.299 | 115.9 | 1.415 | 119400 |
| Hexane | 0.255 | 131.4 | 1.368 | 70000 |
| Octane | 0.197 | 163.2 | 1.312 | 42700 |
| Decane | 0.161 | 195.5 | 1.285 | 25900 |
| Dodecane | 0.136 | 228.1 | 1.268 | 36700 |
| Tetradecane | 0.117 | 260.8 | 1.246 | 19200 |

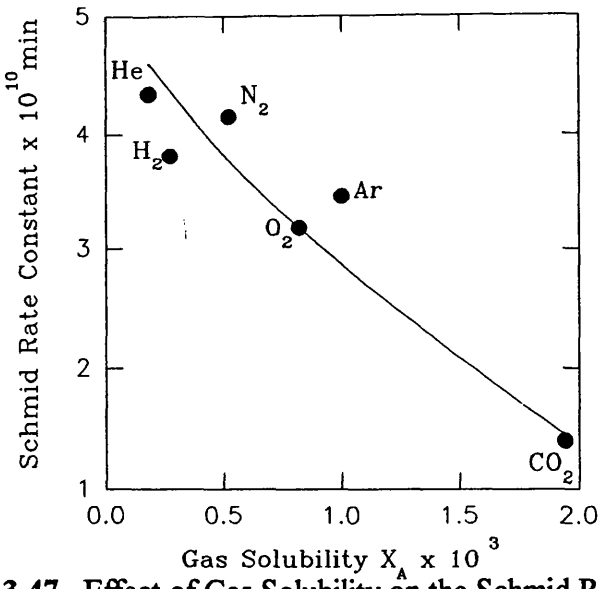


**FIGURE 3.47.** Effect of Gas Solubility on the Schmid Rate Constant for the Sonication of 1% w/v PIB in THF.

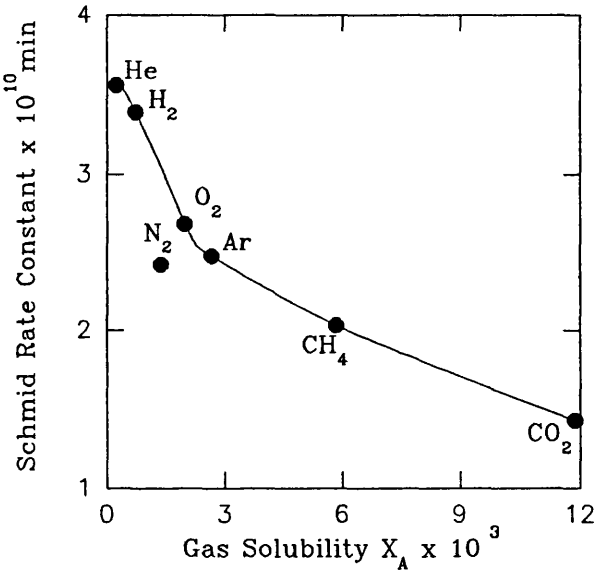


**FIGURE 3.48.** Effect of Gas Solubility on the Schmid Rate Constant for the Sonication of 1% w/v PIB in Hexane.

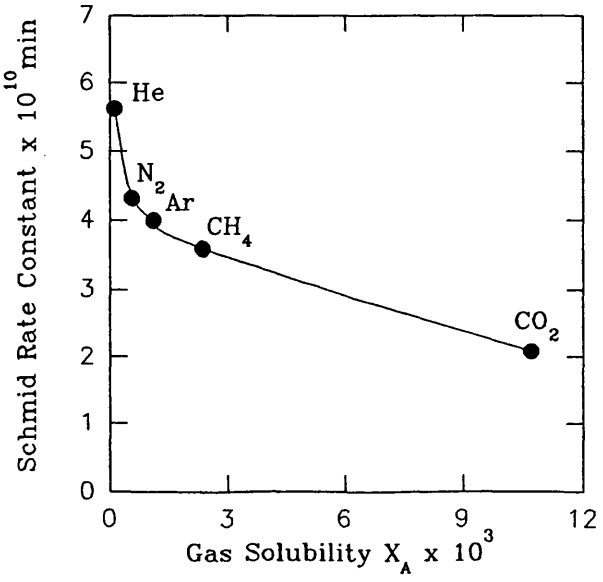


**FIGURE 3.49.** Effect of Gas Solubility on the Schmid Rate Constant for the Sonication of 1% w/v PIB in Toluene.

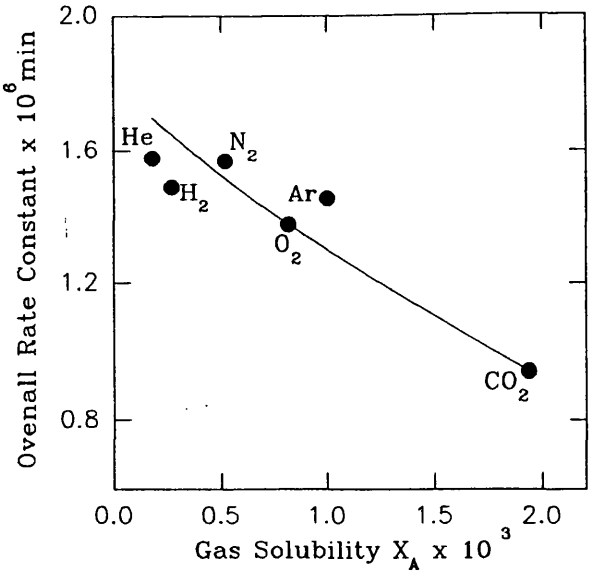


**FIGURE 3.50.** Effect of Gas Solubility on the Ovenall Rate Constant for the Sonication of 1% w/v PIB in THF.

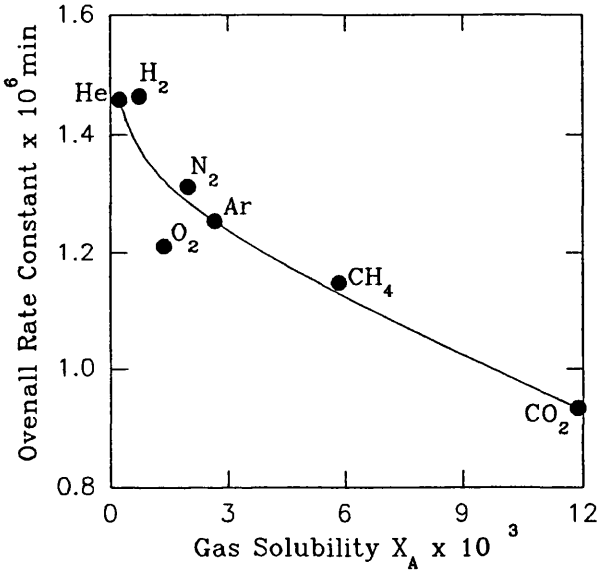


**FIGURE 3.51.** Effect of Gas Solubility on the Ovenall Rate Constant for the Sonication of 1% w/v PIB in Hexane.

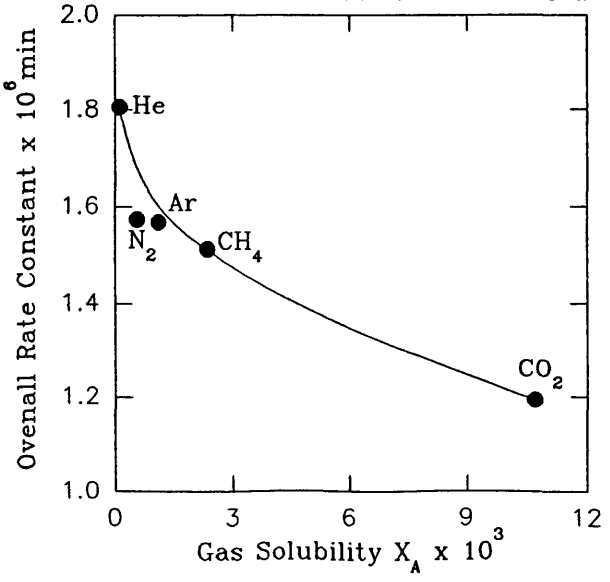


**FIGURE 3.52.** Effect of Gas Solubility on the Ovenall Rate Constant for the Sonication of 1% w/v PIB in Toluene.

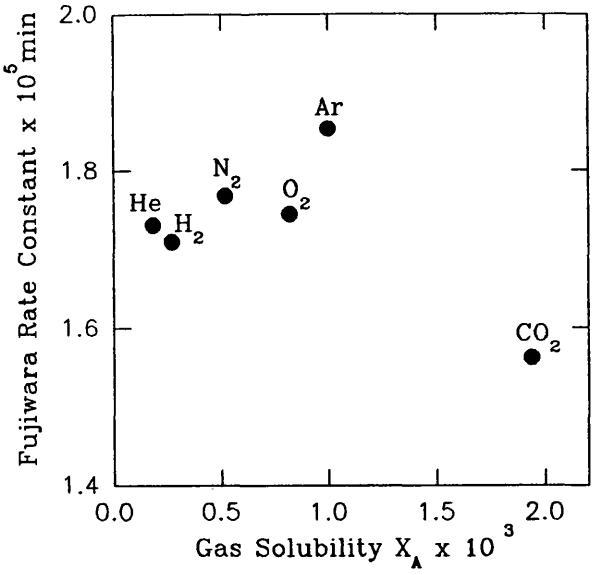


**FIGURE 3.53.** Effect of Gas Solubility on the Fujiwara Rate Constant for the Sonication of 1% w/v PIB in THF.

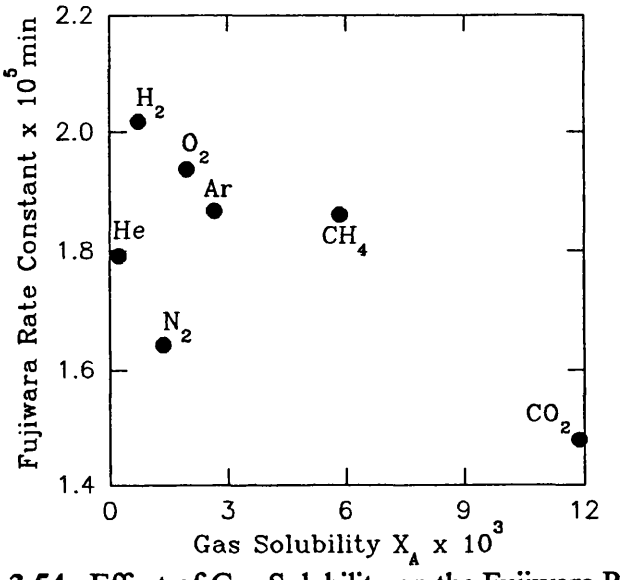


**FIGURE 3.54.** Effect of Gas Solubility on the Fujiwara Rate Constant for the Sonication of 1% w/v PIB in Hexane.

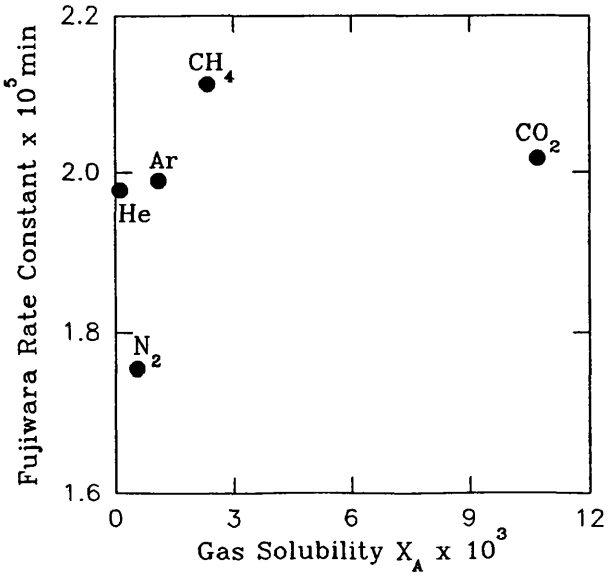


**FIGURE 3.55.** Effect of Gas Solubility on the Fujiwara Rate Constant for the Sonication of 1% w/v PIB in Toluene.

The effect of the solvent on the degradation will be discussed in section 3.7, only the effect of the varying gas solubility will be addressed here.

Figure 3.56 shows the effect of nitrogen gas solubility on the value of $M_{lim}$ for the degradation of polyisobutylene dissolved in n-alkanes. It can be seen that lower limiting molecular weights are reached during the sonication in tetradecane (lower solubility) than in pentane (higher solubility). Correspondingly, faster rates of degradation are observed in solvents with lower gas solubilities, as expected, shown by applying the rate models depicted in figures 3.57 - 3.59. However, other factors also play an important role in the control of the degradation.

## 3.7 Effect of the Nature of the Solvent on the Degradation.

To isolate the effect of the solvent on the degradation a series of n-alkane solvents was chosen that gave a good range of viscosities, heats of vaporisation and differing Flory-Huggins Interaction parameters. All of the 1% w/v polyisobutylene solutions were sonicated at an ultrasonic intensity of 23.9 $Wcm^{-2}$ under an atmosphere of nitrogen at 25°C. A graph showing the variation of number average molecular weight with sonication time is shown in figure 3.60.

Degradation is faster in tetradecane than in pentane and results in a polymer with a lower limiting molecular weight. The value of $M_{lim}$ has already been correlated with the solubility of nitrogen gas in each n-alkane solvent (Table 3.8, figure 3.56).

### 3.7.1 Correlation of the Degradation with the Solvent Viscosity.

The solvent viscosity would be expected to affect the extent of degradation. In the rarefaction cycle of the ultrasonic wave the negative pressure must be able to overcome the cohesive forces in the liquid in order for a cavitation bubble to be formed. An increase in solvent viscosity will raise the cavitational threshold but if cavitation does occur it has been found that the pressures generated are more severe[70].

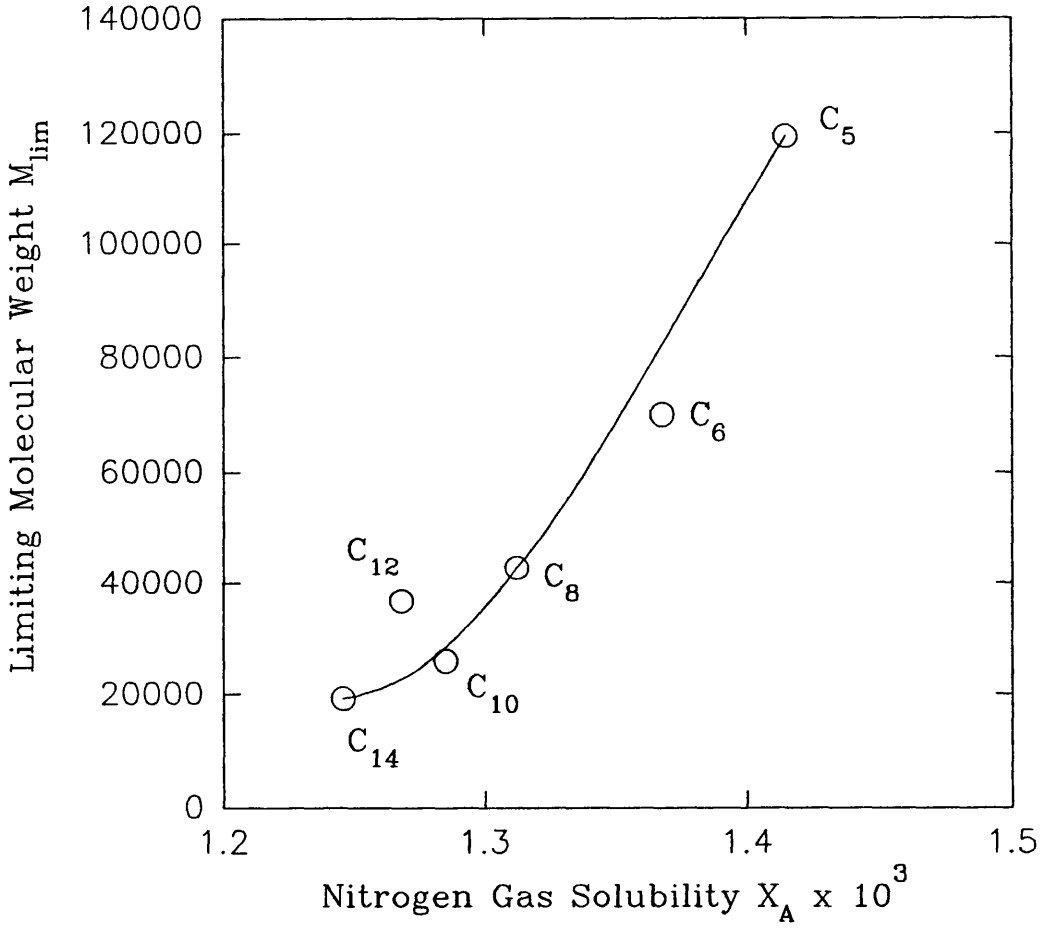


**FIGURE 3.56.** Effect of Nitrogen Gas Solubility on the Limiting Molecular Weight of PIB for the Sonication of a 1% w/v Solution in n-Alkanes.

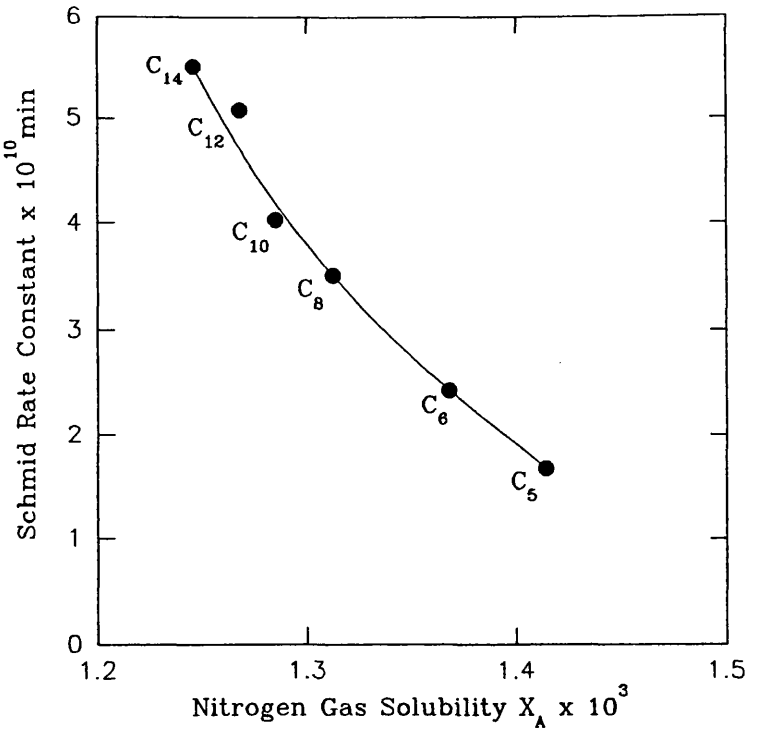


**FIGURE 3.57.** Effect of Nitrogen Gas Solubility on the Schmid Rate Constant for the Sonication of 1% w/v PIB in n-Alkanes.

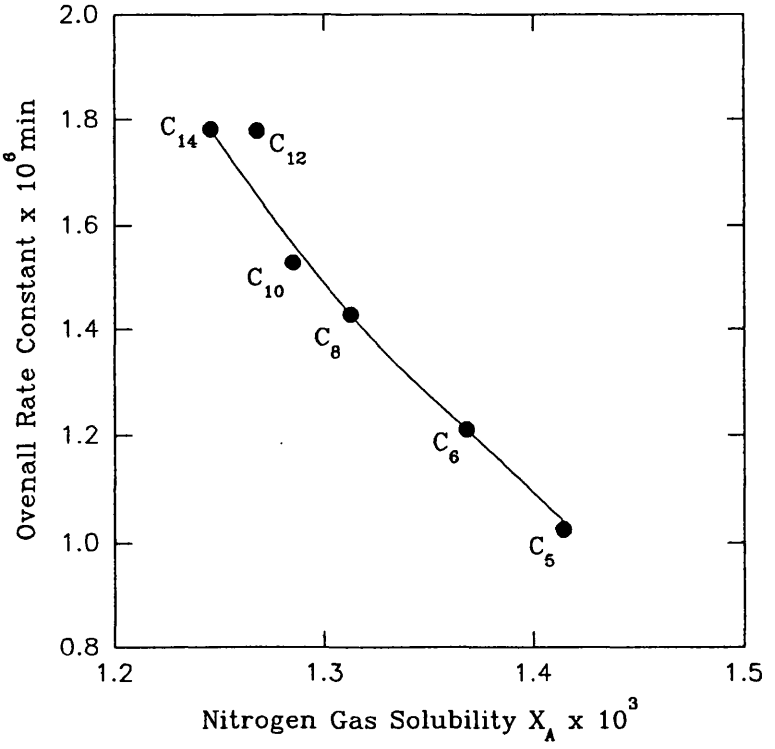


**FIGURE 3.58.** Effect of Nitrogen Gas Solubility on the Ovenall Rate Constant for the Sonication of 1% w/v PIB in n-Alkanes.

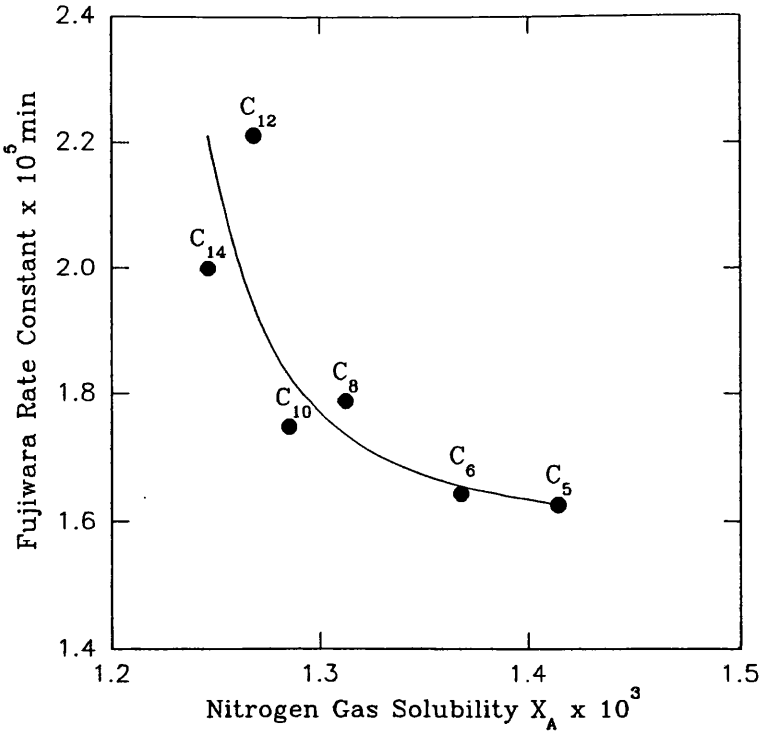


**FIGURE 3.59.** Effect of Nitrogen Gas Solubility on the Fujiwara Rate Constant for the Sonication of 1% w/v PIB in n-Alkanes.

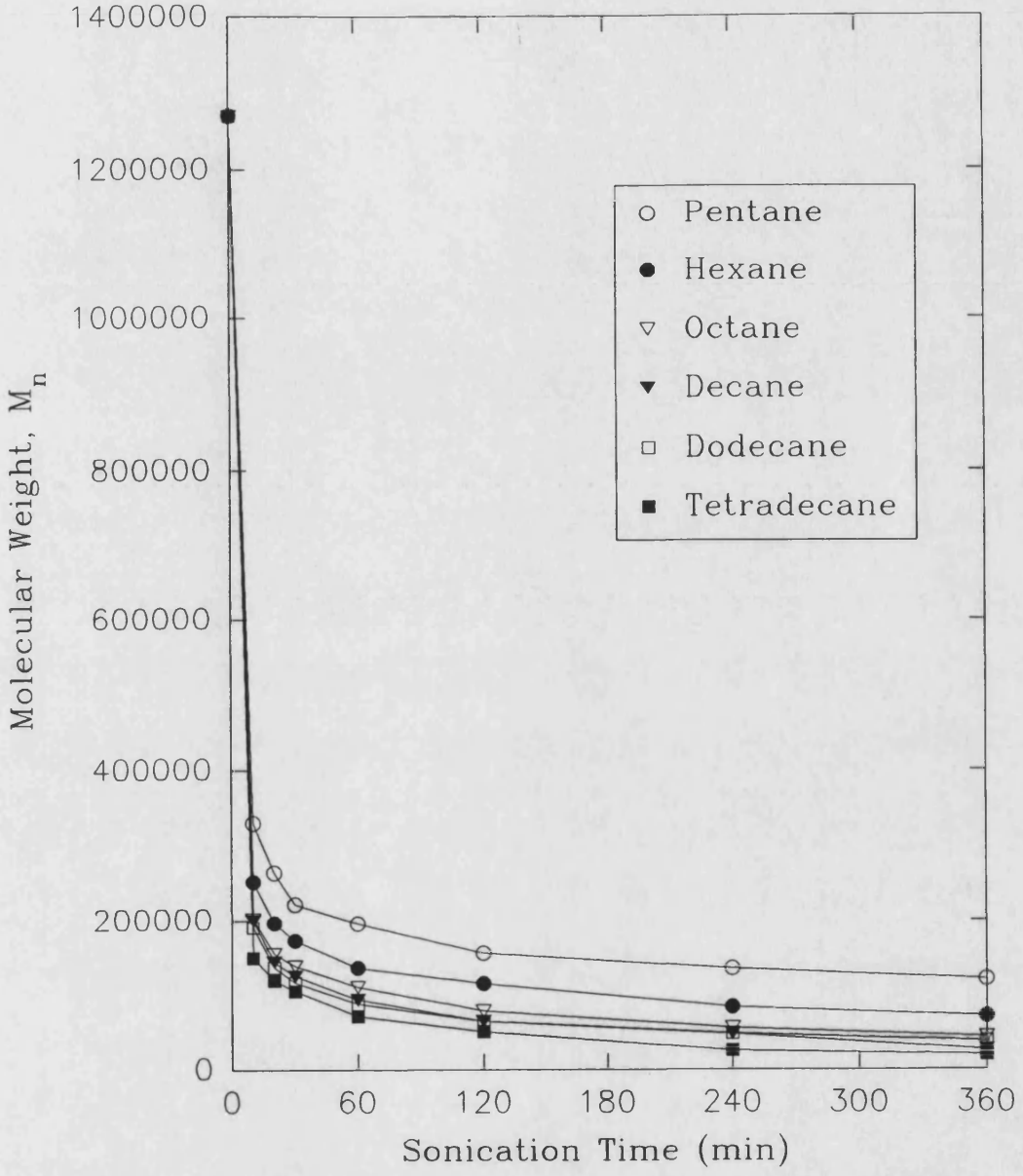


**FIGURE 3.60.** Variation of Number Average Molecular Weight During the Sonication of 1% w/v PIB in Various n-Alkane Solvents.

Viscosity is usually expressed in two ways, absolute or kinematic viscosity. The poise (P) is the unit of absolute viscosity and is equivalent to 0.1 $Nsm^{-2}$. The stoke (St) is the unit of kinematic viscosity and is equal to the absolute viscosity of a fluid in poise divided by its density ($gcm^{-3}$) where 1 stoke is equivalent to $10^{-4}$ $m^2s^{-1}$.

Table 3.9 shows the values of absolute and kinematic viscosity for each of the n-alkanes studied[207].

TABLE 3.9. Viscosities of n-Alkanes.

| n-Alkane | Absolute Viscosity @ 25°C, centipoise (cP) | Kinematic Viscosity @ 25°C, centistokes (cSt) | $M_{lim}$ |
|---|---|---|---|
| Pentane | 0.2240 | 0.3610 | 119400 |
| Hexane | 0.2976 | 0.4545 | 70000 |
| Octane | 0.5136 | 0.7352 | 42700 |
| Decane | 0.8588 | 1.182 | 25900 |
| Dodecane | 1.374 | 1.843 | 36700 |
| Tetradecane | 2.104 | 2.771 | 19200 |

Figures 3.61 and 3.62 show the values of $M_{lim}$ reached in each solvent compared to its absolute and kinematic viscosity. Tetradecane is seen to degrade faster and to a lower $M_{lim}$ despite having the highest viscosity. It can be concluded that providing the cavitational threshold is not too high and that the cohesive forces of the liquid can be overcome during the rarefaction cycle then the shock wave and pressures produced in tetradecane are more severe than in pentane. However, this is not the only factor governing the degradation and its effect may be masked by other more prevalent ones such as the effect of the heat of vaporisation of the solvent or the effect of the Flory-Huggins interaction parameter both of which will be examined in subsequent sections.

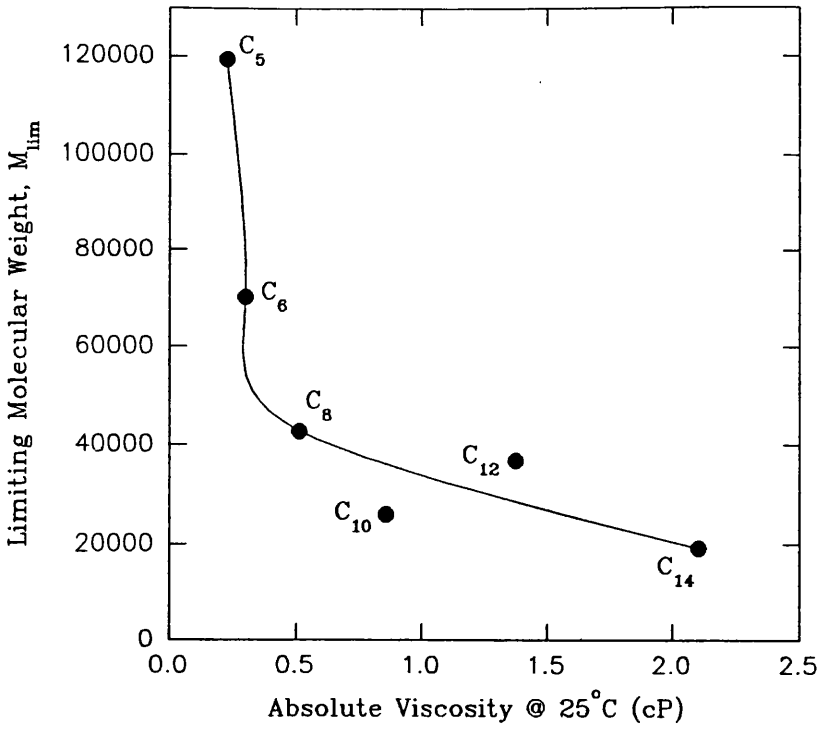


**FIGURE 3.61.** Effect of Absolute Viscosity on the Limiting Molecular Weight of PIB for the Sonication of a 1% w/v Solution in n-Alkanes.

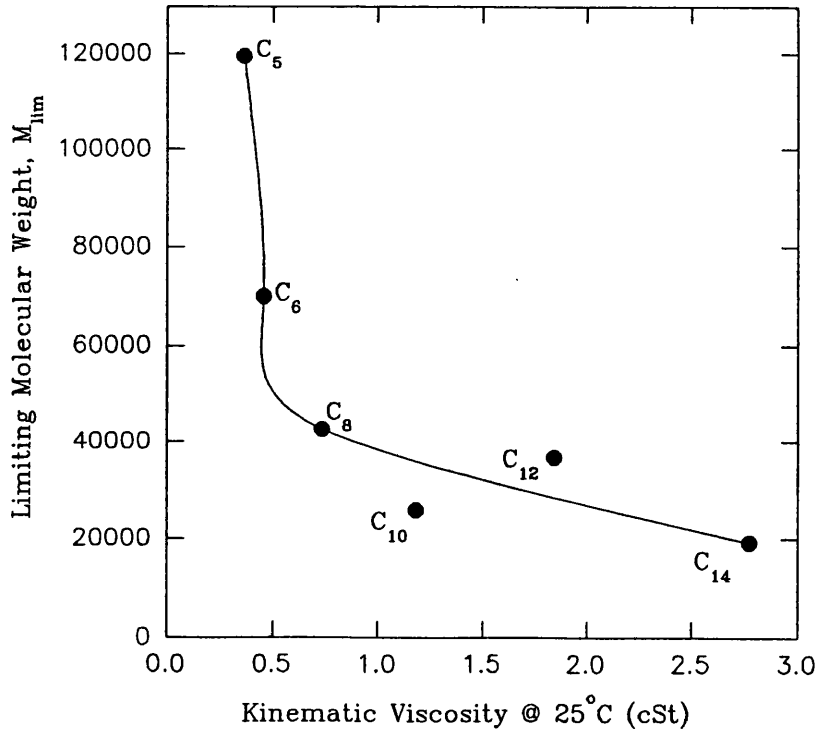


**FIGURE 3.62.** Effect of Kinematic Viscosity on the Limiting Molecular Weight of PIB for the Sonication of a 1% w/v Solution in n-Alkanes.

3.7.2. Correlation of the Degradation with the Heat of Vaporisation of the Solvent.

The amount of vapour inside the cavitation bubbles prior to collapse will determine the severity of the shock wave produced. In solvents where the volatility is high more vapour will enter the bubbles thus contributing to a cushioning effect when the cavity implodes. The heat of vaporisation of the solvent, $\Delta H_{vap}$, should be expected to affect the degradation, the values[208] are shown in Table 3.10.

**TABLE 3.10.** Heats of Vaporisation for n-Alkanes.

| n-Alkane | $\Delta$Hvap / kJmol$^{-1}$ |
|---|---|
| Pentane | 26.42 |
| Hexane | 31.55 |
| Octane | 41.48 |
| Decane | 51.36 |
| Dodecane | 61.29 |
| Tetradecane | 71.13 |

Figure 3.63 shows the effect of the heat of vaporisation on the limiting molecular weight of polyisobutylene. It shows that in solvents possessing a low value of $\Delta H_{vap}$, such as pentane (a more volatile solvent than tetradecane), more vapour enters the cavities cushioning their collapse resulting in a higher value of $M_{lim}$ whereas with tetradecane, less vapour is present inside the bubbles and the implosion is more violent leading to a lower $M_{lim}$ value.

Figures 3.64 - 3.66 show the effect of $\Delta H_{vap}$ of the solvent on the degradation rate constants. The Schmid and Ovenall rate models show a linear relationship throughout the n-alkane series with linear correlation coefficients being 0.989 and 0.973 respectively. Error bars estimated from the GPC molecular weight results have

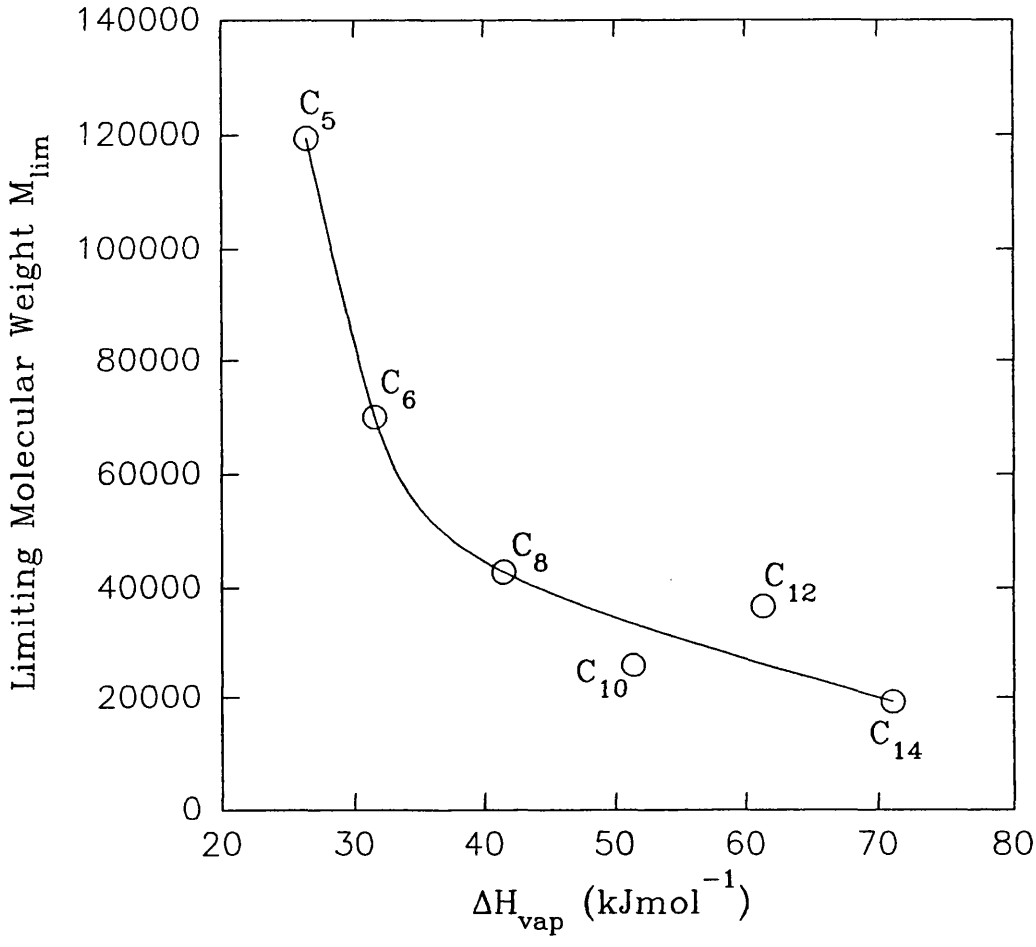


**FIGURE 3.63.** Effect of the Heat of Vaporisation on the Limiting Molecular Weight of PIB for the Sonication of a 1% w/v Solution in n-Alkanes.

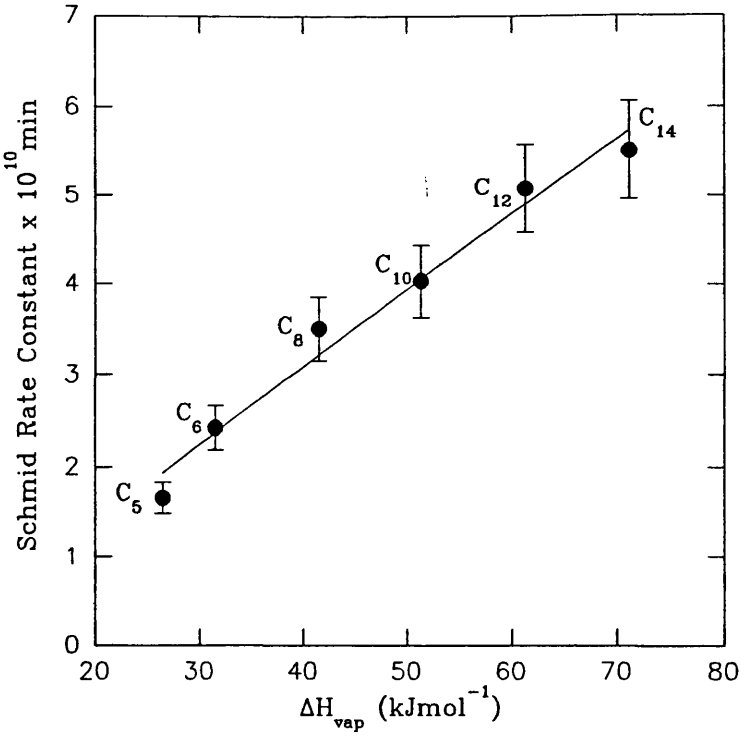


**FIGURE 3.64.** Effect of the Heat of Vaporisation on the Schmid Rate Constant for the Sonication of 1% w/v PIB in n-Alkanes.

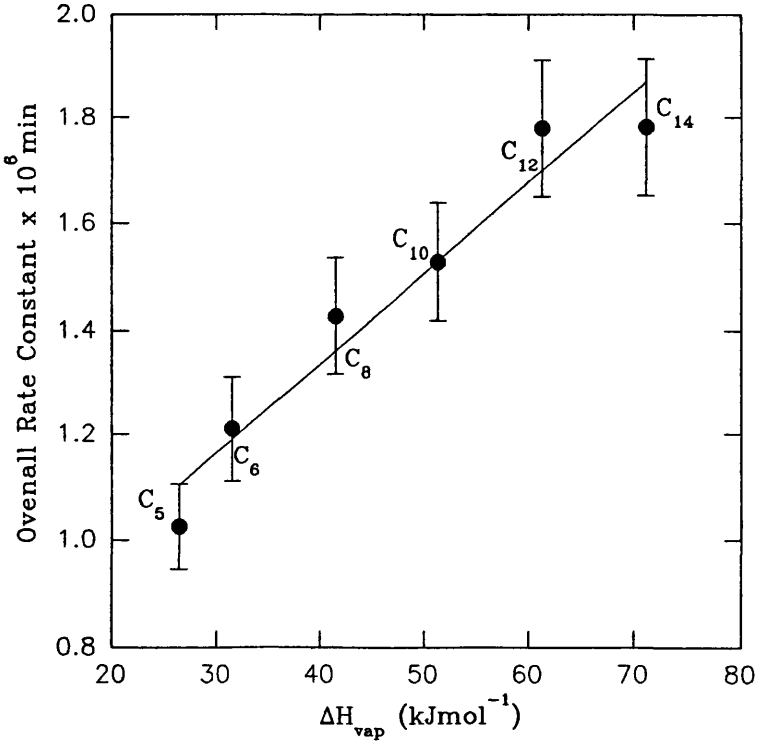


**FIGURE 3.65.** Effect of the Heat of Vaporisation on the Ovenall Rate Constant for the Sonication of 1% w/v PIB in n-Alkanes.

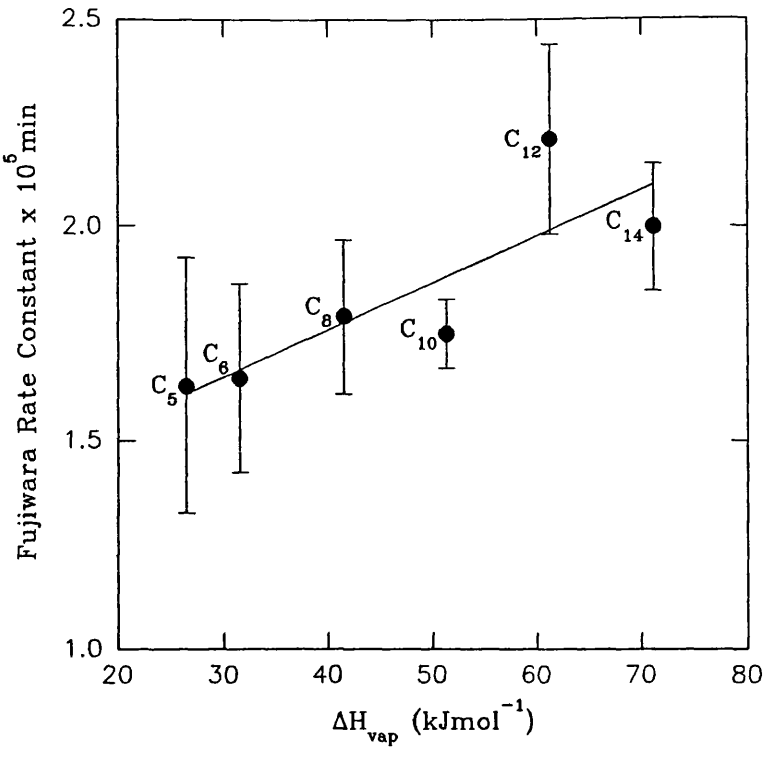


**FIGURE 3.66.** Effect of the Heat of Vaporisation on the Fujiwara Rate Constant for the Sonication of 1% w/v PIB in n-Alkanes.

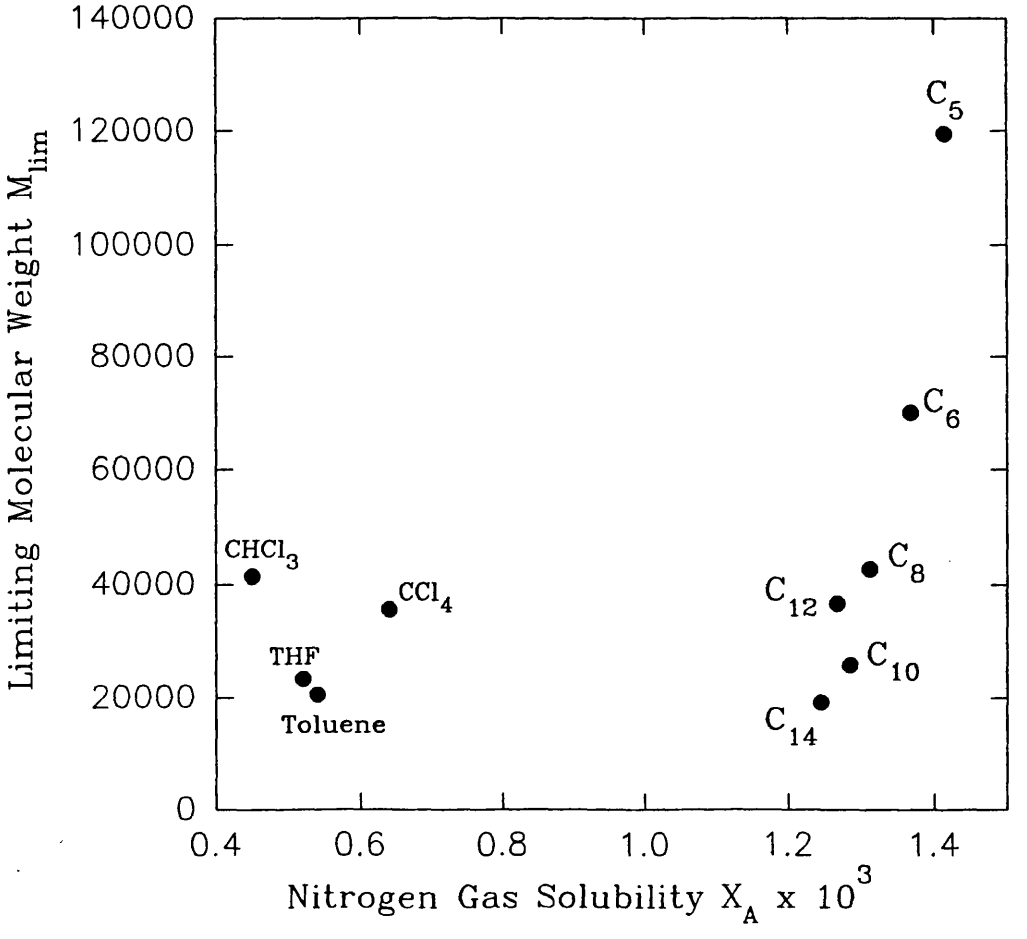


**FIGURE 3.67.** Effect of Nitrogen Gas Solubility on the Limiting Molecular Weight of PIB for the Sonication of a 1% w/v Solution in Various Solvents.

been converted to absolute errors in the rate constants and are as shown on the graphs. Alkane solvents with high heats of vaporisation produce faster rates of degradation.

When other solvents are used such as $CCl_4$, $CHCl_3$, tetrahydrofuran and toluene the graphs show some scatter deviations from these relationships indicating that the solubility of the gas in the solvent and the value of $\Delta H_{vap}$ are not the only contributing factors. Figure 3.67 shows the effect of gas solubility on the value of $M_{lim}$ and figures 3.68 - 3.70 show the effect on the rate constants for the degradation. Figure 3.71 shows the effect of $\Delta H_{vap}$ on the value of $M_{lim}$ and figures 3.72 - 3.74 show the effect on the rate constants. These plots suggest that one parameter alone does not govern the degradation but that a combination of effects is operative and responsible for the control of degradation in solution. A further parameter describing the conformation of the polyisobutylene chains in solution is worthy of investigation.

### 3.7.3 Correlation of the Degradation with the Flory-Huggins Interaction Parameter.

Values for the Flory-Huggins interaction parameter for polyisobutylene in a series of n-alkane solvents were measured so that the effect of the conformation of the chains in solution on the degradation could be studied.

The Flory-Huggins interaction parameter, $\chi$, was calculated using solution viscometry measurements as discussed in section 1.5.1. Values for the intrinsic viscosity were obtained using the conventional extrapolation procedure and these were compared with the two 'single-point' methods introduced in section 1.5.1. A plot showing the conventional extrapolation procedure for three of the n-alkane solvents is shown in figure 3.75 with the values of $[\eta]$ being read as the intercept on the y-axis. For the single-point methods proposed by Solomon and Ciuta[24] and Rudin[32] the lowest concentration results was used in each case. Table 3.11 shows the comparison of the values for $[\eta]$ and the accuracy of the single-point method.

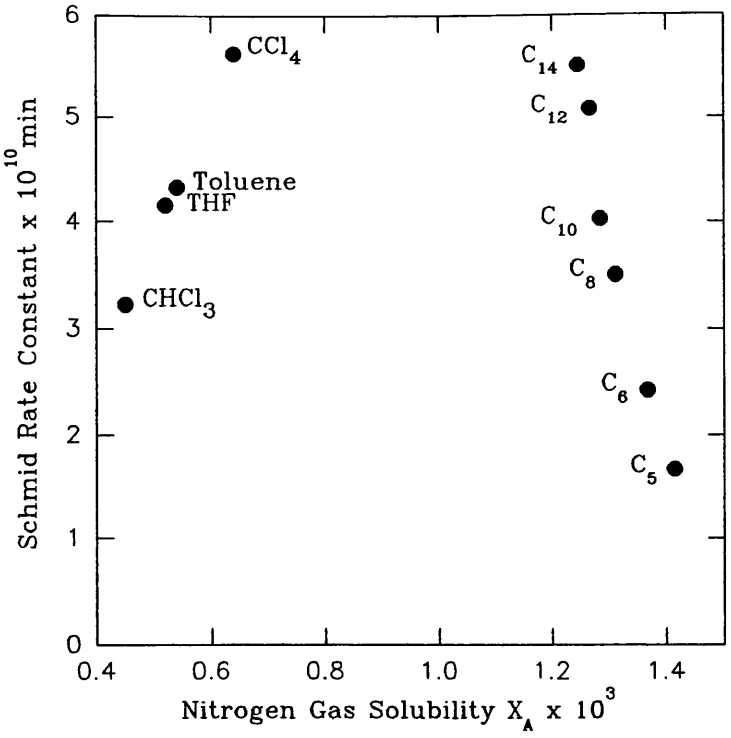


**FIGURE 3.68.** Effect of Nitrogen Gas Solubility on the Schmid Rate Constant for the Sonication of 1% w/v PIB in Various Solvents.

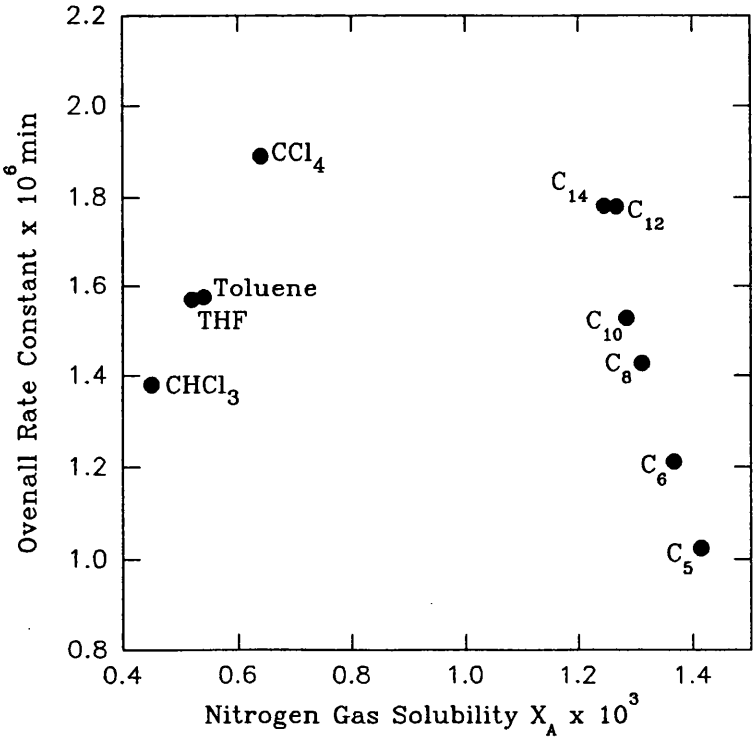


**FIGURE 3.69.** Effect of Nitrogen Gas Solubility on the Ovenall Rate Constant for the Sonication of 1% w/v PIB in Various Solvents.

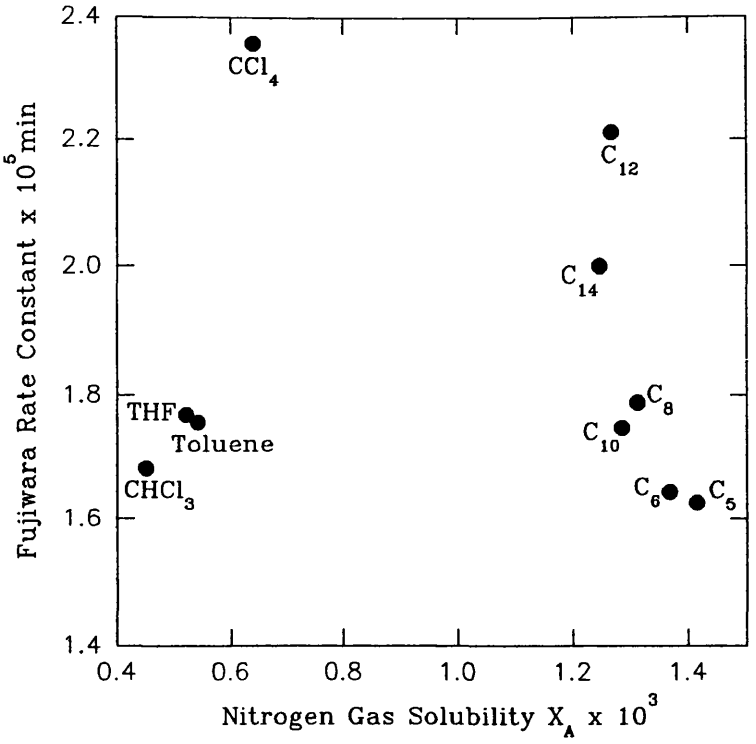


**FIGURE 3.70.** Effect of Nitrogen Gas Solubility on the Fujiwara Rate Constant for the Sonication of 1% w/v PIB in Various Solvents.

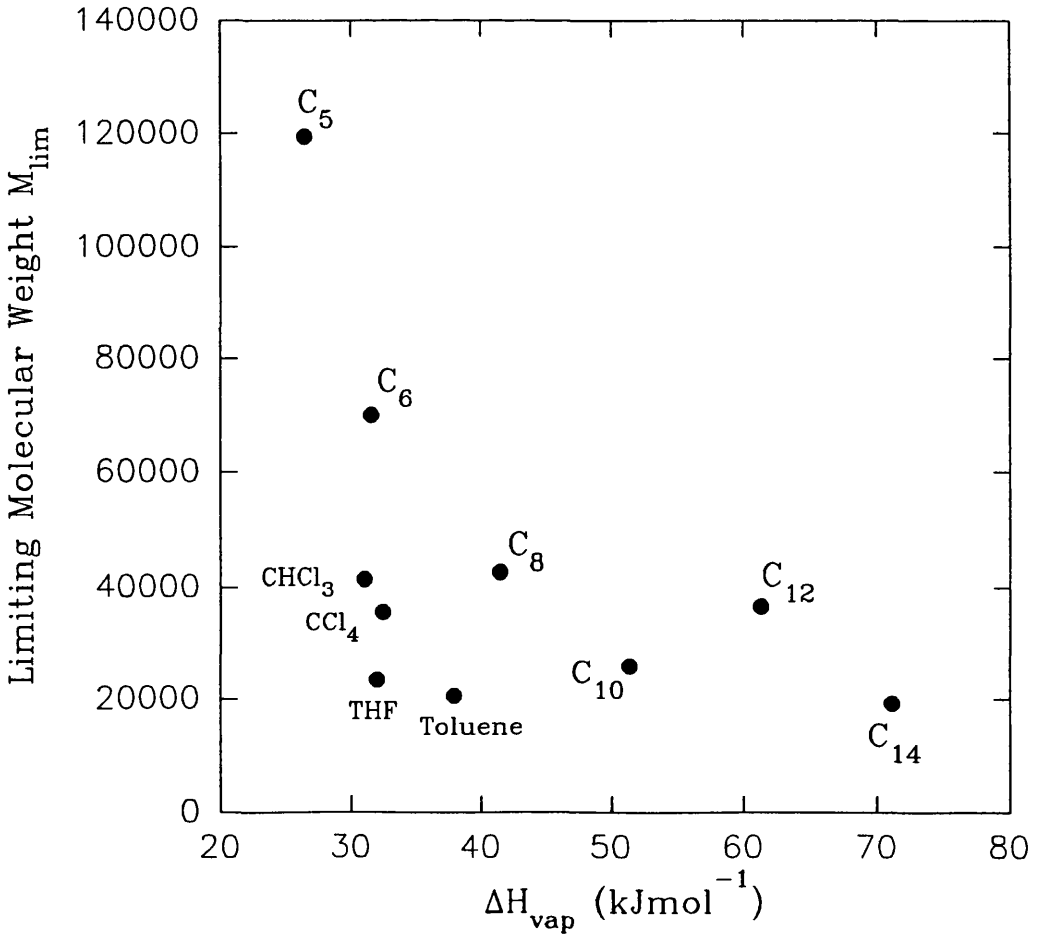


**FIGURE 3.71.** Effect of the Heat of Vaporisation on the Limiting Molecular Weight of PIB for the Sonication of a 1% w/v Solution in Various Solvents.

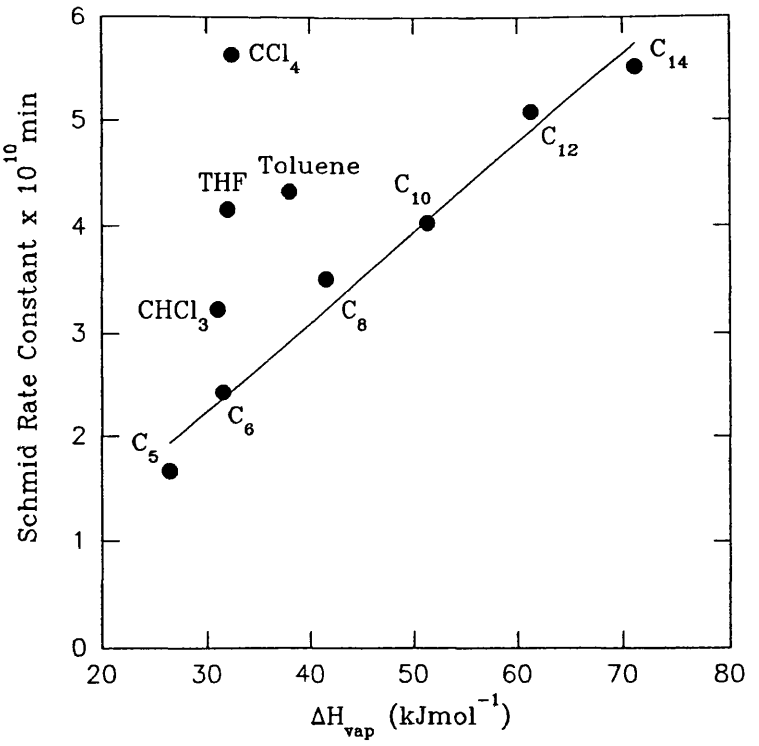


**FIGURE 3.72.** Effect of the Heat of Vaporisation on the Schmid Rate Constant for the Sonication of 1% w/v PIB in Various Solvents.

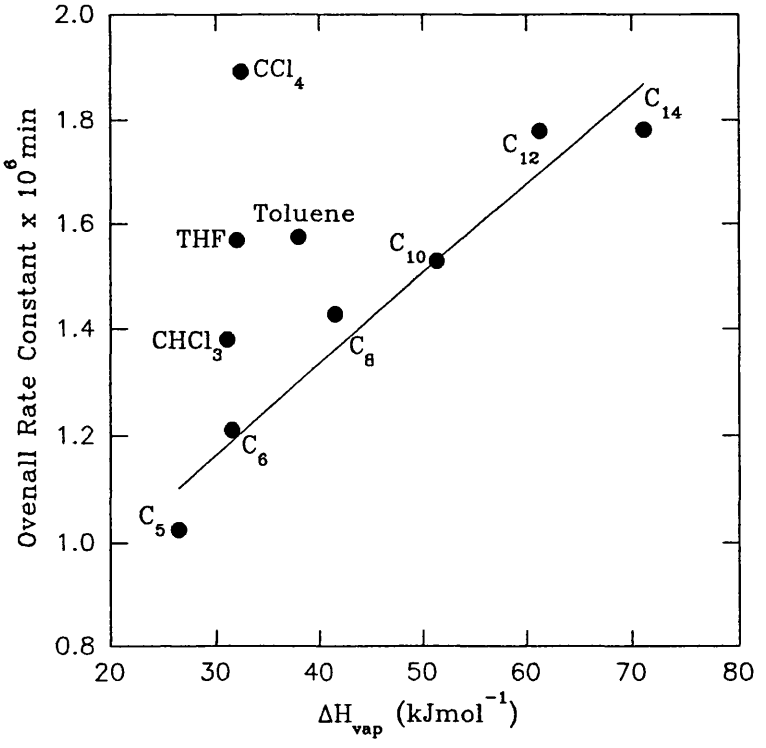


**FIGURE 3.73.** Effect of the Heat of Vaporisation on the Ovenall Rate Constant for the Sonication of 1% w/v PIB in Various Solvents.

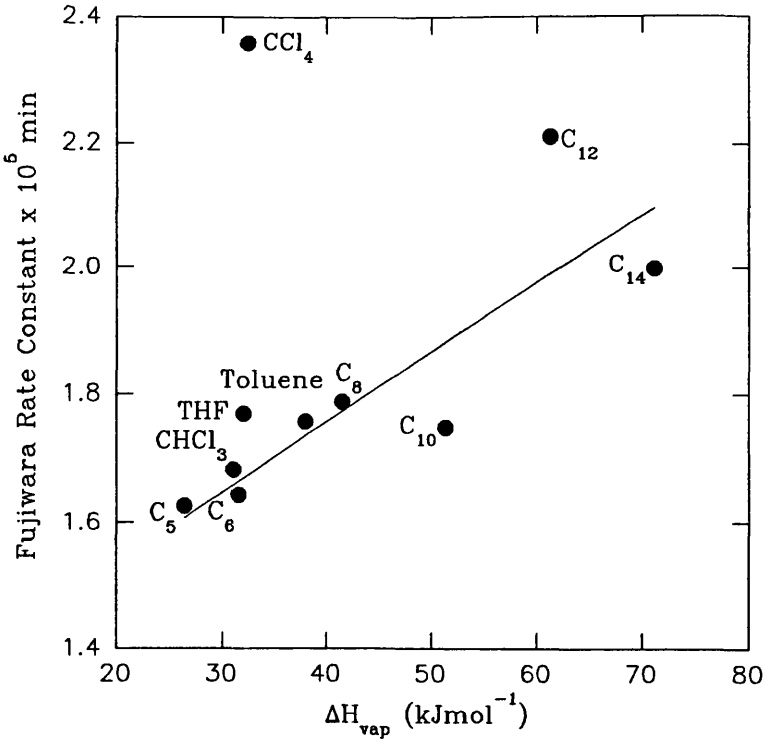


**FIGURE 3.74.** Effect of the Heat of Vaporisation on the Fujiwara Rate Constant for the Sonication of 1% w/v PIB in Various Solvents.

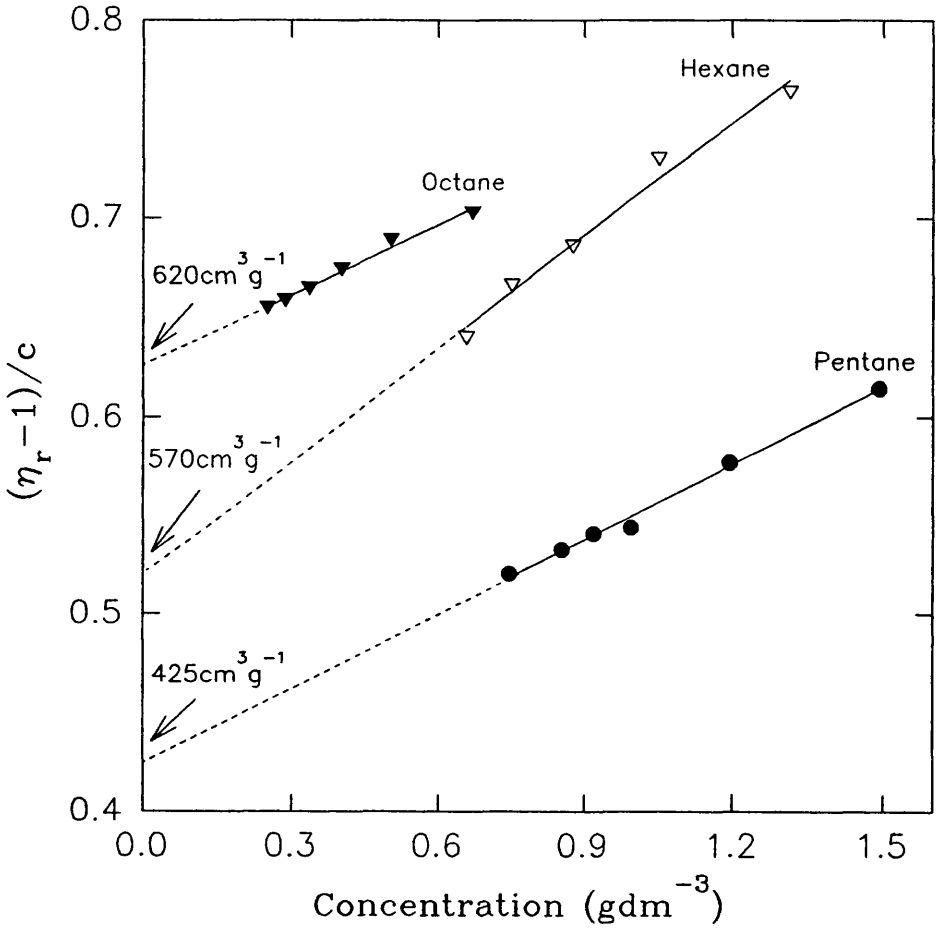


**FIGURE 3.75.** Calculation of the Intrinsic Viscosity of PIB Solutions in n-Alkanes.

TABLE 3.11. Single-Point Determination of Intrinsic Viscosity @25°C.

| | Extrapolated | Solomon & Ciuta | | Rudin | |
|---|---|---|---|---|---|
| n-Alkane | $[\eta]$ / $cm^3g^{-1}$ | $[\eta]$ / $cm^3g^{-1}$ | Δ% | $[\eta]$ / $cm^3g^{-1}$ | Δ% |
| Pentane | 425 | 465 | 9.4 | 476 | 12.0 |
| Hexane | 570 | 567 | 0.5 | 582 | 2.1 |
| Octane | 620 | 620 | 0.0 | 630 | 1.6 |
| Decane | 570 | 575 | 0.9 | 587 | 3.0 |
| Dodecane | 607 | 610 | 0.5 | 620 | 2.1 |
| Tetradecane | 550 | 556 | 1.1 | 565 | 2.7 |

Δ% is the % difference between the single-point and experimentally extrapolated values of $[\eta]$.

The single-point approximation methods appear to give very good predictions of intrinsic viscosity. With the slight exception of pentane, all values fall well within the experimental errors expected in extrapolation of a concentration series. It can be concluded that the models for predicting $[\eta]$ are applicable.

The values of $[\eta]$ were measured so that the Flory-Huggins interaction parameters could be calculated. This calculation was discussed in section 1.5.1. All values of $[\eta]$ calculated were applied to allow a comparison to be drawn. The equations used to calculate $\chi$ were those derived by Kok and Rudin[14-16] (equations 1.28 - 1.30) and by Tseng and Lloyd[36] (equations 1.32 and 1.33).

Table 3.12 shows the calculated values of $\chi$ by applying each of the three equations to the extrapolated and single-point viscosities.

**TABLE 3.12.** Flory-Huggins Interaction Parameters for PIB/n-Alkanes @25°C.

| | χ-EQUATION AND [η] APPLIED | | |
|---|---|---|---|
| | **Kok & Rudin (equation 1.30)** | | |
| **n-Alkane** | **Extrapolated [η]** | **Solomon & Ciuta [η]** | **Rudin [η]** |
| Pentane | 0.490 | 0.488 | 0.487 |
| Hexane | 0.480 | 0.480 | 0.480 |
| Octane | 0.469 | 0.469 | 0.468 |
| Decane | 0.460 | 0.460 | 0.458 |
| Dodecane | 0.459 | 0.459 | 0.458 |
| Tetradecane | 0.459 | 0.458 | 0.457 |
| | **Lloyd 1 (equation 1.32)** | | |
| | **Extrapolated [η]** | **Solomon & Ciuta [η]** | **Rudin [η]** |
| Pentane | 0.493 | 0.491 | 0.491 |
| Hexane | 0.483 | 0.484 | 0.482 |
| Octane | 0.475 | 0.475 | 0.474 |
| Decane | 0.475 | 0.475 | 0.473 |
| Dodecane | 0.466 | 0.466 | 0.465 |
| Tetradecane | 0.470 | 0.469 | 0.468 |
| | **Lloyd 2 (equation 1.33)** | | |
| | **Extrapolated [η]** | **Solomon & Ciuta [η]** | **Rudin [η]** |
| Pentane | 0.490 | 0.487 | 0.486 |
| Hexane | 0.473 | 0.473 | 0.471 |
| Octane | 0.457 | 0.457 | 0.455 |
| Decane | 0.459 | 0.458 | 0.456 |
| Dodecane | 0.443 | 0.443 | 0.440 |
| Tetradecane | 0.451 | 0.449 | 0.447 |

All three equations for $\chi$ yield similar values, however for the purposes of examining the effect of polymer conformation on the degradation the average values of the Kok and Rudin and Lloyd 1 equations will be used as shown in Table 3.13.

TABLE 3.13. Flory-Huggins Interaction Parameters.

| n-Alkane | $\chi$-Parameter |
|---|---|
| Pentane | 0.490 |
| Hexane | 0.482 |
| Octane | 0.472 |
| Decane | 0.467 |
| Dodecane | 0.463 |
| Tetradecane | 0.464 |

By comparing the $\chi$ parameters calculated from single-point estimations of $[\eta]$ with the extrapolated experimental values it can be seen that the values are in close agreement. It can be concluded that 'single-point' intrinsic viscosity measurements are a feasible approach to calculating the Flory-Huggins interaction parameter.

A graph of the effect of $\chi$ on the limiting molecular weight is shown in figure 3.76. It can be seen that when the polymer adopts a more open conformation (lower $\chi$ value) then the polymer is degraded to a greater extent to a lower limiting molecular weight. This behaviour is not unexpected; in solution, an uncoiled polymer chain will experience a greater force across it as it is pulled towards the site of a collapsing cavitation bubble than a chain of the same molecular weight that is coiled. It can be concluded that a polymer dissolved in a good solvents ($\chi$ lower) will experience greater degradation than the same polymer dissolved in a poor solvent ($\chi$ higher).

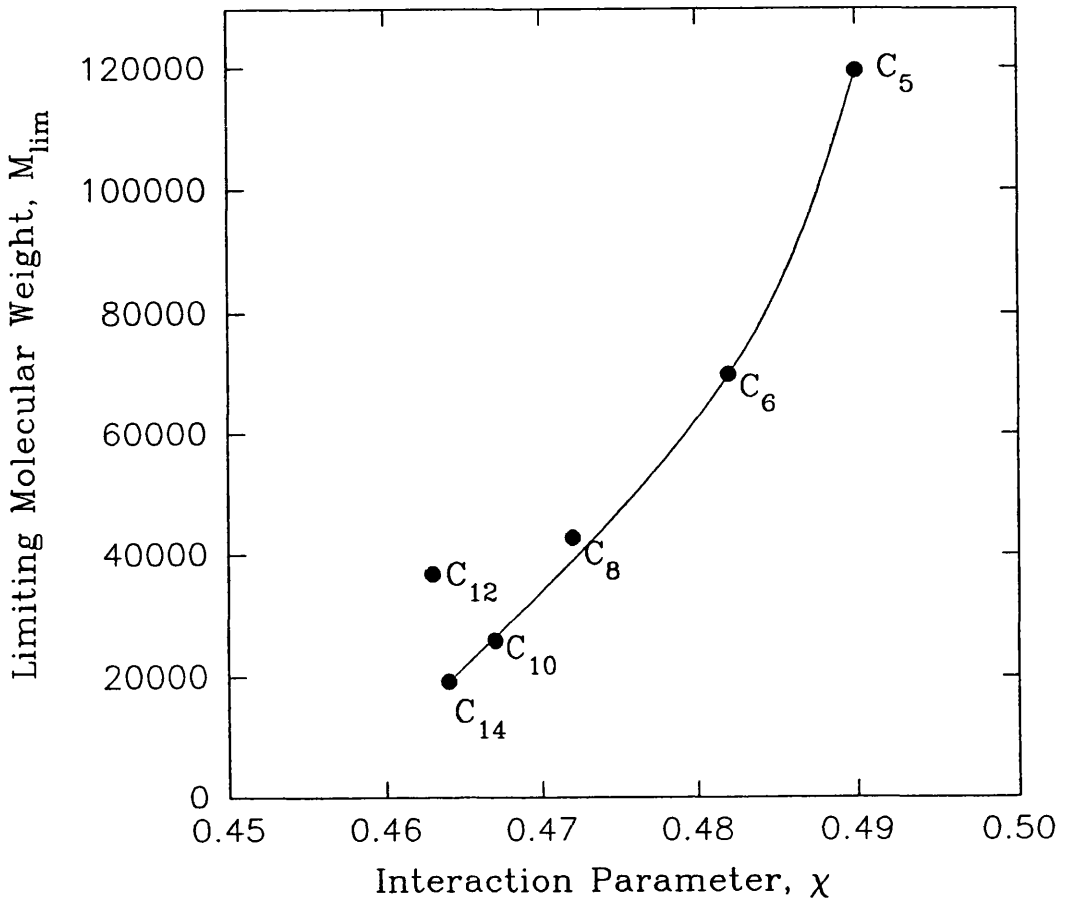


**FIGURE 3.76.** Effect of the Interaction Parameter on the Limiting Molecular Weight of PIB for the Sonication of a 1% w/v Solution in n-Alkanes.

Figures 3.77 - 3.79 show the effect of $\chi$ on the degradation rate constants predicted by the Schmid, Ovenall and Fujiwara rate models. The higher rate constants are observed in solvents possessing lower $\chi$ values.

These results correlate with predictions based on the shear and shock-wave mechanisms for ultrasonic degradation. Both mechanisms predict that the more coiled the conformation the polymer adopts in solution, the less the degradation. Considering the shock-wave mechanism, a highly coiled polymer will be pulled towards a collapsing cavity in a 'tight-ball' configuration. An uncoiled polymer which will have solvent molecules on one side of the polymer chain being pulled towards the collapsing bubble very violently and solvent molecules on the side away from the cavity not experiencing such a large effect, will experience a differential 'pull' on either side of the open polymer chain which will result in chain cleavage.

In conclusion, it is a combination of solvent and polymer properties that dictate the rate and extent of ultrasonic degradation in solution. The various parameters controlling the ultrasonic degradation process have been discussed, it is now possible to address the characterisation of the macromolecular radical products using ESR spectroscopy.

## 3.8 Characterisation of the Products of Ultrasonic Degradation by ESR Spectroscopy.

As already explained in section 1.9, the primary product of the ultrasonic degradation process in most instances is a macroradical. Electron spin resonance (ESR) spectroscopy provides the unique opportunity of absolutely confirming the presence of the radicals and provides information concerning the local environment of radical species leading to the identification of the species isolated.

The macroradicals expected to be produced during sonication are very short-lived and it was not possible to insonate samples directly inside the ESR cavity. To overcome this the technique of radical trapping was used which relies on the efficient trapping of the macroradicals by a highly reactive radical scavenger molecule.

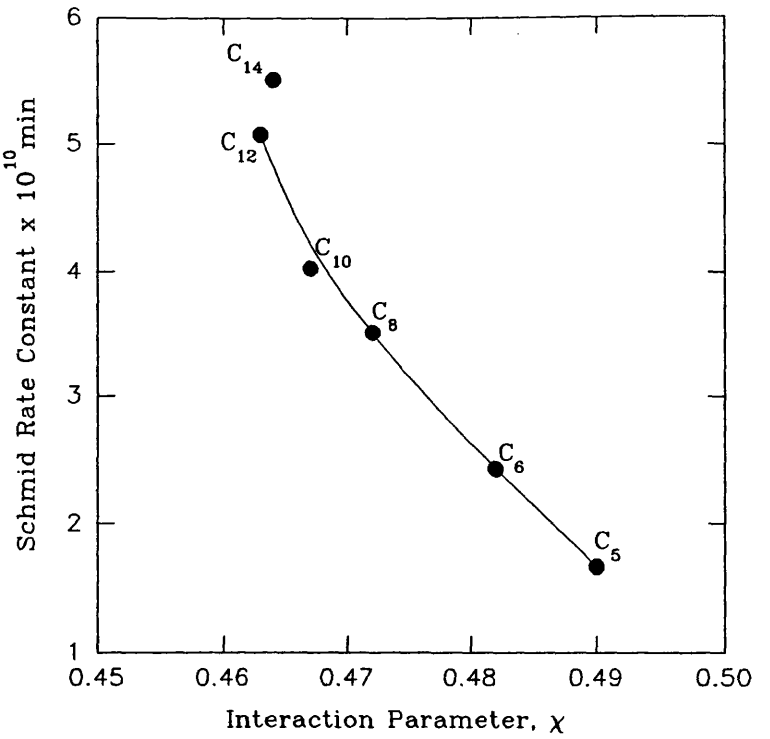


**FIGURE 3.77.** Effect of the Interaction Parameter on the Schmid Rate Constant for the Sonication of 1% w/v PIB in n-Alkanes.

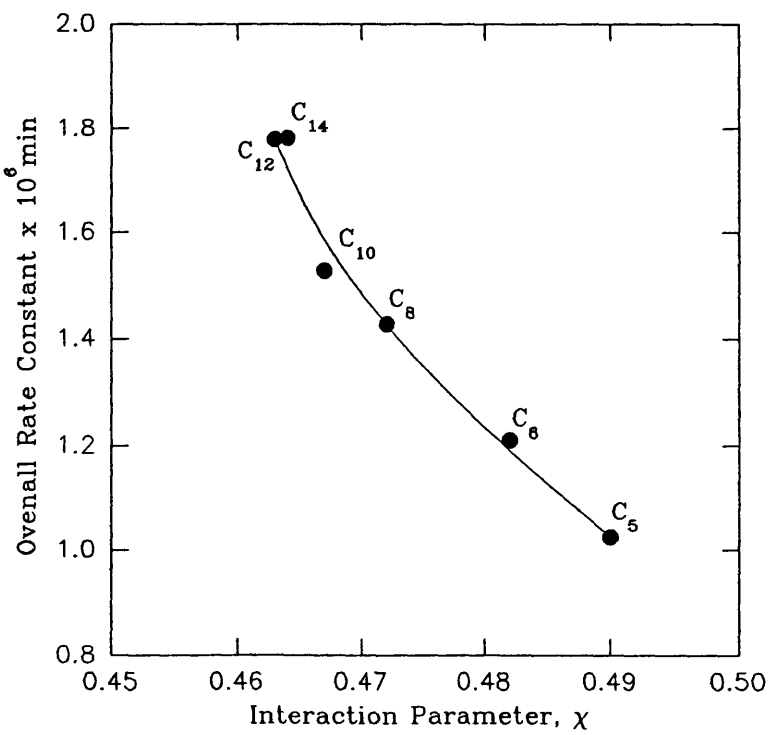


**FIGURE 3.78.** Effect of the Interaction Parameter on the Ovenall Rate Constant for the Sonication of 1% w/v PIB in n-Alkanes.

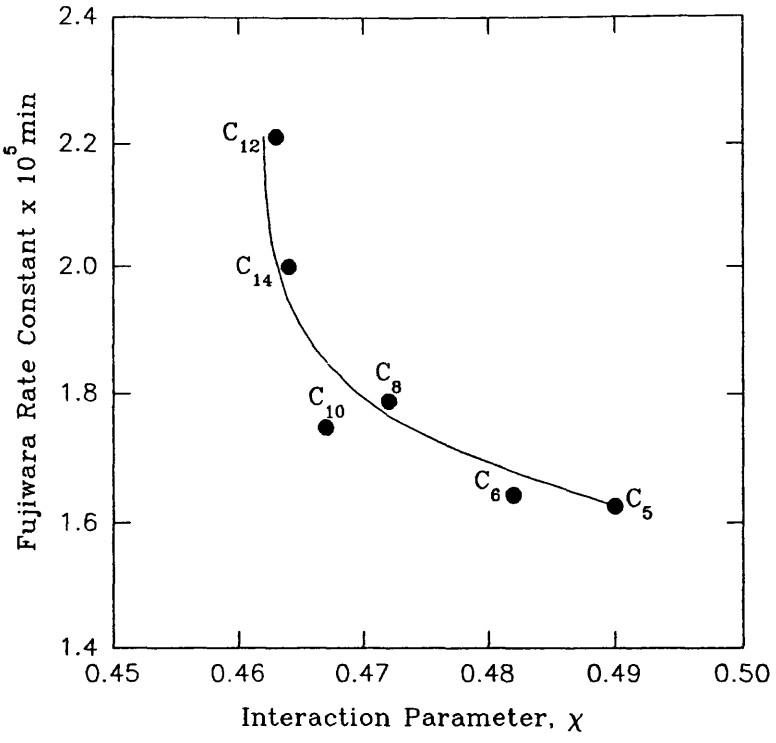


**FIGURE 3.79.** Effect of the Interaction Parameter on the Fujiwara Rate Constant for the Sonication of 1% w/v PIB in n-Alkanes.

Such radical traps include nitrosobenzene (NOB) and N-t-butyl-α-phenylnitrone (TBPN), which react readily with radicals produced ultrasonically as shown in figure 3.80 below.

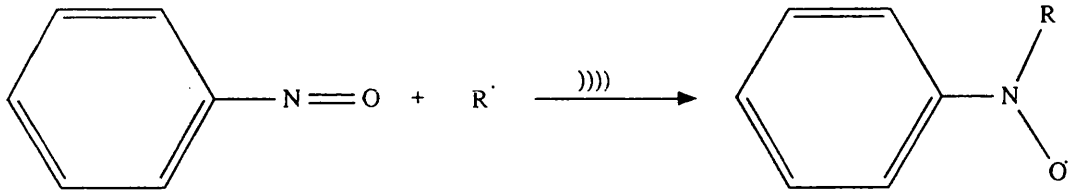


Nitrosobenzene

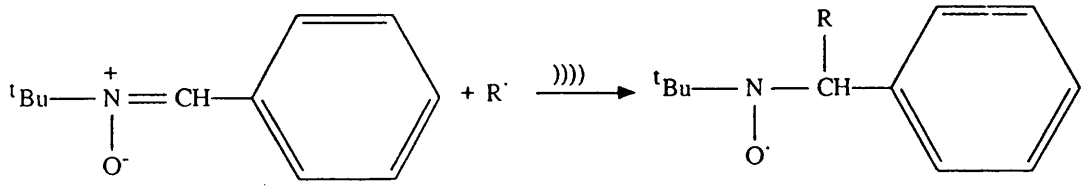


N-t-Butyl-α-phenylnitrone

**FIGURE 3.80.** Action of Radical Traps.

Hence any radicals produced during the sonication are isolated and can be detected by the ESR technique.

The primary signal expected for radicals attached to the nitrosobenzene spin-trap would be a triplet due to splitting with nitrogen. The number of lines appearing in the ESR spectrum can be predicted from the formula (2nI+1) where n is the number of contributing atoms possessing the spin quantum number I. Nitrogen ($^{14}N$) has a spin quantum number equal to one. Each transition in the case of an I=1 atom is equally likely to occur hence the three lines will appear in the ratio of 1:1:1. When nitrogen couples to a radical, such as the ones expected to be produced during an ultrasonic degradation process, the number of lines appearing in the spectrum can be calculated from the formula (2nI+1)(2mI+1) where m is the number of atoms of another type coupling directly with nitrogen and they may have a different spin quantum number, I. Oxygen ($^{16}O$) and carbon ($^{12}C$) both show no overall electron spin, their spin quantum number is zero, hydrogen ($^{1}H$) has a spin quantum number I = ½.

A solution of polyisobutylene was sonicated in tetrahydrofuran in the presence of nitrosobenzene. The first derivative (normal) ESR spectrum is shown in figure 3.81 and the second derivative is shown directly below it in figure 3.82.

The first derivative spectrum shows the expected three line spectrum characteristic of nitrogen. On close examination, and further differentiation of the signal, the fine structure of the radical species is evident. Polyisobutylene would be expected to produce two radical species on sonication which, assuming they react to the same degree with nitrosobenzene, would produce multiple splitting patterns. The structure of the two radicals are shown in figure 3.83.

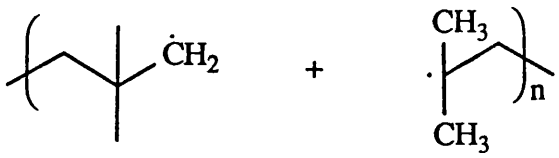


Macroradical "A" Macroradical "B"

**FIGURE 3.83.** Macroradicals Expected from the Ultrasonic Degradation of PIB.

Coupled to nitrogen, as shown in figure 3.80, macroradical A has two equivalent protons on the adjacent methylene group, this should give rise to a triplet of triplets, this is visible in the second derivative spectrum, figure 3.82, beneath the main triplet. Macroradical B has six protons which may appear as being non-equivalent owing to the proximity of the phenyl group present in nitrosobenzene, this would be expected to produce complex multiplets which appear in the second derivative spectrum as satellite peaks on either side of the main resonance signals.

Polyisobutylene was sonicated in the presence of a second trap, TBPN, in an attempt to confirm the results. The spectrum obtained is shown in figure 3.84 and its derivative in figure 3.85. The main nitrogen triplet is split into doublets by the single proton present in the radical trap adjacent to nitrogen. Macroradicals attached to the

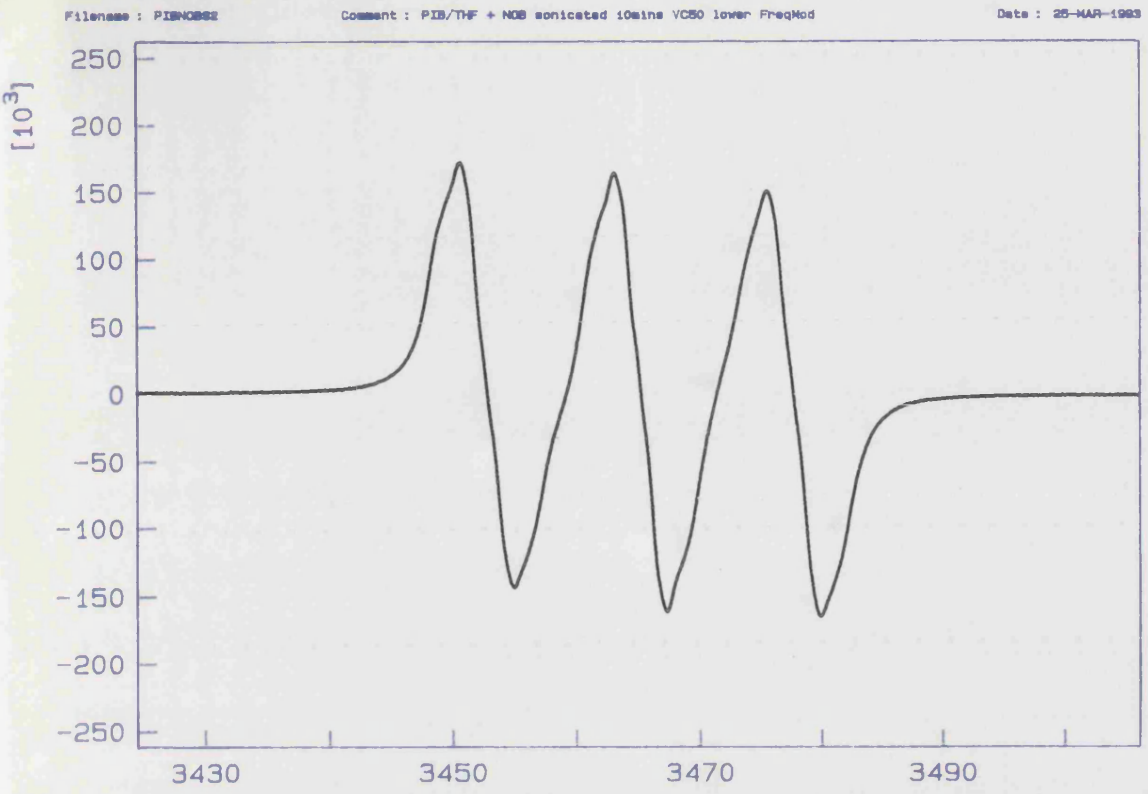


**FIGURE 3.81.** ESR Spectrum of PIB Sonicated in the Presence of Nitrosobenzene.

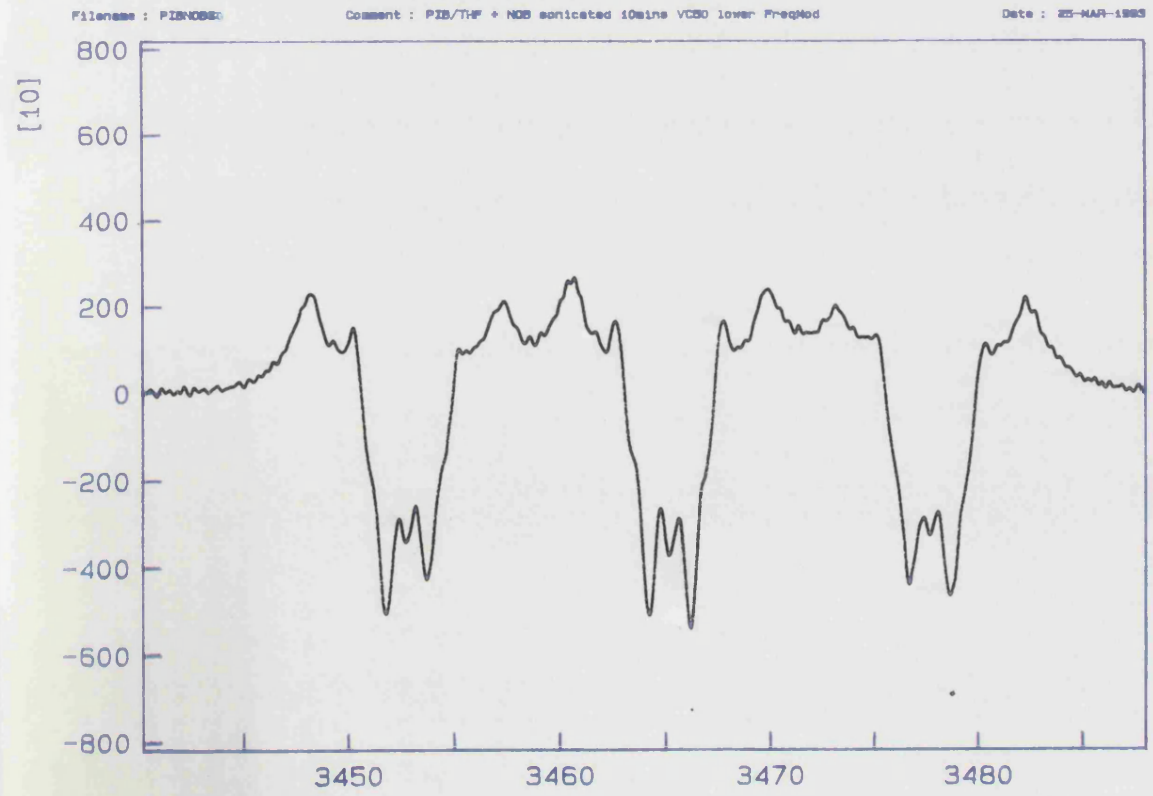


**FIGURE 3.82.** Second Derivative ESR Spectrum of PIB Sonicated in the Presence of Nitrosobenzene.

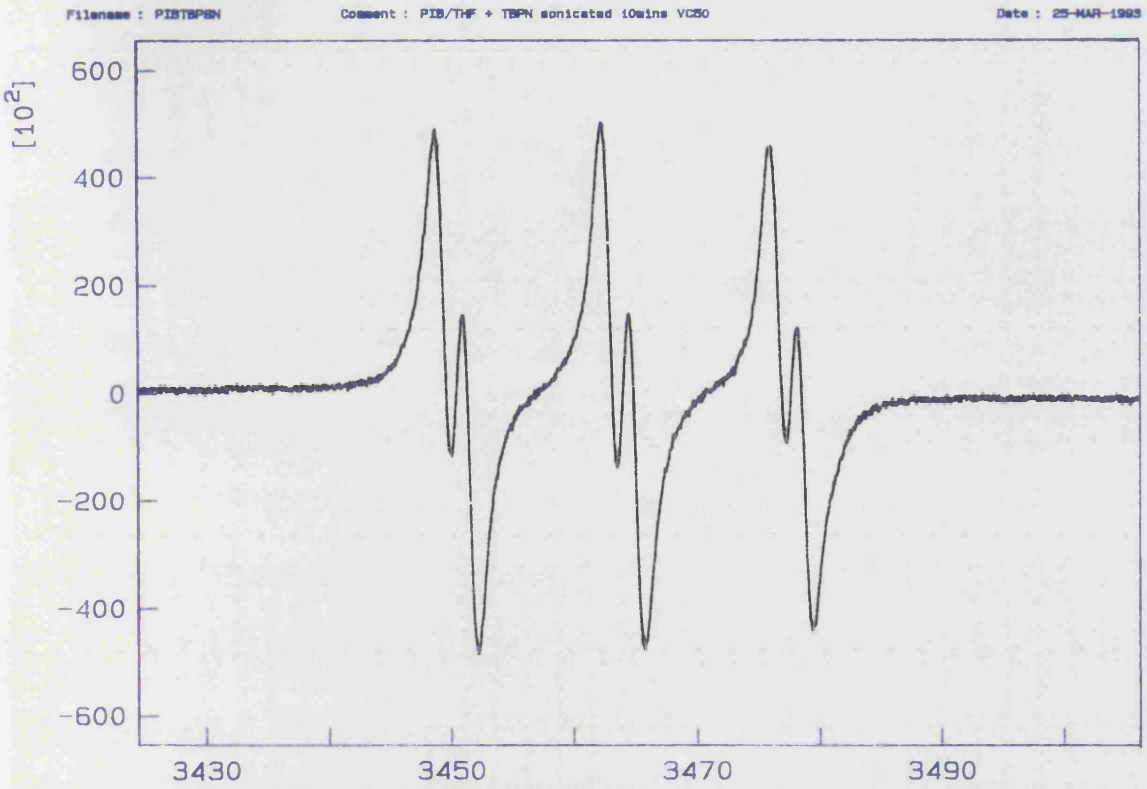


**FIGURE 3.84.** ESR Spectrum of PIB Sonicated in the Presence of N-t-Butyl-α-phenylnitrone.

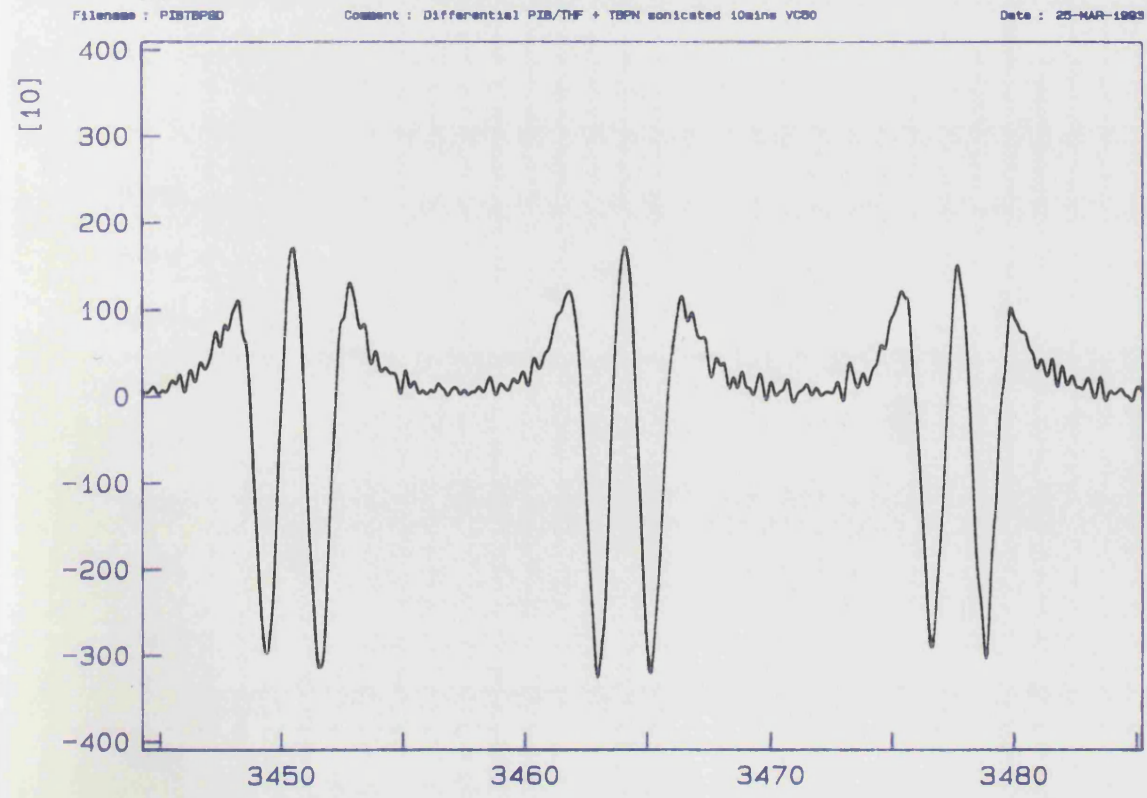


**FIGURE 3.85.** Second Derivative ESR Spectrum of PIB Sonicated in the Presence of N-t-Butyl-α-phenylnitrone.

TBPN molecule are now further away from nitrogen than in NOB and thus the strength of the signal is significantly reduced and is not apparent in the spectrum. It can be concluded that in this study, the choice of radical trap is important in isolating the signal and, although both confirm the production of radicals during sonication, the nitrosobenzene provides a more detailed picture of the radicals.

As a comparison, a solution of polystyrene in tetrahydrofuran was sonicated in the presence of NOB. The ESR spectrum is shown in figure 3.86 with its derivative in figure 3.87. The structures of the radicals expected are shown in figure 3.88.

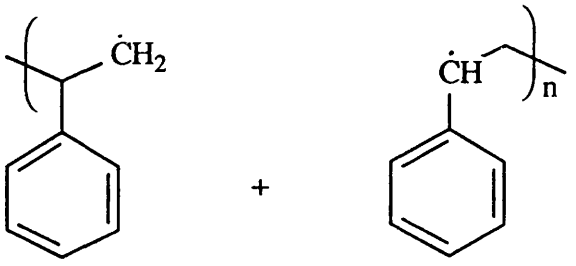


Macroradical "A" Macroradical "B"

**FIGURE 3.88.** Macroradicals Expected from the Ultrasonic Degradation of PS.

Macroradical A, coupled to NOB would be expected to produce a triplet of triplets, as seen in the second derivative spectrum. Furthermore the single proton in macroradical B will split the triplet into doublets. Contributions from ESR-active atoms further away from the radical site add more fine structure to the spectra.

Polystyrene was sonicated in the presence of TBPN and, as with polyisobutylene, the nature of the radical trapped dictates that a detailed picture of the polymer radical is not obtained. The spectrum and its derivative are shown in figures 3.89 and 3.90 respectively. The main nitrogen triplet is split into doublets but the signal is too weak for further characterisation.

The ESR technique has absolutely confirmed that during the ultrasonic degradation of PIB and PS, radicals are produced. The conditions and nature of the reagents used could be modified to assist more accurate determination of the nature of

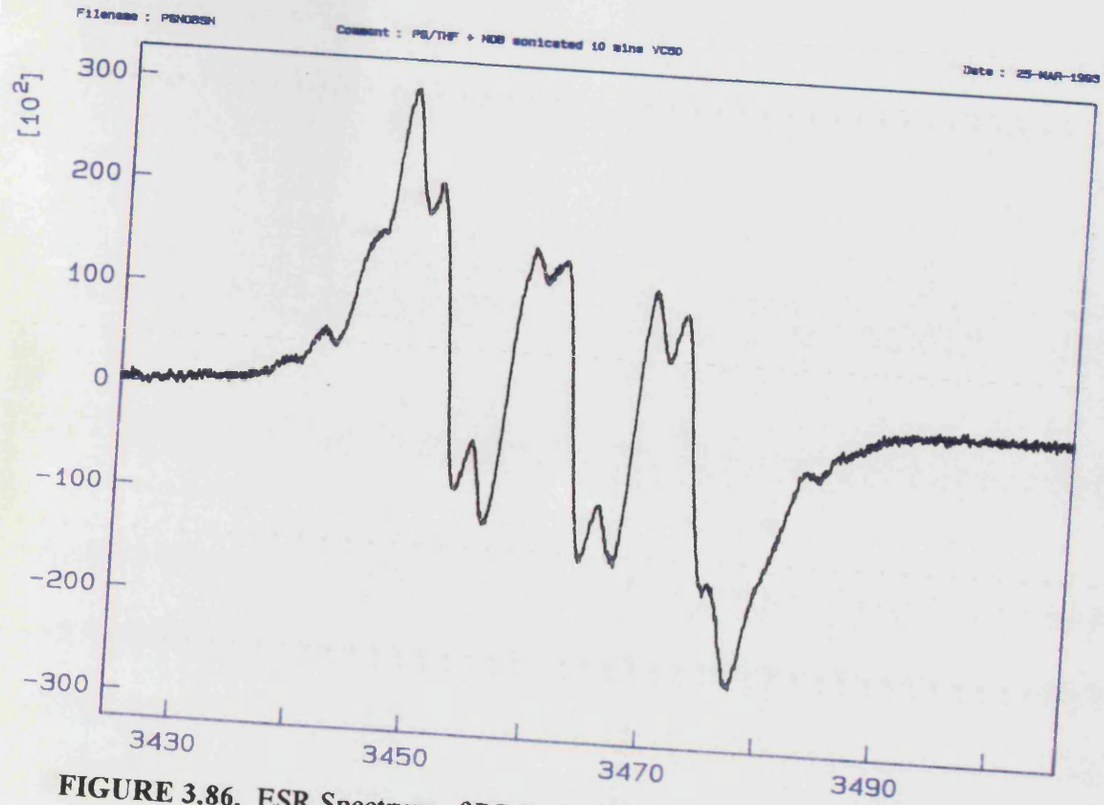


**FIGURE 3.86.** ESR Spectrum of PS Sonicated in the Presence of Nitrosobenzene.

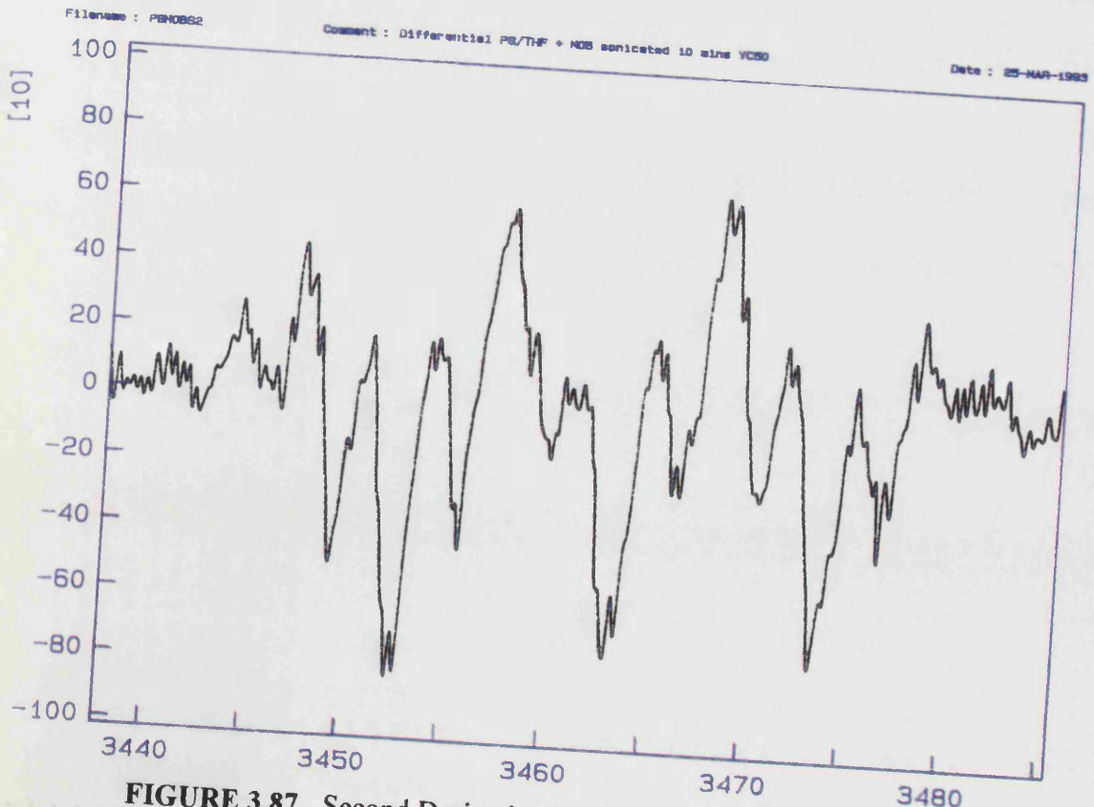


**FIGURE 3.87.** Second Derivative ESR Spectrum of PS Sonicated in the Presence of Nitrosobenzene.

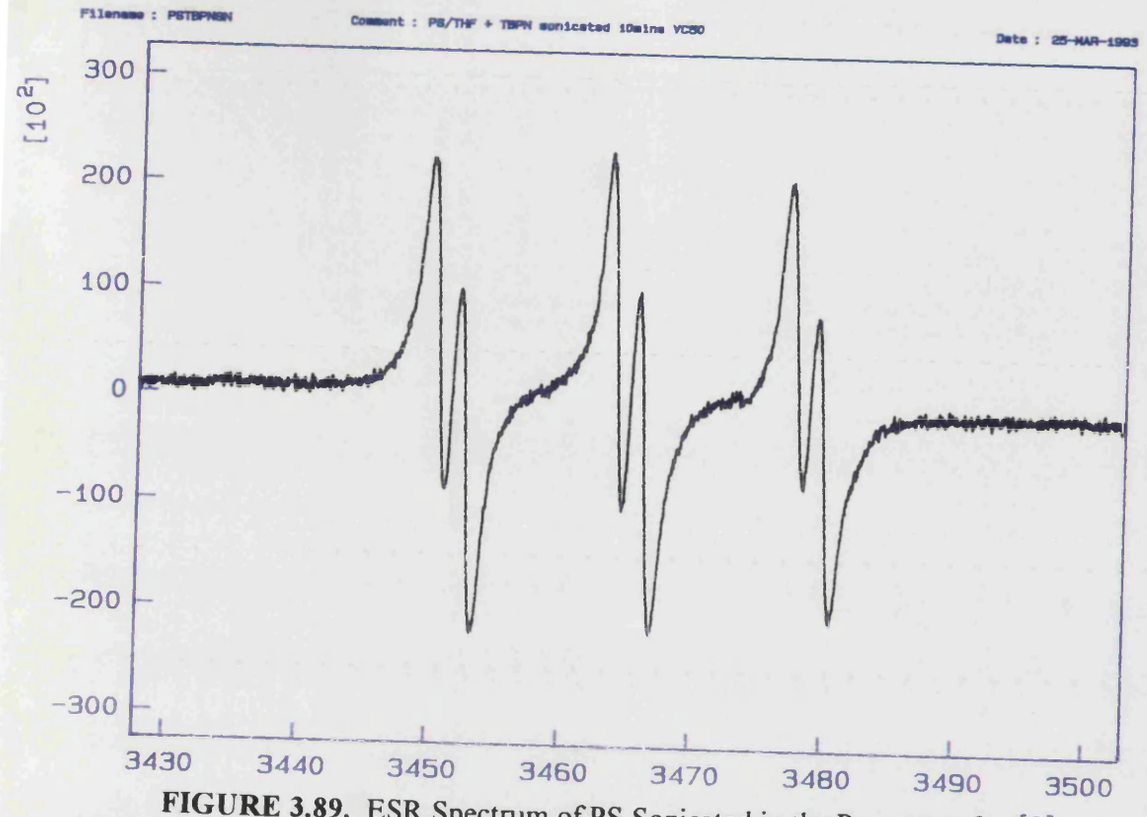


**FIGURE 3.89.** ESR Spectrum of PS Sonicated in the Presence of N-t-Butyl-α-phenylnitrone.

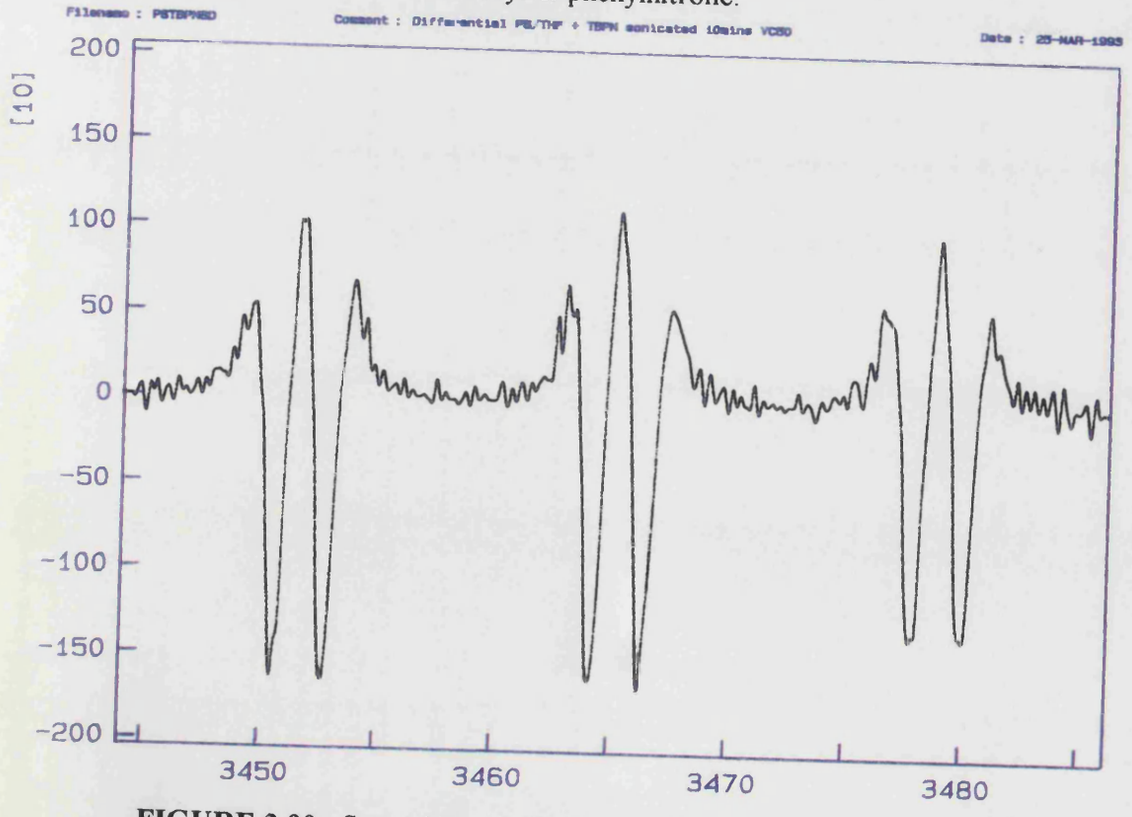


**FIGURE 3.90.** Second Derivative ESR Spectrum of PS Sonicated in the Presence of N-t-Butyl-α-phenylnitrone.

the radicals produced. One notable improvement would be to insonate the polymer solutions *in situ* whilst they are suspended inside the ESR cavity, this would facilitate the possible monitoring of the kinetics of radical production and assist in optimising the conditions for producing functionalised polymers.

One polymer thought to degrade ultrasonically without the production of radical species, as described in section 1.9, is poly(dimethyl siloxane). A solution of PDMS was subjected to ultrasonic treatment identical to that received by PIB, in the presence of TBPN. The spectrum is shown in figure 3.91. Clearly there are no radical species generated (this was repeated in the presence of methanol with identical results) and the ESR signal confirms that the mechanism of degradation of PDMS is non-radical and therefore suggests disproportionation, or a heterolytic cleavage, reaction is occurring.

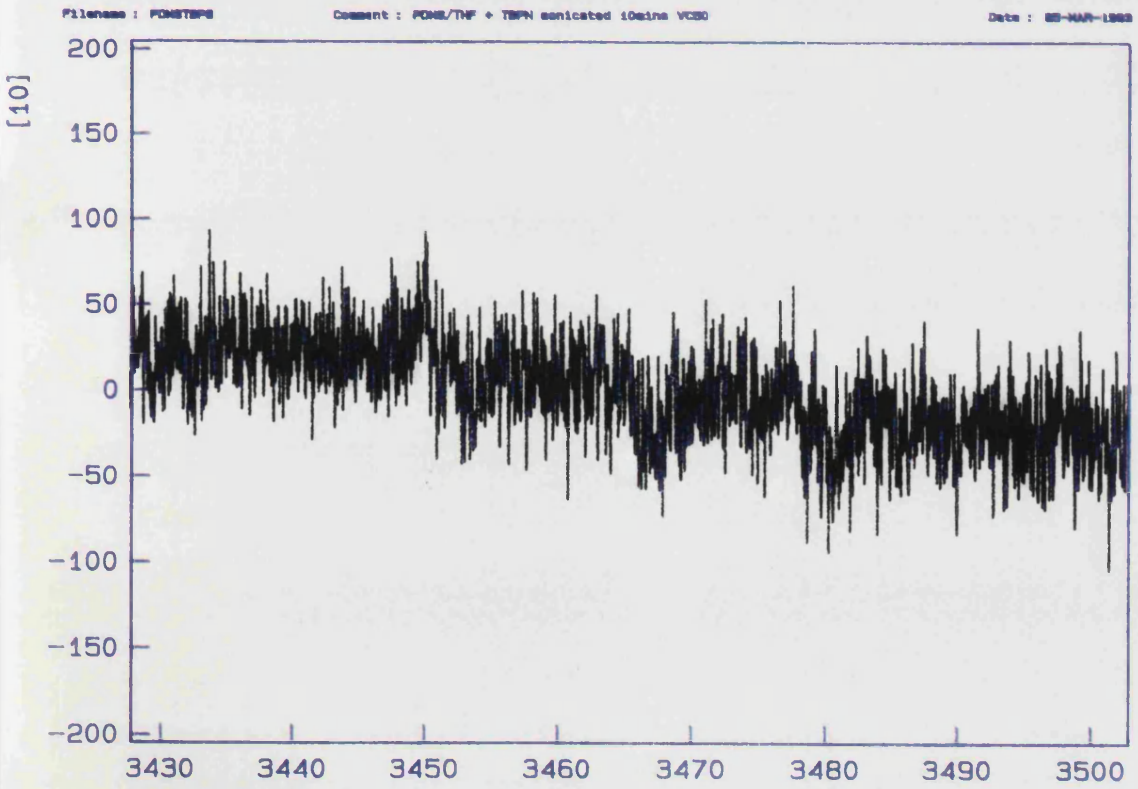


**FIGURE 3.91.** ESR Spectrum of PDMS Sonicated in the Presence of N-t-Butyl-α-phenylnitrone.

# CHAPTER FOUR

# CONTROLLED ULTRASONIC DEGRADATION OF POLYETHYLENE AND POLYPROPYLENE

## 4.1 Controlled Ultrasonic Degradation of Polyethylene and Polypropylene.

Polyethylene and polypropylene are two polymers which attract a high degree of commercial interest due to their wide ranging applications. The market for these materials is of great value and is highly competitive. The control of the properties of the polymers, especially as a result of processing leading to lower polydispersity polymers, is of great industrial importance.

The ultrasonic degradation of polyethylene and polypropylene has not been studied to any great degree, possibly due to the high temperature reaction conditions required for solution sonication and added complications involved in the analysis of molecular weights. Solutions were prepared in decahydronaphthalene at 80°C and this temperature was maintained throughout the sonication by circulating hot water around the temperature controlled jacket in order to ensure the polymer remained in solution. As a feasibility study 1% w/v solutions of polyethylene and polypropylene were sonicated for 24 hours sampling periodically. All of the polymer samples were precipitated into acetone, collected, dried under vacuum and sent to RAPRA Technology Ltd. for analysis. GPC was used to determine molecular weight averages and was performed at 140°C with 1,2-dichlorobenzene as the eluent.

Figures 4.1 and 4.2 show the variation of $M_w$ and $M_n$ with sonication time for polyethylene and polypropylene respectively. From the graphs it can be seen that there is a far greater overall decrease in $M_w$ and only a slight decrease in $M_n$. This narrowing of the molecular weight distribution is shown in figure 4.3. Both samples start with a polydispersity in excess of 6.0 and narrow to approximately 2.0 after 24 hours sonication. This sort of decrease in molecular mass of polymers coupled with a narrowing of the distribution is usually indicative of mechanical degradation. The shock-wave and shear mechanisms proposed for the ultrasonic degradation comply with this observation predicting a mechanochemical process.

For both polymers the GPC chromatograms obtained can be overlaid for the sonication as shown in figures 4.4 and 4.5 for polyethylene and polypropylene respectively. The overlays clearly show that as the polymer is "ultrasonically

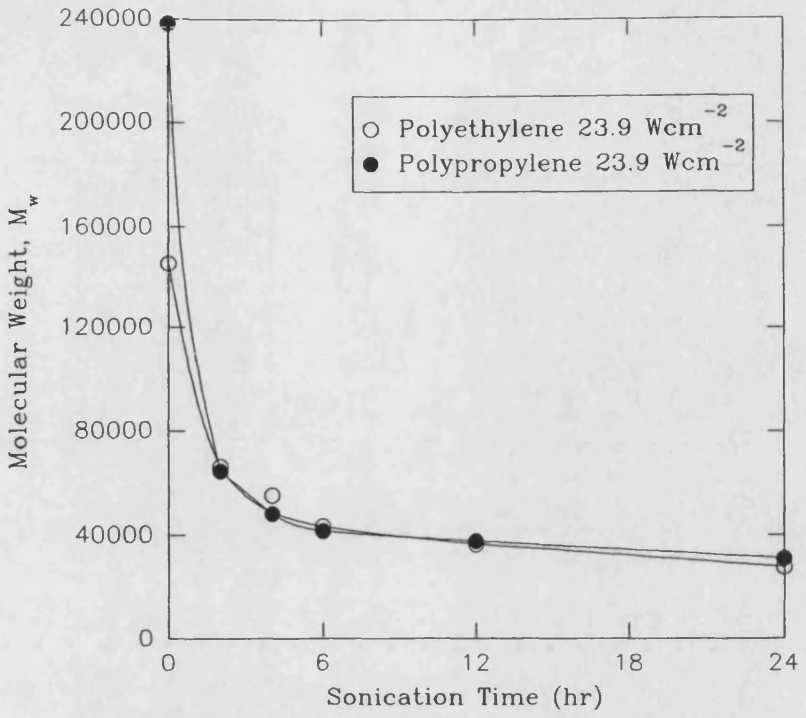


**FIGURE 4.1.** Variation of Weight Average Molecular Weight During the Sonication of 1% w/v Polyethylene and Polypropylene in Decahydronaphthalene.

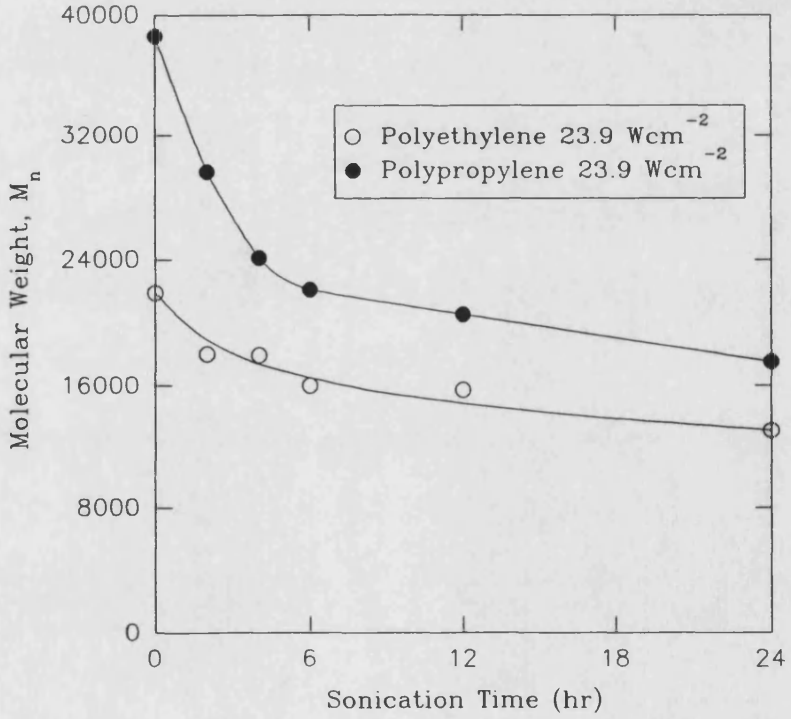


**FIGURE 4.2.** Variation of Number Average Molecular Weight During the Sonication of 1% w/v Polyethylene and Polypropylene in Decahydronaphthalene.

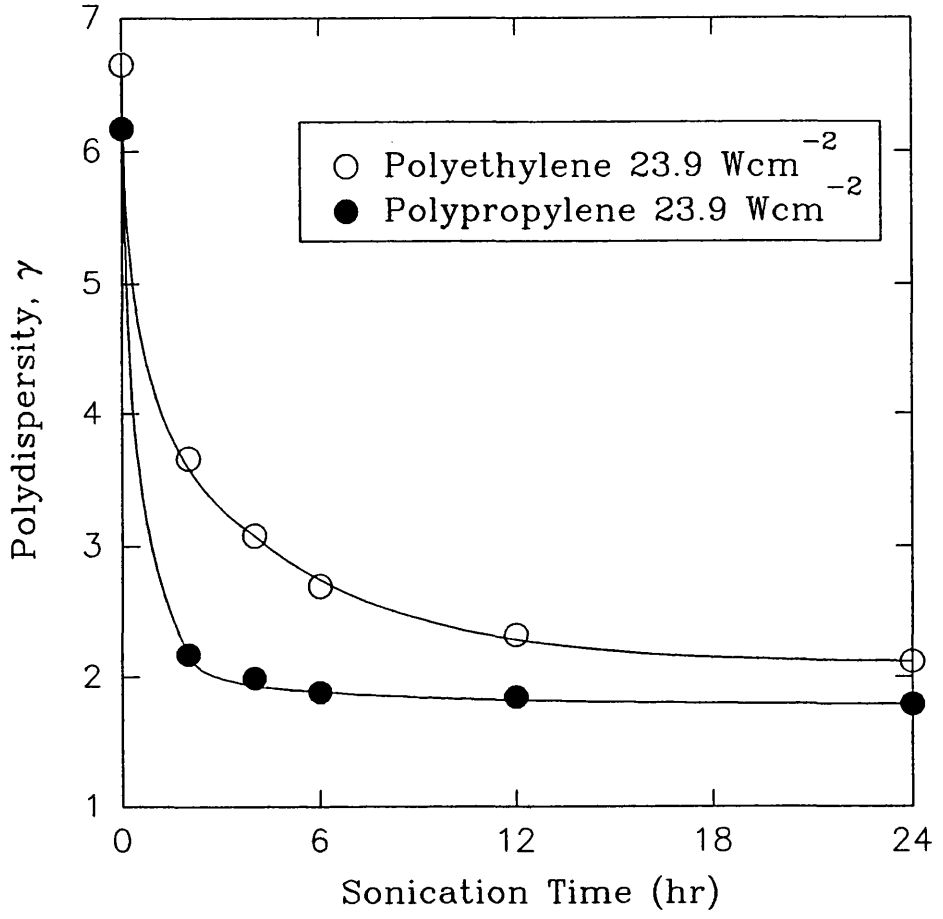


**FIGURE 4.3.** Variation of Polydispersity During the Sonication of 1% w/v Polyethylene and Polypropylene in Decahydronaphthalene.

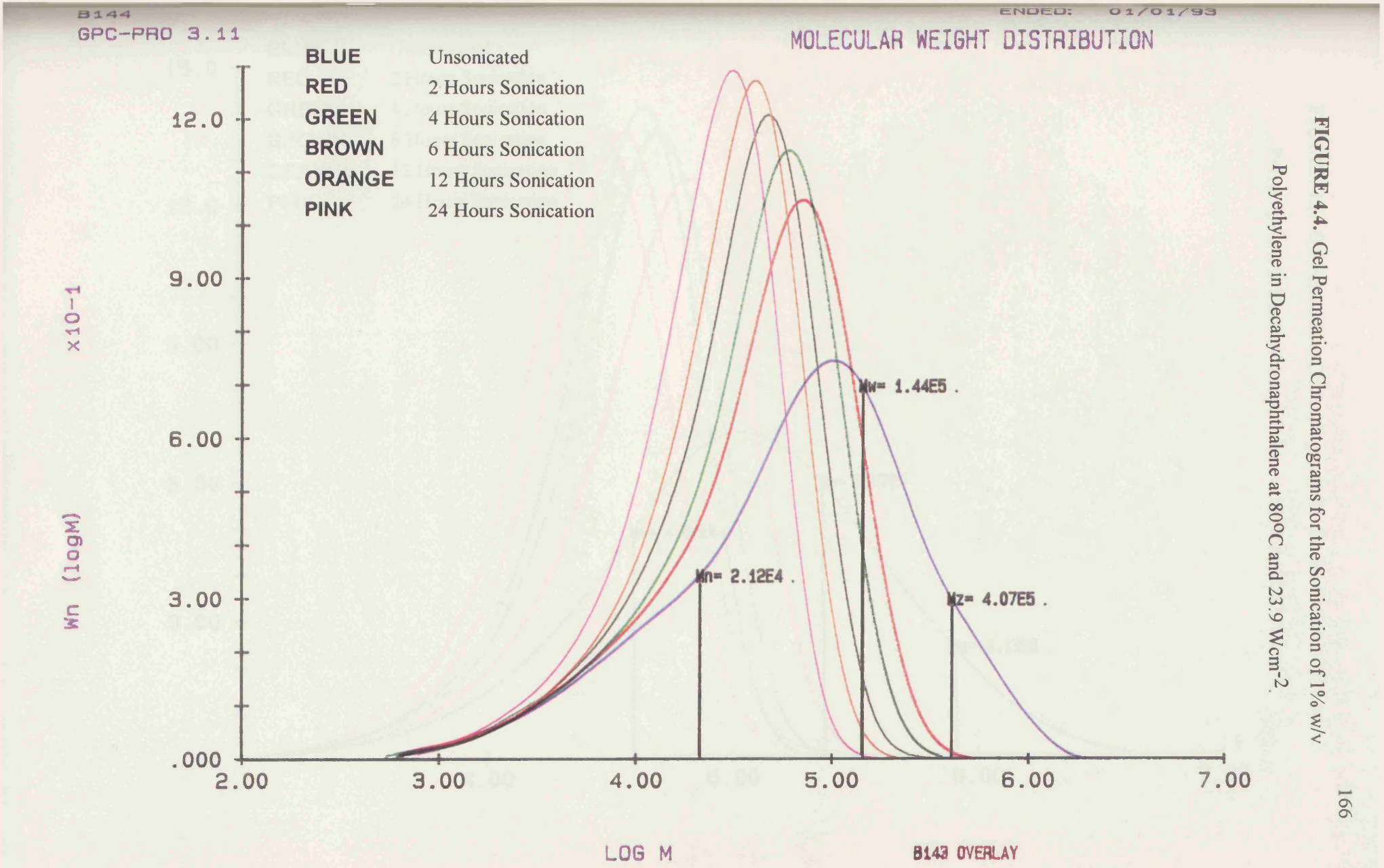


**FIGURE 4.4.** Gel Permeation Chromatograms for the Sonication of 1% w/v Polyethylene in Decahydronaphthalene at 80°C and 23.9 $Wcm^{-2}$.

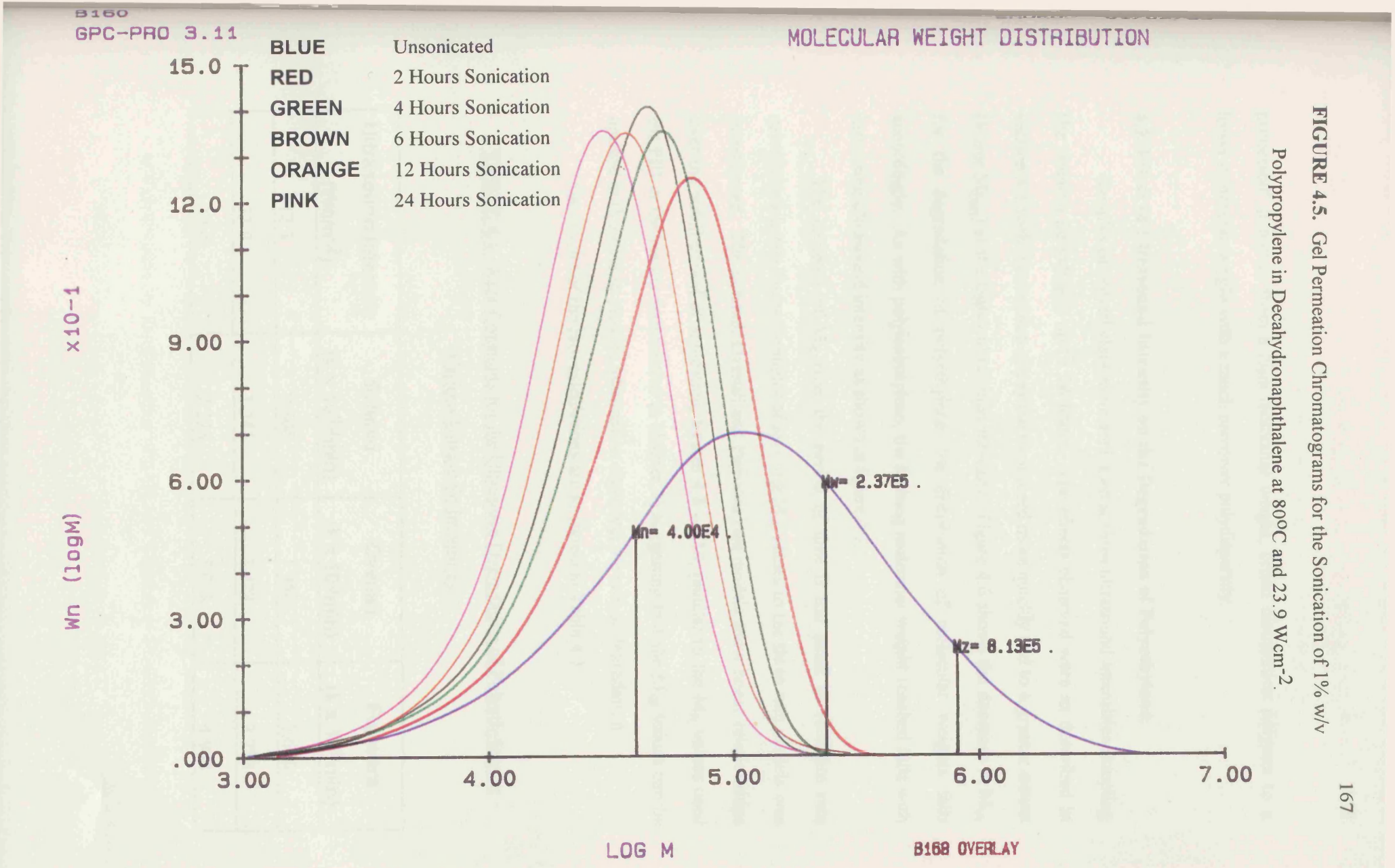


**FIGURE 4.5.** Gel Permeation Chromatograms for the Sonication of 1% w/v Polypropylene in Decahydronaphthalene at 80°C and 23.9 $Wcm^{-2}$.

processed" it moves from a high molecular weight, broad distribution polymer to a lower molecular weight with a much narrower polydispersity.

### 4.2 Effect of Ultrasound Intensity on the Degradation of Polyethylene.

Samples of polyethylene were sonicated at three ultrasound intensities sampling the reaction periodically up to 24 hours. The effects observed were as described in section 4.1 with the reaction appearing to proceed more quickly and to a greater extent (lower $M_{lim}$) at the higher ultrasound intensity. Figure 4.6 shows the decrease in $M_w$ for the degradation of polyethylene, the distribution of molecular weights falls accordingly. As with polyisobutylene, the limiting molecular weight reached falls with increasing ultrasound intensity as shown in figure 4.7.

The decrease of $M_n$ over the period of time is too small to facilitate rate calculations hence the applicability of applying $M_w$ values to the three rate models was investigated. The Schmid, Ovenall and Fujiwara rate models show linear relationships over the initial period of sonication, figures 4.8 - 4.10, (similar to the $M_n$ values used for PIB in the results documented in chapter 3) suggesting that the $M_w$ values can be applied in this case to provide information regarding the rate of degradation.

The results of the rate calculations are as shown in Table 4.1.

**TABLE 4.1.** Rate Constants for the Ultrasonic Degradation of Polyethylene at Various Ultrasonic Intensities.

| Ultrasound Intensity ($Wcm^{-2}$) | Schmid ($k \times 10^{12} min$) | Ovenall ($k \times 10^{9} min$) | Fujiwara ($k \times 10^{6} min$) |
|---|---|---|---|
| 12.3 | 0.506 | 1.950 | 2.606 |
| 23.9 | 1.245 | 3.428 | 3.282 |
| 37.4 | 2.228 | 5.058 | 4.988 |

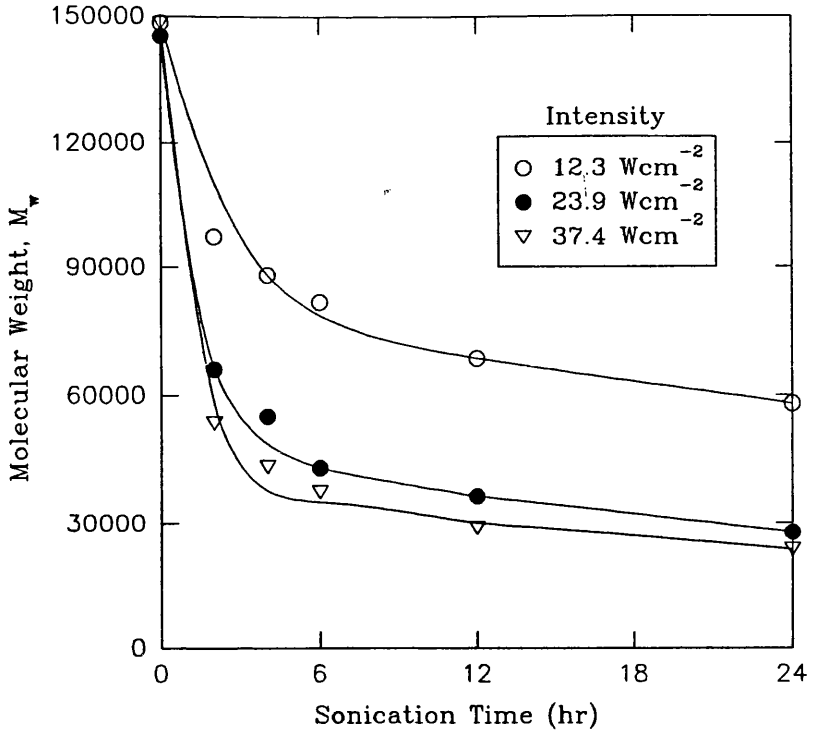


**FIGURE 4.6.** Variation of Weight Average Molecular Weight During the Sonication of 1% w/v Polyethylene in Decahydronaphthalene at Various Ultrasonic Intensities.

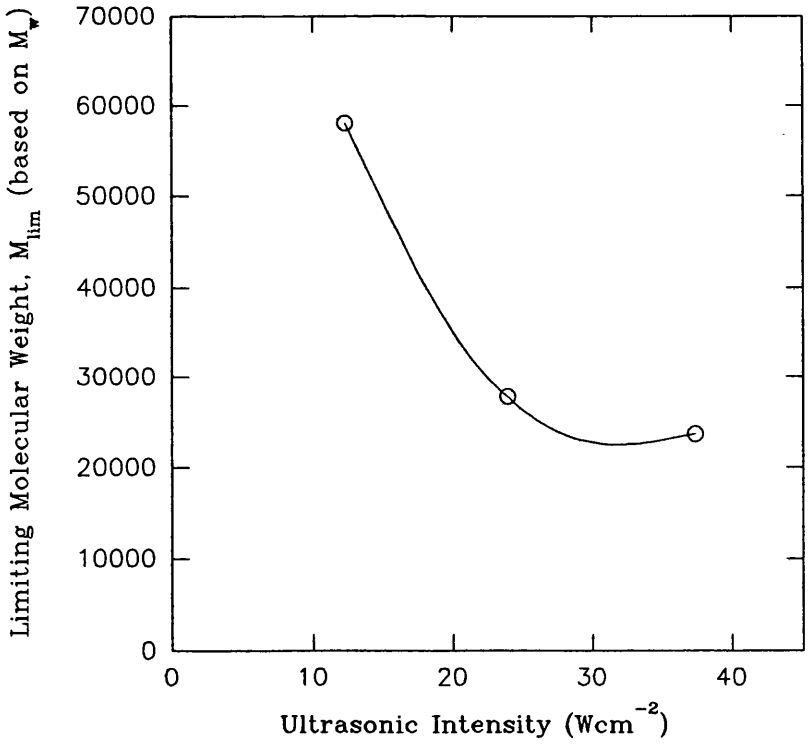


**FIGURE 4.7.** Effect of Ultrasonic Intensity on the Limiting Molecular Weight of Polyethylene for the Sonication of a 1% w/v Solution in Decahydronaphthalene.

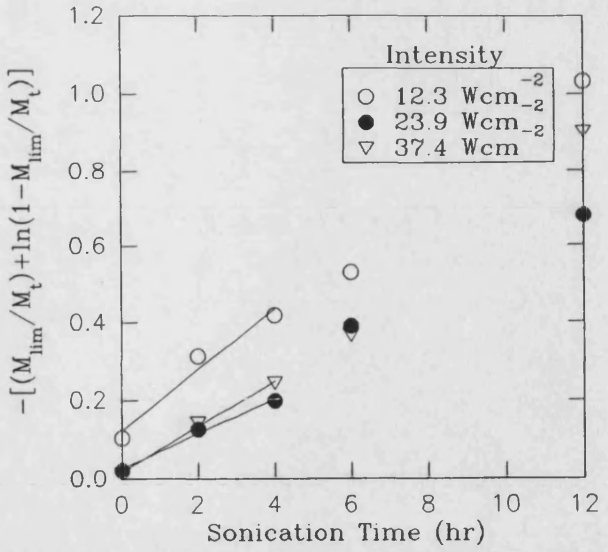


**FIGURE 4.8.** Schmid Rate Model Plot for the Sonication of 1% w/v Polyethylene in Decahydronaphthalene at Various Ultrasonic Intensities.

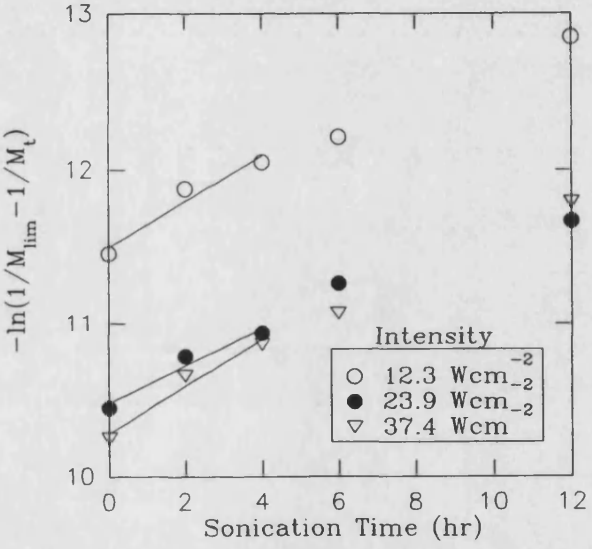


**FIGURE 4.9.** Ovenall Rate Model Plot for the Sonication of 1% w/v Polyethylene in Decahydronaphthalene at Various Ultrasonic Intensities.

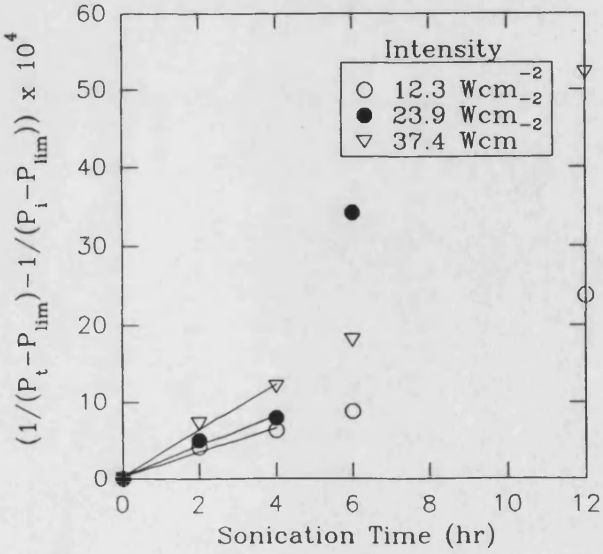


**FIGURE 4.10.** Fujiwara Rate Model Plot for the Sonication of 1% w/v Polyethylene in Decahydronaphthalene at Various Ultrasonic Intensities.

Linear relationships of rate constant against ultrasound intensity were obtained, as with polyisobutylene, for the Schmid and Ovenall models. The linear correlation coefficients for the Schmid and Ovenall models are 0.9994 and 0.9999 respectively, the Fujiwara model produced a linear correlation coefficient of 0.9799. The plots are shown in figures 4.11 - 4.13.

During the ultrasonic degradation process, the macromolecular radicals formed have the opportunity to introduce chain branching to the polymer in solution. This effect has not been previously studied for polyethylene under the influence of ultrasonic irradiation. Figure 4.14 shows schematically how long chain branching can be introduced ultrasonically into polyethylene.

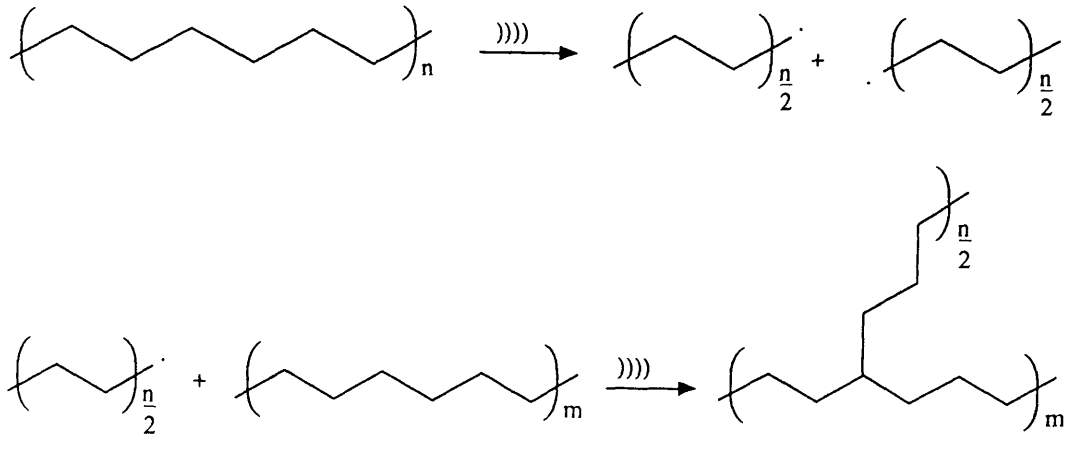


**FIGURE 4.14.** Schematic Representation of Chain Branching Introduced into a Sample of Polyethylene as a Result of Ultrasonic Processing.

## 4.3 Effect of the Degradation on the Degree of Chain Branching.

It was recognised soon after the high-pressure polymerisation of polyethylene by the free-radical mechanism had been developed that the properties of the polymer were different from those to be expected of a polymer of linear structure and that they

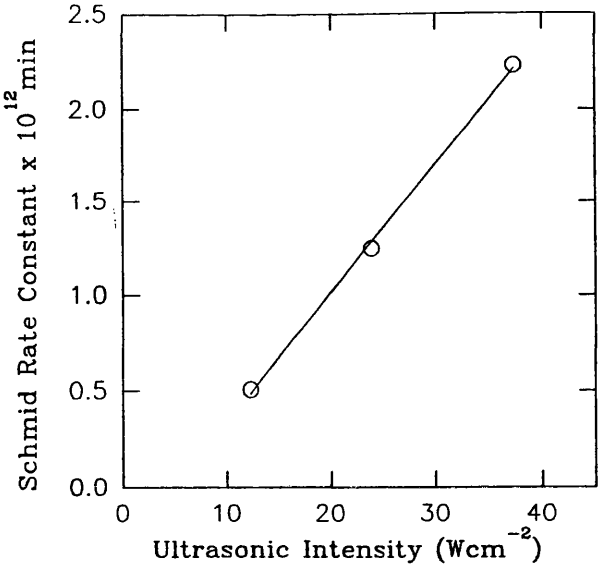


**FIGURE 4.11.** Effect of Ultrasonic Intensity on the Schmid Rate Constant for the Sonication of 1% w/v Polyethylene in Decahydronaphthalene.

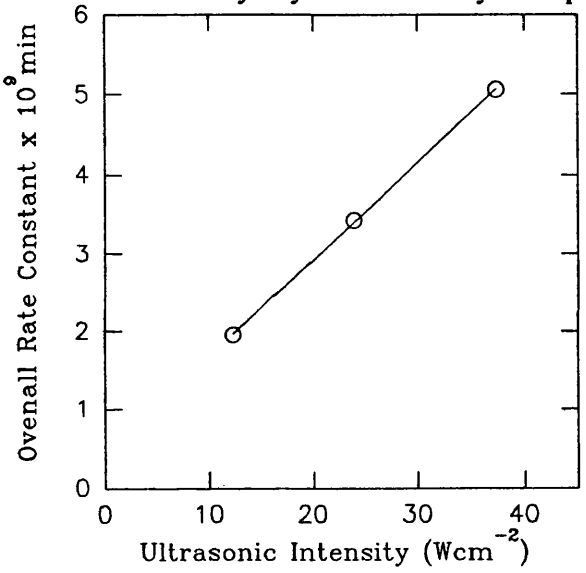


**FIGURE 4.12.** Effect of Ultrasonic Intensity on the Ovenall Rate Constant for the Sonication of 1% w/v Polyethylene in Decahydronaphthalene.

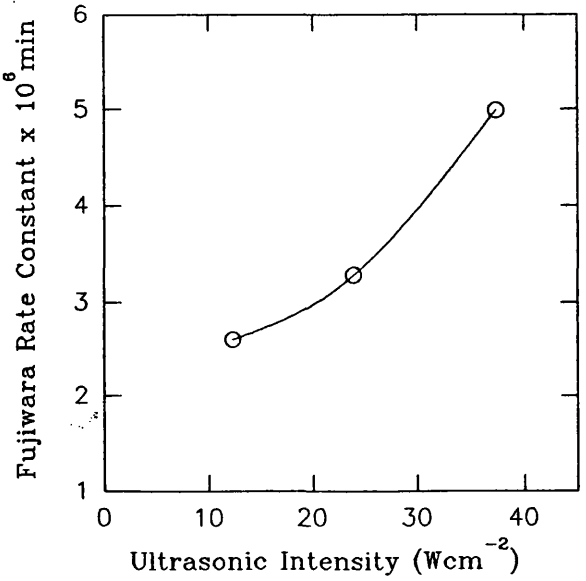


**FIGURE 4.13.** Effect of Ultrasonic Intensity on the Fujiwara Rate Constant for the Sonication of 1% w/v Polyethylene in Decahydronaphthalene.

depended greatly on the conditions of synthesis. Branching in polyethylene had been shown by infra-red spectroscopy[209,210], the presence of methyl groups in the polymer in concentrations appreciably higher than could be accounted for as the end-groups of a linear molecule[211], in fact several methyl groups per 100 carbon atoms. It was concluded that most methyl groups must be at the end of branches. It has also been shown by Roedel[212] that free-radical mechanisms in polyethylene could lead not only to short branches containing a few carbon atoms but, by a mechanism first proposed by Flory[213] involving the attack of growing polymer radicals on dead polymer chains and subsequent propagation from the active centres so produced on the latter, it could produce branches comparable in length with the main chain. Billmeyer[214] showed that the intrinsic viscosities of some branched polyethylene samples were lower than would be expected for linear polymers of the same molecular weight. Hence GPC-viscometry was employed in this study to determine the change in the degree of chain branching following a period of ultrasonic irradiation.

Branching is normally caused by transfer reactions within the polymer molecules. The rheological and mechanical properties of the polymer are greatly influenced by the degree of long chain branching.

The ultrasonic degradation mechanism produces radicals on the chain ends as a results of homolytic cleavage, it was therefore necessary to examine whether branching of the polymers occurred during the sonication and whether a concentrated solution produced more branching due to the closer proximity of the polymer chains. Polymer chains in close contact, in highly concentrated solutions, could undergo inter- as well as intramolecular transfer resulting in the introduction of significantly higher degrees of branching.

The effect of sonication on the degree of chain branching was investigated for polyethylene sonicated at three solution concentrations, 0.25% w/v, 1.00% w/v and 10.0% w/v. Samples were prepared having been subjected to 10, 60 and 360 minutes of ultrasonic irradiation.

The extent of chain branching was studied using GPC-viscometry at RAPRA Technology Ltd.

The GPC-viscometry branching calculations could be carried out in different ways. Mark-Houwink parameters could be used for a sample of polyethylene known to be linear or the degree of chain branching for all sonicated samples could be calculated relative to the starting material, i.e. assuming that to be linear. The latter technique was favourable in this study as this would determine the degree of branching introduced as a direct result of sonication. Table 4.2 shows the results obtained where $\lambda$ is the branching frequency and n is the number of branches per molecule. The underlying theory of the calculations was discussed in section 1.11.1.

**TABLE 4.2.** Chain Branching Results for Sonicated Polyethylene.

| Time (min) | Conc$^n$ (%w/v) | $M_w$ | $M_n$ | $\gamma$ | $\lambda_1$ | $\lambda_2$ | $n_1$ | $n_2$ |
|---|---|---|---|---|---|---|---|---|
| 0 | - | 224000 | 20600 | 10.9 | 0 | 3.9 | 0 | 3090 |
| 10 | 0.25 | 143500 | 22850 | 6.3 | 0.35 | 4.9 | 308 | 4306 |
| 60 | 0.25 | 75550 | 21000 | 3.7 | 1.65 | 14.3 | 1329 | 11550 |
| 360 | 0.25 | 45550 | 15400 | 3.0 | 1.71 | 7.7 | 1013 | 4561 |
| 10 | 1.00 | 163500 | 19050 | 8.7 | 0.20 | 4.3 | 147 | 3151 |
| 60 | 1.00 | 101000 | 16950 | 6.0 | 0.27 | 4.25 | 176 | 2771 |
| 360 | 1.00 | 53850 | 19050 | 2.9 | 2.445 | 10.9 | 1791 | 7986 |
| 10 | 10.0 | 222000 | 23400 | 9.5 | 0.13 | 4.1 | 117 | 3690 |
| 60 | 10.0 | 164000 | 15600 | 10.5 | 0.17 | 4.0 | 102 | 2400 |
| 360 | 10.0 | 129000 | 16850 | 7.6 | 0.205 | 4.0 | 133 | 2592 |

$\lambda_1$ and $n_1$ assume all results are relative to the starting material (assumed to be linear)

$\lambda_2$ and $n_2$ assume that Mark-Houwink parameters for a sample of linear polyethylene are $\alpha = 0.695$, $\log K = -3.29$

In all of the samples there is evidence for chain branching being introduced as a direct result of the ultrasonic degradation process.

In the 0.25% w/v and 1.00% w/v solutions the branching frequency, $\lambda$, increased substantially up until 360 minutes however in the case of the 10.0% w/v solution although branching was introduced it was to a much smaller extent. The most branched sample was the 1% w/v solution after 360 minutes.

It would be expected that the 10.0% w/v polyethylene solution would be the most highly branched due to the close proximity of the chains and hence making hydrogen abstraction along the chain by the radical on the chain end more probable.

After 360 minutes of sonication the 1.00% w/v sample was more branched than the 10.0% w/v sample. The probable reason for this being that there are considerably more chain breaks occurring in the 1.00% w/v sample than in the 10.0% w/v sample as predicted by the concentration studies for polyisobutylene in tetrahydrofuran in section 3.5. This makes the chance of either inter- or intramolecular transfer much more probable.

The 1.00% w/v is also slightly more branched than the 0.25% w/v sample. The concentration study on polyisobutylene would predict that there would be more chain breaks in the 0.25% w/v sample but perhaps in this system the optimum proximity of the chains is reached as the critical overlap concentration is approached and thus resulting in more likelihood of chain transfers.

Various approaches were applied to the results including the number of branches introduced per chain break and it was concluded that no apparent direct relationship between the length of sonication (or the concentration of solution irradiated) and the degree of chain branching introduced existed. The trends observed in the results however show that a degree of long chain branching is introduced into polyethylene as a result of ultrasonic degradation. Attempts were made to correlate this with the concentration of the solution and the period of ultrasonic irradiation.

# CHAPTER FIVE

# SYNTHESIS OF FUNCTIONALISED POLYISOBUTYLENE

## 5.1 Production of Functionalised Polyisobutylene.

A telechelic polymer is a type of functionalised material having two reactive groups[215], normally at the chain ends. It is these end-groups which are capable of reacting to form block copolymers[216].

An alternative method of using polyisobutylene is not as a homopolymer but as a segment in a block copolymer. It is common for copolymers to be composed of two types of segments so that the resulting material possesses some of the properties of each component. If polyisobutylene is to be used as a 'soft' block in a copolymer it is necessary that its molecular weight and functionality can be controlled in a such a way that the polymer has defined end-groups that are reactive or can be converted to reactive end-groups. Two processes are commonly used to make block copolymers. One is living polymerisation where a two- or three-block copolymer is made of isobutylene and a second monomer in one single reaction pot by successively adding the components, for example in the polymerisation of isobutylene followed by that of α-methyl styrene[217]. A second way is to make a difunctional oligomer that is polymerised in a second step to a block copolymer, this second step is often a condensation polymerisation. Neither one of these methods will be discussed in detail but an alternative technique producing functionalised polyisobutylene involving the application of high intensity ultrasound will be proposed and investigated.

It has been possible to produce functionalised polymers by a chain cleavage mechanism which can be initiated by oxidation, reduction and irradiation with light. These methods have the disadvantage that the degradation is random and thus the polydispersity of the resultant functionalised polymer will be high which dictates the properties of the final material.

Ultrasonic degradation of polymers has been shown to be non-random with the production of radicals at the chain ends. This offers the possibility of producing functionalised polymers with well defined chain lengths.

Analysis of functionalised polymers using normal analytical techniques can prove difficult if there is only one functional group per high molecular weight chain.

For the purposes of this study, the functionalised groups attached contained molecules with a strong UV chromophore. The presence of these functionalities can be easily detected and quantified by UV spectroscopy.

To test the feasibility of the ultrasonic technique a solution of polyisobutylene was degraded in the presence of a stable free radical, DPPH. This also gives information on the maximum rate of radical trapping. By calculating the number of radicals trapped it was possible to estimate the efficiency of the process. This was achieved by calculating the number of chain breaks occurring in the parent polyisobutylene molecule and also measuring the number of radicals produced by sonicating pure solvent with DPPH to find the solvent contribution.

DPPH has a strong UV absorbance at 520 nm which decreases as the radical reacts. The extinction coefficient of DPPH in tetrahydrofuran was calculated, using the Beer-Lambert law, by measuring the UV absorbance at 520 nm for a series of concentrations. The results are shown in figure 5.1.

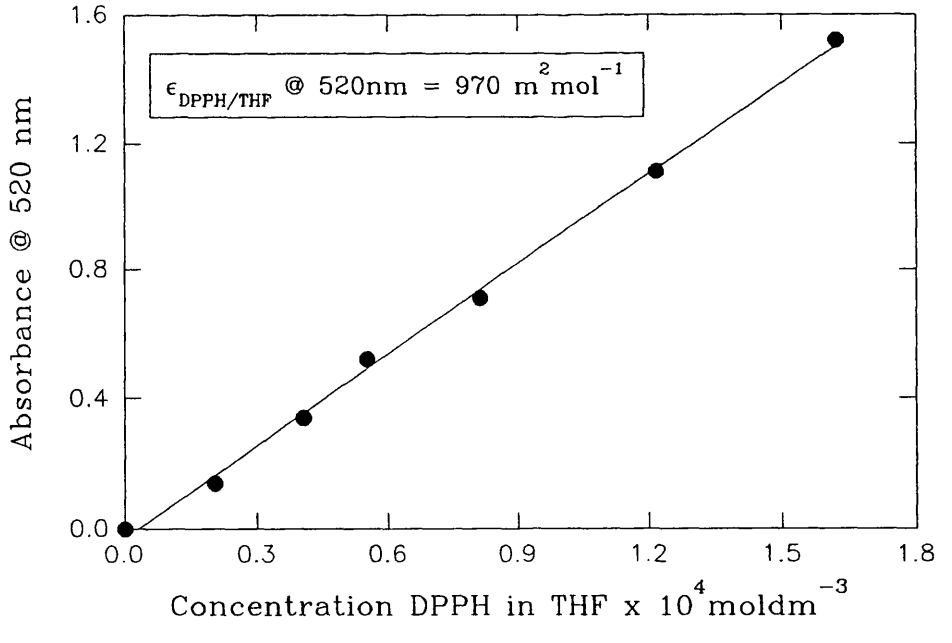


**FIGURE 5.1.** Calculation of the Extinction Coefficient for DPPH in THF.

All of the sonication experiments were performed at 25°C under an atmosphere of nitrogen at an ultrasonic intensity of 23.9 $Wcm^{-2}$.

5.1.1 Sonication of DPPH in THF.

a.) A solution of DPPH in tetrahydrofuran was sonicated in order to calculate the rate of production of radicals as a result of the contribution of the solvent. This is shown in figure 5.2, the rate constant, $k_1$, was found to be,

$$k_1 = 5.99 \times 10^{-6} \text{ moles radicals } dm^{-3}min^{-1}$$

b.) A 1% w/v solution of polyisobutylene dissolved in tetrahydrofuran was sonicated which would yield a rate corresponding to the production of radicals as a result of polymer chain scission plus the solvent contribution. This is also shown in figure 5.2, the rate constant, $k_2$, was found to be,

$$k_2 = 1.271 \times 10^{-5} \text{ moles radicals } dm^{-3}min^{-1}$$

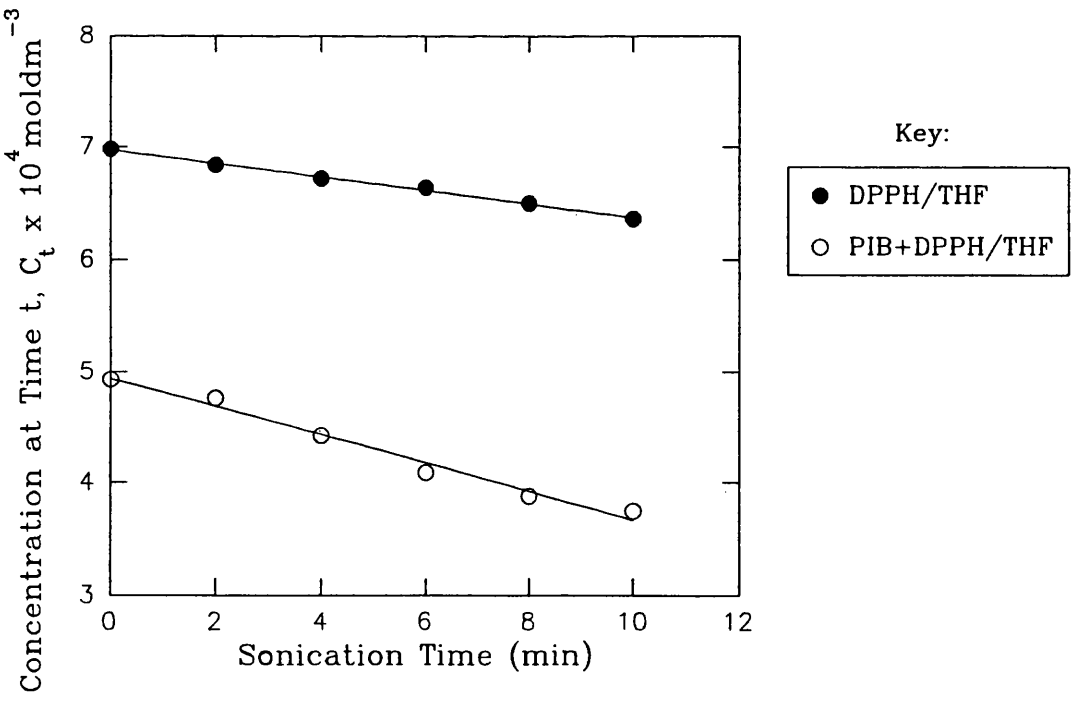


**FIGURE 5.2.** Rate of Consumption of DPPH under Ultrasonic Irradiation.

5.1.2 Calculation of Chain Scissions.

In a 10 minute period of sonication, polyisobutylene, under these conditions, degrades from an initial molecular weight of 1270000 to 234000. Hence for a 1g/100cm$^3$ sample of polymer dissolved in tetrahydrofuran there are 7.874 x $10^{-6}$ moles of polymer chains. The number of chain breaks, N, can be measured,

$$N = \left[ \frac{M_{n,o}}{M_{n,t}} - 1 \right] = 4.427 \qquad 5.1$$

where $M_{n,o}$ and $M_{n,t}$ are the number average molecular weight averages at time t=0 and t=t.

Each chain break produces two radicals, hence,

Moles of radicals produced dm$^{-3}$ per 10 mins = 2 x 4.427 x 7.874 x $10^{-6}$

Number of radicals produced due to chain scissions = 6.97 x $10^{-6}$ moldm$^{-3}$min$^{-1}$

5.1.3 Efficiency of DPPH as a Radical Scavenger.

Therefore by calculating the rate of macroradical production by subtracting the solvent contribution from the rate measured in the polymer solution and by knowing the total number of radicals produced as a result of chain scission, an approximate value for the trapping efficiency can be calculated,

The number of DPPH capped polymers produced = (1.271 - 0.599) x $10^{-5}$

**= 6.72 x $10^{-6}$ moles**

The total number of polymer radicals produced = **6.97 x $10^{-6}$ moles**

$$\text{Efficiency} = \left( \frac{6.72 \times 10^{-6} \text{ moldm}^{-3}\text{min}^{-1}}{6.97 \times 10^{-6} \text{ moldm}^{-3}\text{min}^{-1}} \right) \text{x}100\% = \mathbf{96\%}$$

It can be concluded that the technique has a potential in capping polymer chains and effectively producing functionalised materials.

5.1.4 Sonication of Polyisobutylene in the Presence of Reactive Caps.

In order to functionalise polyisobutylene four molecules were chosen, three of which were bromo-substituted aromatics as these are known to be susceptible to radical attack and the fourth was a dye molecule. In the case of the haloaromatics, when a cap is present on the end of the polymer chain the halogen has been removed and replaced by a long alkyl group hence, in order to spectroscopically analyse these systems, mimic molecules were used to find the extinction coefficients of the capped polymer. The approximate capping efficiency could then be measured.

The caps chosen, and their corresponding mimic molecules are shown in Table 5.1.

Polyisobutylene was sonicated as a solution in tetrahydrofuran in the presence of the capping molecules. The polymers were extensively purified by repeated precipitation to remove unattached chromophore and the UV spectra of the products were obtained. It should be noted that polyisobutylene has no UV absorbance in the region examined. Figure 5.3 shows the UV spectra of Rose Bengal and polyisobutylene with the cap attached and 9-bromoanthracene and polyisobutylene with the cap attached. It is clear that the polymers contain new functionalities. This was further confirmed by recording GPC chromatograms using dual RI and UV detectors at the appropriate wavelength. The RI trace corresponds to the polymer sample whilst the UV responds only to the chromophore in the cap. The retention times of the two peaks were similar in each case confirming that the cap was attached to the polymer chain. Figure 5.4 shows GPC chromatograms for a sample of PIB sonicated with DPPH.

**TABLE 5.1.** Cap Molecules and Mimics Applied.

| Molecular Cap | Mimic Molecule |
|---|---|
| 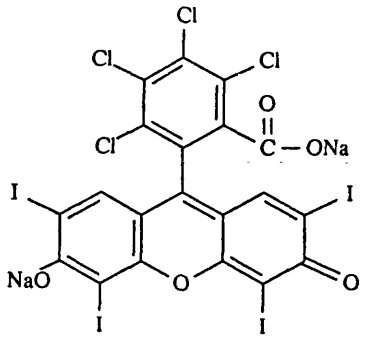 Rose Bengal | 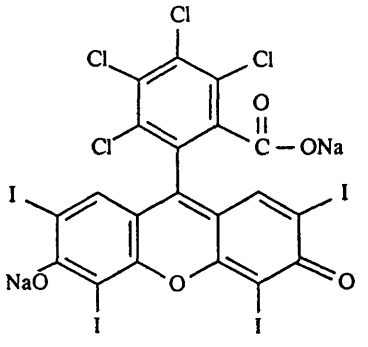 Rose Bengal |
| 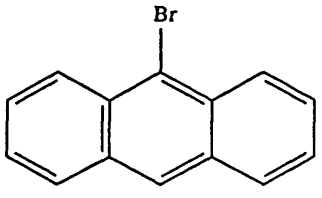 9-Bromoanthracene | 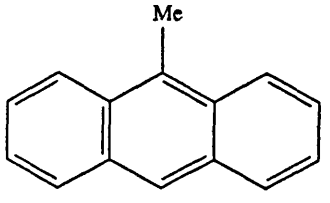 9-Methylanthracene |
| 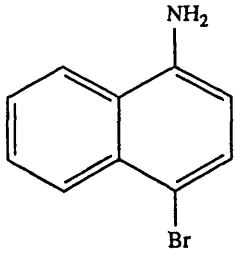 1-Amino-4-bromonaphthalene | 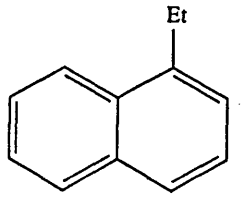 1-Ethylnaphthalene |
| 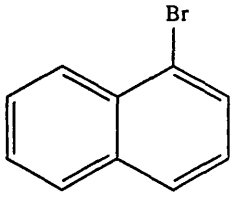 1-Bromonaphthalene | |

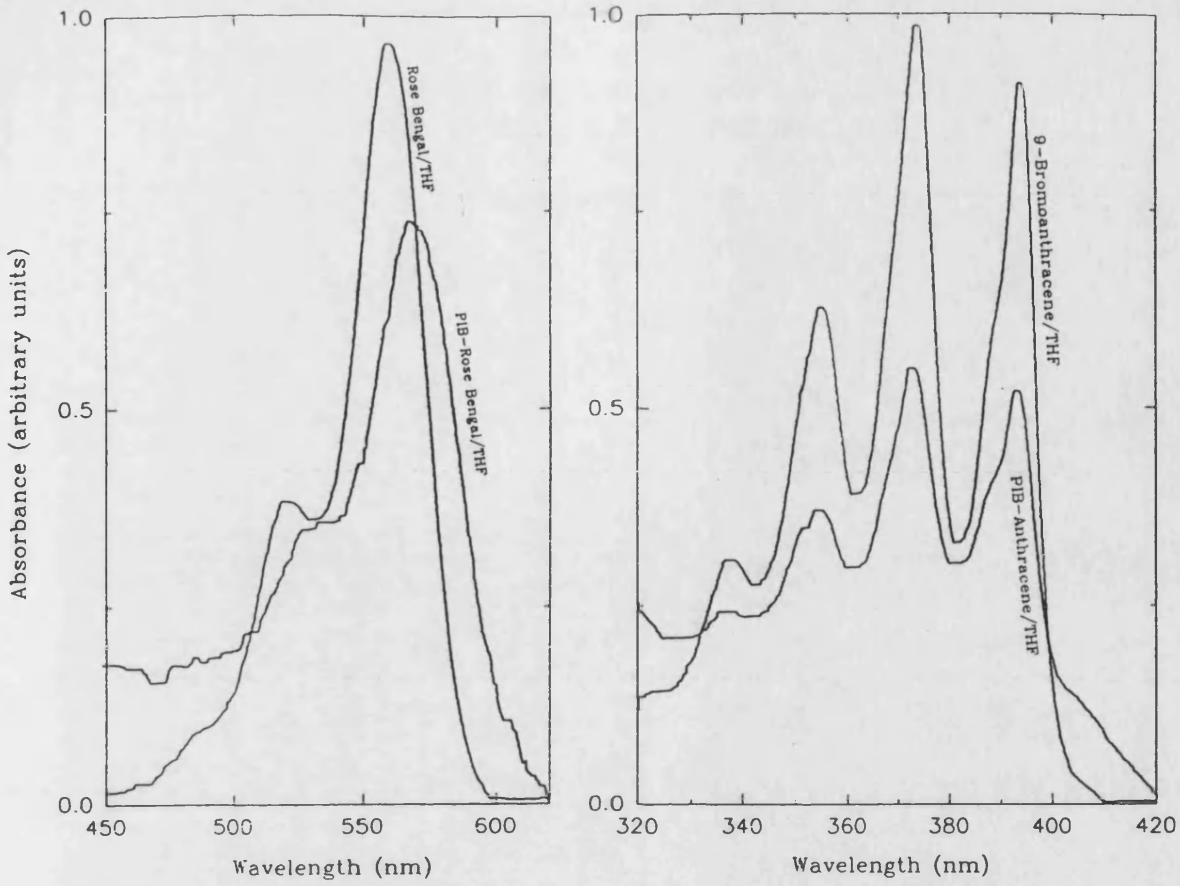


**FIGURE 5.3.** UV Spectra of Rose Bengal and 9-Bromoanthracene in THF and the Corresponding Spectra of the 'Capped' Samples of PIB in THF.

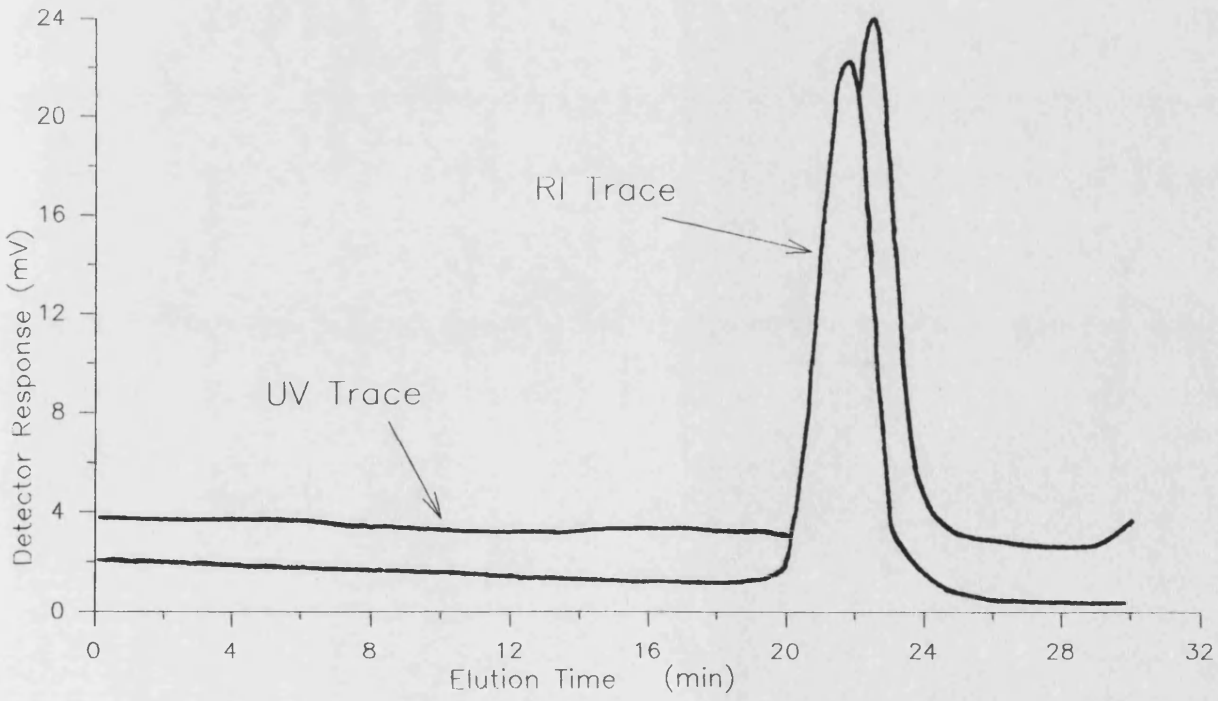


**FIGURE 5.4.** GPC Chromatograms of PIB Sonicated in the Presence of DPPH, Dual Detector Traces (DRI and UV)

The UV trace corresponds only to capped polymer chains.

The extinction coefficients of the molecules were measured in tetrahydrofuran. The values are shown in Table 5.2.

TABLE 5.2. Extinction Coefficients of Molecules.

| Cap / Mimic Molecule | ε in THF ($m^2$ $mol^{-1}$) |
|---|---|
| Rose Bengal | 7020 @ 558 nm |
| 9-Methylanthracene | 945 @ 368 nm |
| 1-Ethylnaphthalene | 467 @ 292 nm<br>27 @ 305 nm |

A known concentration of the capped polymer was prepared in a $10cm^3$ volumetric flask and its UV spectrum recorded. The results are shown in Table 5.3.

TABLE 5.3. Results of Capping Experiments.

| Capping Experiment | Concentration ($g\ dm^{-3}$) | UV Absorbance |
|---|---|---|
| PIB + Rose Bengal | 27.64 | 0.13 @ 558 nm |
| PIB + 9-Bromoanthracene | 29.04 | 0.08 @ 368 nm |
| PIB + 1-Amino-4-bromonaphthalene | 27.18 | 0.104 @ 292 nm |
| PIB + 1-Bromonaphthalene | 22.02 | 0.05 @ 305 nm |

The capping efficiency was calculated as follows, using 1-amino-4-bromonaphthalene as an example.

Concentration of capped polymer in solution = 27.18 g $dm^{-3}$

Absorbance at 292 nm = 0.104

Using the Beer-Lambert law, A = εcl, where A is the absorbance, ε is the molar extinction coefficient, c is the concentration of absorbing species and l is the path length (1cm).

The concentration of cap (using ε for mimic, 1-ethylnaphthalene) is,

$$\frac{0.104}{467\ m^2mol^{-1} \times 1cm} = 2.23 \times 10^{-5}\ moldm^{-3}$$

Assuming one cap per polymer chain, 27.18 g $dm^{-3}$ = 2.23 x $10^{-5}$ mol $dm^{-3}$, hence the effective molecular weight of the polymer with one cap is 1219000. However the molecular weight of the polymer measured by GPC was 234000. It can therefore be concluded that there is only one cap per five polymer chains.

This procedure was repeated for the other caps yielding the following results shown in Table 5.4. In each case the molecular weight of the resulting polymer was 234000.

TABLE 5.4. Results for Capping Efficiency.

| Molecular Cap | Effective Molecular Weight (1 cap/chain) | Capping Efficiency |
|---|---|---|
| Rose Bengal | 14.9 x $10^6$ | 1 cap per 64 chains |
| 9-Bromoanthracene | 3.4 x $10^6$ | 1 cap per 15 chains |
| 1-Amino-4-bromonaphthalene | 1.2 x $10^6$ | 1 cap per 5 chains |
| 1-Bromonaphthalene | 1.2 x $10^5$ | 2 caps per chain (telechelic) |

5.1.5 Discussion of the Functionalisation of Polymers.

The results clearly indicate that a functional group can be attached to a polymer chain as a direct result of ultrasonic irradiation causing chain scissions. From the experiments it can be seen that there is a wide difference between the capping efficiency achieved using the various functionalities.

The calculation of capping efficiencies has been improved by using mimic molecules to calculate the extinction coefficient necessary but it is difficult to obtain an identical copy of the capped material for this purpose.

It appears that the size of the cap molecule plays an important role in determining the likelihood of the radical produced orienting itself into such a position that it will react with the radical on the chain end. The reaction with DPPH with the macromolecular radical was very efficient as the molecule already exists as a stable free radical in great excess in solution whereas the bromoaromatics require bond-breakage to occur in close proximity to a macromolecular radical. Rose Bengal, a very large dye molecule, appeared to only react to a small degree with the polymer undoubtedly due to its size. However its large extinction coefficient made the capped polymer easy to analyse and obtain a UV spectrum. 1-Bromonaphthalene, the smallest molecule, appeared to readily react to form a radical and orient itself to cap a polymer chain. In this case the functionalised polyisobutylene contained two molecules of 1-bromonaphthalene per chain. Hence, assuming the caps reside on the chain ends, this polymer can be said to be a telechelic material.

In summary, the method offers considerable control over the structure of the macroradical and, with careful choice of the functional groups, provides chains effectively capped at both ends with a low polydispersity. Further work is needed in this area before the full potential of copolymerisation reactions using this technique can be realised.

# CHAPTER SIX

# BLOCK COPOLYMER SYNTHESIS USING HIGH INTENSITY ULTRASOUND

## 6.1 Analysis of Copolymers by $^1$H-NMR Spectroscopy.

The knowledge gained from the controlled production of macroradicals under ultrasonic irradiation leads to the opportunity of block copolymer synthesis. In this first approach, the systems sonicated were analysed by $^1$H-NMR spectroscopy in order to confirm the presence of copolymer linkages and attempt a quantitative analysis.

Each system studied proved difficult to separate in terms of removing the residual homopolymers so that the composition of the copolymers could be determined accurately.

The technique of selective precipitation was first tested by mixing solutions of polystyrene and *cis*-polybutadiene and not sonicating the mixture prior to separation. Figures 6.1 and 6.2 show the two $^1$H-NMR spectra of the polymer fractions. Figure 6.1 is the polybutadiene fraction and contains the characteristic methylene groups deshielded by the double bond resonating at 2.09 ppm as a singlet and the vinyl hydrogens absorbing at 5.4 ppm, there is a little polystyrene contamination present. Figure 6.2 is the polystyrene fraction and shows methylene and methine proton resonances in the range 1.1 to 2.4 ppm, aromatic ring hydrogens are represented by the broader bands at lowest field. The band at 6.6 ppm represents the two *ortho* protons and the band at 7.06 ppm arises from the *meta* and *para* hydrogens, there is slight alkane solvent contamination. The spectra show that the technique employed was able to separate the polybutadiene and polystyrene homopolymer mixture.

When styrene is incorporated into an alternating copolymer, the *ortho* hydrogens are not preferentially shielded to the same degree and a single broad peak would be observed for all five ring hydrogens. If the aromatic ring hydrogens, in a sample of pure copolymer, appeared as two bands then it could be assumed that the styrene units were grouped together as in a block copolymer.

Following sonication, the spectra of the separated fractions are less well defined and the isolation of the copolymer was unclear.

Figures 6.3 and 6.4 show the spectra of the separated fractions of the polystyrene and polybutadiene sonication respectively. It is clear that the separation

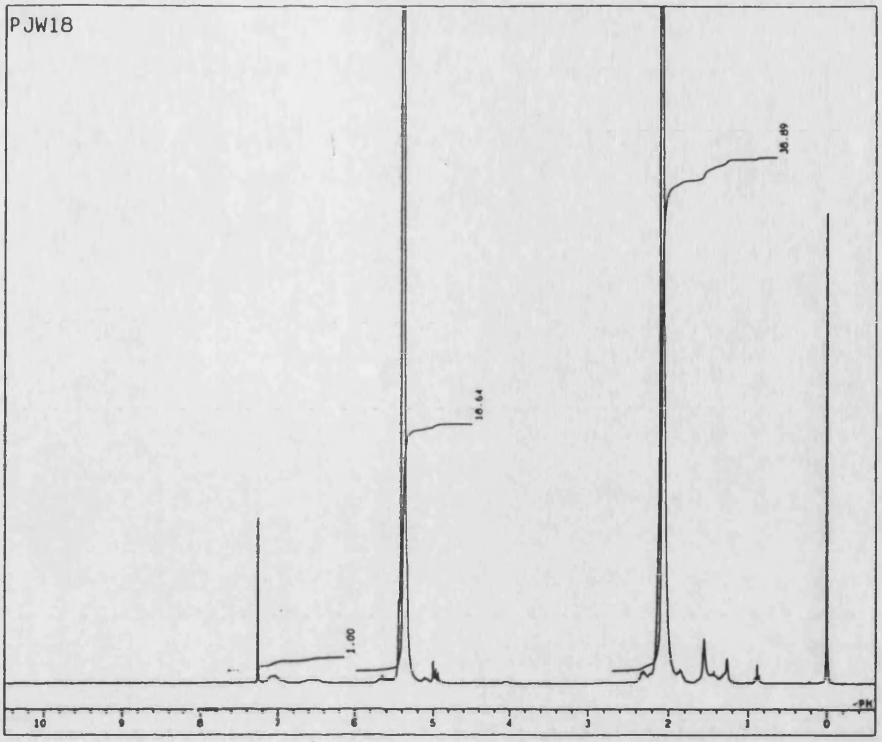


**FIGURE 6.1.** $^{1}$H-NMR Spectrum of the *cis*-Polybutadiene Fraction Separated from an Unsonicated Mixture of Polystyrene and *cis*-Polybutadiene.

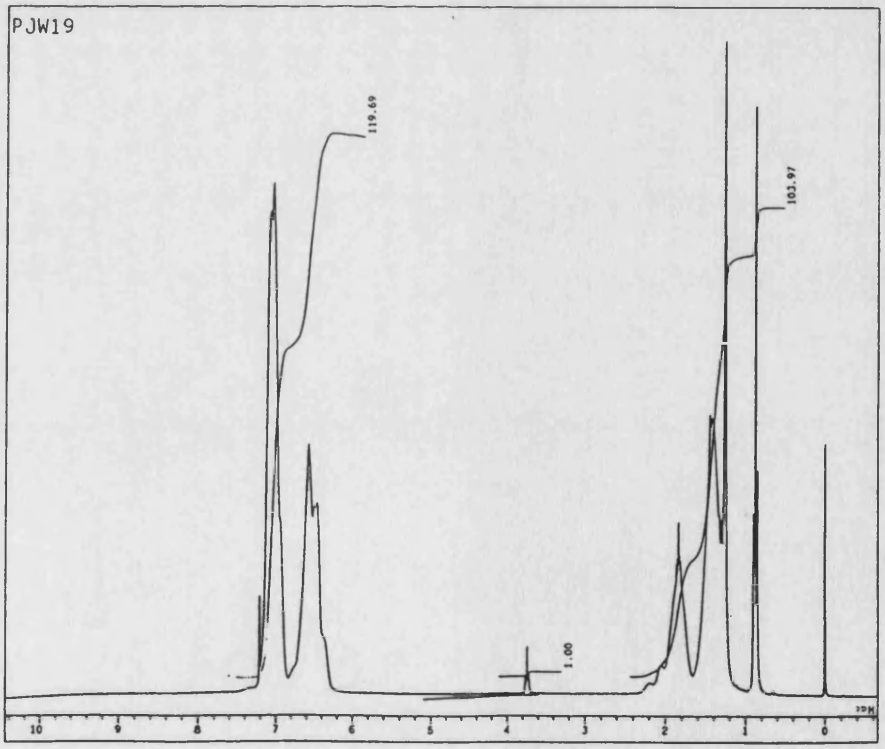


**FIGURE 6.2.** $^{1}$H-NMR Spectrum of Polystyrene Fraction Separated from an Unsonicated Mixture of Polystyrene and *cis*-Polybutadiene.

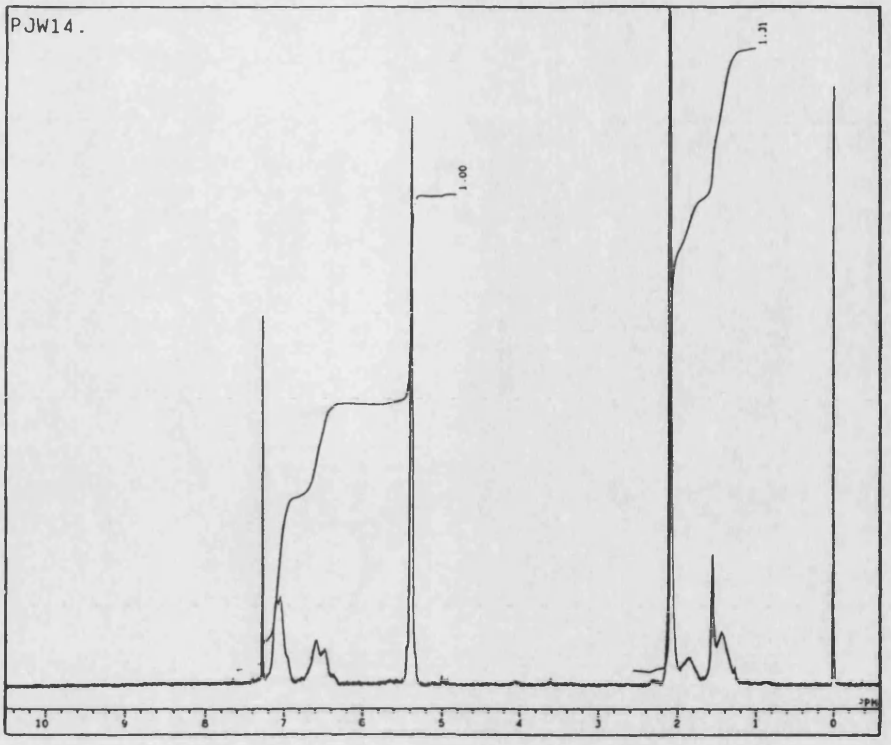


**FIGURE 6.3.** $^{1}$H-NMR Spectrum of Polystyrene Fraction Separated from a Sonicated Mixture of Polystyrene and *cis*-Polybutadiene.

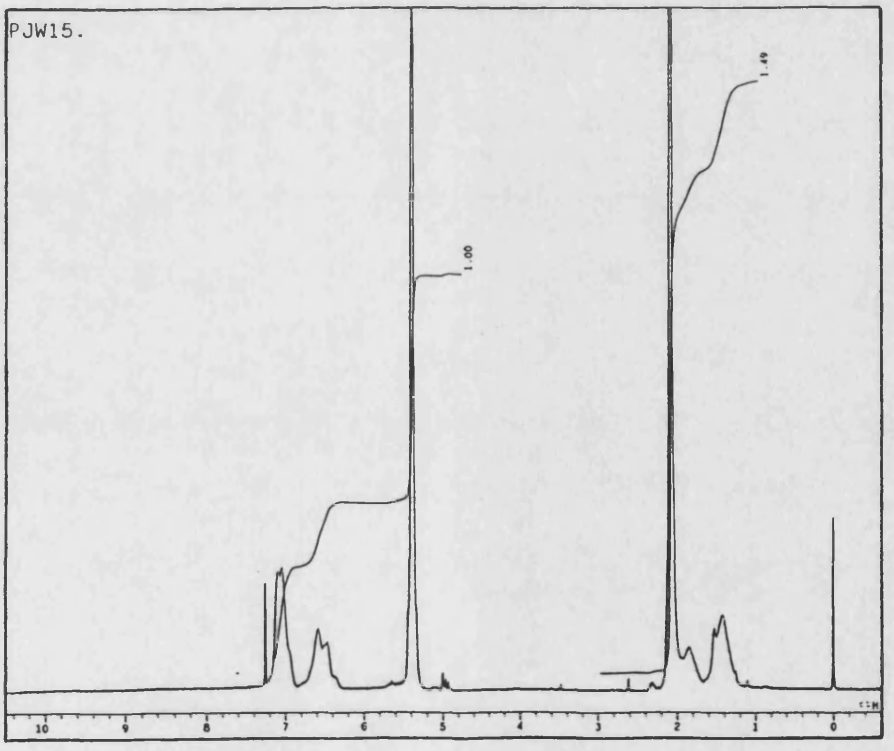


**FIGURE 6.4.** $^{1}$H-NMR Spectrum of the *cis*-Polybutadiene Fraction Separated from a Sonicated Mixture of Polystyrene and *cis*-Polybutadiene.

technique was not so successful as resonances corresponding to both homopolymers are present in each fraction. This contamination is probably due to the formation of copolymer linkages but it cannot be concluded, nor easily characterised, using this procedure.

Figures 6.5 and 6.6 show the spectra of the fractions separated following the sonication of poly(ethylene oxide) and polyisobutylene respectively. PEO would be expected to show methylene resonances, bonded to oxygen (-O-$CH_2$-R), a characteristic of methylene ether groups in the region 3.4 - 3.9 ppm, this is dominant in figure 6.5 but the spectrum clearly contains PIB resonances. Methyl groups in PIB would appear as resonance peaks at 1.10 ppm and the methylene groups at 1.40 ppm, this is dominant in the spectrum shown in figure 6.6, there are other apparent contributions. It remains unclear as to the presence of copolymer linkages.

Similar analysis difficulties were experienced in the other systems examined and it was concluded that NMR could not be used as an accurate method of determining the extent of copolymerisation following ultrasonic reactions of this nature despite claims by other workers. This method of copolymer preparation could not be used to produce significant quantities of pure block copolymers.

It was shown that copolymers were being formed by the mechanism operating during the sonication and an alternative use was investigated. The preparation of *in situ* copolymers to act as compatibilising agents for otherwise immiscible polymer blends is an important application and was studied by SEM.

## 6.2 Characterisation of Polymer Blends and Block Copolymers by Scanning Electron Microscopy.

The size, shape and distribution of components in polymer blends is of primary importance for understanding, and ultimately optimising, properties such as toughness, strength, adhesion, corrosion resistance and processibility. Scanning electron microscopy (SEM) has been used to characterise the blends of various polymer and copolymer mixtures, concentrating on the effect of applying ultrasound to the systems.

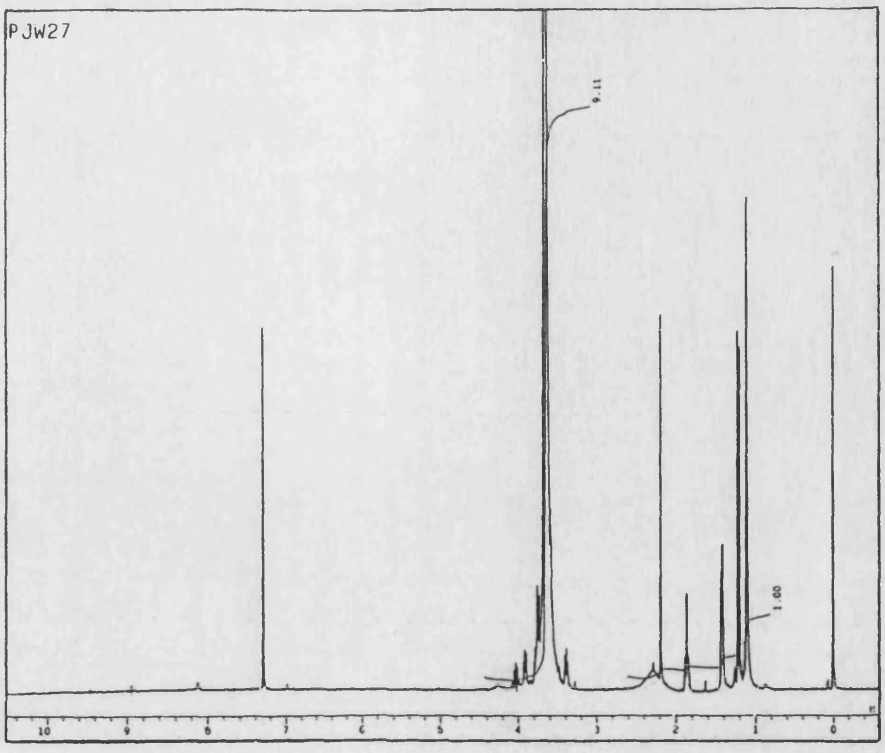


**FIGURE 6.5.** $^{1}$H-NMR Spectrum of the Poly(ethylene oxide) Fraction Separated from a Sonicated Mixture of Poly(ethylene oxide) and Polyisobutylene.

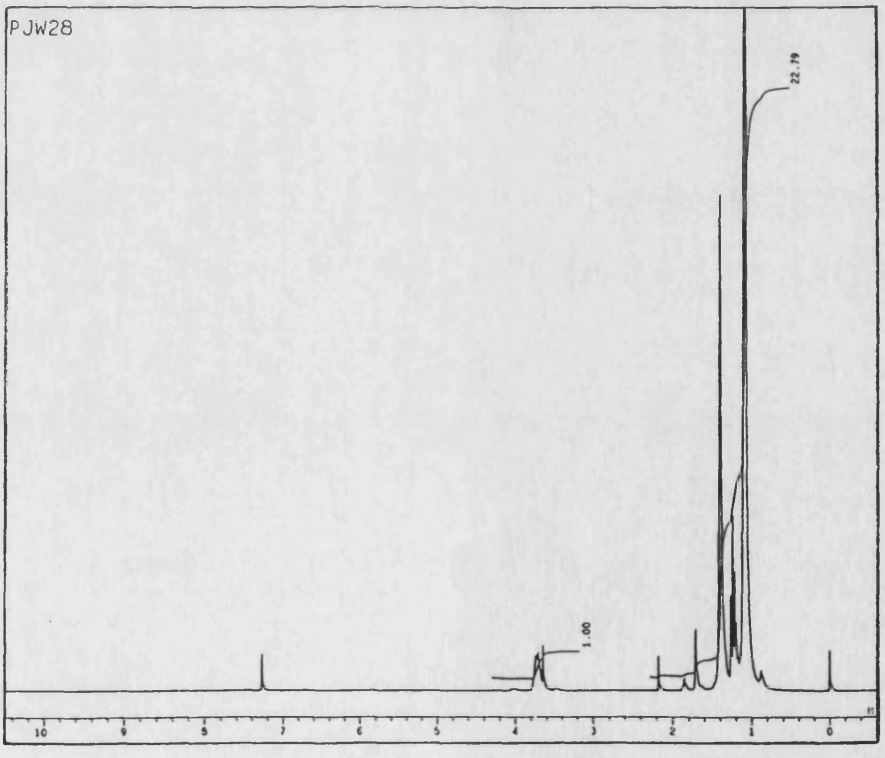


**FIGURE 6.6.** $^{1}$H-NMR Spectrum of the Polyisobutylene Fraction Separated from a Sonicated Mixture of Poly(ethylene oxide) and Polyisobutylene.

a.) Polystyrene + *cis*-Polybutadiene.

The two homopolymers were dissolved in the ratio of 80:20 in toluene as a 1% w/v solution. Thin films were cast from solution directly onto the microscope plates. The solvent was removed slowly under vacuum at a temperature above the glass transition temperatures of both components to ensure that no solvent molecules became trapped in the film and distort the images obtained. The plates were then prepared for SEM by depositing a thin layer of gold on the plate to make the surface conducting. The electron micrographs of the films cast from the unsonicated mixture, shown in figure 6.7 at two different magnifications, show the immiscibility of the homopolymers. Following a period of 6 hours sonication, the appearance of the sample changed dramatically as shown in figure 6.8. The film exhibits large areas of homogeneity and fewer immiscible domains. Sonication inevitably reduces the molecular weight of the polystyrene homopolymer from its initial value of 120000 to approximately 20000 which is a molecular weight comparable to that of the polybutadiene. The sonication process appears to have the effect of solubilising the polystyrene inside the polybutadiene regions producing a miscible blend. The ultrasound has changed the appearance of the micrograph and thus the properties of the resulting blend would be expected to differ greatly from those of the immiscible mixture.

It could be proposed that the inevitable reduction in molecular weight of each component alone could be responsible for the compatibilising effect brought about as a result of sonication. This was investigated by sonicating separate samples of polystyrene and *cis*-polybutadiene alone in toluene under the same ultrasound conditions. The results are the micrographs shown in figure 6.9. The micrographs exhibit immiscible regions and the degree of compatibility cannot be compared with that achieved by sonicating the mixture. It can be concluded that in this system the effect of producing a compatibilised

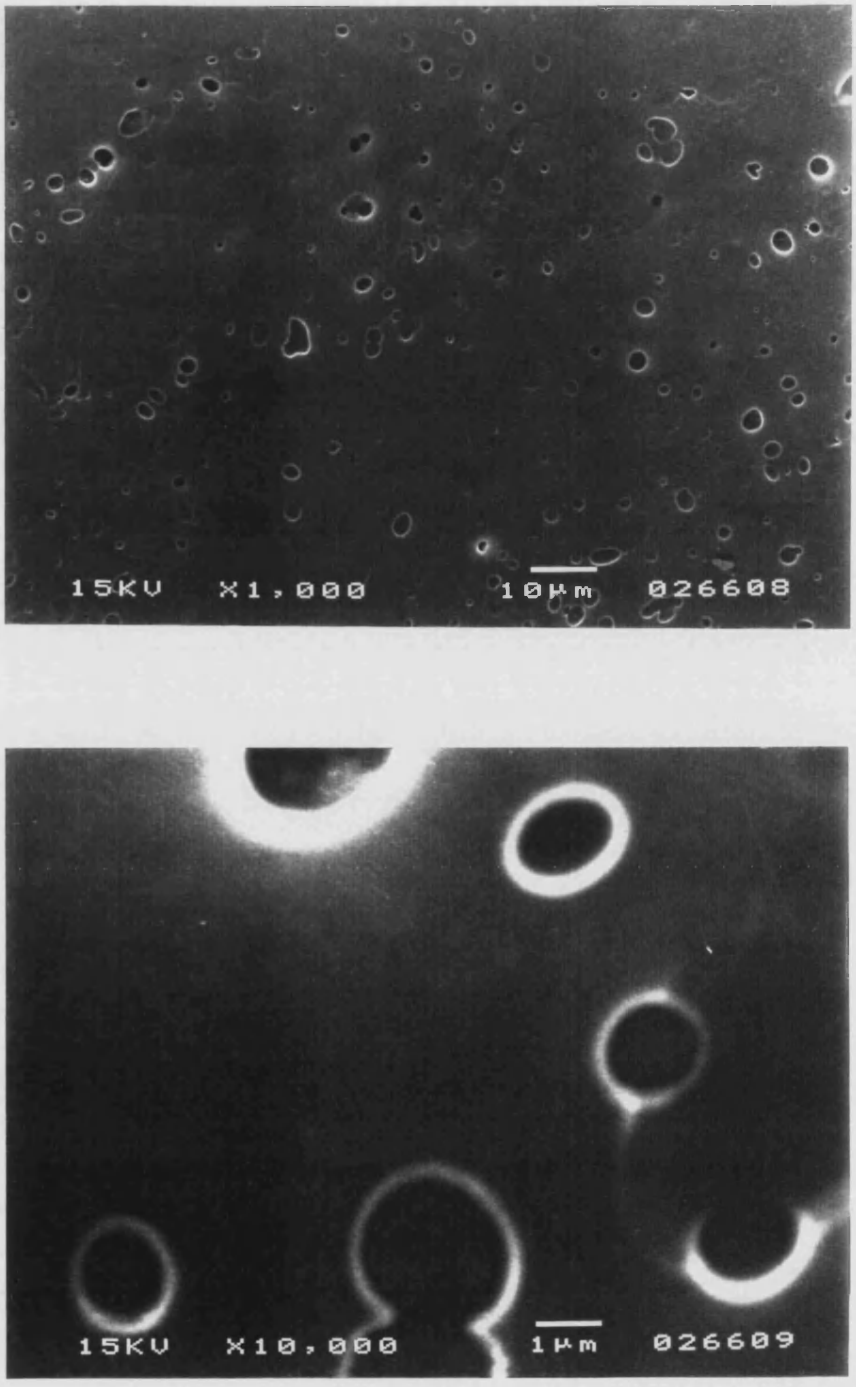


**FIGURE 6.7.** SEM Micrographs of Polystyrene and *cis*-Polybutadiene Unsonicated.

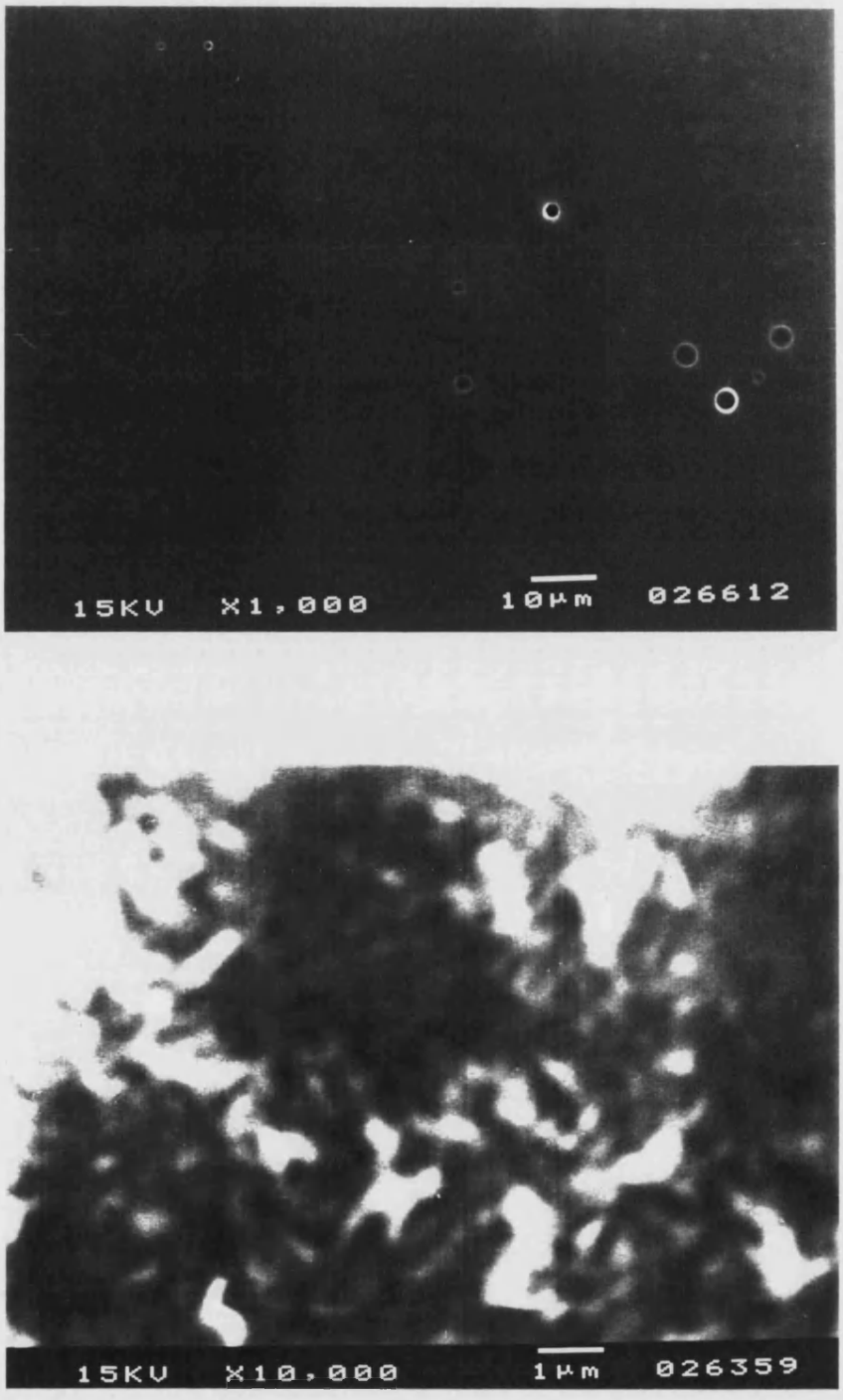


**FIGURE 6.8.** SEM Micrographs of Polystyrene and *cis*-Polybutadiene Sonicated for 6 hours.

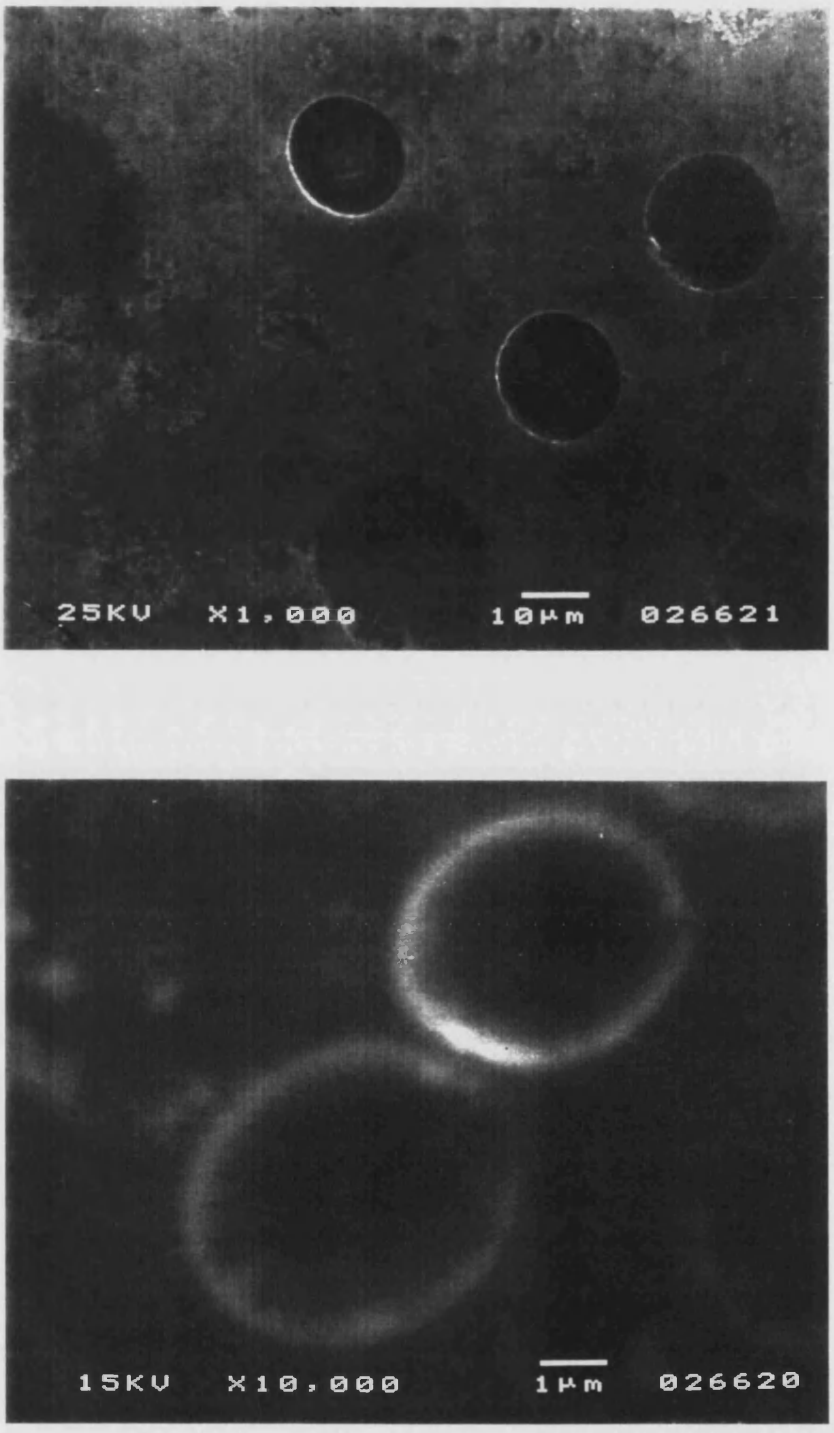


**FIGURE 6.9.** SEM Micrographs of Polystyrene and *cis*-Polybutadiene Mixed Following 6 hours Individual Sonication.

polymer mixture can be attributed directly to the action of ultrasound on the previously immiscible homopolymer mixture; the effect is the same as that expected from incorporating a copolymer.

b.) Polystyrene + Poly(methyl phenylsilane).

The homopolymer mixture in the ratio 80:20 is immiscible under normal conditions as shown in figure 6.10 which clearly shows the incompatibility of the homopolymer pair. Following sonication there is again a marked difference in the appearance of the sample after only 1 hour, as shown in figure 6.11. The ultrasound has the effect of producing a miscible blend of two normally incompatible polymers

c.) Polystyrene + Styrene-Butadiene Copolymer (45% styrene content).

The homopolymer/copolymer mixture was prepared in toluene in the ratio 80:20 and the electron micrographs of the film cast from the unsonicated mixture are shown in figure 6.12 taken at three magnifications. The mixture is immiscible with the copolymer domains clearly in evidence. The domains vary in size with an average diameter of approximately 50 μm. Following sonication there is a marked difference in the appearance of the blend as shown in figure 6.13. Sonication reduces the molecular weight of the two components thus enabling the polystyrene to solubilise inside the copolymer domains during the sonication. This produces a miscible blend and the large domains are no longer present. The micrograph shows areas of compatibilised material and cracks in the films arising from the break-down of the surface as solvent molecules escaped. The domains that remain are greatly reduced in size averaging only 3 - 4 μm.

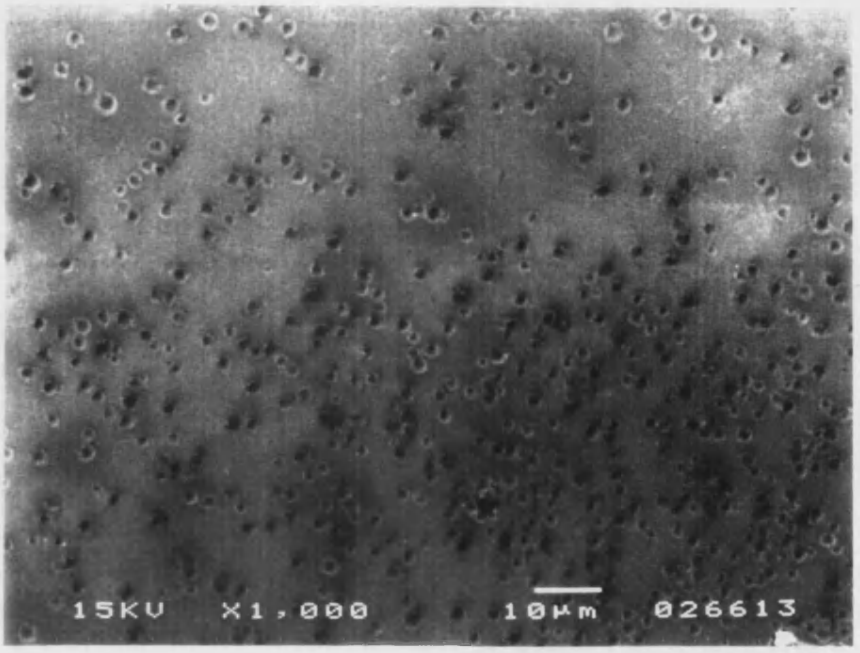


**FIGURE 6.10.** SEM Micrograph of Polystyrene and Poly(methyl phenylsilane) Unsonicated.

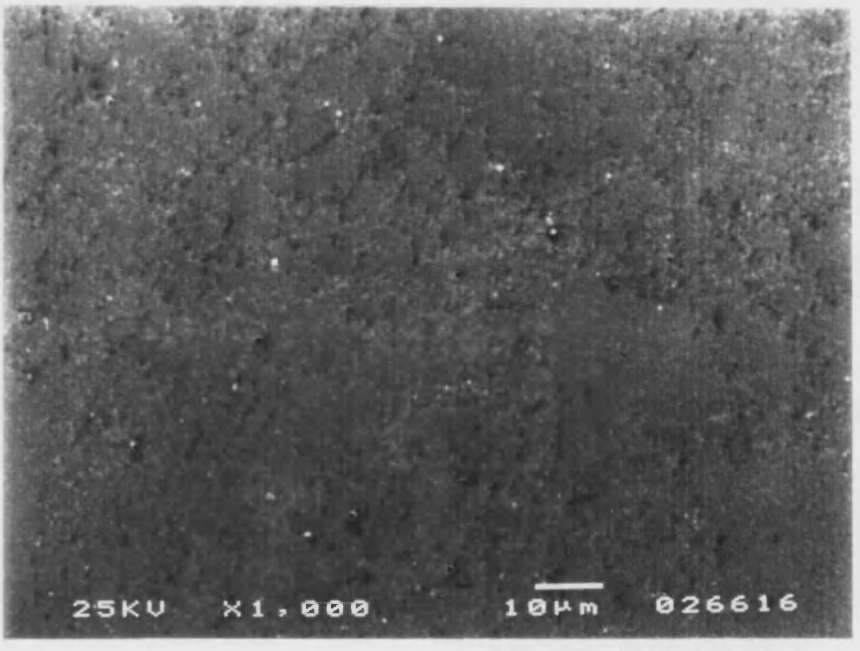


**FIGURE 6.11.** SEM Micrograph of Polystyrene and Poly(methyl phenylsilane) Sonicated for 1 hour.

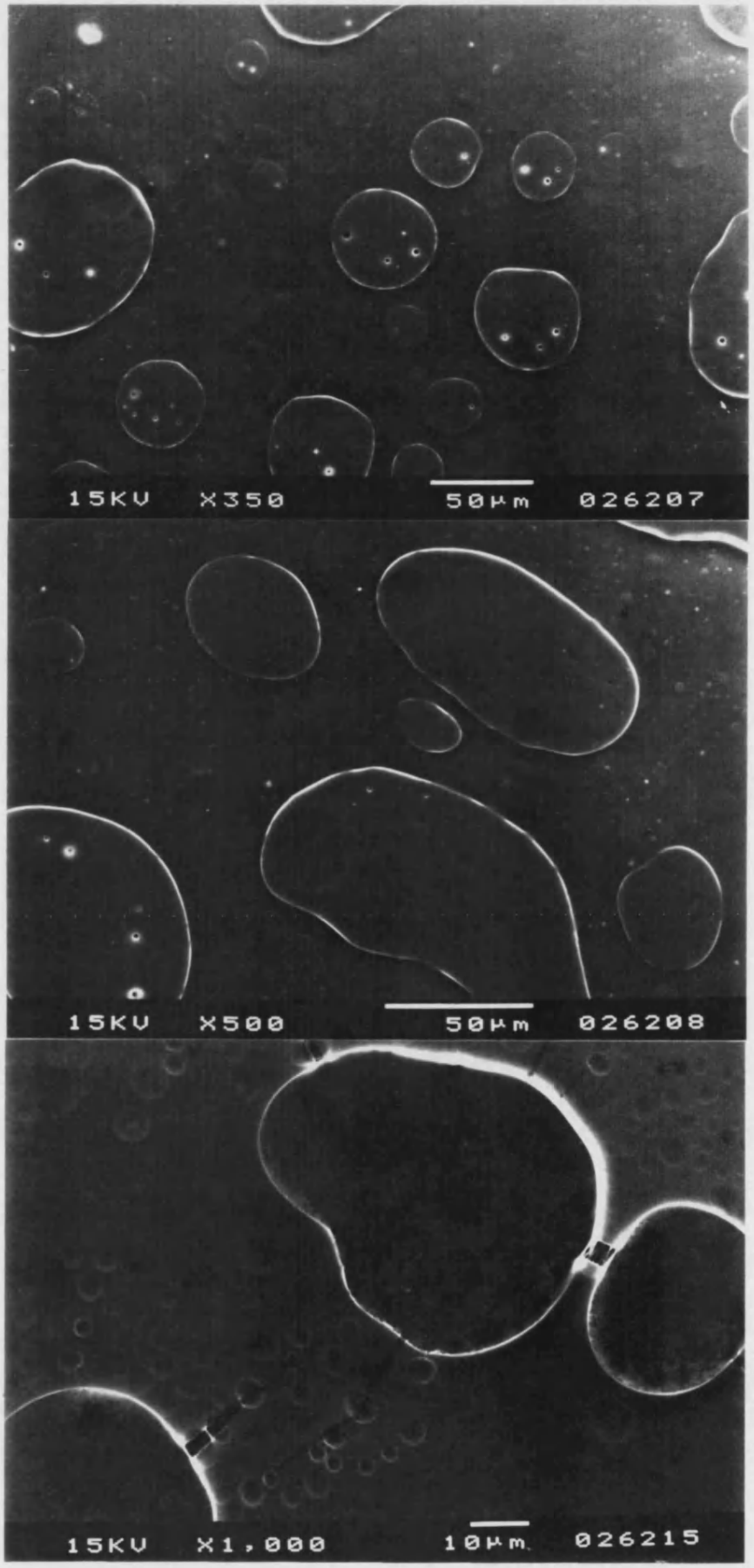


**FIGURE 6.12.** SEM Micrographs of Polystyrene and Styrene-Butadiene Copolymer, Unsonicated.

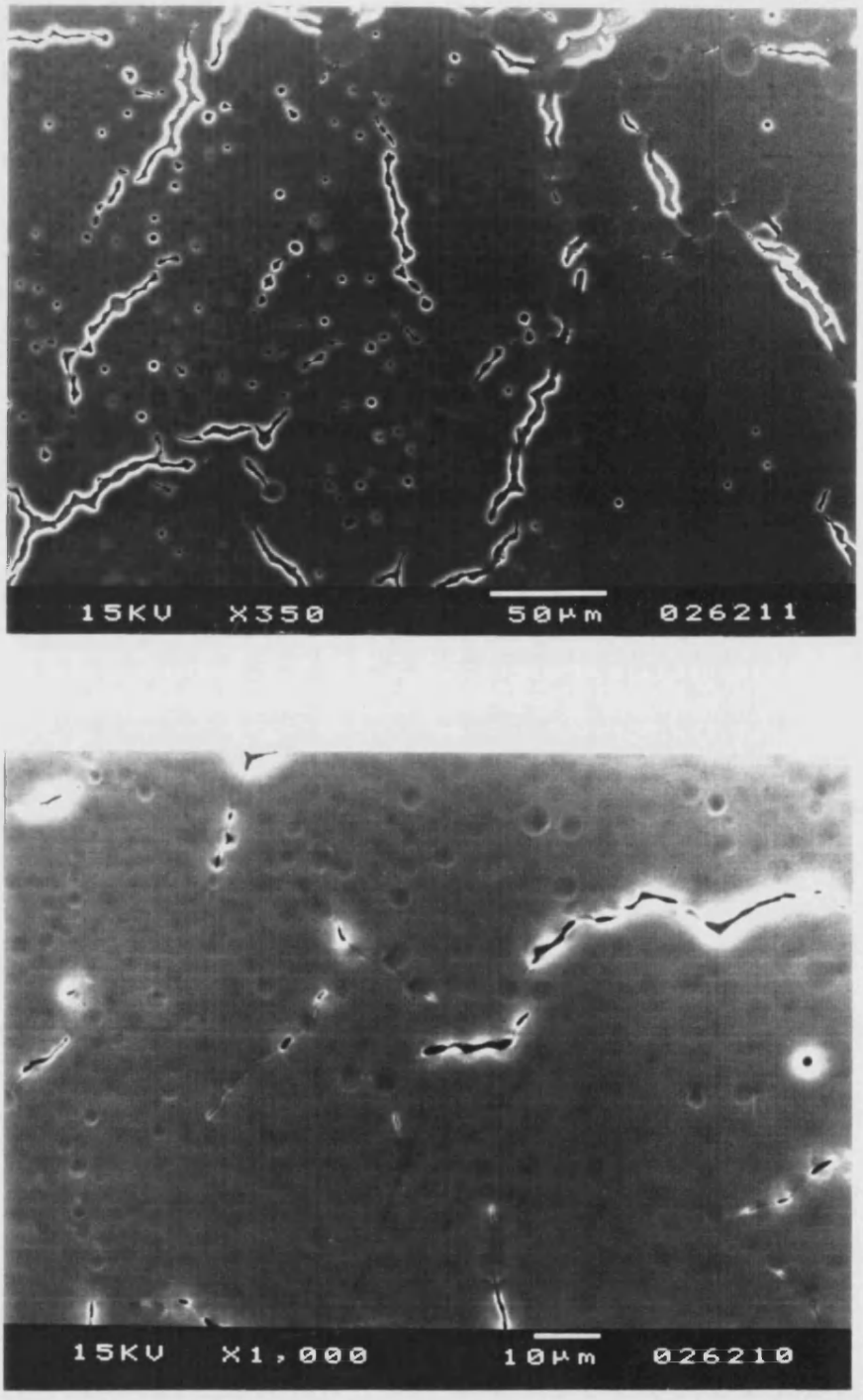


**FIGURE 6.13.** SEM Micrographs of Polystyrene and Styrene-Butadiene Copolymer, Sonicated 6 hours.

6.2.1 Discussion of Studying Polymer Blends by SEM.

Most pairs of high molecular weight polymers are incompatible. SEM studies have shown that the immiscible nature of the systems prior to ultrasonic treatment changes to one corresponding to a compatibilised polymer blend.

The effect is described in terms of the block copolymers formed which allow the homopolymers to be solubilised into respective block copolymer domains composed of like components. This solubilisation effect appears to occur when the molecular weight of the homopolymer is of the same order or less than that of the corresponding block of the copolymer this allows the homopolymer to enter the domain of the copolymer.

The polystyrene and styrene-butadiene copolymer system studied shows that when the molecular weight of the homopolymer is much higher than that of the corresponding block, the copolymer can no longer act as an emulsifier; that is, the block copolymer behaves as if it were incompatible with the corresponding homopolymer and loses the tendency to incorporate the sequences of like homopolymers.

The overall macroscopic effect of introducing a copolymer to the blend is a drastic improvement in the compatibility and ultimately the mechanical strength reducing the problems derived from weak interactions between the immiscible phases. The basis for these improvements is the interfacial activity of the copolymer, which arises from its preferential location at the interphase region causing a reduction in the interfacial tension between the immiscible polymer phases.

The ultrasonic block copolymerisation reaction would be expected to occur at the interface of the immiscible regions as the concentration and likelihood of the macroradicals of homopolymer A and the macroradicals of homopolymer B combining would be at a maximum at the interface. The block copolymers formed at the interface provide unique opportunities for their use *in situ* to compatibilise immiscible polymers. The effect is summarised in figure 6.14.

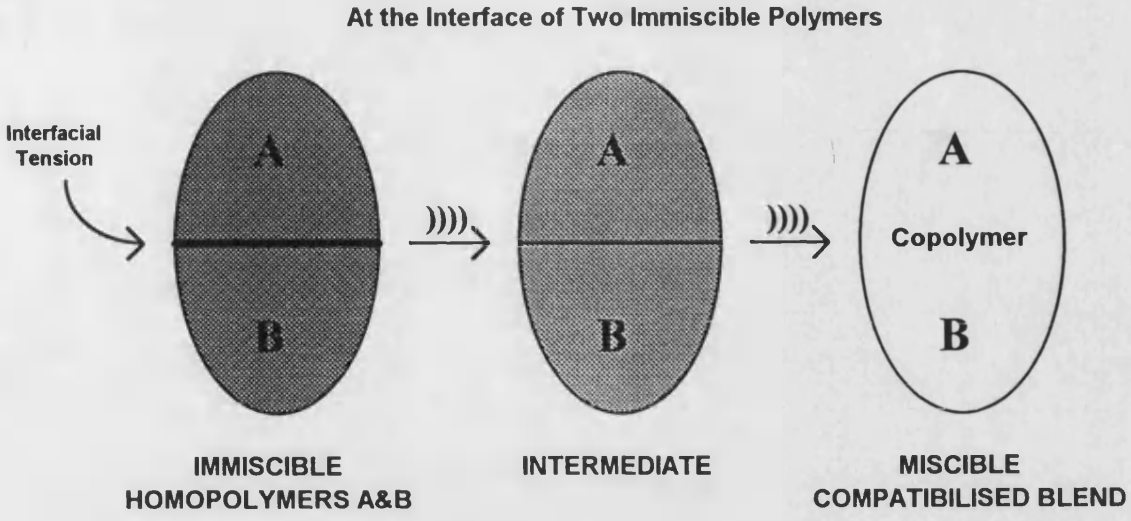


**FIGURE 6.14.** Application of Ultrasound to Incorporate a Block Copolymer at the Interface of Two Otherwise Immiscible Polymers, Reducing Interfacial Tension to Produce a Compatibilised System.

# REFERENCES

1. J. Niezette and A. Linkens, *Polymer*, 1978, **19**, 939.
2. W.B. Smith and H.W. Temple, *J. Phys. Chem.*, 1968, **72**, 4613.
3. J.V. Dawkins, 'Steric Exclusion in Liquid Chromatography of Polymers', ed. J. Janca, New York, 1984.
4. Z. Grubisic, P. Rempp and H. Benoit, *J. Polym. Sci., Polym. Lett. Ed.*, 1967, **5**, 753.
5. F.W. Billmeyer, 'Textbook of Polymer Science', John Wiley & Sons, 1984.
6. P.J. Flory, *J. Chem. Phys.*, 1941, **9**, 660.
7. P.J. Flory, *J. Chem. Phys.*, 1942, **10**, 51.
8. M.L. Huggins, *Ind. Eng. Chem.*, 1943, **35**, 216.
9. M.L. Huggins, *J. Am Chem. Soc.*, 1942, **64**, 1712.
10. O. Smidsrod and J.E. Guillet, *Macromolecules*, 1969, **2**, 272.
11. D. Patterson, Y.B. Tewari, H.P. Schreiber and J.E. Guillet, *Macromolecules*, 1971, **4**, 356.
12. W.R. Krigbaum and P.J. Flory, *J. Am. Chem. Soc.*, 1953, **75**, 1775.
13. P.J. Flory and W.R. Krigbaum, *J. Chem. Phys.*, 1950, **18**, 1086.
14. C.M. Kok and A. Rudin, *J. Appl. Polym. Sci.*, 1981, **26**, 3575.
15. C.M. Kok and A. Rudin, *J. Appl. Polym. Sci.*, 1981, **26**, 3583.
16. C.M. Kok and A. Rudin, *J. Appl. Polym. Sci.*, 1982, **27**, 353.
17. H. Staudinger and W. Heuer, *Ber. Deutsch Chem. Ges.*, 1930, **B63**, 222.
18. M.L. Huggins, *J. Am. Chem. Soc.*, 1942, **64**, 2716.
19. F. Eirich and J. Riseman, *J. Polym. Sci.*, 1949, **4**, 417.
20. T. Alfrey, J.D. Justice and S.J. Nelson, *Trans. Farad. Soc.*, 1946, **B42**, 50.
21. E.O. Kraemer, *Ind. Eng. Chem.*, 1938, **30**, 1200.
22. D.J. Streeter and R.F. Boyer, *Ind. Eng. Chem.*, 1951, **43**, 1979.
23. A. Rudin and R.A. Wagner, *J. Appl. Polym. Sci.*, 1975, **19**, 3361.
24. O.F. Solomon and I.Z. Ciuta, *J. Appl. Polym. Sci.*, 1962, **6**, 683.
25. P.C. Deb and S.R. Chatterjee, *Indian J. Appl. Chem.*, 1968, **31**, 121.

26. T.C. Patton, 'Paint Flow and Pigment Dispersion' p120, Wiley Interscience, New York, 1979.

27. H.U. Khan and G.S. Bhargava, *J. Appl. Polym. Sci., Polym. Lett. Ed.*, 1980, **18**, 803.

28. S.R. Palit and I. Kar, *J. Polym. Sci.*, 1967, **A1(5)**, 2629.

29. P.C. Deb and S.R. Chatterjee, *Makromol. Chem.*, 1969, **125**, 283.

30. J.H. Elliott, K.H. Horowitz and T. Hoodcock, *J. Appl. Polym. Sci.*, 1970, **14**, 2947.

31. A. Rudin and G.B. Strathdee, *J. Paint Technol.*, 1974, **46**, 33.

32. A. Rudin, *J. Appl. Polym. Sci.*, 1975, **19**, 619.

33. T.F. Ford, *J. Phys. Chem.*, 1960, **64**, 1168.

34. D.W. van Krevelen, Properties of Polymers, Elsevier, New York, 1976.

35. B.E. Eichinger and P.J. Flory, *Macromolecules*, 1968, **1**(3), 285.

36. H.S. Tseng and D.R. Lloyd, *Polymer*, 1984, **25**, 670.

37. T.G. Fox and P.J. Flory, *J. Am. Chem. Soc.*, 1951, **73**, 1904.

38. T.G. Fox and P.J. Flory, *J. Phys. Chem.*, 1942, **46**, 151.

39. G.M. Bristow and W.F. Watson, *Trans. Farad. Soc.*, 1958, **54**, 1742.

40. M. Kurata and W.H. Stockmayer, A. Riog, *J. Chem. Phys.*, 1960, **33**, 151.

41. K.K. Chee, *Polymer Commun.*, 1986, **27**, 135.

42. T.J. Mason, *Educ. Chem.*, 1987, **24**(4), 102.

43. G. Kirchoff, *Ann. Phys.*, 1868, **134**, 177.

44. M.A. Margulis, *Ultrasonics*, 1985, **23**(4),157.

45. G.W. Willard, *J. Acoust. Soc. Am.*, 1953, **25**, 669.

46. W.J. Galloway, *J. Acoust. Soc. Am.*, 1954, **26**, 849.

47. M. Greenspan and C.E. Tschiegg, *J. Res. Nat. Bur. Std.*, 1967, **C71**, 229.

48. J.P. Lorimer and T.J. Mason, *Chem. Soc. Rev.*, 1987, **16**(2), 239.

49. B.E. Noltingk and E.A. Neppiras, *Proc. Phys. Soc. (Lond.)*, 1950, **63B**, 674.

50. E.A. Neppiras and B.E. Noltingk, *Proc. Phys. Soc. (Lond.)*, 1951, **64B**, 1032.

51. H.G. Flynn, *Physical Acoustics*, 1964, **1(B)**, 57, Academic Press, New York.

52. K.S. Suslick, S.J. Doktycz and E.B. Flint, *Ultrasonics*, 1990, **28**, 280.

53. M.E. Fitzgerald, V. Griffing and J. Sullivan, *J. Chem. Phys.*, 1956, **25**, 926.

54. F.D. Smith, *Philos. Mag.*, 1935, **19**, 1147.

55. A. Weissler, *J. Appl. Phys.*, 1950, **21**, 171.

56. H.H.G. Jellinek and G. White, *J. Polym. Sci.*, 1951, **6**, 745.

57. H.H.G. Jellinek and G. White, *J. Polym. Sci.*, 1951, **6**, 757.

58. H.H.G. Jellinek and G. White, *J. Polym. Sci.*, 1951, **7**, 33.

59. W. Gaertner, *J. Acoust. Soc. Am.*, 1954, **26**, 977.

60. H.J. Eyring, *J. Chem. Phys.*, 1936, **4**, 283.

61. G.K. Diedrich, P. Kruus and L.M. Rachlis, *Can. J. Chem.*, 1972, **50**, 1743.

62. H.H.G. Jellinek, *J. Polym. Sci.*, 1956, **22**, 149.

63. L. Bergmann, 'Ultrasonics', G. Bell & Sons, New York, 1964.

64. M. Okuyama, *Z. Elektrochem.*, 1955, **59**, 565.

65. J. Curie and P. Curie, *Compt. Rend.*, 1880, **91**, 294.

66. J. Curie and P. Curie, *Compt. Rend.*, 1881, **93**, 1137.

67. F. Galton, 'Inquiries into Human Faculty and Develpoment', Macmillan, 1883.

68. J. Thorneycroft and S.W. Barnaby, *Inst. C. E.*, 1895, **122**, 51.

69. W. Janovski and R. Pohlmann, *Z. Angew. Phys.*, 1948, **1**, 22.

70. T.J. Mason and J.P. Lorimer, in 'Sonochemistry - theory, applications and uses of ultrasound in chemistry', Ellis and Horwood, 1988.

71. E.W. Flosdorf and L.A. Chambers, *J. Am. Chem. Soc.*, 1933, **55**, 3051.

72. A. Szalay, *Z. Phys. Chem.*, 1933, **A164**, 234.

73. A.S. Gyorgyi, *Nature*, 1933, **131**, 278.

74. H. Freundlich and J. Gillings, *Trans. Farad. Soc.*, 1938, **34**, 649.

75. H. Freundlich, *J. Phys. Chem.*, 1937, **41**, 1151.

76. H. Freundlich and K. Sollner, *Trans. Farad. Soc.*, 1936, **32**, 966.

77. E. Heymann, *Trans. Farad. Soc.*, 1935, **31**, 846.

78. F. Brohult, *Nature, (Lond.)*, 1937, **140**, 805.

79. G. Schmid and O. Rommel, *Z. Elektrochem.*, 1939, **45**, 659.

80. G. Schmid, *Phys. Z.*, 1940, **41**, 326.

81. H.H.G. Jellinek, *J. Polym. Sci.*, 1959, **37**, 485.

82. H.W.W. Brett and H.H.G. Jellinek, *J. Polym. Sci.*, 1956, **21**, 535.

83. A.M. Basedow and K.H. Ebert, *Adv. Polym Sci.*, 1956, **22**, 83.

84. A. Henglein, *Makromol. Chem.*, 1954, **14**, 15.

85. A. Henglein, *Makromol. Chem.*, 1955, **15**, 188.

86. H.W. Melville and A.J. Murray, *Trans. Farad. Soc.*, 1950, **46**, 996.

87. M. Tabata, T. Miyazawa, J. Sohma and O. Kobayashi, *Chem. Phys. Lett.*, 1980, **73**, 178.

88. M. Tabata, T. Miyazawa and J. Sohma, Proceedings of the Third Yamada Conference on Free Radicals, Yamada Science Foundation, Osaka, 243, 1979.

89. M. Tabata and J. Sohma, *Eur. Polym J.*, 1980, **16**, 589.

90. J.R. Thomas and D.L. DeVries, *J. Phys. Chem.*, 1959, **63**, 254.

91. J.C. Moore, *J. Polym. Sci.*, 1964, **A2**, 835.

92. G. Gooberman, *J. Polym. Sci.*, 1960, **47**, 329.

93. M.A.K. Mostafa, *J. Polym. Sci.*, 1958, **28**, 499.

94. G. Schmid, C. Schneider and A. Henglein, *Kolloid Z.*, 1956, **148**, 73.

95. G. Goobermann and J. Lamb, *J. Polym. Sci.*, 1960, **42**, 35,

96. G. Goobermann and J. Lamb, *J. Polym. Sci.*, 1960, **47**, 229.

97. R.S. Porter, M. Cantow and J.F. Johnson, *J. Appl., Polym. Sci.*, 1967, **11**, 335.

98. M.T. Shaw and F. Rodriguez, *J. Appl. Polym. Sci.*, 1967, **11**, 991.

99. S.L. Malhotra, *J. Macromol. Sci. Chem.*, 1986, **A23**, 729.

100. C.F. Wu, P.J. Sheth and J.F. Johnson, *Polymer*, 1977, **18**, 822.

101. R.S. Porter and J.F. Johnson, *J. Appl. Phys.*, 1964, **35**(11), 3149.

102. J.F.S. Yu, J.F. Zakin and G.K. Patterson, *J. Appl. Polym. Sci.*, 1979, **23**(8), 2493.

103. H. Fujiwara and K. Goto, *Kogyo Kagaku Zasshi*, 1968, **71**(9), 1430.

104. A. Nakano and Y. Minoura, *Kogyo Kagaku Zasshi*, 1971, **74**(7), 1452.

105. P.A.R. Glynn, B.M.E. Van der Hoff and P.M. Reilly, *J. Macromol. Sci. Chem.*, 1972, **A6**, 1653.

106. P.A.R. Glynn, B.M.E. Van der Hoff and P.M. Reilly, *J. Macromol. Sci. Chem.*, 1973, **A7**, 1695.

107. B.M.E. Van der Hoff and P.A.R. Glynn, *J. Macromol. Sci. Chem.*, 1974, **A8**, 429.

108. B.M.E. Van der Hoff and C.E. Gall, *J. Macromol. Sci. Chem.*, 1974, **A11**, 1739.

109. C.N. Banwell, 'Fundamentals of Molecular Spectroscopy', McGraw-Hill, 1983.

110. M.A.K. Mostafa, *J. Polym. Sci.*, 1958, **33**, 311.

111. G. Schmid and W. Poppe, *Z. Elektrochem.*, 1949, **53**, 28.

112. M.A.K. Mostafa, *J. Polym. Sci.*, 1958, **28**, 519.

113. S.V. Golubev and Y.D. Semchikov, *Isv. Vyssh. Ucheb. Saved. Khim. Khim. Technol.*, 1983, **26**, 1483, [CA 110(12):86238].

114. M.T. Shaw and F. Rodriguez, *J. Appl. Polym. Sci.*, 1967, **11**, 991.

115. C. Keqiang, S. Ye, L. Hiulen and X. Xi, *J. Macromol. Sci. Chem.*, 1985, **A22**, 455.

116. Z. Cao and X. Xu, *Huagong Xuebao*, 1985, **1**, 56, [CA 103(20):16096]

117. B.B. Thomas and W.J. Alexander, *J. Polym. Sci.*, 1957, **25**, 285.

118. T.G. Schoon and G. Rieber, *Angew. Makromol. Chem.*, 1972, **23**, 43.

119. A.M. Basedow and K.H. Ebert, *Makromol. Chem.*, 1975, **176**, 745.

120. A.M. Basedow and K.H. Ebert, *Angew. Chem. Int. Ed. Eng.*, 1974, **13**, 413.

121. M.A.K. Mostafa, *J. Polym. Sci.*, 1958, **33**, 295.

122. T.G. Schoon and G. Rieber, *Angew. Makromol. Chem.*, 1971, **15**, 263.

123. J.R. Thomas, *J. Phys. Chem.*, 1959, **63**, 1725.

124. G. Schmid and E. Beuttenmuller, *Z. Elektrochem.*, 1943, **49**, 325.

125. Y.Y. Nelkenbaum, I.K. Prokofiev and Y.A. Sangalov, *Vysokomol. Soedin. Ser. A*, 1986, **28**, 1058, [CA 106(20):156965].

126. G.J. Price and P.F. Smith, *Polymer Int.*, 1991, **24**, 159.

127. P.F. Smith, Ph.D. Thesis, University of Bath, 1991.

128. G. Schmid and E. Beuttenmuller, *Z. Elektrochem.*, 1944, **50**, 209.

129. S.L. Malhotra, M. Breton and J.M. Gauthier, *J. Macromol. Sci. Chem.*, 1982, **A18**, 1151.

130. G. Schmid and O. Rommel, *Z. Phys. Chem.*, 1939, **A185**, 97.

131. B.B. Thomas and W. Alexander, *J. Polym. Sci.*, 1955, **15**, 361.

132. J.H. deBoer, *Trans. Farad. Soc.*, 1936, **32**, 10.

133. H.H.G. Jellinek and G. White, *J. Polym. Sci.*, 1951, **7**, 21.

134. J.A. Odell and A. Keller, *Polym. Sci., Polymer Phys. Ed.*, 1986, **24**, 1889.

135. R.E. Harrington and B.H. Zimm, *J. Phys. Chem.*, 1965, **69**, 161.

136. M. Okuyama and T. Hirose, *J. Appl. Polym. Sci.*, 1963, **7**, 591.

137. G. Gooberman, *J. Polym. Sci.*, 1960, **42**, 25.

138. T.G. Schoon and G. Rieber, *Angew. Makromol. Chem.*, 1976, **49**, 23.

139. F. Beuche, *J. Appl. Polym. Sci.*, 1960, **4**, 101.

140. D.E. Hughes and W.L. Nyborg, *Science*, 1962, **138**, 108.

141. N.J. Pritchard, D.E. Hughes and A.R. Peacocke, *Biopolymers*, 1966, **4**, 259.

142. N.J. Pritchard and A.R. Peacocke, *Biopolymers*, 1968, **6**, 605.

143. O. Lindstrom and O. Lamm, *J. Phys. Coll. Chem.*, 1951, **55**, 1139.

144. A.A. Berlin and B.S. El'tsefon, *Khim. Nauka. Prom.*, 1957, **2**, 667.

145. I.E. El'Piner, 'Ultrasound : Physical, Chemical and Biological Effects, Consultants Bureau, New York, 1964.

146. P. Kruus, *Ultrasonics*, 1983, **21**, 201.

147. P. Kruus, L.A. Dupond and T.J. Patraboy, *Ultrasonics International*, 502, 1983.

148. G.J. Price, M.R. Daw, N.J. Newcombe and P.F. Smith, *British Polym. J.*, 1990, **23**, 63.

149. G.J. Price, P.F. Smith and P.J. West, *Ultrasonics*, 1991, **29**, 166.

150. G.J. Price, D.J. Norris and P.J. West, *Macromolecules*, 1992, **25**(24), 6447.

151. P. Kruus and T.J. Patraboy, *J. Phys. Chem.*, 1985, **89**, 3379.

152. K.F. O'Driscoll and A.H. Sridharan, *Appl. Polym. Symp.*, 1975, **26**, 135.

153. S.L. Malhotra, *J. Macromol. Sci. Chem.*, 1981, **A18**, 1055.

154. H.W. Melville, *Trans. J. Plastics Inst.*, 1955, **23**, 146.

155. P.E.M Allen, J.M. Downer, G.W. Hastings, H.W. Melville, P. Molyneux and J.R. Urwin, *Nature*, 1956, **117**, 910.

156. S.L. Malhotra and J.M. Gauthier, *J. Macromol. Sci. Chem.*, 1982, **A18**, 783.

157. X. Hu and X. Xu, *Huagong Xuebao*, 1982, **4**, 319, [CA 99(12):88684].

158. M. Sakurai, Y. Torikai and K. Negishi, *Seisan Kenkyu*, 1971, **23**, 272, [CA 76(10):46568].

159. D.J. Buckley, *Trans. N. Y. Acad. Sci.*, 1967, [2] **29**, 735.

160. L. Bohn, *Rubber Chem. Technol.*, 1968, **41**, 495.

161. S. Krause, *J. Macromol. Sci., Rev. Macromol. Chem.*, 1972, 7(21), 251.

162. S. Krause, in 'Polymer Blends', edited by D.R. Paul and S. Newman, Chapter 2, Academic Press, New York, 1978.

163. P.H. Geil, *Ind. Eng. Chem., Prod. Res. Dev.*, 1975, **14**, 59.

164. P.R. Couchman and F.E. Karasz, *J. Polym. Sci., Polym. Phys. Ed.*, 1977, **15**, 1037.

165. D.S. Kaplan, *J. Appl. Polym. Sci.*, 1976, **20**, 2615.

166. T. Nishi, T.T. Wang and T.K. Kwei, *Macromolecules*, 1975, **8**, 227.

167. M.A. Haney, 'Capillary Bridge Viscometer', U.S. Patent #4 463 598 (1984).

168. B.H. Zimm and W.H. Stockmayer, *J. Chem. Phys.*, 1949, **17**, 1301.

169. P. Small, *Adv. Polym. Sci.*, 1975, **18**, 1.

170. R. Dietz and M.A. Francis, *Polymer*, 1979, **20**, 450.

171. D. Constantin, *Europ. Polym. J.*, 1977, **13**, 907.

172. W. Scheinert, *Die Angew. Makromol. Chemie*, 1977, **63**, 117.

173. W.S. Park and W.W. Graessley, *J. Polym. Sci., Polym. Phys. Ed.*, 1977, **15**, 85.

174. L. Marais, Z. Gallot and M. Benoit, *Analysis*, 1976, **4**, 449.

175. A. Servotte and R. de Bruille, *Die Makromol. Chemie*, 1975, **176**, 203.

176. H.L. Wagner and F.L. McCrackin, *J. Appl. Polym. Sci.*, 1977, **21**, 2833.

177. T. Kato, A. Kanda, A. Takahashi, I. Noda, S. Maki and M. Nagasawa, *Polym. J.*, 1979, **11**, 575.

178. D.E. Axelson and W.C. Knapp, *J. Appl. Polym. Sci.*, 1980, **25**, 119.

179. J.W.S. Hearle, J.T. Sparrow and P.M. Cross, 'The Use of the Scanning Electron Microscope', Pergamon, Oxford, 1972.

180. O.C. Wells, 'Scanning Electron Microscopy', McGraw Hill, New York, 1974.

181. J.I. Goldstein and H. Yakowitz, (Eds.), 'Practical Scanning Electron Microscopy', Plenum, New York, 1975.

182. L.C. Sawyer and D. Grubb, 'Polymer Microscopy', Chapman & Hall, 1987.

183. J.R. White and E.L. Thomas, *Rubber Chem. Technol.*, 1984, **57**, 457.

184. P. Echlin and P.J.W. Hyde, *Scanning Electron Microsc.*, 1972, **5**, 137.

185. F.P. Reding and E.R. Walter, *J. Polym. Sci.*, 1959, **38**, 141.

186. R.G. Vadimsky, in 'Methods of Experimental Physics', Vol. 16B, edited by R.A. Fava, Academic Press, New York, 1980, 185.

187. G. Hsiue and C. Yang, *J. Appl. Polym. Sci., Polym. Phys. Ed.*, 1981, **19**, 1255.

188. B.S. El'tsefon and A.A. Berlin, *Vyskomol Soedin*, 1962, **4**, 1033.

189. B.S. El'tsefon and A.A. Berlin, *Polym. Sci. USSR*, 1964, **5**, 668.

190. G. Allen and J.C. Bevington, (Eds.), 'Comprehensive Polymer Science', Pergamon Press, 1989, **1**, 175.

191. G. Schmid, *Z. Phys. Chem.*, 1940, **A186**, 113.

192. D.W. Ovenall, G.W. Hastings and P.E.M. Allen, *J. Polym. Sci.*, 1958, **33**, 207.

193. R. Simha, *J. Appl. Phys.*, 1941, **12**, 569.

194. P.E.M. Allen, G.M. Burnett, G.W. Hastings and D.W. Ovenall, *J. Polym. Sci.*, 1958, **33**, 213.

195. H. Fujiwara and K. Goto, *Polymer Bulletin*, 1990, **23**, 27.

196. T. Sato and D.E. Nalepa, *J. Appl. Polym. Sci.*, 1978, **22**, 865.

197. H.H.G. Jellinek, 'Degradation of Vinyl Polymers', Academic Press, New York, 1955.

198. K. Chen, S. Chen and X. Xu, 33rd IUPAC International Symposium on Macromolecules Conf. Proc., 1990.

199. W. Gerrard, 'Gas Solubilities', Pergamon Press, 1980.

200. R. Battino and H.L. Clever, *Chem. Rev.*, 1966, **66**, 395.

201. R.J. Wilcock, R. Battino, W.F. Danforth and E. Wilhelm, *J. Chem. Thermodynamics*, 1978, **10**, 817.

202. M.B. King and H. Al-Najjar, *Chem. Eng. Sci.*, 1977, **32**, 1241.

203. M.B. King, K. Kassim and H. Al-Najjar, *Chem. Eng. Sci.*, 1977, **32**, 1247.

204. H.L. Clever, C.L. Young and R. Battino, (Eds.) IUPAC Solubility Data Series, Various Volumes, Pergamon Press.

205. J. Makranczy, K. Megyery-Balog, L. Rusz and L. Patyi, *Hung. J. Ind. Chem.*, 1976, **4**, 269.

206. N. B. Vargaftik, 'Tables on the Thermophysical Properties of Liquids and Gases', John Wiley & Sons, 1975.

207. Thermodynamics Research Center Hydrocarbon Project Tables, Thermodynamics Research Center, Texas A&M University.

208. R.R. Dreisbach, 'Physical Properties of Chemical Compounds', Advances in Chemistry Series, Am. Chem. Soc., 1959.

209. J.J. Fox and A.A. Martin, *Proc. Roy. Soc. (Lond.)*, 1940, **A175**, 208.

210. J.W. Thompson and P. Torkington, *Trans. Farad. Soc.*, 1945, **41**, 248.

211. W.M.D. Bryant, *J. Polym. Sci.*, 1947, **2**, 547.

212. M. Roedel, *J. Am. Chem. Soc.*, 1953, **75**, 6110.

213. P.J. Flory, *J. Am. Chem. Soc.*, 1937, **59**, 241.

214. F.W. Billmeyer, *J. Am. Chem. Soc.*, 1953, **75**, 6118.

215. J.R. Ebdon, 'New Methods of Polymer Synthesis', Chapman & Hall, 1991, 162.

216. C.H. Bamford and A.D. Jenkins, *Nature (Lond.)*, 1955, **176**, 78.

217. J.P. Kennedy and R.A. Smith, *J. Polym. Sci., Polym. Chem. Ed.*, 1980, **18**, 1539.